JENNI LEPPINIEMI

The Development of Novel Biomolecular Tools Based on Avidins, DNA and Chitosan

■

ACADEMIC DISSERTATION
To be presented, with the permission of
the Board of the BioMediTech of the University of Tampere,
for public discussion in the Auditorium of
School of Health Sciences, Medisiinarinkatu 3,
Tampere, on May 16th, 2014, at 12 o'clock.

UNIVERSITY OF TAMPERE

JENNI LEPPINIEMI

The Development of Novel Biomolecular Tools Based on Avidins, DNA and Chitosan

Acta Universitatis Tamperensis 1933
Tampere University Press
Tampere 2014

UNIVERSITY
OF TAMPERE

ACADEMIC DISSERTATION
University of Tampere, BioMediTech
Tampere Graduate Program in Biomedicine and Biotechnology (TGPBB)
Finland

Supervised by
Professor Markku S. Kulomaa
University of Tampere
Finland
Docent Vesa P. Hytönen
University of Tampere
Finland

Reviewed by
Professor Reijo Lahti
University of Turku
Finland
Professor Mauri Kostiainen
Aalto University
Finland

The originality of this thesis has been checked using the Turnitin OriginalityCheck service in accordance with the quality management system of the University of Tampere.

Cover design by
Mikko Reinikka

Distributor:
kirjamyynti@juvenes.fi
http://granum.uta.fi

Acta Universitatis Tamperensis 1933
ISBN 978-951-44-9448-2 (print)
ISSN-L 1455-1616
ISSN 1455-1616

Acta Electronica Universitatis Tamperensis 1417
ISBN 978-951-44-9449-9 (pdf)
ISSN 1456-954X
http://tampub.uta.fi

Suomen Yliopistopaino Oy – Juvenes Print
Tampere 2014

For Harri and Toivo

CONTENTS

LIST OF ORIGINAL COMMUNICATIONS

This thesis is based on the following original communications that are referred to in the text by the Roman numerals (I-V).

I **Leppiniemi J**, Määttä JAE, Hammaren H, Soikkeli M, Laitaoja M, Jänis J, Kulomaa MS, Hytönen VP. Bifunctional avidin with covalently modifiable ligand binding site. PLOS ONE 2011, 6(1), e16576.

II **Leppiniemi J**, Grönroos T, Määttä JAE, Johnson MS, Kulomaa MS, Hytönen VP, Airenne TT. Structure of bradavidin – C-terminal residues act as intrinsic ligands. PLOS ONE 2012, 7(5), e35962.

III **Leppiniemi J**, Meir A, Kähkönen N, Kukkurainen S, Määttä JA, Ojanen M, Jänis J, Kulomaa MS, Livnah O, Hytönen VP. The highly dynamic oligomeric structure of bradavidin II is unique among avidin proteins. Protein Science 2013, 22(7), 980-994.

IV Linko V*, **Leppiniemi J***, Paasonen ST*, Hytönen VP, Toppari JJ. Defined-size DNA triple crossover construct for molecular electronics: modification, positioning and conductance properties. Nanotechnology 2011, 22(27), 275610.

V Talvitie E, **Leppiniemi J**, Mikhailov A, Hytönen VP, Kellomäki M. Peptide-functionalized chitosan-DNA nanoparticles for cellular targeting. Carbohydrate Polymers 2012, 89, 948-954.

* = equal contribution

ABBREVIATIONS

3D	three-dimensional
AC	alternating current
AC-IS	alternating current impedance spectroscopy
AFM	atomic force microscopy
AGE	agarose gel electrophoresis
Avd	avidin
bp	base pair
cDNA	complementary DNA
CF	correction factor
CpAvd	circularly permuted avidin monomer
Da	dalton
DC	direct current
DcAvd	dual chain avidin
DcAvd-Cys	dcAvd(I117$C_{5\rightarrow4}$,S16C,V115$H_{6\rightarrow5}$)
DEP	dielectrophoresis
DF	dilution factor
DLS	dynamic light scattering
DMSO	dimethyl sulfoxide
DSC	differential scanning calorimetry
dsDNA	double-stranded DNA
ε	molar extinction coefficient
EDTA	ethylenediaminetetraacetic acid
EGFP	enhanced green fluorescent protein
ESI	eloctrospray ionization
FE-SEM	field emission scanning electron microscopy
FMOC	9-fluorenylmethyloxycarbonyl
FRET	fluorescence resonance energy transfer
FT-ICR	Fourier transform ion cyclotron resonance
ΔG	change in Gibbs energy
ΔH	change in enthalpy
HABA	4-hydroxyazobenzene-2-carboxylic acid
His-tag	polyhistidine tag
HPLC	high-performance liquid chromatography
ITC	isothermal titration calorimetry

K_a	association constant
k_{ass}	association rate constant
K_d	dissociation constant
k_{diss}	dissociation rate constant
LB	Lysogeny broth
Mal-β-ala	N-maleoyl-β-alanine
MI	maleimide
MS	mass spectrometry
NHS	N-hydroxysuccinimide
Ni-NTA	Nickel-nitrilotriacetic acid
NMR	nuclear magnetic resonance
nt	nucleotide
OD_{600}	optical density at 600 nm
PAGE	polyacrylamide gel electrophoresis
PCR	polymerase chain reaction
PDB	protein data bank
PDI	polydispersity index
pDNA	plasmid DNA
PEG	polyethylene glycol
pI	isoelectric point
R	universal gas constant
RH	relative humidity
rpm	revolutions per minute
RT	room temperature
ΔS	change in entropy
SDS-PAGE	sodium dodecyl sulfate polyacrylamide gel electrophoresis
ssDNA	single-stranded DNA
TEG	triethylene glycol
T_m	transition midpoint of heat denaturation
T_r	transition midpoint of oligomeric assembly
Tris	tris(hydroxymethyl)aminomethane
TX	triple crossover
Wt	wild type
Å	ånström (0.1 nm)

TIIVISTELMÄ

Nanobioteknologia ja bionanoteknologia ovat suhteellisen uusia, nopeasti kehittyviä tieteenaloja, jotka hyödyntävät biomolekyylejä. Biomolekyylien luonnolliset ominaisuudet ja toiminta täytyy tuntea hyvin, jotta niitä voidaan hyödyntää moderneissa teknisissä sovelluksissa. Biomolekyylien ominaisuuksia täytyy myös usein muokata joko geneettisesti tai kemiallisesti, jotta ne soveltuvat tiettyyn käyttökohteeseen.

Tämän tutkimuksen tavoitteena oli karakterisoida ja muokata biomolekyylien ominaisuuksia, jotta niistä voitaisiin valmistaa molekyylityökaluja nanobioteknologian ja bionanoteknologian tarpeisiin. Avidiini-proteiinit valittiin muokattaviksi sen vuoksi, että niitä käytetään jo laajalti bioteknologian sovelluksissa, sillä ne sitovat poikkeuksellisen voimakkaasti pientä vitamiini-molekyyliä, D-biotiinia (K_d ~10^{-15} M). Tässä työssä muokattiin aiemmin kehitetyn kaksoisketjuavidiinin (dcAvd) toista ligandin sitoutumispaikkaa muodostamaan kovalentin sidoksen ligandin kanssa. Näin aikaansaatu uusi proteiini, dcAvd-Cys, kykenee sitoutumaan kahdenlaisten molekyylien, tioli-reaktiivisten sekä biotinyloitujen molekyylien kanssa samanaikaisesti, joten sitä voitaisiin hyödyntää molekyylien hallitussa immobilisoinnissa.

Työssä määritettiin kahden avidiinin kiderakenteet suurella tarkkuudella. Rakenteen, biokemiallisen ja biofysikaalisen karakterisoinnin perusteella näiden proteiinien käyttäytyminen poikkeaa aiemmin tutkituista avidiineista. Tetrameerisen villityypin bradavidiinin C-terminaaliset aminohappotähteet vuorovaikuttavat viereisen monomeerin ligandinsitomistaskun kanssa, käyttäytyen kuten monomeerien välinen sisäinen ligandi. Tämä havainto johti bradavidiini-spesifisen Brad-tag:n kehittämiseen, ja Brad-tag:n osoitettiin olevan käyttökelpoinen affiniteettikahva (K_d ~2,5 × 10^{-5} M). Suurin osa tutkituista (strept)avidiineista on tetrameerisia tai dimeerisiä proteiineja, kun taas bradavidiini II:n oligomeerisuusaste osoittautui vaihtelevan ympäröivien olosuhteiden mukaan. Bradavidiini II:n heikkoa oligomerisoitumispyrkimystä voitaisiin hyödyntää fuusioproteiinien kehittämisessä.

Avidiinien ohella tutkittiin kahta erilaista biomolekyylien muodostamaa kompleksia. Ensimmäiseksi hyödynnettiin deoksiribonukleiinihappojen (DNA) ominaisuuksia kehitettäessä määrätyn kokoinen, itsejärjestyvä DNA-rakenne (B–A–B-kompleksi). Kompleksi ohjattiin kullasta valmistettujen nanoelektrodien väliin dielektroforeesin ja tioli-kulta sidoksen avulla. Streptavidiinin avulla osoitettiin, että kompleksi voidaan funktionalisoida muilla molekyyleillä. B–A–B-kompleksin mitattu johtavuus oli lähes olematonta. Kehitetty kompleksi voisi toimia alustana, johon kyettäisiin tarkasti sijoittamaan muita molekyylielektroniikan komponentteja. Toiseksi hyödynnettiin kitosaanin ja DNA:n sähköstaattista vuorovaikutusta valmistettaessa kitosaani-DNA nanopartikkeleita geenien kuljettamiksi. Nanopartikkelit funktionalisoitiin fluoresoivilla leimoilla ja kohdentavilla peptideillä. Soluviljelyanalyysissä nanopartikkelit kulkeutuivat kohdesolujen sisään.

Kokonaisuudessaan tässä työssä tuotettiin monipuolisia molekyylityökaluja, jotka perustuvat muokattuihin avidiineihin, itsejärjestäytyvään DNA-rakenteeseen ja kitosaani-DNA nanopartikkeleihin. Vaikka kehitettyjen työkalujen sovelluskohteet vaihtelevat biosensoripinnoista proteiinien tunnistamiseen ja molekyylitason elektroniikasta geenien kuljettamiseen, eri osatutkimuksissa käytettiin monia samoja menetelmiä ja materiaaleja. Tutkitut ja kehitetyt biomolekyylit lisäävät tietoa, jota tarvitaan parempien molekyylityökalujen valmistamisessa.

ABSTRACT

Biomolecules have a central role in two relatively new, fast-developing scientific disciplines, nanobiotechnology and bionanotechnology. The properties and the behaviour of natural biomolecules need to be well studied and characterized in order to use them in modern technical applications. Quite often a genetic or chemical modification is needed to tailor the biomolecule suitable for a specific application.

The aim of this doctoral thesis was to characterize and modify the properties of biomolecules in order to develop molecular tools for applications in nanobiotechnology and bionanotechnology. Avidin proteins were selected for modification as they are already widely used in biotechnology due to their extraordinary tight affinity for a small vitamin, D-biotin (K_d ~10^{-15} M). In this study, covalent ligand binding was engineered and applied to one binding site of a dual chain avidin (dcAvd). The resulting dcAvd-Cys enabled the subsequent attachment of two different kinds of molecules, thiol-reactive compounds and biotinylated compounds, to the same protein pseudotetramer. This molecule could be a valuable tool for the immobilization of molecules in a controlled way.

The biochemical and biophysical characterization as well as the high-resolution crystallographic 3D-structures of two bradavidins revealed some behavioral traits atypical for avidins. In the tetrameric wild type bradavidin, the C-terminal amino acid residues interact with the ligand-binding site of the neighbouring monomer, thus acting as an intersubunit intrinsic ligand. This finding led to the development of a bradavidin specific Brad-tag, which was demonstrated to be applicable as an affinity tag (K_d ~2.5×10^{-5} M). Most of the characterized avidins are tetramers or dimers, whereas bradavidin II exists in a dynamic oligomeric state depending on the environment. The weak oligomerization tendency of bradavidin II may be of use in the development of fusion proteins.

In addition to avidins, two biomolecular complexes were studied. First, the self-assembling property of deoxyribonucleic acid (DNA) was used to develop a defined sized, self-assembling DNA structure (B–A–B-complex) based on triple crossover (TX) tiles. Dielectrophoresis was used to trap and immobilize the B–A–B-complex between two gold-nanoelectrodes via thiol-gold bonding. The feasibility

to functionalize the complex was demonstrated using streptavidin. The measured direct conductivity of the B–A–B-complex was insignificant, and therefore, the complex may find use as a scaffold material for the precise assembly of other components in molecular electronics. Second, the electrostatic interaction between chitosan and DNA was used to create chitosan-DNA nanoparticles. These were studied as potential carriers for gene-delivery applications. The nanoparticles were functionalized by fluorescent labels and targeting peptides. A cell culture analysis demonstrated that the nanoparticles can be internalized by cells.

In conclusion, this thesis study produced versatile biomolecular tools based on modified avidins, a self-assembling DNA-complex and chitosan-DNA nanoparticles. Although the developed tools may find use in somewhat different end-point applications ranging from biosensor surfaces to protein detection, and from molecular electronics to gene delivery, the methods and materials used were similar in all of the studies. Altogether, the studied and engineered biomolecules provide valuable knowledge for the future development of biomolecular tools.

1 INTRODUCTION

Biotechnology is a well-established and fast-developing scientific discipline. It is defined as "the application of biological organisms, systems, or processes by various industries to learning about the science of life and the improvement of the value of materials and organisms such as pharmaceuticals, crops, and livestock" (American Chemical Society 2013). Nanotechnology can be defined as "the science, engineering and technology conducted at the nanoscale, which is about 1 to 100 nanometers" (United States National Nanotechnology Initiative 2014). In recent years, nanotechnology has become a widely used technology for creating complex and multifunctional materials and devices. One of the biggest challenges in designing nanoscale devices is the production of atomic scale components and assembling them in a controlled way. Therefore, nanotechnology looks for solutions in biology, as biomolecules naturally exist and function at the nanoscale. Nature provides plenty of examples for how biomolecules can form sophisticated complexes to perform specific tasks.

By combining their efforts, nanotechnologists and biotechnologists have created the two relatively new fields of *nanobiotechnology* and *bionanotechnology*. In the literature these two terms are often used interchangeably. However, the term nanobiotechnology should be used to describe the applications of nanotechnology to improve biotechnological processes and products, for example the use of nanoarrays in diagnostics or nanoparticles in drug release. The term bionanotechnology should instead be used when describing the use of biological building blocks to achieve modern technology at the nanoscale. For example, deoxyribonucleic acid, DNA, has been shown to be a promising scaffold material for positioning other components in a controllable way. Therefore, bionanotechnology is not limited to biological applications (Gazit 2007).

The biological function and activity of proteins, nucleic acids and other biological macromolecules are determined by the primary sequence, secondary structure and three-dimensional conformation and sometimes also by the quaternary structure created by both covalent bonding and non-covalent interactions within and among the molecules. The function and interactions of biomolecules are based on molecular recognition and self-assembly or self-

organization, themes which will be discussed later on in this thesis. For example, a ribosomes' spontaneous self-assembly from its numerous individual building blocks (including about 55 different proteins and 3 different ribosomal RNAs (rRNAs) for the bacterial ribosome and, about 82 proteins and 4 rRNAs for the eukaryotic ribosome (Alberts et al. 2002)), is a fascinating example of how molecular recognition is utilized in nature (Niemeyer 2000). To understand the molecular self-assembly mechanisms via non-covalent interactions is as important as developing new covalent coupling routes that link molecules together (Committee on Biomolecular Materials and Processes 2008).

Proteins and oligonucleotides have been successfully applied to organizing nanostructures into macrostructures (Mardyani et al. 2004). When new modified biomolecules become available, they may enable the construction of novel systems with properties that cannot be achieved by traditional methods. For example, it may be possible to produce new intelligent drug or gene delivery systems to speed up biological and medical research or to create better nanobiosensors to increase diagnostic capabilities (Singh et al. 2012). Thus, it is important to study and modify biomolecules to enable the development of novel technologies.

For technological applications, natural biomolecules usually need to be modified. For instance, genetic engineering can be used to introduce active groups into proteins for further modification, or *vice versa*, to block the activities that are not needed or that may be harmful in the final product. Alternatively, biomolecules may be chemically modified, for example probed or labeled using special chemical reactants, or two biomolecules may be joined together directly or using cross-linking agents. However, biomolecules are sensitive to the applied modification techniques and therefore it is important to be able to join two molecules together in the correct conformation. Thus, knowledge of the behaviour of biomolecules is essential when developing new technologies.

2 REVIEW OF THE LITERATURE

2.1 Biological nanomaterials

The prefix 'nano' refers to one-billionth (10^{-9}) of a unit and thus a nanometer is one billionth of a meter or 0.000000001 meter. Nanotechnology has several different kinds of definitions. According to one of them, nanotechnology means the "understanding and control of matter at the nanoscale, at dimensions between approximately 1 and 100 nanometers, where unique phenomena enable novel applications" (United States National Nanotechnology Initiative 2014). Nanoscale materials have at least one dimension at the nanometer scale (Mukhopadhyay 2011). Many biomolecules naturally exist and interact at the nanometer scale (Figure 1), and therefore proteins, viruses and bacteria can be considered biological nanomaterials (Varadan et al. 2009).

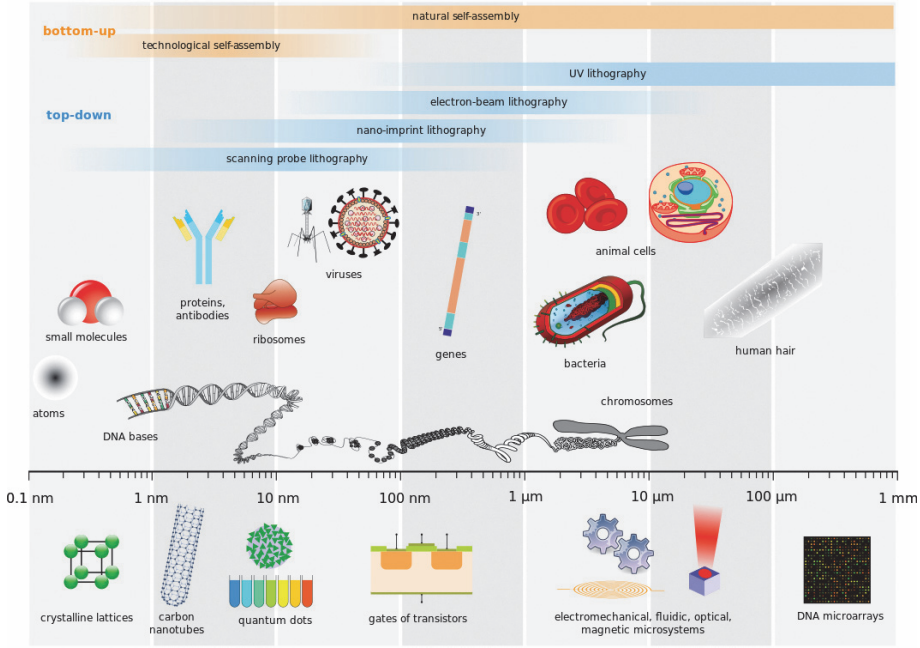

Figure 1. A comparison of the size scales of various biological assemblies and technological devices. Adapted with permission from (Paumier et al. 2009).

2.1.1 Proteins

Proteins are biomolecules, which range from small oligopeptides to huge polymers and exist in many forms in all cells that carry out diverse biological functions. For example, proteins may act as enzymes, hormones, antibodies, transporters and channel proteins, signaling and motor proteins, or they may have a structural or mechanical role (Nelson & Cox 2000). Proteins may interact with other proteins or with other molecules such as ligands, metal ions or macromolecules.

2.1.1.1 Amino acids are structural units of proteins

Proteins are polypeptides made up of 20 common natural amino acids, each of them containing a central carbon (α-carbon) bound to an amino group, a carboxyl group, a hydrogen atom and an identifying side chain. The α-amino group of one amino acid reacts with the α-carboxyl group of another amino acid to create a covalent peptide (amide) bond. The atoms associated with peptide bonds are coplanar and therefore the bonds are rigid and have no rotational freedom, whereas the bonds linked to the α-carbon (N–C_α and C_α–C, specified by the angles ϕ and ψ, respectively) have more freedom of movement. The charge, reactivity, hydrophobicity or hydrophilicity and hydrogen bonding capability of a particular amino acid residue are determined by its side chain, which is free to interact and react with the environment (Hermanson 1996, Nelson & Cox 2000).

Nine of the twenty amino acid residues can be readily modified with common reagents at their functional side chains: aspartic acid (carboxyl), glutamic acid (carboxyl), lysine (primary amine), arginine (guanidine), cysteine (sulfhydryl), histidine (imidazole), tyrosine (phenol), methionine (thioether) and tryptophan (indole) (Figure 2). In addition to these, the N-terminal α-amino and the C-terminal α-carboxylate are also available for modification. While the side chains of amino acid residues can exist in a protonated or unprotonated state, the reactivity of them increases in the unprotonated or ionized state. Each type of ionizable group in a protein has a unique theoretical pK_a. However, the actual pK_a may differ considerably from the theoretical value, depending on the environment of the group. The presence of other amino acid residues in close vicinity, the pH, the temperature, salts, the ionic strength and other environmental parameters can significantly change the microenvironment and thus affect the ionization potential of the amino acid residue (Hermanson 1996). The pH at which the net electric charge of a protein is zero is called the isoelectric point (*pI*).

Hydrophilic amino acid residues such as asparagine, threonine and serine are often post-translationally modified in proteins. Despite the enzymatic modification of these residues, the nucleophilicity of their amide and hydroxyl groups is close to

that of water, rendering them difficult to modify with common reagents under aqueous conditions (Hermanson 1996).

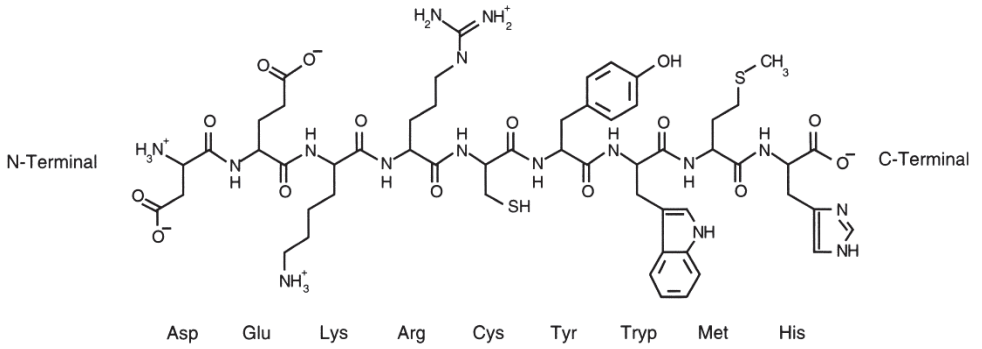

Figure 2. The functionality of the polypeptide can be represented by the nine amino acid residues and the N-terminal α-amino and C-terminal α-carboxylate groups. Adapted from Bioconjugate Techniques, Copyright (1996) with permission from Elsevier (Hermanson 1996).

2.1.1.2 Avidin-biotin technology

Avidin from the chicken egg-white and streptavidin from *Streptomyces avidinii*, collectively known as (strept)avidin, have an extraordinarily tight avidity towards a small vitamin molecule, D-biotin (K_d ~6×10^{-16} M for avidin and K_d ~4×10^{-14} M for streptavidin) (Green 1975, Wilchek & Bayer 1990, Laitinen et al. 2006). Biotin can be relatively easily covalently attached to various materials by its carboxyl group and several commercial biotinylation reagents with different functionalities are available (Hermanson 1996). Compared with most other proteins, avidins can survive in harsh environments. They are highly thermostable (Gonzalez et al. 1999), they tolerate low and high pH (Green 1975, Määttä et al. 2011) and denaturants (Ross et al. 1986) as well as many proteolytic enzymes (Green 1975, Ellison et al. 1995). Therefore, avidins are important tools for numerous applications in biotechnology and life sciences as well as for nanostructure-building approaches in nanotechnology.

In addition to avidin and streptavidin, several other avidins have been identified in the eggs of birds (Green 1975, Hytönen et al. 2003), various vertabrates (Korpela et al. 1981) and amphibians (xenavidin from *Xenopus tropicalis* (Määttä et al. 2009)). Furthermore, fungal (tamavidin 1 and 2 from Tamogitake mushroom (Takakura et al. 2009)), fish-derived (zebavidin from *Danio rerio* (Taskinen et al. 2013)), and also a few bacterial avidins (*Bradyrhizobium japonicum* (bradavidin I and II (Nordlund et al. 2005b, Helppolainen et al. 2008)), *Rhizobium etli* (rhizavidin) (Helppolainen et al. 2007) *Burkholderia pseudomallei* (burkavidin) (Sardo et al. 2011)

and *Shewanella denitrificans* (shwanavidin) (Meir et al. 2012)) have been found. Most avidins have a homotetrameric structure, with the exceptions of rhizavidin and shwanavidin that are homodimers in their native state (Helppolainen et al. 2007, Meir et al. 2012). Recently, zebavidin was also found to form dimers in the absence of biotin but the addition of biotin induced its tetramerization (Taskinen et al. 2013).

Several attempts have been made to independently control the four binding sites in (strept)avidin in order to improve the existing (strept)avidin-biotin technology. A monovalent streptavidin tetramer was produced by combining unmodified and modified subunits at a molar ratio of 1:3 in their denatured state. Rapid refolding resulted in a statistical mixture of tetramers of different compositions. The His-tag in the unmodified subunit enabled the purification of a monovalent form from oligovalent forms using Ni-NTA affinity chromatography by varying the imidazole concentration in the elution (Howarth et al. 2006). In a recent study, negatively charged amino acid residues, such as C-terminal glutamates or multiple aspartates in the surface loop enabled the separation of tetramers of different oligovalencies from each other by ion-exchange chromatography according to the number of negatively charged subunits. Moreover, the *cis*-divalent (1,2) and *trans*-divalent (1,3) forms containing two unmodified and two modified subunits could be separated from each other based on the orientation of the charged tags (Fairhead et al. 2014).

The laborious unfolding and refolding of tetramers could be avoided by the genetic fusion of two or four monomers. For example, dual chain avidin (dcAvd) has been constructed by joining two circularly permuted avidin monomers, circularly permuted avidin 5→4 (cpAvd5→4) and circularly permuted avidin 6→5 (cpAvd6→5) genetically into one polypeptide chain. Thus dcAvd has two binding sites that can be independently modified. Two dcAvd subunits dimerize into a pseudotetramer (Nordlund et al. 2004). Site-directed mutagenesis has yielded dual-affinity dcAvds with two biotin-binding sites with different affinities to biotin (Hytönen et al. 2005). A single chain avidin (scAvd) with four independent binding sites in one polypeptide chain has also been created (Nordlund et al. 2005a) allowing the independent modification of all four binding sites. The same approach has also been applied to streptavidin (Aslan et al. 2005).

2.1.2 Deoxyribonucleic acid

The deoxyribonucleic acid (DNA) molecules in each cell contain the genetic information, i.e. genes needed for the development and function of the organism. In prokaryotic cells, a single circular DNA molecule is located in cytoplasm. It is

packed with proteins and folded tightly into a nucleoid. Eukaryotic nuclear DNA is located in the nucleus and has many levels of packing structures. About 146 base pairs (Alberts et al. 2002) of the dsDNA are wrapped around a histone protein octamer called the nucleosome. Multiple nucleosomes associate to form a chromatin fiber, which may be further folded and looped to ultimately form the chromosomes during cell division. In addition to nuclear DNA, eukayotic cells have dsDNA also in their mitochondria and plant cells also in their chloroplasts. Similarly, most bacteria and even some eukaryotes have small, circular dsDNA molecules called plasmids, which can replicate independently (Rapley 2000, Nelson & Cox 2000). Plasmids can be easily isolated and manipulated and transformed into a new host cell for protein expression.

2.1.2.1 Structural properties of DNA

DNA is composed of deoxyribonucleotides, each of which contains a pentose sugar (2'-deoxy-D-ribose), a nitrogeneous base and a phosphate. Nucleotides differ from each other by their base groups only and a DNA sequence is formed from four different alternating bases; adenine (A), guanine (G), cytosine (C) and thymine (T). The base of a nucleotide is covalently joined to the 1' carbon of the pentose sugar (Figure 3). DNA is a linear molecule, where the nucleotides are covalently linked through phosphodiester linkages, in which the 5'-phosphate group of one nucleotide is joined to the 3'-hydroxyl group of the next nucleotide. Thus, alternating phosphate and pentose residues form the covalent backbone of DNA that has distinct, polar 5' and 3' ends.

Two complementary DNA strands form a helical double stranded structure, dsDNA, where the hydrophilic sugar-phosphate backbone is on the outside of the double helix and the hydrophobic bases project into the helix. The bases of each strand interact with complementary bases of the other strand through hydrogen bonding (Watson & Crick 1953). Two types of base pairs, the so-called Watson-Crick base pairs, interact in dsDNA; A is hydrogen bonded to T through two hydrogen bonds and G is hydrogen bonded to C through three hydrogen bonds. Thus, in dsDNA, regions rich in G-C-pairs are more stable when compared with those containing more A-T-pairs. The DNA strands in a double helix are antiparallel, in other words their 5'-3'-phosphodiester bonds run in the opposite directions.

The double helix can take different conformations, A-DNA, B-DNA or Z-DNA. The most common form found in cells is B-DNA, which is fully hydrated *in vivo*. B-DNA is coiled in the shape of a right-handed double helix and a full turn takes place every ~10.5 base pairs (Wang 1979, Rhodes & Klug 1980). The DNA double helix is further coiled into different levels of supercoils. As an acid, DNA is

negatively charged at neutral (physiological) pH (Hermanson 1996). Surrounding counterions, such as Na^+, K^+, Mg^{2+}, form stable complexes with DNA and affect the conformation of dsDNA. In a recent study, counterions were dialyzed out of a DNA solution in the presence of a strong electric field, which resulted in the precipitation of DNA into amorphous aggregates that redissolved when the counterions were reintroduced (Musheev et al. 2013).

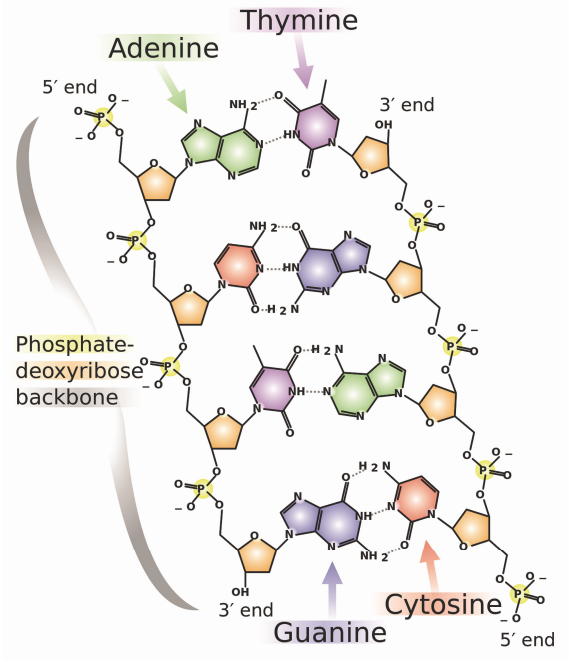

Figure 3. The double-stranded structure of DNA. Adapted with permission from (Ball 2013).

2.1.2.2 DNA as a scaffold

DNA has been shown to be a promising structural construction material, and a whole new field of structural DNA nanotechnology has emerged during the last decades (Seeman 2010). The specificity of Watson-Crick base-pairing through hydrogen bonding allows the programming of DNA strands that hybridize sequence-specificly with the complementary DNA strands. Short DNA double helices have mechanical rigidity and a comparatively high physico-chemical stability making them geometrically predictable. These properties of DNA enable the rational design of a nucleotide sequence to achieve reliable self-assembly (Zhang et al. 2013). Nowadays, it is also possible to synthesize large quantities of DNA oligomers with chemical modifications at a reasonable cost (Gazit 2007).

Usually, synthetic oligonucleotides are designed to first self-assemble into nanometer-scale motifs. Using sticky ends, i.e. single stranded overhangs complementary to other DNA motifs, allow the use of oligonucleotides as building blocks for larger, micron- or even millimeter scale structures (Winfree et al. 1998, Zheng et al. 2009). Many different geometries of self-assembling DNA structures have been realized, for instance chains (Aldaye et al. 2009), double crossover (DX) and triple crossover (TX) tiles (Fu & Seeman 1993, LaBean et al. 2000), lattices (Winfree et al. 1998), DNA nanotubes (Aldaye et al. 2009, Liu et al. 2004), and three dimensional structures such as a cube (Chen & Seeman 1991), a tetrahedron (Goodman et al. 2004) and an octahedron (Zhang & Seeman 1994). Joyce at al. introduced the concept of folding a long single strand with the aid of five smaller strands into the shape of a DNA octahedron (Shih et al. 2004). Rothemund et al. extended the concept to DNA origami and folded a long scaffold strand into complex two dimensional shapes such as a square, rectangular, star, smiley etc., with the aid of hundreds of short 'staple' strands (Rothemund 2006). Later on, the technology used in DNA origami was extended to the assembly of three-dimensional shapes (Douglas et al. 2009a). Recently, finite complex two-dimensional shapes were self-assembled from hundreds of distinct single stranded tiles (SST). Each SST is built entirely out of concatenated sticky ends and acts as a pixel in a molecular canvas. More than 100 different shapes were created by selecting pixels (Wei et al. 2012). The concept was extended from 2D to 3D and more than 100 distinct structures were assembled (Ke et al. 2012).

Self-assembling DNA structures have also been functionalized by several methods such as avidin-biotin technology (Niemeyer et al. 1999, Li et al. 2004, Park et al. 2005b, Yan et al. 2003), protein-aptamer technology (Liu et al. 2005, Li et al. 2006) or covalent attachment, for example using thiol-functionalized DNA-strands to bind gold nanoparticles (Le et al. 2004, Zheng et al. 2006, Sharma et al. 2006). The DNA-directed assembly of proteins has the potential for constructing artificial spatially well-defined multienzyme complexes, which cannot be made by conventional chemical crosslinking or genetic engineering (Niemeyer et al. 2002). DNA structures may also template the assembly of nonbiological materials such as nanoparticles and carbon nanotubes (Maune et al. 2010) as nanoelectronics components and nanomechanical devices (Committee on Biomolecular Materials and Processes 2008, Aldaye et al. 2008). The advantage of DNA nanostructures compared with other self-assembling biopolymers is that the interactions and surface features can be predicted and programmed for the precise positioning of other nanoparticles and biopolymers (Fu et al. 2012). In addition, the DNA origami can be self-assembled into arbitrary two and three-dimensional non-periodic shapes, whereas most other self-assembling approaches, which are based on proteins (King et al. 2012) or peptides (Zhao & Zhang 2007, Gradisar et al.

2013) produce periodic structures. Isothermal DNA strand-displacement reactions have been used in dynamic DNA nanotechnology to design systems with an autonomous behaviour (Zhang & Seelig 2011, Zhang et al. 2013), but this field is not in the scope of this thesis and will not be discussed in more detail.

2.1.3 Polysaccharides

Polysaccharides belong to carbohydrates that have a characteristic polyhydroxylic aldehyde or polyhydroxylic ketone structure. Polysaccharides are formed from numerous monosaccharides bound to a chain by an acetal linkage (also called an O-glycosidic bond). In an acetal linkage, the hydroxyl group of C1 (carbon 1) of one sugar is joined to the hydroxyl group of C4 or C6 of another sugar. Polysaccharide synthesis is enzymatically controlled, but it does not occur from a template, and therefore, each polysaccharide molecule will have its own unique molecular weight, usually expressed as an average (Hermanson 1996).

Functional groups of monosaccharides include either an aldehyde or a ketone, several hydroxyls and possibly amine, carboxylate, sulfate or phosphate groups. These groups can be targeted by modification reactions. Polyhydroxylic structures make polysaccharides polar molecules, but still they may not be fully soluble in water. Solubility is usually dependent on polymer weight and 3D-structure (Hermanson 1996). Common natural polysaccharides include starch, cellulose and chitin, just to name a few. Polysaccharides are also covalently bound to some proteins and lipids. The structure and properties of the chitin-derivative chitosan are discussed in more detail, as it belongs to the scope of the thesis.

2.1.3.1 Chitosan

Chitosan is a linear, random copolymer of β-(1→4)-N-acetyl-D-glucosamine and β-(1→4)-D-glucosamine produced by partial alkaline deacetylation from chitin (Figure 4), which is the principal structural component of the exoskeleton of crustaceans and insects and found in the cell wall of fungi and yeast. Chitosan may be defined as a chitin derivative that is water soluble under acidic conditions (Rinaudo 2012). The lowest degree of deacetylation of chitosan reported in the literature ranges from 40 to 60 % (Sorlier et al. 2001, Brugnerotto et al. 2001, Balázs & Sipos 2007) and the molecular weight ranges from 50 to 2000 kDa (Hejazi & Amiji 2003). D-glucosamines contain a free $–NH_2$ at the C2 position (Rinaudo 2012). These amines have a pK_a value of approximately 6.5 and thus at an acidic pH these amine groups become protonated rendering chitosan a positively charged, soluble polyelectrolyte (Yi et al. 2005, Mao et al. 2001). The solubility of chitosan is dependent on the degree of acetylation, pH, the ionic strenght, the acid

used for protonation, and whether the acetyl groups are distributed randomly or in a periodic manner along the chain (Rinaudo 2012).

Chitosan is naturally biodegradable and generally considered a biocompatible and non-toxic material (Rinaudo 2012). However, chemically modified chitosans may compromize the biocompatibility, and therefore require assessment of biocompatibility (Halim et al. 2012). Solubilized chitosan can be processed as gels, films and fibers for biomedical applications (Rinaudo 2012). Chitosan and its derivatives have also been studied for their potential as delivery agent for peptides, proteins, antigens, plasmid DNA and also drugs (Muzzarelli 2012).

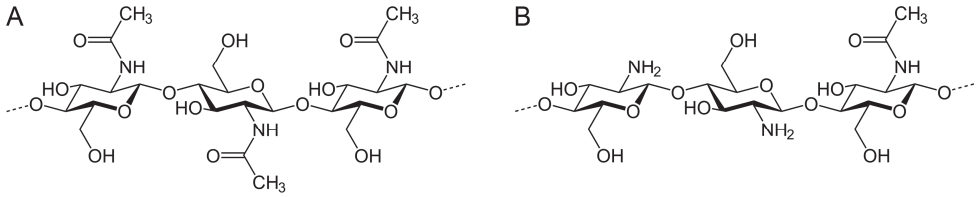

Figure 4. The chemical structure of **A**) chitin and **B**) chitosan. Adapted with permission from (Chitosan synthese 2008).

2.1.3.2 Chitosan as a gene carrier

Chitosan is a positively charged cationic polymer able to form electrostatic complexes with negatively charged macromolecules. Because of this behaviour, chitosan has been widely studied as a non-viral gene carrier. Although viral vectors have demonstrated higher gene transfection efficiency, non-viral carriers are seen as a safer alternative as their benefits may include a lower host immune response, easier and cheaper production in large quantities and better long-term stability in storage (Corsi et al. 2003, Mao et al. 2001). Optimal gene carriers should transport genetic material to the host without toxicity and they should be able to protect DNA until it reaches its target, the nucleus (Mansouri et al. 2004). Therefore, a carrier system must be small enough to be internalized into cells and to enter the nucleus intact, and it must evade degradation by extracellular nucleases and also resist deactivation by other extracellular components (Uchegbu et al. 2009).

Chitosan can effectively complex with DNA and protect it from degradation by nucleases (Mansouri et al. 2004). Chitosan-DNA polyplexes are formed at an acidic or neutral pH, where chitosan is highly or partially ionized (Ferrari et al. 2012). The polyplex formation is an entropically driven process that can be obtained by simply mixing solutions of chitosan and plasmid DNA resulting in the self-assembly of oppositely charged components (Janes et al. 2001, Ahmed & Narainhmed 2010, Ferrari et al. 2012). However, the polyplexes obtained this way may have a large size distribution and heterogeneous morphology (Janes et al. 2001). In another

method called complex coacervation, an addition of a dilute salt, sodium sulfate to the DNA solution, is used as a desolvating agent. When desolvation is combined with the careful adjustment of blending conditions such as the mixing speed and the temperature of the solutions, monodisperse and spherical nanoparticles can be obtained (Mao et al. 2001).

The degree of deacetylation, the molecular weight and the weight and charge ratio of chitosan to DNA have been shown to affect the complexation of chitosan and DNA as well as the transfection efficiencies of these complexes. The conditions to complex chitosan and DNA should be optimized to achieve a strong enough binding to be able to condense and protect DNA against nucleases, but still weak enough to permit the intracellular or intranuclear release of DNA (Ishihara et al. 2012, Ferrari et al. 2012). To achieve efficient gene delivery to specific cells, targeting ligands such as small molecules, peptides and proteins have been conjugated to chitosan-DNA nanoparticles (Jain & Amiji 2012).

2.2 Molecular recognition

Molecular recognition or biorecognition plays an essential role in all biological processes. For example, protein-protein association, enzyme catalysis, cellular signaling, antibody-antigen as well as protein-ligand interactions involve two or more molecules interacting with each other at high affinity and specificity. Molecular recognition involves a combination of non-covalent interactions such as ionic or hydrogen bonding, hydrophobic effects, van der Waals interactions and electrostatic interactions. Surface complementarity has an important role in molecular recognition as well (Baron & McCammon 2013, Wilchek et al. 2006). As an example, the avidin-biotin interaction is based on several hydrogen bonds and hydrophobic effects. In addition to these, biotin has a structurally optimal cavity inside the β-barrel of the avidin monomer. The combination of several weak interactions results in an extraordinary tight affinity between avidin and biotin (K_d ~10^{-16} M) (Green 1975, Wilchek & Bayer 1990, Laitinen et al. 2006).

2.2.1 Molecules are recognized by induced fit and conformational selection

The specificity of enzyme-substrate reactions was explained by the *lock-and-key* – model by Emil Fisher in 1894 (Fischer 1894, Bosshard 2001). However, this rigid fit was not able to explain all enzyme reactions, and in 1958 Daniel Koshland formulated the concept of the *induced fit*, where the binding of a substrate induces some conformational changes making the binding site more favorable for the

substrate (Koshland 1958). Since then, this principle has been used to describe all kinds of molecular recognition processes. Both of the proposed concepts treat the protein as if it exists in a single stable conformation under specific experimental conditions. However, instead of being stable, proteins are inherently dynamic and have many different conformations. Recent experiments have supported an alternative mechanism for conformational selection, which states that all protein conformations pre-exist and the ligand selects the most favored one. After binding, the complex undergoes a population shift, redistributing the conformational states. The combination of induced fit with conformational selection would probably be the best way to describe the interaction between molecules that do not have an optimal fit in the beginning (Bosshard 2001, Boehr et al. 2009). The initial binding by conformational selection is followed by the optimization of side-chain and backbone interactions by an induced fit mechanism, which makes the surfaces more complementary to each other.

2.2.2 Thermodynamics and ligand-binding kinetics of molecular recognition

The simple reversible binding or association reaction between a target molecule A and a ligand B to form a bimolecular complex AB can be presented by an equilibrium equation (1):

$$A + B \leftrightarrow AB \tag{1}$$

The association constant of the reaction is defined as (2):

$$K_a = \frac{[AB]}{[A]\times[B]} \tag{2}$$

where [AB] is the concentration of the formed complex, [A] that of the free molecule A and [B] of the free ligand B. The affinity between two molecules is often defined by the dissociation constant, K_d that is the equilibrium constant for the release of the ligand. K_d is an inverse of the association constant defined as (3):

$$K_d = \frac{[A]\times[B]}{[AB]} = \frac{1}{K_a} \tag{3}$$

K_d is the equivalent of the molar concentration of the ligand at which half of the available ligand-binding sites are occupied. K_d is directly linked to the kinetic properties of the reaction by the following equation:

$$K_d = \frac{k_{diss}}{k_{ass}} \quad (4)$$

where k_{diss} is the dissociation rate constant and k_{ass} the association rate constant (Privalov 2012). The formation of an initial association complex involves the translational and rotational diffusion of the molecules, which is followed by conformational changes in the molecules (Zhou & Bates 2013). The rate of diffusion can be increased by favorable Coulombic electrostatic forces (Selzer et al. 2000). The rate of dissociation instead, is linked to short range interactions such as van der Waals interactions, hydrogen bonds, hydrophobic effects and salt bridges between the binding partners (Selzer et al. 2000).

The strength of the binding reaction is governed by the energy change of the process and the relationship of the equilibrium constants with the thermodynamics can be expressed as:

$$\Delta G = -RTln(K_a) \quad (5)$$

where ΔG is the change in the Gibbs energy of the interaction, R is the universal gas constant and T is the absolute temperature. K_a or K_d can be measured using several experimental techniques such as fluorescence, circular dichroism, equilibrium dialysis or surface plasmon resonance. Calorimetry can be used to determine the change in the enthalpy (ΔH) of interaction and the K_a of the binding. In an exothermic binding reaction, energy is released as heat into the solution and in an endothermic reaction heat is absorbed from the solution. The change in the entropy (ΔS) of the interaction can be calculated using the following equation:

$$\Delta G = \Delta H - T\Delta S \quad (6)$$

which applies at a constant temperature and constant pressure. For spontaneously occurring processes ΔG is negative, whereas for unfavorable reactions ΔG is positive, and an initial state is favored (Allen 2009).

X-ray crystallography is an important tool for studying the 3D-structure of a protein and its interacting molecular counterparts, although it provides only snapshots of the dynamic protein structure (Wilchek et al. 2006). Molecular docking studies can be helpful in depicting molecular structure and function, when crystallographic structures are not available. Other techniques such as fluorescence, spectrophotometry and circular dichroism can also be used to study molecular recognition processes (García-Fuentes et al. 2011).

2.3 Self-assembly and self-organization

Self-assembly is the spontaneous association of molecules into larger coordinated structures and it is the principal method that nature uses to achieve complexity (Aldaye et al. 2008) in processes including protein folding, the assembly of DNA and the formation of bilayers, micelles and vesicles (Lindoy et al. 2012). Typically, self-assembly is a reversible process driven by energy minimization according to the thermodynamic principles (Committee on Biomolecular Materials and Processes 2008). Self-assembly is mainly based on weak, non-covalent intermolecular or colloidal forces such as hydrogen bonds, van der Waals interactions, hydrophobic forces, π-π interactions, steric interactions, depletion forces, and solvation/hydration forces (Lee 2011). Some studies have also inferred that self-assembly involves covalent bonding (Tanoue et al. 2011, Baek et al. 2013, Björk et al. 2013).

The most remarkable natural self-assembling molecule is DNA. Two complementary single-stranded DNA molecules (ssDNA) hybridize spontaneously and sequence-specifically to form dsDNA structures. A number of non-covalent interactions, such as hydrogen-bonding, base stacking, electrostatic forces and hydrophobic effects, drive this process (Lin et al. 2009). The A-T and G-C base pairing through hydrogen bonding allows the programming of DNA strands that are highly specific for the complementary DNA strands (Niemeyer 2000). Although the energy of the interaction in a single base pair is quite small (a G-C-pair is stabilized by three hydrogen bonds and an A-T-pair by two hydrogen bonds, as was previously mentioned), the overall energy of double-stranded DNA is quite high when tens, hundreds or thousands of base pairs are formed between the DNA-strands (Gazit 2007).

The term self-assembly is often mixed up with self-organization. Halley & Winkler distinguished these two terms according to a thermodynamic basis and provided a definition: "Self-organization is a dissipative nonequilibrium order at macroscopic levels, because of collective, nonlinear interactions between multiple microscopic components. This order is induced by interplay between intrinsic and extrinsic factors, and decays upon removal of the energy source" (Halley & Winkler 2008). According to this definition the term dynamic self-assembly (Whitesides & Grzybowski 2002) could also be considered a synonym for self-organization. To avoid confusion, the term self-organization is used in this thesis.

Self-assembly and self-organization are based on molecular recognition and both of them are essential for biological systems. All living matter is made of simple building blocks that form complex networks, molecular machines and cellular structures by self-assembly, self-organization or their interactions. The term *bottom-up* is used to describe the hierarchical self-assembly or self-organization

process starting from the molecular level and ending up in larger scale ordered assemblies (Gazit 2007). Adopting the way of nature, the combination of these processes can be used in attempts to generate highly ordered structures. For example, sometimes molecules can get stuck in a kinetic trap and cannot spontaneously self-assemble and achieve a higher order. These limitations can be overcome by guiding or directing the organization using an electric or magnetic field or shear force to align the assembling particles. In dynamic molecular combing (DMC) DNA molecules are allowed to bind spontaneously to a silanized cover slip and vertical pulling of the cover slips from the solution results in the irreversible fixing and aligment of parallel DNA fibers for the fluorescent hybridization of DNA probes (Bensimon et al. 1994, Michalet et al. 1997). Alternatively, templated self-assembly uses scaffolds or templates to provide patterns for ordering the building blocks. These templates may support the formation of a desired structure in case there are competing structures with similar free energies (Committee on Biomolecular Materials and Processes 2008). For example, DNA has been used as a building block to direct the assembly of other molecules into larger structures, as already discussed in section 2.1.2.2.

2.4 Modification of biomolecules

Biomolecules may need to be modified or tailored to have suitable properties for a certain specific application. For example, biomolecules which are to be immobilized on a surface through covalent coupling need chemically active groups on their surface at the correct position and orientation. If two molecules are conjugated together by a site-directed method, both of them need an active group on their surface. When biomolecules do not have the desired functional groups for a specific modification, they may be introduced by chemical or genetic means.

2.4.1 Genetic engineering

Genetic engineering, also called recombinant DNA technology, has become a widely used and popular technique for modifying nucleic acids and proteins, for example to introduce or to block specific functional groups or regions on proteins at the genetic level (Carroll 1993, Nelson & Cox 2000). A gene of interest may be isolated from the genome of an organism. However, the majority of eukaryotic genes contain non-coding, intervening regions called introns, in between the amino acid coding regions, called exons. During RNA transcription, the introns are removed or spliced out to produce the mature messenger RNA (mRNA) that can direct the synthesis of a polypeptide chain. The mature mRNA can be isolated, and

with the aid of the enzyme reverse transcriptase, transcribed to create a copy of complementary DNA (cDNA) in a multistep process. The resulting double-stranded cDNA molecules can be inserted into a plasmid vector for further protein expression in bacteria, yeast, insect or mammalian cells (Nelson & Cox 2000).

Molecular biology enables the modification of a DNA sequence to alter the amino acid sequence of the target proteins. The common approach of rational site-directed mutagenesis is to introduce a point mutation, insertion or deletion into the gene sequence (Carter 1986) or ligate parts of different genes in a new combination to produce fusion proteins (Nelson & Cox 2000). Quite often the complexity of biological systems makes the rational design of mutagenesis extremely difficult. Therefore, proteins or parts of the proteins may be exposed to random mutagenesis or directed evolution methods to create libraries of protein variants. These libraries can then be screened for proteins with desired recognition properties and functionalities in a process called "biopanning" (Cobb et al. 2012).

The production of cDNA especially from eukaryotic genes requires much effort and may not be cost effective. Alternatively, many cDNAs are available in cDNA libraries. Nowadays, commercially produced synthetic DNA is increasingly used as its production speed has increased and costs have decreased. More importantly, using synthetic DNA enables the optimization of the codon usage of the protein coding sequences to enhance the expression in heterologous hosts (Welch et al. 2009).

2.4.2 Chemical modification

Quite often the native structure of a biomolecule needs to be chemically tailored to provide functional groups for modification, especially in oligonucleotides and carbohydrates (Rozkiewicz et al. 2010). Usually, existing groups can be reacted with a modification reagent that contains or produces a desired function upon binding. A chemical group can be converted into a different one. For example, an amine could be converted into a sulfhydryl with an appropriate reagent. The same principle can be used to alter groups of rather low reactivity to make them more reactive. For example, a cysteine in a disulfide bond in a protein can be selectively reduced to form an active sulfhydryl (thiol). In addition, spacer arms could be used for extending the reactive group away from the surface of a biomolecule to minimize the steric hindrance in conjugation (Hermanson 1996).

A stoichiometrically controlled and directed modification is more difficult to achieve through a chemical modification than by genetic engineering. Proteins, for example, usually have several functional groups present and available or accessible, and therefore the result of the modification may be statistical and lack the control

of the stoichiometry and regioselectivity of the modified site. One common strategy for modification is thus the introduction of a sulfhydryl group (Di Marco et al. 2010) as many cross-linkers and modification agents are targeted to it. The modification is restricted to limited sites as the occurrence of sulfhydryls in biomolecules is usually low when compared with that of amines or carboxylates. In addition to the importance of introducing reactive groups into biomolecules, it may be equally important to block specific groups to prevent them from participating in modification reactions. Usually a chemical group is covalently coupled to a relatively inert group to eliminate its reactivity (Hermanson 1996).

The chemical modification of a protein is called chemical mutagenesis, when the amino acid side chain is chemically converted into another one (Chalker & Davis 2010). This concept was reported already in 1966 when the serine protease subtilisin was chemically converted into a cysteine protease (Neet & Koshland 1966, Polgár & Bender 1966). However, chemical mutagenesis was largely replaced by the easier and more specific recombinant DNA technology. In chemical mutagenesis, a precursor or a chemical mutagenesis handle is incorporated into the amino acid sequence of a protein to provide access to a different functional amino acid side chains. Dehydroalanine has been proposed as a common chemical mutagenesis handle that would in principle provide access to aromatic, aliphatic, acidic and basic amino acid residues due to its suitable chemistry, although much research is still needed to accomplish these tasks. In addition, a better way to incorporate dehydroalanine into a protein structure is needed. Since chemical mutagenesis can be performed post-expression on folded proteins, the risk of misfolding during protein expression can be avoided. Chemical mutagenesis may allow rapid access to natural, unnatural and modified side chains and could be used as an additional technology together with genetic engineering (Chalker & Davis 2010).

Click chemistry involves the joining of small units together quickly and reliably and has become an attractive alternative or complementary technology for conventional chemistry in bioconjugation (Nwe & Brechbiel 2009). Click chemistry focuses on carbon-heteroatom bond formation. Reactions exhibit a large thermodynamic driving force to proceed rapidly and favor a reaction with a single reaction product. These irreversible reactions include, among others, cycloadditions of unsaturated species such as the copper-catalyzed Huisgen cycloaddition or azide-alkyne [3+2] dipolar cycloaddition; nucleophilic ring-opening reactions; carbonyl chemistry such as the formation of oxime ethers, hydrazones and aromatic heterocycles; and carbon-carbon multiple bonds, such as epoxidation, dihydroxylation and aziridination. Click reactions enable the modification of one biomolecule while leaving others untouched.

The benefits of click reactions include the fact that they are bio-orthogonal, i.e. neither the reactants nor their product's functional groups interact with functionalized biomolecules. In addition, the reactions can be performed easily under mild conditions at room temperature and usually in aqueous solutions (Kolb et al. 2001, Nwe & Brechbiel 2009). The drawback of some click reactions is the use of copper as a catalyst, which may be toxic *in vivo*. The metal-free azide-alkyne [3+2] dipolar cycloaddition has been developed, but it produces a mixture of regioisomeric products, which may be harmful for the application (Nwe & Brechbiel 2009). Other metal-free click reactions have been developed as well, but they involve rather large complicated reactive groups, which may be a disadvantage in many applications (Becer et al. 2009).

2.5 Assembly of biomolecules

When biomolecules are used in various applications, they usually need to be assembled, for example conjugated with some other molecules or immobilized onto a surface to perform a specific task. The assembly of biomolecules can be achieved by using a non-covalent or covalent interaction.

2.5.1 Non-covalent interaction

Non-covalent interactions are relatively weak chemical interactions including ionic bonds, hydrogen bonds, van der Waals forces and hydrophobic effects. The conformation of a macromolecule is usually stabilized by multiple non-covalent interactions (Lodish et al. 2000).

2.5.1.1 Physisorption

One of the simplest and fastest ways to immobilize biomolecules is by physisorption (physical adsorption) via hydrophobic or polar interactions (Figure 5A). In this approach proteins are adsorbed nonspecifically onto a surface and can potentially detach from the surface and become exchanged by the proteins in the solution if the buffer and surface charges are altered (Aydin et al. 2012). DNA is negatively charged at neutral (physiological) pH and the phosphate groups of the DNA backbone can bind strongly to positively charged objects. This interaction can be exploited for attaching DNA to surfaces, for example to poly-L-lysine coated glass (Diehl et al. 2001). Physical adsorption between DNA and a positively charged polymer, such as chitosan can be used to form nanoparticles.

Although the simplicity of physisorption is beneficial, a major drawback is the nonspecificity of the interaction. The adsorbed molecules are randomly oriented, and therefore, this interaction is not the best choice when molecules need to be directed in a specific orientation or inserted in a specific density. However, for example in microarrays, protein adsorption results in a situation where usually enough protein molecules are in the proper orientation to bind with the analyte (Zhu & Snyder 2003). The size of nanoarrays, on the other hand is significantly reduced compared with microarrays and they require uniform protein immobilization with optimized bioactivity (Wingren & Borrebaeck 2007). For example avidin has been adsorbed on glass cover slips to enable the immobilization of biotin-labeled molecular beacon probes for the development of DNA arrays (Yao & Tan 2004).

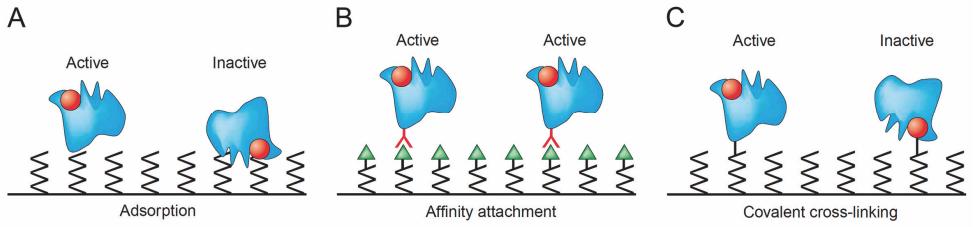

Figure 5. A comparison of protein immobilization by **A**) adsorption/physisorption, **B**) affinity attachment and **C**) covalent attachment. Adapted from Current Opinion in Chemical Biology, Copyright (2003) with permission from Elsevier (Zhu & Snyder 2003).

2.5.1.2 *Affinity interaction*

The term affinity defines the attraction of molecules for each other and can be used to describe molecular recognition. Biological binding reactions can range from transient low affinity interactions (K_d ~10^{-4} M for a weak protein-protein interaction (Luna et al. 2013)) to very stable high-affinity interactions (K_d ~10^{-15} M for (strept)avidins (Green 1975, Wilchek & Bayer 1990, Laitinen et al. 2006)). Affinity interactions include **affinity tags** that are usually introduced into fusion proteins using recombinant DNA technology and are widely used for protein detection and purification (Cuatrecasas & Wilchek 1968, Uhlén 2008). Affinity tags are also useful tools for the site-directed immobilization of molecules on surfaces (Figure 5B). An affinity tag at the amino or carboxyl terminus of a fusion protein will target the protein to its specific binding partner on the surface, and should result in the uniform orientation of the attached proteins on the surface (Zhu & Snyder 2003).

Affinity tags include everything from small peptides to full proteins. Small tags may not need to be removed for downstream applications. Large peptides or proteins may be used as a fusion partner for instance to increase the solubility of a

target protein, but may then need to be removed for several applications, such as crystallization (Terpe 2003) or nuclear magnetic resonance (NMR) spectrocopy analyses. One of the most widely employed affinity tags is the His-tag (Arnau et al. 2006), which consists of an oligopeptide of several histidine residues that can be used in metal-chelating chromatography (Hochuli et al. 1987, Hochuli et al. 1988). Several known affinity tags bind to avidin (Meyer et al. 2006, Gaj et al. 2007), neutravidin (Meyer et al. 2006, Gaj et al. 2007) or streptavidin (Schmidt et al. 1996, Korndörfer & Skerra 2002, Skerra & Schmidt 1999, Meyer et al. 2006, Gaj et al. 2007, Lamla & Erdmann 2004, Perbandt et al. 2007), (summarized in Table 1). In addition, monoclonal antibodies have been produced against peptide tags, such as the c-myc-tag (Hilpert et al. 2001) or the FLAG-tag (Einhauer & Jungbauer 2001, Wegner et al. 2002a).

Table 1. A summary of the properties of different avidin binding peptide tags compared with some other commonly used affinity tags.

Tag	Sequence (residues)	Size (kDa)	Receptor	K_d (M)	PDB entry	References
Avi-tag	DRATPY (6)	0.72	Avidin, NeutrAvidin	2.8×10^{-5} 1.2×10^{-5}	[a]	(Meyer et al. 2006)
AviD-tag	Divalent DRATPY (6 + spacer + 6)	1.44 + spacer	Avidin, NeutrAvidin	[a]	[a]	(Gaj et al. 2007)
Nano-tag$_{15}$	fMDVEAWLGAR VPLVET (formyl-Met + 15)	1.81	Streptavidin	4.0×10^{-9}	[a]	(Lamla & Erdmann 2004)
Nano-tag$_9$	fMDVEAWLGAR (formyl-Met + 9)	1.18	Streptavidin	1.7×10^{-8}	[a]	(Lamla & Erdmann 2004)
Nano-tag	fMDVEAWL (formyl-Met + 6)	0.89	Streptavidin	$< 2.0 \times 10^{-8}$	2G5L	(Perbandt et al. 2007)
Strep-tag	AWRHPQFGG (9)	1.06	Streptavidin	3.7×10^{-5}	1RST	(Schmidt et al. 1996)
Strep-tag II	WSHPQFEK (8)	1.06	Streptavidin SA mutant 1 i.e. StrepTactin SA mutant 2	7.2×10^{-5} 1×10^{-6} 1×10^{-6}	1RSU 1KL3 1KL5	(Schmidt et al. 1996, Korndörfer & Skerra 2002, Skerra & Schmidt 1999)
SBP-tag	MDEKTTGWRG GHVVEGLAGE LEQLRARLEH HPQGQREP (38)	4.31	Streptavidin	2.5×10^{-9}	[a]	(Keefe et al. 2001)
Poly-His	HHHHHH (2-10, usually 6)	0.84	Ni^{2+}-NTA, Co^{2+}-CMA	1.0×10^{-5} for mono-NTA, 1.0×10^{-8} for Tris-NTA	[a]	(Lata et al. 2005, Huang et al. 2009)
c-myc	EQKLISEEDLN (11) EQKLISEEDL (10)	1.32 1.20	9E10 monoclonal antibody	$\sim 5.0 \times 10^{-7}$	2OR9	(Hoogenboom et al. 1991, Fuchs et al. 1997, Hilpert et al. 2001, Wegner et al. 2002b)
FLAG-tag	DYKDDDDK (8)	1.01	Anti-FLAG monoclonal antibody M1, M2, or M5	6.7×10^{-9} for M2	[a]	(Hopp et al. 1988, Einhauer & Jungbauer 2001, Wegner et al. 2002a)

[a] Not available

Another widely applied affinity-based technology uses the extreme affinity of the **(strept)avidin-biotin interaction**, which is based on several hydrogen bonds (11 in the case of avidin (Livnah et al. 1993)), hydrophobic contacts and shape complementarity. The (strept)avidin-biotin interaction can be used for example for protein immobilization by physisorbing (strept)avidin to a surface and coupling biotin covalently to the protein of interest. Due to the (strept)avidin-biotin interaction, this results in a reduction in the interaction between the protein and the surface, and thus an increase in the protein's activity. However, the proteins will be oriented randomly, which can drastically lower their activity (Aydin et al. 2012). Nowadays, automated DNA synthesis can be routinely used to prepare biotinylated oligonucleotides, which may serve as a scaffold for (strept)avidin conjugates in DNA-based nanomaterials (Niemeyer et al. 1999, Yan et al. 2003, Li et al. 2004, Park et al. 2005b). In addition, the avidin-biotin interaction can be used to build DNA-chips. Avidin, for instance, has been chemically immobilized onto a sensor surface and incubated with a biotinylated DNA probe to detect genes by DNA hybridization (Jin et al. 2009).

The base-pairing of nucleic acid strands, which allows the design of complex self-assembling DNA structures, already discussed in chapters 2.1.2.2 and 2.3, can also be seen as an affinity interaction. This interaction is also used in DNA-microarrays (DNA chips), where specific DNA sequences, probes, are covalently attached to a surface for hybridazation with cDNA, for example to monitor the expression of a large number of genes in parallel (Schena et al. 1995).

2.5.2 Covalent interaction

Covalent bonds provide a stable mechanishm for conjugating biomolecules. The most common reactive groups present on proteins are primary amine, carboxylate, sulfhydryl, or phenolate, which are easy to derivatize (Hermanson 1996, Aydin et al. 2012). Although many common bioconjugation reagents used with proteins do not react with nucleic acids, some particular sites of bases, sugars of phosphate groups can be modified in reactions that are mostly unique to DNA or RNA. The functional groups of polysaccharides may include either an aldehyde or a ketone and hydroxyl, amine, carboxylate, sulfate or phosphate groups (Hermanson 1996). Overall, amines and sulfhydryls are often functionalized, and therefore they will be discussed in more detail.

The most commonly used crosslinking and modification reagents contain reactive groups capable of coupling with amines. The amine-coupling proceeds mostly through acylation or alkylation. The reactions are rapid and result in a high yield of stable amide or secondary amine bonds (Hermanson 1996). N-

hydroxysuccinimide (NHS) esters are probably the most common amine-reactive modification reagents available. NHS or sulfo-NHS ester containing molecules react with nucleophiles with the release of a NHS or sulfo-NHS group to yield an acylated product (Figure 6A). The reactions with primary and secondary amines create stable amide and imide linkages.

Coupling reactions with sulfhydryl-containing molecules proceed mainly through alkylation or disulfide exchange. Most of these reactions occur rapidly and produce a high yield of stable thioether and disulfide bonds. Maleic acid imides (maleimides) contain a double bond that may react through alkylation with sulfhydryls to form stable thioether bonds (Figure 6B) (Hermanson 1996). The sulfhydryl group of cysteine is the most reactive functional group on a protein, especially in its deprotonated state (Mattson et al. 1993).

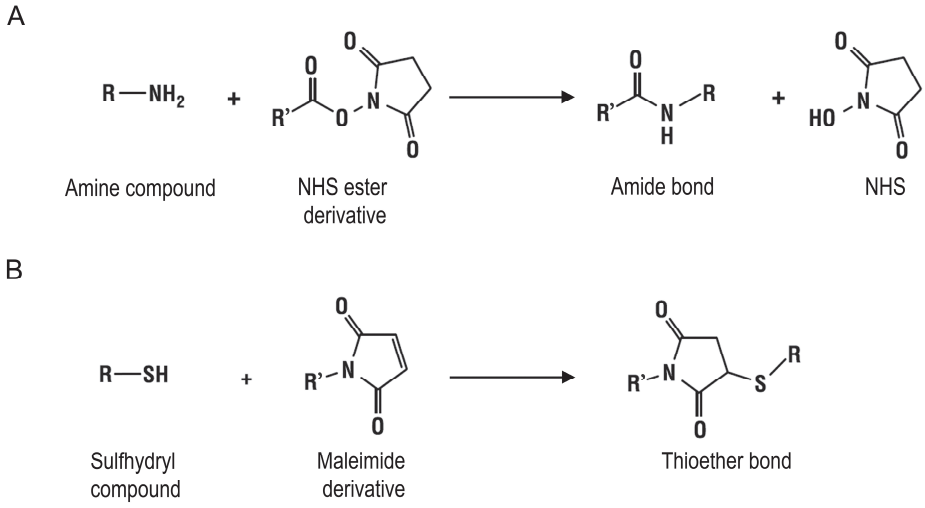

Figure 6. The coupling reaction of **A**) an amine with a NHS-ester and **B**) a sulfhydryl with maleimide. Modified from Bioconjugate Techniques, Copyright (1996) with permission from Elsevier (Hermanson 1996).

2.5.2.1 Bioconjugation of biomolecules

Bioconjugation involves two or more molecules linked together by highly stable covalent bonds to form a novel complex with the combined properties of its individual components (Hermanson 1996). The choice of a bioconjugation strategy depends on the physicochemical and biochemical properties of the molecules to be conjugated (Di Marco et al. 2010).

Biomolecules can be chemically coupled to other biomolecules either directly or by using bi- or multifunctional cross-linking reagents, which contain two or more

reactive ends capable of attaching chemically to specific functional groups. The bifunctional cross-linker reagents may contain reactive end-groups with the same functionality (homobifunctional) or different functionality (heterobifunctional) and they may be used in one- or multistep processes. Cross-linking two different molecules together using a homobifunctional cross-linker in a single step lacks the control of the reaction, as many different types of intermediates may be produced. Usually the use of heterobifunctional cross-linkers in multistep-process offers the greatest degree of control of the reaction. The smallest available reagents for bioconjugation are zero-length cross-linkers that conjugate two molecules by forming a bond containing no additional atoms (Hermanson 1996). Steric hindrance can be diminished by introducing a spacer arm between conjugated molecules to achieve more active complexes. The spacer can be selected to have almost any desired length and it may be rigid, flexible, hydrophilic or hydrophobic, charged or neutral and it may contain cleavable groups (Hermanson 1996, Rozkiewicz et al. 2010).

Bioconjugation may also involve the labeling or modification of macromolecules by tags and probes containing groups that can be detected based on their fluorescence, radioactivity, visible chromogenic character or affinity toward another molecule, for example utilizing avidin-biotin technology (Hermanson 1996). Biotin is an important player in various biochemical and cellular processes, and therefore each organism has an enzyme called biotin protein ligase to covalently attach biotin to acceptor proteins (Cronan & Reed 2000). For example in *E. coli*, the biotin holoenzyme synthetase/bio repressor (BirA) attaches biotin covalently to Lys122 of the biotin carboxyl carrier protein (BCCP) in acetyl-CoA carboxylase (Cronan 2001). BCCP may be used as a fusion partner to produce biotinylated proteins, as for instance *E. coli* is capable of metabolically biotinylating the fusion proteins (Germino et al. 1993). For localized drug or gene delivery, nanoparticles may need to be conjugated with targeting peptides and sometimes linker molecules between the peptide and particle are needed.

2.5.2.2 Covalent immobilization of biomolecules to a surface

The performance of immobilized biomolecules on a surface is dependent on the chemical and physical properties of the surface as well as the biomolecules, including their distance from the surface and the orientation and the density of the immobilized biomolecules on the surface (Rozkiewicz et al. 2010). Proteins are structurally and chemically complex and heterogeneous molecules sensitive to denaturation, dehydration or oxidation, which results in the loss of their structure and biochemical activity. Therefore, proteins are especially sensitive to the applied immobilization methods (Rozkiewicz et al. 2010). The activity and proper function

of immobilized proteins on a surface strongly depend on their ability to bind their receptor in the correct conformation. For example, direct attachment may result in steric constraints that affect the reactivity when compared with a protein in solution (Di Marco et al. 2010). Thus, the orientation and spacing between proteins on the surface are important. Protein immobilization can lead to a site-directed or random orientation (Aydin et al. 2012).

Biomolecules can be immobilized to functionalized or nonfunctionalized surfaces by direct attachment or by using cross-linkers between the functionalized surface and the biomolecule. For example, thiol groups adsorb strongly to a clean gold surface forming a strong bond of a partially covalent nature (Love et al. 2005, Jadzinsky et al. 2007, Häkkinen 2012) and this direct adsorption can be used as an immobilization method, which does not require a surface modification, although passivation should be performed after immobilization to block the remaining gold areas (Rozkiewicz et al. 2010). The covalent immobilization of biomolecules to surfaces usually offers greater control than non-covalent adsorption (Figure 5C). However, covalent immobilization could also be random, if active functional groups exist arbitrarily or are widely distributed on the molecule (Rozkiewicz et al. 2010). When both the surface and the biomolecule contain multiple sites for receptors and ligands, biomolecules may become deformed when immobilized (Rowe et al. 2012).

3 AIMS OF THE STUDY

The aim of the study was to develop biomolecules suitable for nanobiotechnology and bionanotechnology. In the first part of the study the properties of different avidins were characterized and modified. In the second part of the study, biomolecular complexes were produced and their applicability was evaluated.

More specifically, the aims of the study were:

I To chemically modify avidin and dcAvd to enable their use in covalent bioconjugation.

II To solve the crystallographic structure of wt bradavidin. To study whether the C-terminal amino acid residues could be used as an affinity tool.

III To solve the crystallographic structure of bradavidin II and characterize its biophysical properties.

IV To design a self-assembling defined-sized DNA construct that could be applied to molecular electronics.

V To study the nanoparticle formation from chitosan and DNA, and to functionalize the formed nanoparticles by targeting peptides and fluorescent labels. To characterize the cellular targetability of the particles.

4 MATERIALS AND METHODS

4.1 Engineered proteins (I-III)

4.1.1 Construction of protein expression vectors

To obtain Avd(S16C) and dcAvd(I117$C_{5\rightarrow4}$,S16C,V115$H_{6\rightarrow5}$), referred to as dcAvd-Cys, the cDNAs of avidin, cpAvd6→5 and cpAvd5→4 were modified by site-directed mutagenesis using the QuikChange (Stratagene, La Jolla, CA, USA) or the megaprimer methods (Sarkar & Sommer 1990). The mutated forms of cpAvd6→5(S16C, V115H) and cpAvd5→4(I117C) were ligated and the full-length dcAvd-Cys was subcloned into the pFastBac vector (Invitrogen, Carlsbad, CA, USA). For avidin, Avd(S16C) and bradavidin II, the DNA encoding the bacterial signal peptide OmpA from *Bordetella avium* was placed in front of the protein-encoding sequence to obtain efficient bacterial secretion (Hytönen et al. 2004) and such cassettes were subcloned into pET101/D-TOPO®. Brad-tag–EGFP fusion proteins were generated using the pHis-EGFP plasmid (Saeger et al. 2012) as template in a polymerase chain reaction (PCR) and the primers contained the Brad-tag sequence. The amplified PCR-products were extracted from an agarose gel and subcloned into expression vectors. The construction of the pBVboostFG vector containing the core-bradavidin and wt bradavidin is described in detail in (Nordlund et al. 2005b). The expression vectors used in this study are summarized in table 2. All constructs were confirmed by DNA sequencing (ABI PRISM 3100 Genetic Analyzer, Applied Biosystems).

4.1.2 Protein expression

For the proteins produced in bacteria, the expression plasmids were transformed into *E. coli* BL21-AI or *E. coli* BL21 Star™(DE3) (Invitrogen) by heat shock transformation according to the manufactures protocol. The cells were plated onto LB plates containing the appropriate antibiotics (and 0.1 % glucose for avidins) and incubated overnight at 37°C.

Table 2. Summary of protein expression vectors, host cells, culture systems and purification methods used in protein expression.

Protein (communication)	Expression vector	Expression host	Culture method	Culture medium	Induction	Affinity chromatography	Elution buffer
Avidin (I)	pET101/D-TOPO®	*E. coli* BL21-AI	Bottle culture, 28 °C, 220 rpm	LB with 0.1 % glucose, 100 µg/ml ampicillin, tetracycline 5 µg/ml [a]	1 mM IPTG, 0.2 % (w/v) L-arabinose	2-iminobiotin	50 mM CH_3COONa, 100 mM NaCl (pH 4)
Avd(S16C) (I)	pET101/D-TOPO®	*E. coli* BL21-AI	Bottle culture, 28 °C, 220 rpm	LB with 0.1 % glucose, 100 µg/ml ampicillin, tetracycline 5 µg/ml [a]	1 mM IPTG, 0.2 % (w/v) L-arabinose	2-iminobiotin	50 mM CH_3COONa, 100 mM NaCl (pH 4)
Core-bradavidin (II)	pBVboostFG	*E. coli* BL21-AI	Fermentor	LB with 0.1 % glucose, 7 µg/ml gentamycin [a] / fermenting medium with 7 µg/ml gentamycin	0.25 mM IPTG, 0.2 % (w/v) L-arabinose	2-iminobiotin	0.1 M acetic acid (pH 3)
Wt bradavidin (II)	pBVboostFG	*E. coli* BL21-AI	Fermentor	LB with 0.1 % glucose, 7 µg/ml gentamycin [a] / fermenting medium with 7 µg/ml gentamycin	0.25 mM IPTG, 0.2 % (w/v) L-arabinose	2-iminobiotin	0.1 M acetic acid (pH 3)
Brad-tag–EGFP (II)	pET101/D-TOPO®	*E. coli* BL21 Star™(DE3)	Bottle culture, 28 °C, 220 rpm	LB with 100 µg/ml ampicillin	1 mM IPTG	Brad-tag	50 mM Na-carbonate, 1 M NaCl, pH 11
Brad-tag–EGFP–His-tag (II)	pET101/D-TOPO®	*E. coli* BL21 Star™(DE3)	Bottle culture, 28 °C, 220 rpm	LB with 100 µg/ml ampicillin	1 mM IPTG	Ni-NTA	50 mM NaH_2PO_4, 300 mM NaCl, 250 mM imidazole, pH 8
EGFP–Brad-tag (II)	pET101/D-TOPO®	*E. coli* BL21 Star™(DE3)	Bottle culture, 28 °C, 220 rpm	LB with 100 µg/ml ampicillin	1 mM IPTG	Not performed [b]	Not performed [b]
EGFP–His-tag–Brad-tag (II)	pET101/D-TOPO®	*E. coli* BL21 Star™(DE3)	Bottle culture, 28 °C, 220 rpm	LB with 100 µg/ml ampicillin	1 mM IPTG	Not performed [b]	Not performed [b]
Bradavidin II (III)	pET101/D-TOPO®	*E. coli* BL21-AI	Fermentor	LB with 0.1 % glucose, 100 µg/ml ampicillin, tetracycline 5 µg/ml [a] / fermenting medium with 100 µg/ml ampicillin	0.25 mM IPTG, 0.2 % (w/v) L-arabinose	2-iminobiotin	0.5 M acetic acid (pH 3)
DcAvd-Cys (I)	pFastBac, (Bac-to-bac)	*E. coli* DH10Bac, *Spodoptera frugiperda* Sf9 [c]	Bottle culture, 28 °C, 125 rpm	HyClone SFX-Insect cell culture medium w/o biotin	1:100 recombinant virus / transfected cells	2-iminobiotin	50 mM CH_3COONa, 100 mM NaCl (pH 4)

[a] The composition of the seed culture medium that was transferred to the final culture in fermenting medium (Appendix 1).
[b] Protein purification was not performed as the protein expression level was relatively low based on an immunoblot analysis.
[c] *E. coli* DH10Bac were used for the generation of a bacmid that was transfected into *Spodoptera frugiperda* Sf9 cells to generate recombinant baculoviruses.

Colonies were picked and cultured overnight in a seed culture of 10 ml of Lysogeny broth (LB) medium including the appropriate supplements (Table 2) at 27-28°C with rotation at 220 rpm. Then bacterial suspension was diluted to a final volume in culture medium and the cultivation was continued until the optical density at 600 nm (OD_{600}) reached 0.2-0.5, after which the protein expression was induced. The bottle cultivation was continued an additional 18 hours, after which the cells were collected by centrifugation (4000 g, 10 min, 4°C).

For fermentor production, three colonies were picked and cultured overnight in 5 ml of LB medium with the appropriate supplements (Table 2) at 27°C with continuous rotation. Then 1.5 ml of each culture was transferred to 200 ml of fermenting medium (Appendix 1) containing the appropriate antibiotics (Table 2) and incubated overnight at 27°C with continuous rotation. From these seed cultures, 400 ml were diluted to a final volume of 4 liters to start fermentation in a Labfors Infors 3 fermentor (Infors HT, Bottmingen, Switzerland) at 28°C. The oxygen concentration was maintained at 30 % by controlling the air flow and the agitation speed (150-1200 rpm). When the oxygen concentration could not be maintained above 20 % or when the OD_{600} reached 20, the temperature was decreased to 25°C and the cultures were induced (Table 2) and fermentation was continued for 12 hours. The resulting cell mass was collected by centrifugation (4000 g, 10 min, 4°C).

DcAvd-Cys (I) was produced in *Spodoptera frugiperda* insect cells using the Bac-To-Bac® baculovirus expression system (Invitrogen) as instructed by the manufacturer. The pFastBac expression vector was transformed into *E. coli* DH10Bac cells to create a recombinant bacmid, which was purified and transfected into *Spodoptera frugiperda* Sf9 insect cells. The primary stock of recombinant baculoviruses was collected from the culture medium and used for a larger scale production of recombinant dcAvd-Cys. Approximately 2×10^8 Sf9 cells were seeded to a final volume of 100 ml of biotin-free HyClone SFX-Insect cell culture medium (Thermo Fisher Scientific, Waltham, MA, USA) in a 250 ml Erlenmayer flask. A primary stock was added in a ratio of 1:100 and the infected cells were cultured for 72 hours at 28 °C with rotation at 125 rpm. The cells were pelleted by centrifugation (500 g, 10 min, RT).

4.1.3 Protein purification

Pelleted cells were suspended in the appropriate buffers and lyzed using either a sonicator or a homogenizator (EmulsiFlex C3, Avestin Inc., Ottawa, Canada). Cell lysates were centrifuged (15 000 g, 30 min, 4 °C) and the supernatants were filtered using a 0.2 μm filter cloth. Avidin proteins were purified in a single step using 2-

iminobiotin affinity chromatography (Affiland S. A., Ans-Liege, Belgium) (Hofmann et al. 1980, Airenne et al. 1997) and Brad-tag–EGFP fusion proteins containing a His-tag (II) were purified using Ni-NTA metal-affinity chromatography (Qiagen GmbH, Hilden, Germany) as instructed by the manufacturer. The proteins were eluted in one ml fractions with the elution buffer (Table 2). Brad-tag–EGFP fusion proteins without a His-tag were purified from clarified cellular lysates with core-bradavidin agarose, as described in section 4.1.6.2.

The protein concentration was determined with a UV/Vis spectrophotometer (NanoDrop 1000 Spectrophotometer, Thermo Scientific, Wilmington, DE, USA) by measuring the absorbance at 280 nm. The purity of the protein was analyzed by SDS-PAGE. The protein was denaturated by heating at 95 °C for ten minutes in SDS-PAGE sample buffer with or without a reducing agent (β-mercaptoethanol). Samples were separated by SDS-PAGE on a 15 % gel and the gel was stained with Coomassie Brilliant Blue.

4.1.4 Bioconjugation with maleimide

Maleimides were coupled to free thiols in the ligand-binding sites of Avd(S16C) (I) and dcAvd-Cys (I). Maleimide (Sigma-Aldrich, St. Louis, MO, USA) and N-maleoyl-β-alanine (Mal-β-ala, Sigma-Aldrich) in dimethyl sulfoxide (DMSO) were added in a 100-fold molar excess to the protein solution in a 50 mM Na-phosphate buffer (pH 7.0) containing 100 mM NaCl. The samples were incubated at RT for one hour.

4.1.5 Characterization of ligand binding

4.1.5.1 Isothermal titration calorimetry

Isothermal titration calorimetry (ITC) was performed to analyze the ligand-binding affinities of core-bradavidin (II) towards a synthetic peptide, named Brad-tag (GenScript, Piscataway, NJ, USA), Brad-tag–EGFP–His-tag or D-biotin (Fluka Chemie GmbH, Buchs, Switzerland); wt bradavidin (II) towards D-biotin and bradavidin II (III) towards desthiobiotin or D-biotin. Core-bradavidin and wt bradavidin were dialyzed against a 50 mM sodium phosphate (pH 7.0) buffer containing 100 mM NaCl, whereas bradavidin II was dialyzed against 0.5 M acetic acid (pH 3). The ligands were dissolved in the last dialysates to ensure identical buffer conditions for proteins and ligands. Samples were degassed by stirring for 5 min in a MicroCal™ ThermoVac instrument at a temperature of 0.5 degrees lower

than the measurement temperature. The measurements were performed at 15, 25 or 40 °C in a VP-ITC MicroCalorimeter instrument (GE Healthcare, MicroCal, Northampton, MA, USA). Proteins were titrated with repeated additions of ligands in 10 µl or 15 µl aliquots.

Competitive ITC was performed for core-bradavidin by first titrating with the Brad-tag, which was followed by competitive titration with biotin. Similarly, bradavidin II was first titrated with desthiobiotin followed by competitive titration with biotin. The data were analyzed with the Microcal Origin 7.0 (MicroCal LLC, Northampton, MA, USA) software. The observed reaction heats were corrected by subtracting the heat of dilution caused by the titration of the ligand alone into the buffer. K_a, ΔH and n (stoichiometry) were obtained using the non-linear least-squares fit of the corrected reaction heats for each titration step. K_d, ΔG and ΔS were calculated using equations 3, 5 and 6.

4.1.5.2 Dissociation analysis of biotin

The biotin-binding properties of avidin (I), Avd(S16C) (I) and dcAvd-Cys (I) were studied at RT by a dissociation analysis of two different biotin-conjugates, a fluorescently labelled biotin (BF560-biotin™, ArcDia Ltd, Turku, Finland) and a radioactive biotin ([8,9-^{3}H]biotin, PerkinElmer, Waltham, MA, USA). BF560-biotin™ in a 50 mM Na-phosphate buffer (pH 7.0) containing 650 mM NaCl was excited at 560 nm and the emission was detected at 576 nm for 300 seconds using a QuantaMaster™ spectrofluorometer (Photon Technology International, Inc., Lawrenceville, NJ, USA). Then a two-fold molar excess of the protein was added and the binding was monitored for 300 seconds as quenching of the fluorescence. The fluorescence recovery was measured for one hour after the addition of a 100-fold molar excess of free D-biotin. Each measurement was performed twice.

Proteins were incubated overnight with the radioactive ^{3}H-biotin in a 50 mM Na-phosphate buffer (pH 7.0) containing 100 mM NaCl and 10 µg BSA per ml to prevent non-specific binding. The unbound ^{3}H-biotin was separated by centrifugal ultrafiltration (Vivaspin 500 centrifugal concentrators with 30,000 MWCO, Sigma-Aldrich). Then a 1000-fold molar excess of cold biotin was added and the released ^{3}H-biotin was separated from the protein-ligand complex at different time points by ultrafiltration. The radioactivity of the filtrate was analyzed in a Wallac 1410 liquid scintillation counter (Wallac Oy, Turku, Finland). Triplicates of each sample were measured at each time point.

The dissociation rate constants (k_{diss}) and the fraction of bound fluorescent or radioactive biotin at each time point were determined using the equation (7):

$$-k_{diss}t = \ln\left(\frac{(x_t - x)}{(x_t - x_0)}\right) = \ln(fraction\ bound) \quad (7)$$

where x_t is the total amount of fluorescent/radioactive ligand before the addition of protein, x is the free biotin at each time point and x_0 is the amount of free ligand in the presence of protein just before the addition of the competing biotin (Klumb et al. 1998). The first 500 s were omitted from the data to eliminate the effect of the fast initial-phase characteristic of the avidin-BF650-biotin™ interaction (Hytönen et al. 2005).

4.1.5.3 Biolayer interferometry

The specificity of core-bradavidin (II) towards the Brad-tag–EGFP–His-tag fusion protein was studied by biolayer interferometry using a ForteBio Octet RED384 instrument (FortéBio, Menlo Park, CA, USA) and the Data Acquisition 7.0 software (FortéBio). First, the baseline for the anti-Penta-HIS biosensor (FortéBio) was measured for 200 s in the measurement buffer containing 50 mM sodium phosphate (pH 7.0) and 100 mM NaCl. Then, Brad-tag–EGFP–His-tag (0.03 mg/ml) was incubated with the sensor for 400 s. After a 10-second washing step in the measurement buffer, the biosensor was moved to a solution containing core-bradavidin (0.06 mg/ml) for 200 s. Wt bradavidin, avidin, streptavidin or rhizavidin solutions (0.06 mg/ml) were studied as controls. Finally, the biosensor was exposed to the measurement buffer and the dissociation of bound protein was measured for 600 s. The experiment was repeated using higher core-bradavidin (0.5 mg/ml) and control protein (1.2 – 2 mg/ml) concentrations and slightly longer incubation times.

Solutions containing core-bradavidin and avidin in the presence of a ~100-fold molar excess of biotin were analyzed as negative controls. In another control experiment, a His-tagged EYFP with terminal cysteine residues (Hytönen, Saeger & Vogel, unpublished) was studied for the functionalization of the anti-penta-HIS sensor, followed by incubation with different avidins. Also, a plain anti-penta-HIS biosensor was exposed to core-bradavidin and chicken avidin both in the absence and presence of biotin.

The measurements were performed at 30 °C using a stirring speed of 1000 rpm and the distance of the tip from the surface was 4 mm. Black 96-well plates (Greiner Bio-One GmbH, Frickenhausen, Germany) were used for the biosensor analyses, a 1:1 Langmuir binding model was fitted to the buffer-subtracted binding curve using the Data Analysis 7.0 software (FortéBio). The raw data was exported from the instrument and processed with MS Excel for preparation of the graphs.

4.1.6 Characterization of Brad-tag–EGFP fusion proteins

4.1.6.1 Immunoblot analysis

The expression of the Brad-tag–EGFP fusion proteins (II) was studied by an immunoblot analysis. Proteins were blotted onto a nitrocellulose filter and detected by incubating with a primary antibody against GFP (Anti-GFP Epitope Tag Polyclonal Antibody, Thermo Scientific) at a 1:2000 dilution. This was followed by incubation with a secondary antibody - alkaline phosphatase (AP) conjugate (anti-rabbit IgG-AP, Sigma) at a 1:30000 dilution and AP was reacted with 5-bromo-4-chloro-3-indolyl phosphate (BCIP) and nitro-blue tetrazolium (NBT) to yield a coloured precipitate.

4.1.6.2 Purification of Brad-tag–EGFP fusion proteins with an immobilized core-bradavidin resin

Core-bradavidin (II) was coupled to a NHS-activated resin, Sepharose™ 4 fast flow, NHS-4FF (Affiland, Liège, Belgium) through amine coupling according to the intructions of manufacturer. Purified Brad-tag–EGFP–His-tag or a cleared cellular lysate containing Brad-tag–EGFP was incubated with the core-bradavidin resin (0.2 ml) on a rolling shaker for one hour at 4 °C. Then the resin was transferred to a column and washed ten times with one ml of binding buffer (50 mM Tris-HCl, 100 mM NaCl, pH 7.5) and again ten times with one ml of wash buffer (50 mM Tris-HCl, 1 M NaCl, pH 7.5). Finally, the protein was eluted in one ml fractions with 50 mM Na-carbonate, 1 M NaCl, pH 11. Samples of fractions were analyzed by SDS-PAGE on a 15% gel and the sample tubes were photographed under UV-light to visualize the elution profile.

To evaluate whether the EGFP fusion proteins were concentrated into the resin via the Brad-tag, samples of core-bradavidin resin were prepared by mixing with the binding buffer in the absence and presence of biotin. Then, the Brad-tag–EGFP–His-tag fusion protein was incubated with resin using an orbital shaker with continuous shaking for 10 min and the resin was left to settle by incubation without shaking for 10 min before the sample tubes were photographed under UV-light.

4.1.6.3 Fluorescence emission

Fluorescence emission was used to verify the Brad-tag-EGFP fusion protein (II) expression and purification. A QuantaMaster™ spectrofluorometer (Photon Technology International, Inc., Lawrenceville, NJ, USA) was used to excite the sample at 485 nm and the emission spectra was detected from 495 nm to 635 nm.

The measurements were performed at RT in 50 mM Tris-HCl, 100 mM NaCl, pH 7.5. The emission spectrum of the buffer was subtracted as the baseline.

4.1.7 Fluorescence resonance energy transfer

A fluorescence resonance energy transfer (FRET) experiment was performed to study whether two different kinds of ligands can be bound to the same dcAvd-Cys pseudotetramer (I). DY560-maleimide (DY560-MI) and DY633-biotin from Dyomics GmbH (Jena, Germany) were used as the FRET donor and acceptor, respectively. First, the degree of labeling was determined. A five-fold molar excess of DY560-MI was added to proteins in a 50 mM Na-phosphate buffer (pH 7.0) containing 100 mM NaCl and incubated for two hours at RT protected from light. The free dye was removed by dialysis and the absorption spectrum for the protein-dye conjugate was recorded with a PerkinElmer Lambda 35 UV/Vis spectrometer (PerkinElmer Life and Analytical Sciences). The absorption maxima at 280 nm and 560 nm were used to calculate a *dye/protein ratio* (11) according to a formula derived from the Lambert-Beer law for the absorption maximum of the dye (8) and for the absorption maximum of the protein at 280 nm (9) adjusted by a correction factor, *CF*, (10) contributed by the dye absorbance at 280 nm.

$$c_{dye} = \frac{A_{max}}{\varepsilon' \times l} \tag{8}$$

where ε' is the molar extinction coefficient of the fluorescent dye

$$c_{protein} = \frac{A_{280} - (A_{max} \times CF)}{\varepsilon \times l} \times DF \tag{9}$$

where ε is the molar extinction coefficient of the protein and *DF* is a dilution factor.

$$CF = \frac{A_{280}(dye)}{A_{560}(dye)} \tag{10}$$

$$\frac{Dye}{protein} = \frac{c_{dye}}{c_{protein}} \tag{11}$$

In the FRET experiment, a QuantaMaster™ spectrofluorometer (Photon Technology International, Inc., Lawrenceville, NJ, USA) was used to excite the sample at 559 nm and to detect the emission spectra from 570 nm to 700 nm at RT. The emission spectrum was measured for the dcAvd-Cys-DY560-MI

conjugate before and after the addition of DY633-biotin. The emission spectrum for DY633-biotin alone, and DY633-biotin incubated with dcAvd-Cys without DY560-MI were measured as controls. In addition, free biotin was incubated with the dcAvd-Cys-DY560-MI conjugate and the emission was measured before and after the addition of DY633-biotin. The fluorescence intensities of the measured emission spectra were corrected for the sample dilution.

4.1.8 Analysis of thermal stability

4.1.8.1 Differential scanning calorimetry

The unfolding temperatures of core-bradavidin (II), wt bradavidin (II) and bradavidin II (III) were analyzed by a MicroCal™ VP-Capillary DSC System (GE Healthcare, MicroCal, Northampton, MA, USA). Core-bradavidin and wt bradavidin were analyzed in a 50 mM sodium phosphate (pH 7.0) buffer containing 100 mM NaCl. Bradavidin II aggregated at pH 7 and therefore was analyzed in 0.5M acetic acid (pH 3), in a 50 mM sodium phosphate buffer containing 100 mM NaCl (pH 5) and in a 25 mM ammonium acetate buffer (pH 6.8). Protein concentrations in the analyses were ~0.2 mg/ml for core-bradavidin and wt bradavidin, and 0.2 mg/ml; 0.4 mg/ml and 0.6 mg/ml for bradavidin II.

Samples were degassed by stirring for 5 min at 20 °C by MicroCal™ ThermoVac. Thermograms were recorded from 20 °C to 130 °C using a scan rate of 2 °C/min and each sample was scanned twice. The measurements were conducted in the absence and in the presence of biotin using ~3:1 molar ratio of biotin per protein subunit. A small amount of DMSO (0.1 %) was included in the bradavidin II samples to make the biotin soluble at low pH. The Microcal Origin 7.0 software was used for analysing the data.

4.1.8.2 SDS-PAGE

The oligomeric state of avidin (I), Avd(S16C) (I), dcAvd-Cys (I) and bradavidin II (III) was studied by a thermal treatment in the presence of sodium dodecyl sulfate (SDS). Protein samples in the absence and in the presence of D-biotin (Fluka Chemie GmbH, Buchs, Switzerland) were acetylated *in vitro* using sulfo-NHS-acetate (Pierce) to decrease their isoelectric point in order to avoid precipitation by SDS (Bayer et al. 1996). An equal volume of SDS-PAGE buffer with β-mercaptoethanol was added to avidin, Avd(S16C) and dcAvd-Cys and samples were heated to selected temperatures between RT and 100 °C for 20 min. For bradavidin II, an SDS-PAGE buffer without β-mercaptoethanol was used as in the method described earlier (Bayer et al. 1996) and samples were heated to 20 °C or to

80 °C for 20 min. Biotin was added prior to the heat treatment and the samples were incubated for 5 minutes before heating. The oligomeric states of the proteins were analyzed by SDS-PAGE on a 15 % gel stained with Coomassie Brilliant Blue (Bayer et al. 1995) or silver for bradavidin II.

4.1.9 Structural analysis

4.1.9.1 X-ray crystallography

The X-ray crysrallographic analysis of wt bradavidin (II) was performed in collaboration with the group of Professor Mark Johnson (Åbo Akademi University, Turku, Finland). Briefly, suitable conditions for crystallization were screened using the Classics™ (Nextal Biotechnology) screen by the vapour diffusion and sitting drop method. Before crystallization, a saturated solution of an azo dye HABA (<10 mg/ml) was added to the wt bradavidin solution (0.4 mg/ml in 50 mM sodium acetate, pH 4) in 1:10 (v/v) ratio. The crystals were formed at 22 °C. The X-ray diffraction data were collected at the MAX-lab beam line I911-2 (Lund, Sweden) using a MarCCD detector. A more detailed description is given in the original communication (II).

The X-ray crystallographic structures for bradavidin II (III) were solved in collaboration with the group of Professor Oded Livnah (The Hebrew University of Jerusalem, Jerusalem, Israel). Three different kinds of crystal structures were obtained: two forms without biotin (apo Form-A and apo Form-B) and one biotin-complex. The crystals were obtained with the microbatch method at 20 °C using appropriate combinations of precipitants and additives. A bradavidin II–biotin complex was obtained by incubating the protein (3.9 mg/ml in 0.5 M acetic acid, pH 3) with a saturated D-biotin solution (1.5 mg/ml in 0.5 M acetic acid) for 0.5 h at 4 °C before crystallization. Crystallographic data for all bradavidin II forms were collected at the European Synchrotron Radiation Facility (ESRF), Grenoble, France. The data were collected at 100 K using an Oxford Cryosystem Cryostream cooling device. The beamlines and detectors used for the different forms were as follows: for apo Form-A, beamline ID14-4 on an ADSC Q315 CCD detector; for apo Form-B, beamline ID-29 on a PILATUS 6M pixel detector and for bradavidin II–biotin complex, beamline ID-29 on an ADSC Q315 CCD detector. The methods are described in more detail in the original communication (III).

4.1.9.2 Mass spectrometry

Mass spectrometric (MS) experiments (I, III) were performed in collaboration with Professor Janne Jänis (University of Eastern Finland, Joensuu, Finland) with a Fourier transform ion cyclotron resonance (FT-ICR) mass spectrometer (APEX-Qe™; Bruker Daltonics, Billerica, MA, USA) equipped with eloctrospray ionization (ESI). The aim was to analyze the coupling efficiency of maleimide to the free cysteine of Avd(S16C) (I) and avidin was analyzed as a control. A ten-fold molar excess of maleimide (Sigma-Aldrich, St. Louis, MO, USA) in HPLC-grade DMSO was mixed with the proteins, and subsequently incubated at RT for 15–30 min before the measurements. The desalted protein samples (untreated or treated with maleimide) in a 10 mM ammonium acetate buffer (pH 6.8) were further diluted with an acetonitrile/water/acetic acid (49.5:49.5:1.0, v/v) solution for denaturing MS. Avidin and Avd(S16C) samples with or without a maleimide treatment were also digested in solution with trypsin using a 1:40 trypsin to protein ratio to verify the presence of the maleimide-coupled residue.

For bradavidin II (III), the aim was to analyze the oligomeric state of the protein under different conditions. Thus, bradavidin II was buffer-exchanged with 10 mM ammonium acetate (pH 6.8) before analysis and the samples were further diluted with 25 mM ammonium acetate (pH 6.9) for native MS experiments or with acetonitrile/water/acetic acid (49.5:49.5:1.0, v/v) for denaturing MS.

4.1.9.3 Dynamic light scattering

A dynamic light scattering (DLS) instrument Zetasizer Nano ZS (Malvern Instruments Ltd., Worcestershire, UK) was used to determine the hydrodynamic diameter of bradavidin II (III) samples at different buffer conditions. The samples (100 µl) were measured at 25 °C using a scattering angle of 173°. The hydrodynamic diameters were determined from a cumulants analysis of six parallel measurements and the molecular weight estimates were calculated using a globular protein standard curve provided by the instrument's manufacturer. A molecular weight of 12.24 kDa was used as the M_w of the monomer to determine the protein oligomeric state.

A DLS thermal scanning experiment was also performed for bradavidin II. The temperature of the sample (300 µl) in a quartz cuvette (Hellma 104-QS, Hellma GmbH & Co. KG, Müllheim, Germany) was gradually increased from 20 °C to 90 °C in 5 °C steps, and the sample was incubated for 5 min at each temperature before the measurement. The obtained molecular weight estimates and derived count rates were plotted at different temperatures.

4.2 DNA triple crossover construct (IV)

In order to study the potential of a DNA complex for the patterning other components for molecular electronics, defined-sized DNA templates were designed that could be immobilized between electrodes to study their conductance behaviour.

4.2.1 Design of a TX tile construct

Defined-sized DNA templates were designed based on previously published triple crossover motifs (TX tiles) (Li et al. 2004, Park et al. 2005a). Two different kinds of tiles, *tile A* and *tile B,* were designed so that they were able to assemble into a complex of three tiles in the following order: *tile B – tile A – tile B* (B–A–B-complex). As the previously reported TX tiles formed long, continuous arrays, the following changes to the constructs were made: first, the sticky ends were modified. Three different kinds of sticky ends (*a*, *b* and *c*) of eight nucleotides (nt) in lenght were designed for *tile A* and used symmetrically at the both ends, which enabled *tile A* to be rotated by 180° and still have the sticky ends in the same orientation at the both ends. Accordingly, the sticky ends of tile B were *a'*, *b'* and *c'* at the one end. The sticky ends (12 nt) at the other end of *tile B* shared an identical sequence (*d*) so that they could be assembled with complementary strands (*d'*) functionalized with thiol groups at their 5' end. The thiol-functionalization was added in order to be able to position and immobilize the structures between gold nanoelectrodes through S-Au bonding. Secondly, the sticky ends were changed to start from the same horizontal location in each helix, thus enabling *tiles B* to assemble at both ends of *tile A*. Third, the crossover points of *tile A* were designed to have 16 base pairs in between, corresponding to 1.5 turns of B-DNA double helices, and enabling the same natural orientation for helices when *tile B* was assembled on both sides of *tile A*. The length of the full B–A–B-complex with thiol groups at both ends was 167 bases, corresponding to 15.9 full turns of the DNA double helices.

With the above restrictions in mind, DNA sequences for 14 different oligonucleotides were modified from previously published structures (Li et al. 2004, Park et al. 2005a). To minimize alternative associations, i.e. undesired sequence complementarity, the M-fold web server (Zuker 2003, The Mfold Web Server 1995) was used to predict possible secondary structures and sequences were modified when needed. In each tile, the undesired complementary subsequences were limited to five adjacent base pairs with the restriction of two of them being A-T pairs, or on a rare occasion to six adjacent base pairs with the restriction of four of them being A-T pairs. Undesired C-G pairing in parallel was restricted to be

three at maximum. DNA sequences are presented in the original communication (IV, Figure S1, Table S1).

To study the functionalization properties of the B–A–B-complex, a biotinylated hairpin was added to similar TX tiles. Instead of using two biotins in the hairpin as in previous studies (Li et al. 2004), only one biotin with a more flexible 15-atom triethylene glycol (TEG) linker was used to optimize the binding with streptavidin.

4.2.2 Fabrication of the TX tile construct

The B–A–B-complex was formed in a TAE Mg^{2+} buffer (40 mM Tris (pH 7.6), 1 mM ethylenediaminetetraacetic acid (EDTA), 19 mM acetic acid, 12.5 mM magnesium acetate). Ligation was performed to make the complex more stable for DEP trapping. For this purpose, T4 polynucleotide kinase (New England Biolabs) was used to add phosphates to the 5' end of each DNA strand (PAGE- or high performance liquid chromatography (HPLC)-purified, Biomers GmbH, Ulm, Germany), except the 5' thiol-modified strand (HPLC-purified, Integrated DNA technologies, Coralville, Iowa, USA). Each strand was modified separately by incubating for one hour at 37 ºC in T4 DNA ligase buffer in the presence of T4 polynucleotide kinase.

A two-fold molar concentration of strands forming *tile B* (B-strands) were mixed with strands forming *tile A* (A-strands) to achieve an appropriate concentration of each tile. In addition, a three-fold molar concentration of the 5' thiol-modified strands compared with the B-strands was used in order to hybridize them with each sticky end *d* of the *tile B*. Complexes were formed by heating the mixture to up to 90 ºC and by cooling it down to 20 ºC at a rate of 0.01 ºC/s in a PCR-machine (Biometra GmbH, Goettingen, Germany). T4 DNA ligase (New England Biolabs) was used to catalyze the formation of phosphodiester bonds between the 5' phosphate and 3' hydroxyl groups of the adjacent strands of the annealed complexes. Ligation reactions were incubated for two hours in the dark at room temperature and then stored at 4 ºC. Theoretically, the obtained complex contained a 0.29 μM concentration of *tile A* and a 0.58 μM concentration of *tile B*. The folding of separate *tiles A* and *B* and complete B–A–B-complex formation was analyzed by agarose gel electrophoresis (AGE) on a 1.5 % gel.

For functionalization studies with streptavidin, the same strands previously used in the DNA triple crossover molecules (TX tiles, (Li et al. 2004)) were purchased from Biomers GmbH, except strand 3 (IV, Figure S2, Table S2) with an internal biotin-TEG modification was purchased from (TAG Copenhagen, Copenhagen, Denmark). TX tile constructs were formed in 20 mM Tris (pH 7.6), 2 mM EDTA, 12.5 mM $MgCl_2$ by heating and cooling by the same procedure as described for the

B–A–B-complex. The final concentration of each strand, as well as the TX molecules, was 1 μM. Streptavidin at the ratio 1:1 per TX tile was added to the annealed solution and incubated overnight at 4 ºC before AFM imaging.

4.2.3 Analysis of the TX tile construct

4.2.3.1 Atomic force microscopy

The formation of the B–A–B-complex and streptavidin functionalization through biotin-modification of the TX tiles were analyzed by atomic force microscopy (AFM). A sample of 5 μl was incubated on a freshly cleaved mica surface for 3 min at RT and then washed with 10 μl of deionized water and gently dried under a nitrogen stream. AFM-imaging was performed by the tapping mode under ambient conditions using a Dimension 3100 AFM using NanoScope IVa controller (Veeco Instruments, NY, USA).

4.2.3.2 Dielectrophoretic trapping

Alternating current dielectrophoresis (AC-DEP) trapping (Kuzyk et al. 2008, Linko et al. 2009) was applied to the thiol-modified B–A–B-complex to position it in a controlled way between two gold nanoelectrodes that were fabricated by standard electron beam lithography on a SiO_2 substrate. Before the experiment, TX tile constructs were filtered and transferred into a buffer (6.5 mM Hepes, 1 mM magnesium acetate and ~2 mM NaOH to adjust pH to 7) of lower conductivity ($\sigma \approx 300$ μS cm^{-1}) using Millipore Microcon YM-100 spin filters (MW cutoff of 100 kDa).

An AC voltage of 1.2-1.5 V at a frequency of 11 MHz was applied between two fingertip-type gold nanoelectrodes (width of 30-50 nm and the gap between them 45-55 nm (Figure 11D and E) to produce the trapping field. A sample of 10 μl of spin-filtered B–A–B-complexes (1-10 nM) was pipetted onto the chip and the trapping voltage was applied for 3-5 minutes. To reduce the concentration of Mg^{2+} ions after trapping, samples were gently washed with 3 mM Hepes, 2 mM NaOH buffer (pH ≈ 7) and also with distilled water and dried under a nitrogen flow. The control samples did not contain any DNA in the buffer, and they underwent similar DEP and washing steps as the B–A–B-complexes. The trapping results were verified by AFM-imaging. Samples containing only one intact and correctly aligned structure were selected for a conductivity analysis.

4.2.3.3 Electrical / Conductivity measurements

DC-conductivity measurements were performed by changing a battery powered bias voltage between -0.3 V and 0.3 V while measuring the current and voltage by a computer equipped with a data acquisition card (National Instruments PXI-1031) via DL-Instruments 1211 current preamplifier and DL-Instruments 1201 voltage preamplifier. For alternating current impedance spectroscopy (AC-IS) measurements the same preamplifiers and two Stanford Research 830 Lock-In amplifiers, controlled through a GBIP connection by a computer running a homemade LabVIEW AC-IS program were used. All electrical measurements were performed in an electromagnetically shielded room. The sample, i.e. the B–A–B-complex immobilized between gold electrodes, was placed inside a humidity-tight chamber, where the relative humidity (RH) during the measurements was adjusted by a small constant flow of either dry nitrogen or DI-water vapor saturated air. Samples were measured in a dry environment of RH ~5 % and also at humid state of RH=90 %. RH and temperature were continuously measured with a Honeywell HIH-3602-A humidity sensor.

The alternating current impedance spectroscopy (AC-IS) measurements were performed at an RH of 90 % and a frequency ranging from 0.01 Hz - 100 kHz. The used excitation was a sinusoidal voltage with zero offset (V_{dc}=0) and an amplitude of 50 mV_{rms}. First, the dry and empty sample, i.e. only the nanoelectrodes, was measured. Then three parallel measurements were performed for both the samples containing only buffer (controls) and the samples containing the B–A–B-complex. A more detailed description is given in the original communication (IV).

4.3 Chitosan-DNA nanoparticles (V)

4.3.1 Preparation of nanoparticles by complex coacervation

Chitosan nanoparticles containing plasmid DNA (pDNA) were prepared by complex coacervation technology. First, ultrapure chitosan (PROTASAN UP B 80/20 with a molecular weight of 250 kDa and a degree of deacetylation of 86 % from FMC BioPolymer/NovaMatrix, Sandvika, Norway) was let to dissolve in a 100 mM acetic acid, 100 mM sodium acetate buffer overnight. Then, the pH of the chitosan solution was adjusted to 5.5 with 10 M NaOH and the solution was filtered with a 0.2 μm syringe filter before use. The plasmid Id2.3 (Promega Corp., Madison, WI, USA) encoding green fluorescent protein (GFP) was diluted in a 5 mM sodium sulfate solution. The chitosan and pDNA solutions were heated to 55 °C, followed by the immediate addition of the plasmid solution into the chitosan solution. Finally, the mixture was vortexed for 30 s and then incubated at RT for 30 min to complete the nanoparticle formation. The following chitosan to pDNA weight ratios were used: 1:4, 1:2, 1:1, 2:1, 4:1, and 8:1.

4.3.2 Verification of the DNA binding capacity by agarose gel electrophoresis

Agarose gel electrophoresis (AGE) was used to analyze the capacity of chitosan to bind with pDNA at weight ratios 1:4, 1:2, 1:1, 2:1, 4:1, and 8:1. Naked pDNA and nanoparticle samples were mixed with a loading dye and run on a 0.8 % agarose gel in a Tris–borate EDTA (TBE) buffer at 80 V (400 mA) for 1 h. The gel was prestained with the SYBR® Safe DNA gel stain (Invitrogen) and visualized under UV light using a Bio-Rad ChemiDocTM XRS molecular imager (Bio-Rad Laboratories, Inc., Hercules, CA, USA). The naked pDNA and the nanoparticles with the chitosan to pDNA weight ratios of 1:4 and 4:1 were digested with the PstI restriction enzyme (Fermentas, St. Leon-Rot, Germany) to analyze whether chitosan nanoparticles can protect the plasmid and the samples were analyzed by AGE as described above.

4.3.3 Coupling of targeting peptides and a fluorescent dye to nanoparticles

Targeting peptides for the chitosan nanoparticles (V) were designed based on a published TrkB binding sequences (Ma et al. 2003) and adding the cleavage site for

the TeV protease between the N-terminal cysteine and the TrkB binding sequence. For the targeting peptide PEP (CENLYFQSG**SMAHPYFAR**) and for the scrambled control peptide cPEP (CENLYFQSGAYHMSAPFR), the recognition sequence for the TeV protease is presented underlined and the TrkB binding sequence in bold text. Peptides were synthesized using a 9-fluorenylmethyloxycarbonyl group (FMOC) as the amino-protecting group (Carpino & Han 1972) by Storkbio (Tallinn, Estonia), and their purity (>90 %) was verified by (HPLC) and their identity confirmed by mass spectrometry.

Peptides and a fluorescent DyLight 405 NHS ester (Thermo Scientific, Rockford, IL, USA) were coupled to amines at the surface of a chitosan nanoparticle after particle formation. Peptides were conjugated in a two-step reaction (V, Figure 1) using succinimidyl- ([N-maleimidopropionamido]-ethyleneglycol)ester (NHS-PEG_n-MI) crosslinkers (Thermo Scientific) with varying PEG spacer arm lengths and molecular weights: PEG_2 (17.6 Å, 425.39 g/mol), PEG_6 (32.5 Å, 601.60 g/mol), and PEG_{12} (53.4 Å, 865.92 g/mol).

For conjugation, the pH of the nanoparticle solution was increased to 7.0–7.2 by adding PBS buffer (100 mM sodium phosphate, 100 mM sodium chloride, pH 8). A 50-fold molar excess of crosslinker and a 16-fold molar excess of fluorescent dye to chitosan were mixed with the nanoparticle solution and incubated at RT for 1 h. Then, a 50-fold molar excess of peptide to chitosan was added into the nanoparticle solution and the incubation was continued at RT for 30 min. Samples were dialyzed against a PBS buffer (50 mM sodium phosphate, 100 mM sodium chloride, pH 5.3) using a dialysis membrane with a molecular weight cutoff of 12,000–14,000 Da. The dialyzed nanoparticle solutions were stored at 4 °C.

4.3.4 Characterization

4.3.4.1 Dynamic light scattering

The hydrodynamic diameters of the chitosan nanoparticles (V) were determined with a dynamic light scattering (DLS) instrument Zetasizer Nano ZS, similarly as described in 4.1.9.3. Each chitosan nanoparticle sample (100 µl) was measured twice with three parallel measurements at 25 °C. The polydispersity index (PDI) was recorded for each sample as a measure of the broadness of the particle size distribution. If a Gaussian size distribution is assumed, the polydispersity index can be calculated from the cumulants analysis by the following equation:

$$PDI = \frac{\sigma^2}{d^2} \tag{12}$$

where σ is the standard deviation and *d* is the intensity-weighted mean diameter derived from the cumulants analysis. The PDI is dimensionless, for values smaller than 0.1, the sample is typically referred to monodisperse and values greater than 0.7 indicate a very broad size distribution.

4.3.4.2 Laser Doppler velocimetry

The zeta potential for the chitosan nanoparticles (V) was determined by laser Doppler velocimetry (LDV) using the Zetasizer Nano ZS (Malvern Instruments Ltd., Worcestershire, UK) with a Smoluchowski measurement model. The measurements were performed at 25 °C in disposable folded capillary cells. Each sample was measured three times.

4.3.4.3 Field emission scanning electron microscopy

The morphology of the chitosan nanoparticles (V) was studied using field emission scanning electron microscopy (FE-SEM, Zeiss ULTRA plus, Carl Zeiss NTS GmbH, Oberkochen, Germany). Before sample manufacturing, the nanoparticle solutions were dialyzed against a PBS buffer (pH 5.3) or sterile water. Then a drop of the nanoparticle solution was pipetted onto a copper grid and incubated for a few minutes and excess solution was removed with filter paper. Both carbon-coated and non-coated FE-SEM samples were examined.

4.3.4.4 Cell culture studies

The targeting efficiency of the peptide-functionalized chitosan nanoparticles (V) was analyzed by a suspension culture of EDTA-detached RAW 264 cells naturally expressing the TrkB receptor. The nanoparticles were added to the cell suspensions at a 1:5000 dilution with 10^6 cells per sample, incubated for one, six, or 22 hours at room temperature in 5 mM Hepes containing 135 mM NaCl (pH 7.4), washed four times with PBS and then fixed in 4 % paraformaldehyde in PBS. The fixed cells were analyzed using a Becton Dickenson FACSAria flow cytometer (BD Biosciences, Franklin Lakes, NJ, USA). A TeV protease treatment was used to investigate whether the particles were bound to the receptors or internalized into the cells. The TeV protease was added to the cells before the addition of the nanoparticles and the cells were treated and analyzed as described above.

5 SUMMARY OF THE RESULTS

5.1 Covalent modification of the ligand binding site in avidin and dual chain avidin (I)

Because of the extreme biotin-binding affinity of avidin it is difficult to develop novel ligands that are capable of competing with biotin. Thus, a ligand-binding site for covalent ligand binding was developed, by replacing serine 16 with a cysteine (I, Figure 1). The resulting chemically reactive thiol group can be covalently modified with thiol-reactive agents, such as maleimide-containing reagents, under chemically mild conditions. The S16C mutation was introduced into avidin and to the cpAvd6→5 subunit of dcAvd(I117$C_{5\rightarrow4}$, V115$H_{6\rightarrow5}$), which is capable of folding only into one disulfide-locked form (Hytönen et al. 2006) resulting in Avd(S16C), and dcAvd(I117$C_{5\rightarrow4}$,S16C,V115$H_{6\rightarrow5}$), referred to as dcAvd-Cys (I, Figure 3A). The modification site was carefully selected so that Cys16 is located inside the binding site and thus unable to form a disulfide with any other avidin subunit, which would potentially cause oligomerization.

Avd(S16C) and dcAvd-Cys were successfully purified by 2-iminobiotin chromatography, indicating that their biotin-binding activity was retained, although one hydrogen bond was lost as a result of the S16C-mutation. The free thiol-group of Avd(S16C) was chemically modified with maleimide (MI), which was verified by ESI FT-ICR mass spectrometry as a mass increase of +97 Da (I, Figure 2). The covalent thioether linkage formed with high efficiency, as the amount of unreacted protein in the sample was very low. The mass of wt avidin did not change upon maleimide treatment, indicating a high specificity for the reaction. Similar results were obtained using N-ethylmaleimide. In addition, the covalent binding of maleimide to Cys16 was shown to be specific by trypsin digestion (I, Table S1).

5.1.1 Ligand binding analysis

Based on a fluorescent biotin and radioactive biotin dissociation analysis, the S16C mutation had only a mild effect on the ability of avidin to bind biotin, as the quenching of the fluorescence and the amount of free ^{3}H-biotin were fairly equal

between avidin, Avd(S16C) and dcAvd-Cys. However, Avd(S16C) had a decreased affinity for biotin, detected as a 15- and 18-fold faster dissociation rate (k_{diss}) than avidin, as determined by fluorescent biotin and ^{3}H-biotin, respectively (Table 3 and I, Figure 3). For dcAvd-Cys the recovery of fluorescence after a one-hour displacement with free biotin was 50 % and thus between of those for avidin (85 %) and Avd(S16C) (15 %). The dissociation rate for dcAvd-Cys was about five-fold faster than that for wt avidin and about three-fold slower than for Avd(S16C). As dcAvd-Cys has two S16C-modified and two unmodified binding sites it seemed to behave as a hybrid of wt avidin and Avd(S16C). The maleimide, which was covalently coupled to Cys16, inhibited biotin binding and further decreased the affinity of modified avidins for biotin. When a larger maleimide derivative, N-maleoyl-β-alanine (Mal-β-ala) was conjugated to the Avd(S16C), biotin was still able to bind to Avd(S16C)-Mal-β-ala complex, but the affinity was decreased significantly and the dissociation of the bound ^{3}H-biotin reached 100 % within six hours.

Table 3. The dissociation analysis of wt avidin, Avd(S16C) and dcAvd-Cys using fluorescent biotin (BF560-biotin) and radioactive biotin (^{3}H-biotin). The results for samples coupled with maleimide (MI) or N-maleoyl-β-alanine (Mal-β-ala) are also shown.

	Fluorescent biotin BF560 dissociation			Radioactive ^{3}H-biotin dissociation		
	Quenching of fluorescence [%]	k_{diss} [s^{-1}]	Recovery of fluorescence after an hour [%]	Free ^{3}H-biotin [%]	k_{diss} [s^{-1}]	Released ^{3}H-biotin after 24 hours [%]
Avidin	66.5±1.3	2.4×10^{-5}	13.7±0.9	2.7±0.1	6.0×10^{-7}	7.2±0.3
Avd(S16C)	61.0±0.6	3.7×10^{-4}	85.7±2.6	14.6±1.6	1.1×10^{-5}	85.6±1.6
dcAvd-Cys	63.2±7.3	1.3×10^{-4}	52.3±2.2	5.1±0.6	2.9×10^{-6}	24.7±0.5
Avidin + MI	69.6±22.9	3.0×10^{-5}	16.2±4.9	2.7±0.1	6.0×10^{-7}	7.4±0.3
Avd(S16C) + MI	36.1±0.7	ND[a]	88.1±5.7	25.6±0.1	ND[a]	93.8±0.8
Avd(S16C) + Mal-β-ala	41.7±1.2	ND[a]	92.7±1.3	34.9±0.4	ND[a]	102.9±1.1
dcAvd-Cys + MI	45.0±5.3	ND[a]	26.3±7.8	16.5±0.3	ND[a]	14.4±0.7

[a] Could not be reliably determined because of a very rapid recovery of the fluorescence / release of ^{3}H-biotin after the addition of free D-biotin.

5.1.2 Dual chain avidin able to bind two different kinds of ligands

A fluorescence resonance energy transfer (FRET) experiment demonstrated that maleimidylated molecules could be introduced into the S16C-modified sites of dcAvd-Cys. A fluorescent maleimide (MI) derivative, DY560-MI acted as a donor (I, Figure S2A) by reacting with a thiol in the cpAvd6→5 subunit and fluorescent biotin, DY633-biotin (I, Figure S2B) was used as an acceptor to react with the unmodified biotin-binding sites in the cpAvd5→4 subunit (Figure 7A). The

complex was excited at 560 nm, which resulted in a quenching of the donor emission by 73 % and an increase in the acceptor emission (Figure 7C) indicating energy transfer and the coexistence of both fluorescent labels in the same pseudotetramer, because FRET is restricted to small distances (10 to 100 Å (Gell et al. 2006)).

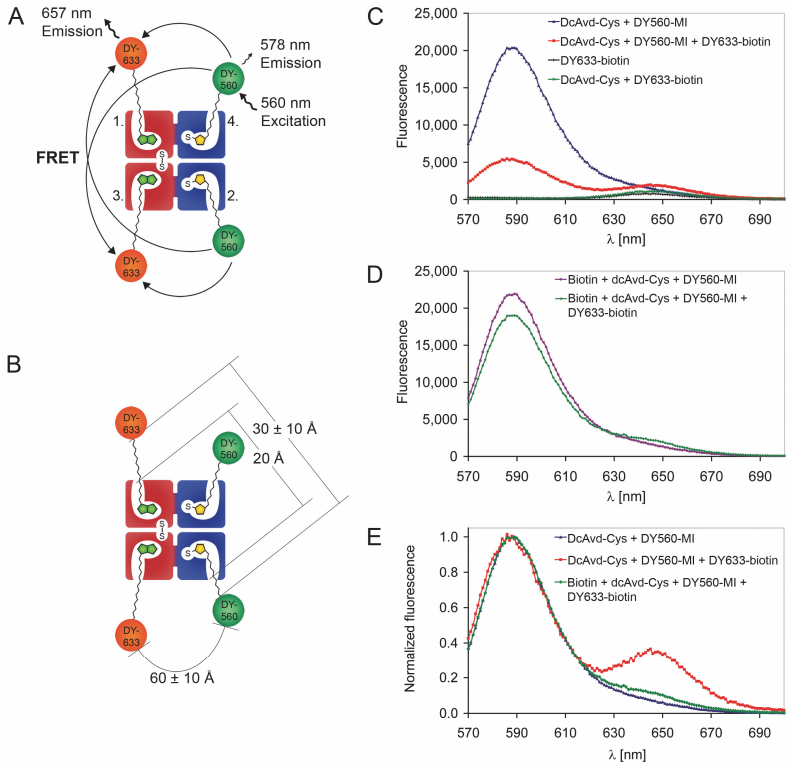

Figure 7. A FRET experiment with dcAvd-Cys. (**A**) A schematic showing a donor (DY560-maleimide, DY560-MI) coupled to the Cys16-modified binding sites and an acceptor (DY633-biotin) bound to the unmodified binding sites of dcAvd-Cys. (**B**) A schematic showing that the distances between the fluorescent labels attached to the same side of the dcAvd-Cys molecule are limited to 30 ± 10 Å. In contrast, the distance between the labels bound to another cpAvd5→4 - cpAvd6→5 pair over the symmetry axis of the avidin is ~60 ± 10 Å. (**C, D**) DcAvd-Cys with a FRET donor and acceptor was excited at 560 nm and the fluorescence intensity was measured. The data corrected for the sample dilution are shown. (C) DcAvd-Cys coupled with DY560-MI was measured in the absence and presence of DY633-biotin. As a control, the DY633-biotin label alone or incubated with dcAvd-Cys was measured. (D) DcAvd-Cys coupled with DY560-MI was incubated with biotin and measured before and after the addition of DY633-biotin. (**E**) The fluorescence spectra normalized according to the maximum fluorescence at 590 nm of dcAvd-Cys coupled with DY560-MI. Samples in the absence and presence of DY633-biotin and with and without biotin are shown. Modified with permission from I.

The maximal distance between the neighboring cpAvd5→4 and cpAvd6→5 (subunits one and two, or three and four) would be ~30±10 Å and for the other cpAvd5→4 and cpAvd6→5 pair (subunits one and four, or three and two) this would be ~60±10 Å (Figure 7B). When the unmodified binding sites of the cpAvd5→4 subunit were blocked with biotin before the addition of DY633-biotin, the emission of the donor was quenched less than 13% (Figure 7D). The fluorescence spectra normalized according to the maximum fluorescence at 590 nm illustrates the increase in the acceptor emission of dcAvd-Cys in the presence of both the FRET donor and the acceptor (Figure 7E). For samples blocked with biotin before the addition of the FRET acceptor, the increase in acceptor emission is insignificant (Figure 7D and E).

The conjugation efficiency of DY560-MI determined as a degree of labeling was 0.6±0.1 for the dcAvd-Cys pseudotetramer and 0.6±0.1 for the Avd(S16C) tetramer (I, Table S2), which was measured as a control. This may indicate some steric hindrance between adjacent biotin-binding sites as described by (Gruber et al. 1998). For wt avidin, no bound DY560-MI was detected indicating the specificity of the reaction.

5.2 Bradavidins have unique structural features (II, III)

The X-ray crystallographic structures of wild type (wt) bradavidin (the apo form) and bradavidin II (two apo forms and one biotin complex) were solved. All structures displayed an eight-stranded antiparallel β-barrel-fold typical for avidins. The conserved hydrophobic and polar residues in the biotin-binding sites of bradavidins are highlighted in a sequence alignment with avidin (Figure 8). Both bradavidins contained a disulfide bridge stabilizing the L3,4-loop, as in rhizavidin (Meir et al. 2009). The essential parts of the determined wt bradavidin and bradavidin II structures in comparison with Avd(S16C) and dcAvd-Cys, are listed in Table 4. The structures are briefly described below and in more detail in the original communications (II and III).

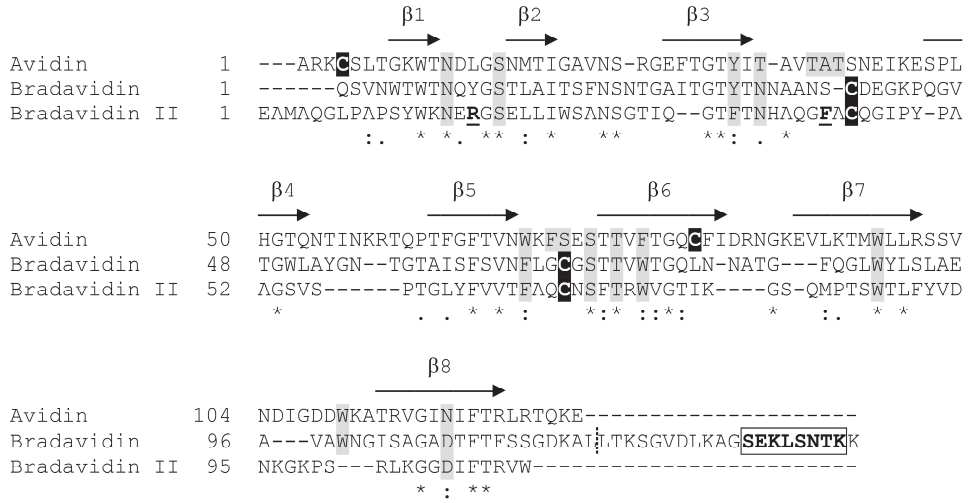

Figure 8. A sequence alignment of avidin, wt bradavidin and bradavidin II showing the concerved amino acids (*), strong group similarities (:) and weak group similarities (.). The locations of the β-strands according to the structure of chicken avidin are indicated by arrows. The residues in close contact with biotin are shown with a grey background and the cysteine residues forming intramonomeric disulfides are shown in white letters on a black background. The truncation site for core-bradavidin is shown as a vertical dash line. The C-terminal Brad-tag sequence of wt bradavidin is bordered and shown in bold letters. Arg17 and Phe42 are important for biotin-binding in bradavidin II, and are shown in bold and underlined letters.

5.2.1 Wt bradavidin has an intrinsic ligand

Wt bradavidin was crystallized in the presence of the azo dye HABA and the crystallographic structure was solved at a resolution of 1.78 Å (PDB 2Y32; II, Table 1). Wt bradavidin assembled into homotetramers, but surprisingly, HABA was not identified in the final structure of the tetramer. Instead, the biotin-binding site of subunit I was occupied by C-terminal amino acid residues from subunit III, (and *vice versa*), and similarly, subunits II and IV interacted with each other (II, Figure 1A). Specifically, the C-terminal tail left the original subunit from the closed-end of the β-barrel and extended into the ligand-binding site of the neighbouring subunit so that residues 130-138 were part of the neighbouring subunit (II, Figure 1B, C and D). Three of the C-terminal residues; Glu131, Lys132 and Leu133 folded deepest into the ligand-binding pocket and occupied the site equivalent to the biotin-binding site of avidin (II, Figure 4). Several non-covalent interactions stabilized the binding of this intersubunit ligand.

Table 4. A comparison of the main structural details of Avd(S16C), dcAvd-Cys, wt bradavidin and bradavidin II.

	Avd(S16C)	**DcAvd-Cys**	**Wt bradavidin**	**Bradavidin II**
Structure	- Homotetramer - 8-stranded β-barrel - 128 amino acids - Theoretical M_w 14.4 kDa - Theoretical pI 9.6 - Flexible L3,4-loop adopts closed conformation in the biotin complex - Glycosylation site at Asn17 - Disulfide between Cys4 and Cys83	- Pseudotetramer - Genetic fusion of two 8-stranded β-barrels - 271 amino acids - Theoretical M_w 30.1 kDa - Theoretical pI 9.8 - CpAvd5→4 and cpAvd6→5 genetically fused together using a tripeptide (SGG) - Original N and C-termini connected with hexapeptide linkers (GGSGGS) - Disulfides between Cys4 and Cys83 in both cpAvd5→4 and cpAvd6→5 subunits [a]	- Homotetramer - 8-stranded β-barrel - 138 amino acids - Theoretical M_w 14.4 kDa - Theoretical pI 6.3 - C-terminal residues 130-138 of subunit I folds within the ligand-binding site of subunit III (and *vice versa*) and similarly subunits II and IV interact together - Residues after β8-strand make short 3/10-helix, and then turn towards neighbouring subunit - Disulfide between Cys39 and Cys69	- Monomer, forms transient oligomers - 8-stranded β-barrel - 112 amino acids - Theoretical M_w 12.2 kDa - Theoretical pI 9.4 - Five of the seven loops are β-turns (L1,2, L4,5, L5,6, L6,7, L7,8) - Flexible L3,4-loop critical for biotin binding has the same size than in most avidins - Disulfide between Cys44 and Cys69
Oligomeric assembly	- Val115 forms hydrophobic contacts in the center of tetramer - 1-2 interface: Trp110 from L7,8-loop forms part of the biotin-binding pocket of the neighboring subunit - 1-3 interface: van der Waals interaction by Met96, Val115, Ile117 - 1-4 interface involves extensive polar and hydrophobic interactions, particularly important being Asn54 and Asn69	- 1-3 interface: $I117C_{5\rightarrow4}$ forms stabilizing disulfide bridge between cpAvd5→4 domains [a] - 1-3 interface: $V115H_{6\rightarrow5}$ destabilizes protein resulting in dynamic oligomerization process and thus enhances the formation of disulfide bridge between cpAvd5→4 domains [a]	- Tetramer is stabilized by non-covalent intersubunit interactions, many of which are unique to bradavidin I - Tyr90 from each subunit locates in the center of tetramer having major role in the assembly of tetramer	- Interface contacts between subunits missing - Lys103 (corresponds to Val115 of avidin) is an obstacle for oligomer assembly - Phe72, Tyr61 and Arg74 (corresponding to Thr76, Gly65 and Val78 of 1-4 interface of avidin) would cause clashes between oligomers

	Avd(S16C)	DcAvd-Cys	Wt bradavidin	Bradavidin II
Ligand-binding site	- Trp70, Phe72, Phe79 Trp97 form hydrophobic box for biotin together with Trp110 from neighboring subunit - S16C results in loss of one hydrogen bond with biotin when compared to wt avidin - Cys16 in the ligand-binding site able to couple with thiol-reactive agents - Asn12, Tyr33, Thr35 and Asn118 make four hydrogen bonds with the heteroatoms of ureido ring of biotin - Biotin sulfur may interact with Thr77 - Thr38, Ala39, Thr40, Ser73 and Ser75 form five hydrogen bonds with carboxylate oxygens of valeryl-tail of biotin	- $S16C_{6\rightarrow5}$ results in loss of one hydrogen bond with biotin when compared to wt avidin [a] - Cys16 in the ligand-binding site can be coupled with thiol-reactive agents - Biotin-binding mode of cpAvd5→4 is similar than in avidin - Biotin-binding mode of cpAvd6→5 differs from avidin, as the side-chains of Phe72 and Ser73 are in different conformation when compared to avidin or cpAvd5→4 [a] (Hytönen et al. 2006)	- Conserved hydrophobic and polar residues involved in biotin-binding - Glu131, Lys132 and Leu133 of subunit I fold deepest into the ligand-binding pocket of the neighboring subunit III, and occupy the site equivalent to the biotin-binding site of avidin - Binding of the C-terminal ligand is stabilized by several non-covalent interactions - C-terminus causes opening or widening of the ligand binding pocket	- Conserved hydrophobic residues Phe66, Trp75 and Trp90 - Phe42 from L3,4-loop compensates the lack of conserved Trp from L7,8-loop - Conserved H-bond interactions with biotin, missing conserved Tyr from β3 replaced by Phe3 - Disulfide bridge interacting with biotin - In the biotin complex the L3,4-loop adopts a closed conformation forming two conserved H-bond interactions; Ans37 with ureido nitrogen and Ala43 with carboxylate oxygen - Arg17 from L1,2-loop seals the biotin-binding site from the side of the bicyclic ring

[a] Numbering according to wt avidin.

The bound C-terminus might have caused the opening or widening of the ligand-binding pocket when compared with other avidin proteins. In addition to having an intrinsic ligand, wt bradavidin showed some differences in its secondary structure elements and loops between the known avidin structures. The composition of the amino acids playing important roles at the interfaces differed from those in avidin too (II, Figure S2).

5.2.2 Bradavidin II crystals suggest a monomeric protein

Bradavidin II was crystallized both in the absence and presence of biotin. The asymmetric units of bradavidin II crystals contained one (apo Form-A, resolution 1.9 Å, PDB 4GGR), two (apo Form-B, resolution 1.7 Å, PDB 4GGT), or four (biotin complex, resolution 1.75 Å, PDB 4GGZ) subunits (III, Table I). However, the subunits showed no common canonical avidin oligomer assembly, suggesting a monomeric protein. The structural alignment showed that the interface contact between the subunits of tetramers (avidin and streptavidin) or dimers (rhizavidin and shwanavidin) are missing in bradavidin II (III, Figure 1). The hydrophobic Val115 in the center of the avidin tetramer is replaced by Lys103 in bradavidin II. In addition, Thr76, Gly65 and Val78 of the 1-4 interface in avidin are replaced by Phe72, Tyr61 and Arg74 in bradavidin II (III, Figure 9). All these changes would reduce or prevent the oligomeric assembly seen in the tetrameric avidins characterized earlier.

Hydrophobic and polar residues in the biotin-binding site of bradavidin II were mostly conserved, but the conserved Tyr (Tyr30 in avidin) in β3 was replaced by Phe35 (Figure 8 and III, Figure 4). In addition, bradavidin II lacks a Trp (Trp110 in avidin) residue in its L7,8 loop that is critical for the high biotin-binding affinity and oligomeric assembly of tetrameric avidins. This loss was compensated by Phe42 in the L3,4 loop (Figure 8 and III, Figures 2 and 3). Moreover, the L1,2 loop of bradavidin II contains Arg17 in a unique position sealing the biotin-binding site from the side of the bicyclic ring (III, Figure 2). The crystal structures contained a L3,4 loop in two distinct conformations; open and closed.

5.2.3 Ligand-binding analysis of bradavidins

According to the crystal structure, the C-terminal amino acid residues of wt bradavidin acted as intersubunit ligands with their neighbouring subunits. This was studied in more detail using isothermal titration calorimetry (ITC). The affinity of D-biotin towards wt bradavidin (K_d ~2.2 × 10^{-7} M) was significantly lower than towards the C-terminally shortened core-bradavidin (K_d < 10^{-9} M) that exceeded

the sensitivity limit of the ITC. The binding affinity of the C-terminal amino acids (SEKLSNTK, named to Brad-tag) to core-bradavidin was studied using a synthetically produced peptide. The binding of the Brad-tag to core-bradavidin was temperature dependent, being endothermic (ΔH = 1.1 ± 0.2 kcal/mol) at 15 °C and exothermic (ΔH = -4.4 ± 0.3 kcal/mol) at 40 °C, but could not be determined at 25 °C, presumably because this was the thermal transition temperature between the endothermic and exothermic binding modes (Table 5 and II, Figure 5). The dissociation constants were 2.5×10^{-5} M at 15 °C and 2.6×10^{-5} M at 40 °C.

A competitive binding experiment involved the saturation of core-bradavidin with the Brad-tag, followed by a second titration with biotin. The sum of the measured binding enthalpy of core-bradavidin titrated with the Brad-tag and the enthalpy of the competitive titration with biotin were almost equal to the binding enthalpy of the non-competitive titration of core-bradavidin with biotin at all three temperatures (II, Figure 5D), further indicating that the Brad-tag was bound to core-bradavidin. The Brad-tag showed no interaction when titrated to avidin, streptavidin or rhizavidin at 40 ºC (II, Figure S6), suggesting a specificity for core-bradavidin.

Table 5. The thermodynamic parameters of the ligand binding properties of core-bradavidin, wt bradavidin and bradavidin II analyzed by ITC. Modified with permission from II and III.

Protein	Ligand	T [ºC]	pH	ΔH [kcal mol^{-1}]	-TΔS [kcal mol^{-1}]	ΔG [kcal mol^{-1}]	K_d [M]
Core-bradavidin	Brad-tag	15	7	1.7 ± 0.2	-7.7	-6.1	$2.5 \pm 0.5 \times 10^{-5}$
Brad-tag / core-bradavidin	Biotin	15	7	-17.3 ± 0.0	ND[a]	ND[a]	$<10^{-9}$
Core-bradavidin	Biotin	15	7	-15.9 ± 0.1	ND[a]	ND[a]	$<10^{-9}$
Core-bradavidin	Brad-tag–EGFP	15	7	-0.5 ± 0.1	-6.8	-7.3	$2.8 \pm 0.8 \times 10^{-6}$ [b]
wt Bradavidin	Biotin	15	7	-18.9 ± 0.1	10.1	-9.1	$1.3 \pm 0.1 \times 10^{-7}$
Core-bradavidin	Brad-tag	25	7	ND[c]	ND[c]	ND[c]	ND[c]
Brad-tag / core-bradavidin	Biotin	25	7	-20.5 ± 0.1	ND[a]	ND[a]	$<10^{-9}$
Core-bradavidin	Biotin	25	7	-20.1 ± 0.1	ND[a]	ND[a]	$<10^{-9}$
Core-bradavidin	Brad-tag–EGFP	25	7	-1.0 ± 0.1	-6.5	-7.5	$3.1 \pm 1.0 \times 10^{-6}$ [b]
wt Bradavidin	Biotin	25	7	-18.8 ± 0.2	9.7	-9.0	$2.4 \pm 0.2 \times 10^{-7}$
Core-bradavidin	Brad-tag	40	7	-4.4 ± 0.3	-2.2	-6.6	$2.6 \pm 0.3 \times 10^{-5}$
Brad-tag / core-bradavidin	Biotin	40	7	-21.4 ± 0.1	ND[a]	ND[a]	$<10^{-9}$
Core-bradavidin	Biotin	40	7	-26.4 ± 0.1	ND[a]	ND[a]	$<10^{-9}$
wt Bradavidin	Biotin	40	7	-17.6 ± 0.6	8.3	-9.3	$3.1 \pm 0.8 \times 10^{-7}$
Bradavidin II	Desthiobiotin	40	3	-21.7 ± 0.3	11.8	-9.9	$1.2 \pm 14.6 \times 10^{-7}$
Bradavidin II / desthiobiotin	Biotin	40	3	-23.1 ± 0.1	8.5	-14.6	$6.6 \pm 1.5 \times 10^{-11}$
Bradavidin II	Biotin	40	3	-26.5 ± 0.4	ND[a]	ND[a]	$<10^{-9}$

[a] K_d could not be determined as it exceeded the sensitivity limit of the ITC.
[b] A rough estimate because the noise level in the thermogram was relatively high.
[c] Could not be determined.

The affinity of bradavidin II towards biotin exceeded the sensitivity limit of the instrument. Therefore, we decided to use a displacement method, which allows the determination of the binding isotherm of a ligand that is competitively inhibited with ligand binding to an identical binding site with a weaker affinity than the displacing ligand. The K_d may be solved when the affinities of the two ligands do not differ in their K_d more than six orders of magnitude (Sigurskjold 2000). Bradavidin II was first titrated with desthiobiotin (the concentration ranging from 15 to 500 μM), followed by a competitive titration with biotin (75 μM) to precisely determine the affinity. The analysis revealed a $K_d = 1.2 \pm 0.2 \times 10^{-7}$ M for the bradavidin II–desthiobiotin complex, and the displacement of 500 μM desthiobiotin by biotin revealed a $K_d = 6.6 \pm 1.5 \times 10^{-11}$ M for the bradavidin II–biotin complex (Table 5 and III, Figure 5).

5.2.4 Oligomeric state of bradavidin II

A DLS analysis revealed a dynamic oligomeric state for Bradavidin II. At pH 3 (0.5 M acetic acid), below a concentration of 0.4 mg/ml, the protein was mostly monomeric (Figure 9A and C) even though the temperature was raised from 20 to 90 °C (Table 6). At a higher protein concentration (>1 mg/ml) oligomers were observed and the protein aggregated at increasing temperatures with a transition temperature (T_r) of 50 °C (Table 6). Biotin had a stabilizing effect as no aggregation was observed at 90 °C even at a protein concentration of 1 mg/ml. When the pH was increased to 5 (50 mM sodium phosphate, 100 mM NaCl, 0.1 % DMSO), oligomers were detected already at room temperature, but the presence of biotin stabilized the protein (Figure 9B), as the onset of aggregation was detected at higher temperatures compared with samples without biotin (Table 6). Bradavidin II was poorly soluble in a phosphate buffer at pH 7 (50 mM sodium phosphate, 100 mM NaCl), as precipitation was even visually observable and mostly aggregates were observed by DLS.

The oligomeric state of bradavidin II was also analyzed by native mass spectrometry in 25 mM ammonium acetate (pH 6.8). At a low concentration (0.25 mg/ml) bradavidin II was mostly monomeric with a small amount of dimeric protein. At an increasing concentration the amount of the oligomeric forms increased and at concentration of 1 mg/ml, bradavidin II was mostly trimeric, but no aggregation was observed (III, Figure 8). The addition of biotin did not cause significant changes in the oligomeric distribution (data not shown).

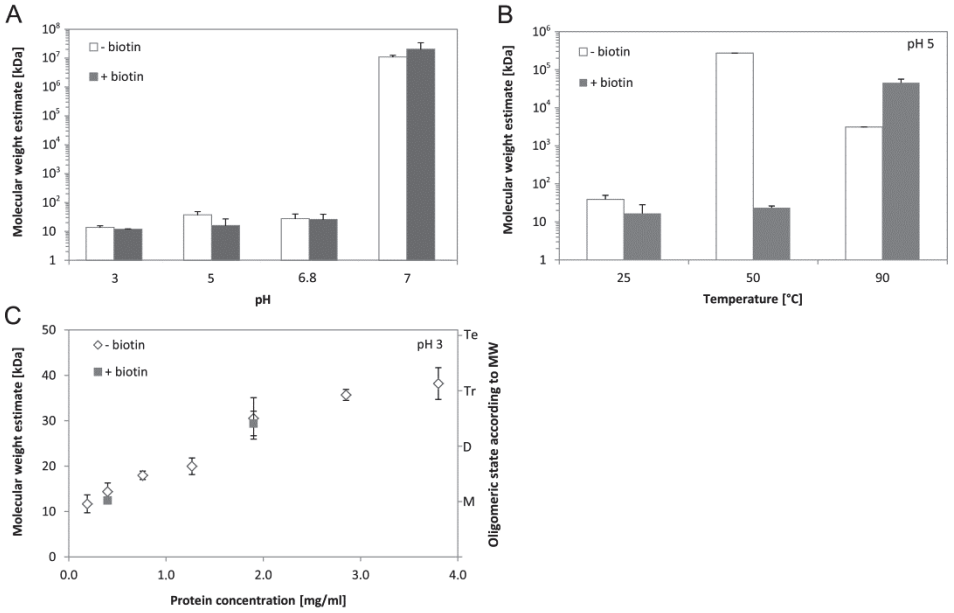

Figure 9. The DLS analyses of bradavidin II in the following buffers: a 0.5 M acetic acid containing 0.1 % DMSO (pH 3), a 50 mM Na-phosphate buffer containing 100 mM NaCl and 0.1 % DMSO (pH 5), 25 mM ammonium acetate containing 0.1 % DMSO (pH 6.8) and a 50 mM Na-phosphate buffer containing 100 mM NaCl (pH 7). **A**) The oligomeric state of bradavidin II (0.4 mg/ml) at different pH values. **B**) The oligomeric state of bradavidin II (0.4 mg/ml) at pH 5 varied at different temperatures. **C**) At pH 3, the oligomeric state of bradavidin II increased with an increasing protein concentration, both in the absence and presence of biotin. M indicates monomer (12.24 kDa), D indicates dimer (24.48 kDa), Tr indicates trimer (36.72 kDa) and Te indicates tetramer (48.96 kDa). Modified with permission from III.

5.2.5 Thermal stability of bradavidins

The thermal stability of bradavidins was studied by DSC. The melting temperatures (T_m) for wt bradavidin in the absence and in the presence of biotin were quite similar (96.2 ± 0.1 ºC and 101.7 ± 0.1 ºC, respectively; Table 6) and the stabilizing effect of biotin was far less pronounced than that observed for core-bradavidin (T_m values 73.2 ± 0.3 ºC and 97.9 ± 0.2 ºC; in the absence and in the presence of biotin, respectively; Table 6). Both wt bradavidin and core-bradavidin showed irreversible unfolding in a DSC analysis that is typical for avidins.

Bradavidin II was thermally less stable than wt bradavidin (Table 6), as was expected, because the oligomerization of avidins usually increases their thermal stability (Laitinen et al. 2001) and because wt bradavidin is a tetrameric protein, whereas bradavidin II forms loose oligomers. The thermal stability of bradavidin II increased when the pH was increased from 3 to 5. A further stabilizing effect was

not detected when the pH was increased to 6.8. At pH 7, the protein aggregated and could not be measured. The presence of biotin significantly stabilized bradavidin II under all pH conditions measured. The T_m was found to be slightly dependent on protein concentration in the presence of biotin. Unexpectedly, bradavidin II showed partially reversible unfolding at pH 3 in the presence of biotin, but under all other measured conditions, the unfolding was irreversible (III, Figure 6).

Table 6. The thermal stability of core-bradavidin, wt bradavidin and bradavidin II analyzed by differential scanning calorimetry (DSC) and dynamic light scattering (DLS). Modified with permission from II and III.

Protein	DSC		DLS	
	T_m –biotin [ºC]	T_m +biotin [ºC]	T_r –biotin [ºC]	T_r +biotin [ºC]
Core-bradavidin (pH 7, ~0.2 mg/ml)	73.2±0.3	97.9±0.2		
Wt bradavidin (pH 7, ~0.2 mg/ml)	96.2±0.02	101.7±0.1		
Bradavidin II (pH 3, 0.2 mg/mL)	50.9±1.4	83.9±0.7		
Bradavidin II (pH 3, 0.4 mg/mL)	50.3±1.1	84.6±0.8	NT[b]	NT[b]
Bradavidin II (pH 3, 0.6 mg/mL)	50.3±0.9	85.2±1.3		
Bradavidin II (pH 3, 1.0 mg/mL)			50	NT[b]
Bradavidin II (pH 5, 0.2 mg/mL)	66.5	90.4		
Bradavidin II (pH 5, 0.4 mg/mL)	66.3	93.2	50	75
Bradavidin II (pH 5, 0.6 mg/mL)	66.5	85.7[a]		
Bradavidin II (pH 5, 1.0 mg/mL)			NT[b]	NT[b]
Bradavidin II (pH 6.8, 0.2 mg/mL)	62.4	88.4		
Bradavidin II (pH 6.8, 0.4 mg/mL)	63.3	90.0		
Bradavidin II (pH 6.8, 0.6 mg/mL)	63.7	90.9		
Bradavidin II (pH 7, 0.25 mg/mL)			45	65
Bradavidin II (pH 7, 0.4 mg/ml)			ND[c]	ND[c]

[a] A weak second peak corresponding to the apo form was observed (T_m = 67.2 °C), most likely indicating the presence of protein forms not accessible to biotin (aggregates).
[b] No clear transition identified.
[c] Could not be determined as the protein was heavily aggregated.

5.2.6 Brad-tag-fusion proteins

The potential of using the Brad-tag as an N- or C-terminal affinity tag was studied by creating four different Brad-tag-EGFP fusion proteins (II, Figure 6A) with and without a histidine tag (His-tag). According to a spectrofluorometric analysis of cellular lysates, all recombinant EGFPs were expressed in *E. coli*. However, only the N-terminally tagged Brad-tag–EGFP and Brad-tag–EGFP–His-tag were clearly

recognized by an antibody against GFP in an immunoblotting analysis (II, Figure 6B) and therefore selected for further analysis.

The Brad-tag–EGFP–His-tag fusion protein prepurified with Ni-NTA affinity chromatography was found to concentrate within the core-bradavidin conjugated sepharose resin as observed under UV-light (Figure 10A). As a control experiment, the resin was incubated with free biotin before the addition of the Brad-tag–EGFP–His-tag, and showed no concentrating effect of the fusion protein, indicating that biotin could efficiently prevent the Brad-tag–core-bradavidin interaction. In another experiment, cleared cellular lysates from a Brad-tag–EGFP cultivation were incubated with a core-bradavidin-conjugated resin and the Brad-tagged EGFP was separated from other proteins (Figure 10B), although washing led to a relatively rapid dissociation (~5-10 column volumes). The emission spectrum of the isolated Brad-tag–EGFP protein strongly resembled that of free EGFP (Figure 10C).

The ITC analysis of the Brad-tag–EGFP–His-tag and core-bradavidin showed a slightly exothermic binding (Table 5 and II, Figure 5), but the low protein concentrations led to relatively high noise levels in the thermograms and only a very rough estimate of K_d ~3.0×10^{-6} M was obtained.

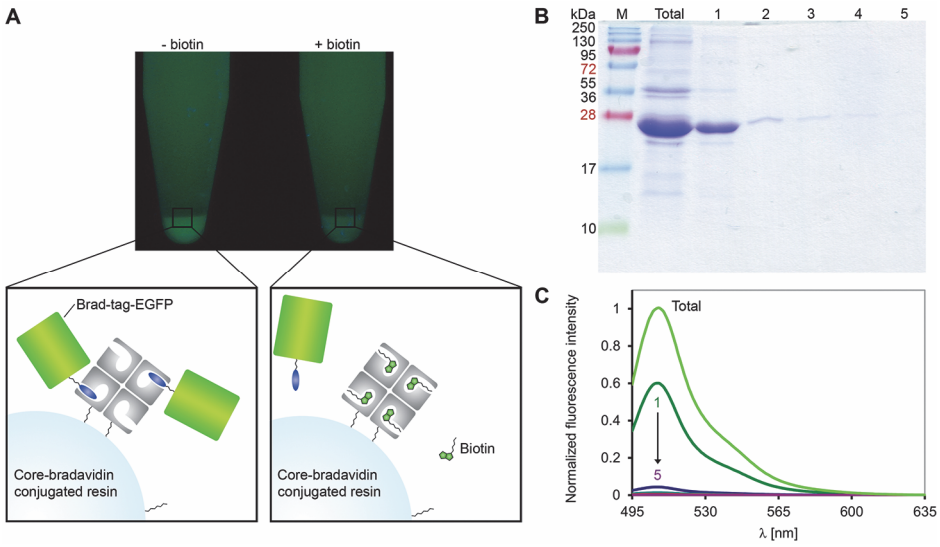

Figure 10. The purification of an EGFP fusion protein using an N-terminal Brad-tag. **A**) The Brad-tag–EGFP–His-tag was incubated with the core-bradavidin resin in the absence and in the presence of biotin and photographed under UV-light. **B**) An SDS-PAGE analysis for N-Brad-tag–EGFP-C. A cleared cellular lysate (total) of the Brad-tag–EGFP was incubated with a core-bradavidin-conjugated resin. Washing led to the elution of samples 1 to 5. **C**) The fluorescence spectra for a cleared cellular lysate (total) and eluted samples 1 to 5 from the purification experiment for Brad-tag–EGFP. Adapted with permission from II.

The specificity of the Brad-tag towards core-bradavidin was studied with a biolayer interferometry biosensor. Anti-Penta-HIS biosensors functionalized with the Brad-tag–EGFP–His-tag fusion protein showed clear binding only for core-bradavidin (at protein concentration 0.06 mg/ml), whereas wt bradavidin, avidin, streptavidin or rhizavidin showed a similar behavior as a sample with buffer only (II, Figure 8). At higher protein concentrations, core-bradavidin (0.5 mg/ml) showed some non-specific binding to non-functionalized anti-penta-HIS sensors), both in the absence and in the presence of biotin (II, Figure S7). Importantly, the presence of biotin was able to inhibit core-bradavidin binding to the Brad-tag–EGFP–His-tag-functionalized surface, thus confirming the specificity of the assay.

5.3 Defined-sized DNA construct for molecular electronics (IV)

5.3.1 Preparation of biotin-functionalized TX tiles

The gradual folding of individual *tiles A* and *B* (IV, Figure S1) and the whole B–A–B-complex (Figure 11A) from 14 different oligonucleotides (IV, Table S1) were analyzed by AGE on a 1.5 % gel. The folding of all of them was successful, although the yield for the *tile A* formation was lower than that for *tile B*. The length of the designed B–A–B-complex was 167 bases, corresponding to 57 nm and 15.9 full turns of the DNA double helix. AFM-imaging of the B–A–B-complexes (Figure 11B) dried on mica surfaces showed numerous complexes with a length of ~50-60 nm and a height of ~1.5 nm indicating the formation of correct-sized complexes.

The streptavidin-biotin interaction was used to illustrate that the designed B–A–B-complex could be functionalized by other substances. However, the incubation of streptavidin (size ~4 × 5 × 5.6 nm) (Rosano et al. 1999) with a solution containing biotinylated B–A–B-complexes (theoretical size ~2 × 57 nm) would probably result in a situation where a single streptavidin was bound to multiple biotinylated B–A–B-complexes, and thus the formation of correct complexes would not be resolved by AFM. Therefore, biotinylated hairpins were added to very similar TX tiles (IV, Figure S2) that were capable of forming long, continuous arrays. According to previous studies, two biotins per hairpin are needed to enable the tight binding of streptavidin to DNA (Li et al. 2004, Yan et al. 2003). However, those studies used a short linker between DNA and biotin, and the length of the linker is known to be an important factor in tight biotin binding (Marek et al. 1997, Gruber et al. 1997). Here, only one biotin was attached to the hairpin by a flexible 15-atom triethylene glycol (TEG) linker to optimize the binding with streptavidin.

The successful streptavidin assembly was verified by AFM (Figure 11C) and the same concept could be applied to functionalize the B–A–B-complex.

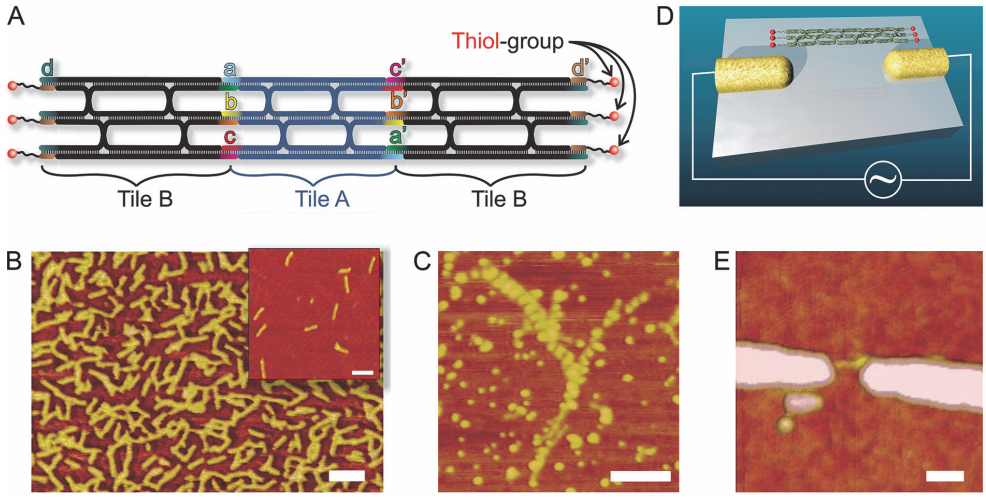

Figure 11. The design and analysis of the TX tile DNA assembly. **A**) A schematic view of the B–A–B-complex. **B**) AFM images of B–A–B-complexes dried on a mica surface, the scale bars are 100 nm. **C**) An AFM image of biotin-TEG modified TX tile chains functionalized with streptavidin, the scale bar is 100 nm. **D**) A schematic view of the dielectrophoretic trapping of the B–A–B-complex. **E**) An AFM image of a single B–A–B-complex trapped between the gold nanoelectrodes, the scale bar is 50 nm. Modified with permission from IV.

5.3.2 DEP trapping of the TX tile

Dielectrophoresis (DEP) is a phenomenon in which a polarizable particle, neutral or charged, is subjected to an inhomogenous electric field, where the electric field densities are unequal. This results in a net electric force, i.e. a dielectric force, which acts on the particle, and therefore results in the translational motion of the particle. DEP can be used for example to manipulate, orientate and separate many kinds of objects (Pohl 1978). Here, DEP trapping was used to guide the TX tile constructs (B–A–B-complexes) between the electrodes. TX tile constructs were filtered into a trapping buffer (6.5 mM Hepes, 1 mM magnesium acetate and ~2 mM NaOH to adjust the pH to 7) with low conductivity ($\sigma \approx 300$ μS cm^{-1}) before trapping. The optimal trapping results were obtained using an AC voltage of 1.2-1.5 V at a frequency of 11 MHz applied to gold nanoelectrodes for 3 to 5 minutes. The thiol-functionalization at the ends of the *tiles B* enabled the positioning and immobilization of structures between the gold nanoelectrodes through S-Au

bonding (Tuukkanen et al. 2007). After trapping, the samples were washed gently. Successful trapping resulted in the alignment of only one intact B–A–B-complex between the electrodes, as detected by AFM analysis (Figures 11D and E). Only succesfully trapped samples were selected for a conductivity analysis.

5.3.3 Conductivity of the TX tile construct

The conductivity of molecular electronic components is of great interest, and therefore the B–A–B-complex was analyzed by measuring its DC (direct current) conductivity and using an AC impedance spectroscopy. Under dry conditions (RH ~5 %) samples containing the B–A–B-complex had a resistance of the order of TΩ and were thus insulating. The samples were then measured at an RH of 90 % and the B–A–B-complex showed almost linear *IV*-curves with a resistance of ~15-20 GΩ, when the DC voltage was changed from -0.3 to 0.3 V (IV, Figure 3a). The control samples, which contained a trapping buffer without DNA and had underwent similar DEP trapping and washing procedures, produced linear *IV*-curves with larger resistances of ~30 GΩ or more (IV, Figure 3a).

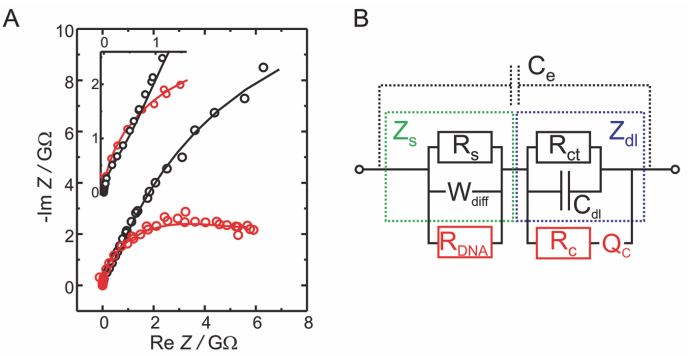

Figure 12. AC impedance spectroscopy. **A**) Cole-Cole plots and data fittings of a control sample (black circles and black solid curve, respectively) and a typical sample containing a single TX tile construct (the B–A–B-complex) in the gap (red circles and red solid curve). **B**) Equivalent circuit models of a control sample (black components) and a DNA sample (black and red components). C_e is the measured self-capacitance of the electrodes. R_s represents the small current through the "electrolyte" and the diffusive element W_{diff} describes the diffusion of the ions on the SiO_2 surface. A parallel combination of W_{diff} and R_s forms the series impedance Z_s (green) and in series with this, there is a double-layer impedance Z_{dl} (blue) comprised of the double-layer capacitance, C_{dl} (formed by ions on the electrode-"electrolyte" interface) and charge-transfer resistance, R_{ct} (the charge moving through the double-layer). R_{DNA} describes the resistance of the B–A–B-complex and R_c together with Q_c the contact impedances between the construct, linker and electrodes (Linko et al. 2009, Barsoukov & Macdonald 2005). Adapted with permission from IV.

The AC-IS was applied to study the details of electrical conductivity. First, an empty sample, i.e. only the nanoelectrodes was analyzed under dry conditions (RH ~5 %) and the obtained data was fitted to the equivalent circuit model of the setup, i.e., a simple model of parallel capacitance and resistance. The acquired values for the leakage current (described by the resistor $R_e \approx 0.3$ TΩ) and self-capacitance ($C_e \approx 7$ pF) were kept constant during other data analysis and fittings. Then, the AC-responses of the control samples were measured at a RH of 90 % and fitted with the equivalent circuit model (Figure 12B) that was a modified Randles circuit previously used for analysing the conductivity of a DNA origami (Linko et al. 2009). The fittings gave the resistance (R_s) for the control samples (i.e. "electrolyte") ~1-4 GΩ and the charge-transfer resistance (R_{ct}) 20-30 GΩ (Table 7). The sum of these two resistors roughly corresponded to the observed DC-resistance (~15-20 GΩ). The high resistance of the charge-transfer process through the double-layer could explain the poor DC-conductivity.

Finally, the AC-conductance for samples containing the B–A–B-complex was measured and compared with the control samples. The Cole-Cole-plots of samples and controls were quite similar, except for differences in the low frequency tail (Figure 12A). Therefore, the observed behavior of the samples was described by adding three elements, R_{DNA}, R_c and Q_c to the equivalent circuit of the control samples (Figure 12B). More details are presented in original communication IV.

For the B–A–B-complex, the observed ohmic conductivity $R_{s||DNA}$ was typically ~1-2 GΩ, and thus only about half of the R_s of the control (Table 7). When compared with previous studies, the conductivity through a single TX tile construct is lower than that measured for the origami ($R_{s||DNA}$ ~70 MΩ at RH = 90 %). For the B–A–B-complex and the origami, W_{diff} increased when compared with the control; Table 7). Therefore, the presence of DNA enhances the diffusion of ions along the construct via gathered water molecules. The observed ohmic conductivity for the B–A–B-complex was found to be just due to enhancement of the conductivity of the "electrolyte".

Table 7. Results from the fittings of the equivalent circuits of an empty dry sample, a typical control sample and a TX tile construct sample (control and TX tile construct are the same samples as in Figure 12A). The values in parenthesis are not fitted, but fixed based on the fitting of the dry and empty sample or the control sample. Adapted with permission from IV.

Sample	$R_s/R_{s\|\|DNA}$ [GΩ]	W_{diff} [$ps^{½}Ω^{-1}$]	C_{dl} [pF]	R_{ct} [GΩ]	R_c [GΩ]	Q_c [$ns^{nQ}Ω^{-1}$]	n_Q	R_e [TΩ]	C_e [pF]
Dry	-	-	-	-	-	-	-	0.3	6.8
Control	1.3	13	26	26	-	-	-	(0.3)	(6.8)
TX tile construct	0.9	29	1.8	(26)	1.5	0.13	0.3	(0.3)	(6.8)

5.4 Chitosan nanoparticles for gene delivery (V)

5.4.1 Formation of chitosan-DNA nanoparticles

Nanoparticle formation was studied using different chitosan to pDNA weight ratios. The average hydrodynamic diameters of nanoparticles varied from 163±36 nm to 581±194 nm as determined with a DLS analysis (Figure 13A). At chitosan to pDNA weight ratios from 1:2 to 4:1, nanoparticles showing monomodal size distributions were successfully formed. The polydispersity indexes were elevated at low (w:w 1:4) and high (w:w, 8:1) chitosan to pDNA weight weight ratios (Table 8) and also the size distribution became bimodal, which may indicate aggregating nanoparticles or the presence of free molecules, i.e. a more heterogeneous sample. The zeta potentials of the nanoparticles varied from −49 mV to +28 mV (Table 8, Figure 13A, measured at pH ~5.5). At weight ratios from 2:1 to 8:1, the zeta potential remained at a level of approximately +28 mV, indicating the condensation of pDNA. The FE-SEM analysis revealed the chitosan–pDNA nanoparticles to be spherical, with an estimated size of 40 nm (Figure 13B). In addition, aggregating nanoparticles were observed. The FE-SEM was performed in the dry state and the DLS analysis in an aqueous nanoparticle suspension, which may explain the large size differences between these assays.

The AGE-analysis showed that in the nanoparticles prepared at the chitosan to pDNA weight ratios of 1:4 and 1:2, some plasmid migrated freely in the gel, suggesting that not all of the pDNA was tightly coated by chitosan (Figure 13C). When using a chitosan to pDNA weight ratio higher than 1:2, the chitosan was able to completely harvest the DNA, as all of the DNA remained in the gel loading wells. For nanoparticles containing an excess amount of plasmid (w:w, 1:4), digestion with the PstI restriction enzyme resulted in the release of most of the DNA in two fragments of expected sizes, 4120 bp and 1197 bp. For nanoparticles containing an excess amount of chitosan (w:w, 4:1), no released DNA was detected on the gel after the PstI digestion suggesting that chitosan protected the plasmid and therefore the majority of the plasmids was located inside the particle.

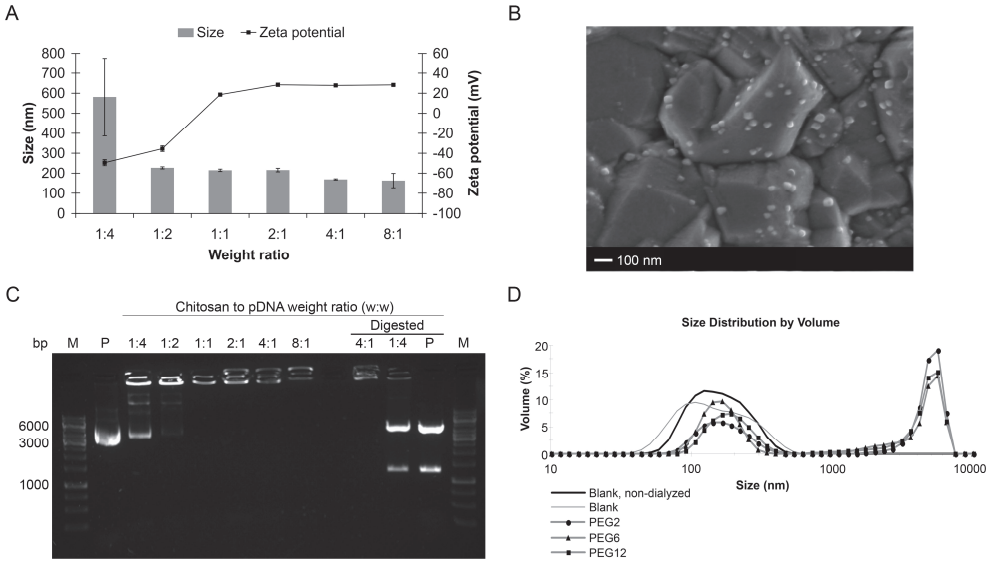

Figure 13. The analysis of chitosan-pDNA nanoparticles. **A**) The size (average hydrodynamic diameter) and the zeta potential of nanoparticles using different chitosan to pDNA weight ratios (w:w). **B**) A FE-SEM analysis of nanoparticles (prepared using a 4:1 chitosan to pDNA weight ratio) on a copper grid. **C**) An agarose gel electrophoresis analysis of chitosan-pDNA nanoparticles. M indicates the molecular weight marker and P indicates the plasmid. **D**) Particle size distribution by volume of chitosan-pDNA nanoparticles functionalized with a fluorescent Dylight 405 and different crosslinkers conjugated with the peptide PEP. Nanoparticles without any functionalization (blank) were used as a control. Modified with permission from V.

5.4.2 Functionalization of nanoparticles

Nanoparticles prepared using a chitosan to pDNA weight ratio of 4:1 were selected for functionalization studies because they were able to bind the pDNA completely according to AGE. In addition, they had a monomodal particle size distribution with a particle size of 169±3 nm and a zetapotential of 28 mV. The nanoparticles were functionalized in two steps. First, a fluorescent dye (Dy Light 405 NHS ester) and a heterobifunctional crosslinker (NHS-$PEG_{2/6/12}$-MI) were conjugated to amine groups in chitosan to generate particles containing functional groups attached via a stable amide bond. In the second step the N-terminal cysteine of the peptide (PEP or cPEP) was conjugated to the maleimide group of the crosslinker to form a stable thioether bond (Hermanson 1996). The successful coupling of fluorescent labels to nanoparticles was verified by fluorescence microscopy (unpublished results) and a fluorescence-activated cell sorting (FACS) analysis. The

presence of peptides on the surface of nanoparticles was verified by a Bradford assay (unpublished results).

The functionalization of nanoparticles with a fluorescent label, crosslinker and peptide resulted in an increased size of 159±13 to 193±13 nm, (Table 8) and also induced some aggregation, since large particles with a diameter ~5 μm appeared in all of the functionalized particles (Table 8, Figure 13D). The zeta potential of dialyzed blank nanoparticles and the peptide-functionalized nanoparticles varied between +18 and +20 mV at pH 5.3 (Table 8), indicating that functionalization does not significantly change the zeta potential of the particles.

Table 8. A dynamic light scattering analysis of chitosan-pDNA nanoparticles. The average hydrodynamic diameter by volume, the distribution of the hydrodynamic diameter by volume, the polydispersity index (PDI), and the zeta potential of non-functionalized and functionalized nanoparticles at different chitosan to pDNA weight ratios (w:w). Adapted with permission from V.

Sample	Average diameter [nm]	Distribution of diameter by volume [nm]. Percentual amount of each population by volume [nm] is indicated in parenthesis. [a]		PDI	Zeta potential [mV]
Non-functionalized nanoparticles:					
w:w 1:4	581 ± 194	18 ± 2 (6 %)	662 ± 272 (91 %)	0.362 ± 0.097	-49.4 ± 3.0 [b]
w:w 1:2	227 ± 5	227 ± 5 (100 %)		0.139 ± 0.008	-35.4 ± 2.8 [b]
w:w 1:1	215 ± 6	215 ± 6 (100 %)		0.107 ± 0.017	+18.6 ± 0.7 [b]
w:w 2:1	216 ± 9	216 ± 9 (100 %)		0.187 ± 0.011	+28.4 ± 1.7 [b]
w:w 4:1	169 ± 3	169 ± 3 (100 %)		0.188 ± 0.012	+27.8 ± 1.1 [b]
w:w 8:1	163 ± 36	33 ± 3 (11 %)	190 ± 61 (89 %)	0.248 ± 0.017	+28.3 ± 0.9 [b]
Functionalized nanoparticles:					
w:w 4:1, blank	166 ± 3	166 ± 3 (100 %)		0.215 ± 0.004	+19.6 ± 1.3 [c]
w:w 4:1, PEG_2		173 ± 6 (40 %)	5000 ± 390 (60 %)	0.259 ± 0.040	+18.9 ± 1.4 [c]
w:w 4:1, PEG_6		159 ± 13 (49 %)	4740 ± 1050 (51 %)	0.285 ± 0.053	+19.8 ± 1.6 [c]
w:w 4:1, PEG_{12}		193 ± 13 (44 %)	4860 ± 540 (53 %)	0.275 ± 0.058	+17.5 ± 0.8 [c]

[a] Size distributions containing <5 % of the total amount of particles are not shown.

[b] Particle solution, pH ~5.5.

[c] Nanoparticles in the dialysis buffer, pH 5.3.

5.4.3 Nanoparticles targeted to cells

The targetability of functionalized nanoparticles was studied by FACS. The nanoparticles functionalized with the TrkB binding peptide (PEP) showed enhanced binding to cells in a specific and time-dependent manner (Table 9) as compared with those functionalized with a control peptide (cPEP). The length of the PEG spacer arm positively correlated with the cell attachment efficiency as the

longest spacer gave the highest specificity between targeting and scrambled peptides, as well as the highest absolute level of binding of the nanoparticles.

The cells in the presence of the TeV protease showed lower fluorescence in all experimental groups (Table 9) as expected, since the protease can specifically remove an affinity peptide from the termini of the PEG spacer. However, when the TeV protease was added to the cells before the addition of the nanoparticles, the PEP-functionalized particles still showed higher fluorescence when compared with the cPEP-functionalized particles. This may be due to fast nanoparticle internalization as the measured fluorescence should result from internalized nanoparticles. Alternatively, the TeV protease was not efficient in cleaving the peptides.

Table 9. The fluorescence of cells incubated for 1, 6 and 22 hours with chitosan-pDNA nanoparticles. The nanoparticles were functionalized with crosslinkers of varying PEG spacer arms lengths and targeting peptides (PEP) or scrambled control peptides (cPEP). As a control measurement, the fluorescence of cells incubated for 22 hours in the presence of the TeV protease is shown. The results are presented as the mean*10^3 ± CV*10^3. Adapted with permission from V.

	PEG_2		PEG_6		PEG_{12}	
Incubation time	**PEP**	**cPEP**	**PEP**	**cPEP**	**PEP**	**cPEP**
1 h	7.5 ± 0.1	3.7 ± 0.2	8.0 ± 0.1	1.7 ± 0.1	9.2 ± 0.1	2.9 ± 0.3
6 h	10.5 ± 0.1	5.0 ± 0.3	12.7 ± 0.1	3.2 ± 0.3	10.8 ± 0.1	4.2 ± 0.3
22 h	19.3 ± 0.1	9.5 ± 0.2	21.6 ± 0.1	17.0 ± 0.3	22.9 ± 0.1	6.9 ± 0.3
22 h TeV protease	15.2 ± 0.1	6.6 ± 0.2	17.0 ± 0.1	12.4 ± 0.3	20.6 ± 0.1	5.7 ± 0.3

6 DISCUSSION

6.1 Feasibility of characterized biomolecular complexes

The properties and the feasibility of the developed biomolecules and their complexes produced in this study are discussed in the following sections.

6.1.1 Bifunctional avidin (I)

The bifunctionality of the dcAvd-Cys pseudotetramer was demonstated in a FRET experiment by conjugating a fluorescent maleimide to S16C-modified binding sites and by adding fluorescent biotin conjugates to the unmodified sites. The quenching of the donor emission by 73 % and the increase in the acceptor emission by 24 % were a clear indication of FRET, in other words, an indication of the close proximity of the fuorophore and the quencher. For the best quenchers nearly 100 % quenching of the fluorescence has been achieved (Kokko et al. 2007), and thus the FRET observed here was not very efficient, possibly due to anti-cooperative binding. In the avidin tetramer, the four binding-sites are arranged in a pairwise manner (Livnah et al. 1993). It has been suggested that fluorescent biotin derivatives with non-optimized spacers might bind anti-cooperatively to avidin (for example 14 atoms with fluorescein-biotin (Gruber et al. 1998)) when two fluorescent derivatives bound to a pair of adjacent biotin-binding sites can directly contact each other resulting in steric repulsion and slow association kinetics (Gruber et al. 1998). Instead, the biotin-4-fluorescein with a short four-atom spacer showed fast, non-cooperative and strong binding (Kada et al. 1999). The determined degree of labeling with a maleimidylated fluorochrome was 0.6±0.1 per dcAvd-Cys pseudotetramer and also 0.6±0.1 per Avd(S16C) tetramer, suggesting anti-cooperative binding. Therefore, the FRET could be optimized by optimizing the spacer lengths between the fluorophores, maleimide and biotin.

DcAvd-Cys proteins (I) could be chemically coupled to various substrates using maleimide linkers. Such functionalized materials would enable the subsequent attachment of two different kinds of molecules; thiol-reactive compounds and biotinylated compounds. The strategy for introducing a cysteine in the binding site

could be applied to single chain avidin (scAvd, where four binding sites are in one polypeptide chain) in combination with other known mutations to create tetrafunctional avidins. For example, an avidin variant, which prefers to bind testosterone over biotin, has been identified using the Phage display method (Riihimäki et al. 2011). In addition, an inactive binding site could be generated, for example, using a combination of the mutations S16R (Kopetzki et al. 2002) and N118M (Määttä et al. 2008). In the case of streptavidin, the combination of the mutations N23A, S27D and S45A resulted in the inactivation of the binding site (Howarth et al. 2006). The corresponding mutations for residues Asp12, Ser16 and Thr35 in avidin could be suitable for the development of an inactive form of avidin. An inactive binding site might be desirable, if the binding of the avidin tetramer to only one biotin or biotinylated molecule were preferred. The novel tetrafunctional avidin could be useful in applications, where assembly at the molecular level is required to create, for example, catalytic multienzyme complexes.

The drawback of dcAvd-Cys is its positive charge (theoretical pI 9.8), which may result in nonspecific interactions with negatively charged molecules at a physiological pH and thus limit its use for example in self-assembling DNA technology. However, avidins with a neutral or acidic charge have been successfully produced by replacing some arginine and lysine residues with neutral or acidic amino acids (Marttila et al. 1998). Therefore, engineering via mutagenesis or ordering a synthetic gene to produce a neutral dcAvd-Cys would be quite straightforward, although the folding and sufficient production of the neutral dcAvd-Cys should be experimentally studied.

6.1.2 Functional affinity tag, the Brad-tag (II)

The crystal structure at the atomic level resolution (1.78 Å) of wt bradavidin revealed that the C-terminus of each subunit folded into the ligand-binding site of the neighboring subunit so that subunits I & III and II & IV interacted with each other. In the DSC analysis the addition of biotin stabilized the C-terminally shortened core-bradavidin (T_m increased from ~73 ºC to ~98 ºC), whereas wt bradavidin was more stable than core-bradavidin and the stabilizing effect of biotin on wt bradavidin was mild (T_m increased from ~96 ºC to ~102 ºC). According to the ITC analysis, biotin had a significantly lower affinity for wt bradavidin (K_d ~2.2 × 10^{-7} M) than for core-bradavidin, which exceeded the sensitivity limit of the ITC-instrument (K_d < 10^{-9} M). Additionally, the affinity of a synthetically produced Brad-tag towards core-bradavidin was ~2.5 × 10^{-5} M. These results proved that the C-terminal Brad-tag acts as an intrinsic ligand and competes with biotin or at least biotinylated ligands for the ligand-binding site in wt bradavidin.

This was the first time when an intersubunit intrinsic interaction was reported for avidins. The full-length streptavidin (its structure solved with the N-terminal T7-tag) also has C-terminal residues folding into the biotin-binding site of the same subunit, thus acting as an intrasubunit intrinsic ligand (Le Trong et al. 2006). The biological function of the C-terminus of wt bradavidin is not known. The amino acid sequence SEKLSNTK (Brad-tag) also exists in the C-terminus of rhodavidin fom *Rhodopseudomonas palustris* (Sardo et al. 2011). Rhodavidin is highly homologous in sequence to wt bradavidin (76 % sequence identity; II, Figure 2) suggesting it may have a similar tertiary structure. However, rhodavidin was unable to bind to 2-iminobiotin sepharose and therefore was not purified and characterized in more detail (Sardo et al. 2011). Probably the C-terminal Brad-tag sequence was able to compete with 2-iminobiotin. Similarly, the purification of wt bradavidin by 2-iminobiotin was not as efficient as for core-bradavidin. Therefore, we would assume that biotin affinity chromatography could be a potentially suitable method for the purification of rhodavidin.

The functionality of the Brad-tag as an affinity tag was demonstrated by producing Brad-tag–EGFP fusion proteins and using core-bradavidin conjugated agarose beads to separate them from the other proteins in cleared cellular lysates. The ITC analysis revealed a rough estimate of K_d ~3.0±0.9 × 10^{-6} M for Brad-tag–EGFP–His-tag towards core-bradavidin and the biosensor sandwich assay also revealed the binding affinity at the micromolar range. More importantly, the Brad-tag interaction was shown to be specific for core-bradavidin, as the ITC and biosensor analyses revealed no interaction at least with avidin, streptavidin of rhizavidin.

Although the 25 μM affinity of the Brad-tag towards core-bradavidin was comparable with that of the original Strep-tag towards streptavidin (K_d ~37 μM) (Schmidt et al. 1996), it was still not high enough for efficient protein purification compared with the affinities of the Strep-tag II–streptactin pair (K_d ~1 μM) and the His-tag–Ni^{2+}-NTA pair (K_d ~10 μM) (Lata et al. 2005, Huang et al. 2009), which are commonly used in affinity purification. However, the details of the crystal structure of wt-bradavidin could be potentially exploited by rational design to produce a modified Brad-tag with an increased affinity towards core-bradavidin. Alternatively, the Brad-tag sequence could be applied to randomization and phage-display selection to find peptides with a higher affinity.

Brad-tag having an increased affinity towards core-bradavidin could find use in protein detection and purification, for example in combination with other tags in tandem affinity purification, TAP (Rigaut et al. 1999, Li 2010). Alternatively, the use of two Brad-tag sequences in a tandem fashion could increase the affinity because consecutive tags would bind to two neighboring binding sites in core-bradavidin. The use of two Strep-tag II sequences in tandem (named One-STrEP-

tag) has improved the purification yield of poorly expressed protein complexes in only one purification step (Junttila et al. 2005, BioTechniques - Strep-tag® and One-STrEP-tag for Protein-protein Interaction Analysis 2009) and also the tandem Avi-tag, named AviD-tag, resulted in a higher purification yield when compared with a single Avi-tag (Gaj et al. 2007).

6.1.3 Bradavidin II as a model for oligomerization independent protein development (III)

The crystallographic structure of bradavidin II suggested a monomeric protein and pointed out clear obstacles for a stable tetrameric or dimeric assembly. In native mass spectrometry and a DLS analysis, bradavidin II was found to be in a dynamic oligomeric state dependent on the environment. The observed dynamic oligomericity is unique among avidins that are mostly homotetramers, with the exceptions of dimeric rhizavidin (Helppolainen et al. 2007), and shwanavidin (Meir et al. 2012). Additionally, zebavidin exists as a dimer in the absence of biotin, but the addition of biotin induces its tetramerization (Taskinen et al. 2013). However, the oligomericity of other proteins, such as arylsulfatase and LptA has been reported to depend on the pH and concentration, respectively (Merten et al. 2012, Abzalimov et al. 2013). Active avidin and streptavidin monomers have been produced by applying mutations that prevent aromatic interactions and hydrophobic effects at subunit interfaces (Laitinen et al. 2003, Lim et al. 2013).

The observed dynamic oligomericity of bradavidin II is in conflict with a previous study (Helppolainen et al. 2008), where bradavidin II was proposed to be a tetramer based on gel filtration. However, in that study the mass spectrometry was performed only under denaturing conditions and the oligomericity could not be stated by that method. Therefore, the gel filtration analysis was the only method supporting the statement. This result could have been associated with a leaky stop codon, as the native mass spectrometry and SDS-PAGE revealed the appearance of two different sized protein forms in the current study (III, Figure S1). We found no clear gel filtration elution profile for homogeneous bradavidin II produced from an expression vector carrying two stop codons (unpublished results). According to these findings, gel filtration alone should be considered an insufficient method for judging the oligomeric state of a protein, which has been shown in several other studies (Philo 2006, Arakawa et al. 2010, Yumioka et al. 2010).

Bradavidin II was found to be a high affinity biotin-binding protein, although the affinity measured by competitive ITC was about five orders of magnitude weaker (K_d ~7×10^{-11} M) when compared with that of avidin (K_d ~6×10^{-16} M) (Wilchek & Bayer 1990). In bradavidin II, a conserved Tyr (Tyr33 in avidin) from

the β3 is replaced by a Phe35 that lacks the hydroxyl group and is therefore unable to form a hydrogen bond with the ureido oxygen of biotin. The missing conserved Trp (Trp110 in avidin) in the L7,8 loop may also contribute to the decrease in the affinity for biotin.

The knowledge about which amino acid residues at the bradavidin II surface prevent its tight packing into dimers or tetramers resulting in dynamic behaviour could be applied in novel biotin-binding protein development. In addition, bradavidin II could find use as a biotin-binding tag in fusion proteins instead of avidin and streptavidin, which as tetramers may perturb the oligomeric state of the target (Lim et al. 2013) or disturb the folding of large fusion partners.

6.1.4 Self-assembling TX tile construct (IV)

In order to design and develop a nanodevice, suitable scaffolds for the precise positioning of components such as proteins, gold nanodots and other such molecules or particles are needed. The remarkable self-assembling capacity and ease of modification of DNA has made it a very promising scaffolding material. Most of the earlier published self-assembling DX and TX tiles formed long, continuous structures (Winfree et al. 1998, Li et al. 2004, Le et al. 2004, Park et al. 2005a). In this study (IV) defined-sized self-assembling DNA structures were designed that could be used as a scaffolding material, for example, in molecular electronic devices for the positioning of other components such as proteins, gold nanodots etc.

Although the design of individual *tiles A* and *B* and the full B–A–B-complex was successful, the yield of the *tile A* formation was notably lower than that of the *tile B* according to an AGE-analysis (unpublished results). Therefore, it is possible that the correct assembly was limited by some constrains not observed by the methods used (i.e. the M-fold web server for the minimization of alternative association and undesired sequence complementarity, and AGE and AFM for the visualization of formed complexes). To increase the yield, the undesired sequence complementarity of oligonucleotides might need to be further diminished. Because of the complexity of the design, the sequences can nowadays be designed with advanced computer programs such as Tiamat (Williams et al. 2009), GIDEON (Birac et al. 2006) and Uniquimer (Wei et al. 2006). Programs such as caDNAno (Douglas et al. 2009b) and SARSE (Andersen et al. 2008) are useful for the design of DNA origamis.

The yield of a single B–A–B-complex correctly aligned between nanoelectrodes after the DEP trapping was rather low. The AFM imaging after trapping revealed that in addition to the B–A–B-complexes, also fragments, possibly individual *tiles A*

and *B*, were present in the sample. This might mean that the addition of a phosphate group to the 5' end of a DNA strand by a kinase or the following ligation was not efficient to produce structures stable enough for DEP trapping. Chemically 3' or 5'-phosphorylated oligonucleotides are commercially available and these might have resulted in better ligation. On the other hand, the folding of *tile A* or *B* may not have been stable enough, and therefore it is possible that the fragments observed in the sample represent a fraction of DNA components, which did not form stable assemblies.

The conductance was concluded to be mainly due to the ionized water molecules adsorbed to the DNA helices. However, although the direct electronic conductivity of the defined-sized B–A–B-complex via base pairs was insignificant, the complex could be used as a scaffold for organizing other components. In the present study (IV), a streptavidin assembly on the TX tiles modified with only one biotin at the end of a flexible triethylene glycol (TEG) linker was proven efficient, and could be applied to functionalize the B–A–B-complex by the modified avidin proteins, for example those studied in communications I-III. In order to show the usability of the B–A–B-complex in molecular electronics, both *tiles A* and *B* have later been modified by a ssDNA that basepairs with complementary strands attached to gold nanoparticles. The B–A–B-complex was functionalized with three gold nanoparticles and DEP trapped between nanoelectrodes. By optimizing the size of the gold nanoparticles, the formed complex could function as a single electron transistor, which has already been preliminarily demonstared, although the process still requires careful optimization (Tapio 2012).

6.1.5 Targetable chitosan-DNA nanoparticles (V)

Chitosan-pDNA nanoparticles were rendered targetable by covalently modifying the amines of chitosan with a heterobifunctional crosslinker and a targeting peptide. The functionalization increased the hydrodynamic diameter of the nanoparticles 4-16 %. The PDI became elevated and larger aggregates with a diameter of ~5 μm were also detected. The zeta potential decreased from +28 mV to +20 mV upon dialysis when the pH was decreased from ~5.5 to 5.3 when the buffering components were changed. Typically, the zeta potential increases with a decrease in the pH. However, in addition to the pH, the zeta potential is dependent also on the concentration of chitosan and DNA and the amount of salt in the suspension medium (Nimesh et al. 2010), and changes in these after dialysis may explain the decrease in the zeta potential. The functionalization of the primary amines on the surface of the nanoparticles only mildly altered the zeta potential as it remained between +18 and +20 mV. Previously, the zeta potential of the

chitosan-pDNA complexes decreased when the amount of endosomolytic peptides on the surface of the particles increased (MacLaughlin et al. 1998). The functionalized nanoparticles were relatively stable, although their zeta potential was moderate (~18-20 mV). Typically, particles in colloids are more stable when the zeta potential is highly negative (<−30 mV) or highly positive (>+30 mV).

The functionalization of the nanoparticles with a TrkB binding peptide enhanced binding to the target cells in a time-dependent manner. Those nanoparticles, where the peptides were attached to the longest PEG crosslinker, had the highest specificity between targeting and scrambled control peptides, and they resulted in the best binding efficiency to the cells. The lowest sterical hindrance with the longest spacer could explain the result. The higher hydrophilicity of the longer PEG spacers also could reduce the unspecific binding by van der Waals interactions. Treatment with the TeV protease caused a decrease in the fluorescence in all samples (Table 9). As TeV cleaves off the targeting peptide, the remaining measured fluorescence was expected to result from the internalized nanoparticles. In additional studies (unpublished results), where the nanoparticles were incubated with the cells for one or 12 hours before the addition of TeV, the fluorescence was higher than for samples pretreated with TeV, suggesting the rapid internalization of particles containing the targeting peptide. In addition, the particle uptake was enhanced when the length of the PEG spacer arm increased.

The natural biodegradability and good biocompatibility of chitosan and the relatively easy coupling with DNA and functionalizability through amines has made chitosan an attractive material for gene delivery (Jayakumar et al. 2010). Successful gene delivery requires that the DNA is sufficiently protected, but still released intracellularly. This delicate balance between chitosan and DNA is difficult to achieve and makes the design of non-viral gene carriers challenging (Strand et al. 2010). In this study, the samples where chitosan was able to protect DNA completely, even after PstI-digestion, were functionalized and used in cell culture studies. However, they resulted in low GFP expression levels indicating low gene transfer efficiency (unpublished results). The unpacking of the DNA from chitosan particles has been reported to be a relatively inefficient process (Ahmed & Narainhmed 2010) and actually the excess of a polycation has been shown to be important in enhancing transfection efficiency by promoting the release of polyplexes from the endo-lysosomal vesicles (Thibault et al. 2011). Therefore, a better gene transfer efficiency might have been obtained by using a higher chitosan to pDNA ratio. In addition, the specific combination of molecular weight and the degree of deacetylation that is dependent on the amine to phosphate ratio and the pH, is important for determining transgene expression (Lavertu et al. 2006).

6.1.6 Summary of the potential applications for modied biomolecules

The potential applications for the modified biomolecules developed in this study are summarized in the Table 10. It is important to remember that further studies are still needed before those applications will become a reality. Especially, the commercialization of the products would require much effort and should be conducted together with companies in the field.

Table 10. Examples of potential applications for produced modified biomolecules.

Field	Application	Suggestion
Diagnostics	Functional biosensor surface	DcAvd-Cys (I) immobilized covalently on a surface through maleimide coupling may enable detection of biotinylated binding partners
	Protein detection	Wt bradavidin (II) on sensor surface could be used for the detection of biotinylated ligands with high affinity. The C-terminal sequence would compete for a bionylated ligand leading to low-affinity binding.
Biotechnology	Protein purification	Brad-tag-core-bradavidin technology (II) could be used in affinity or tandem affinity purification
	Generation of fusion protein	Bradavidin II (III) could act as a biotin-binding tag for a fusion partner
Medicine	Controlled gene delivery	Chitosan-DNA nanoparticles (V) would enable targeting to specific cells
Molecular electronics	A single electron transistor	B–A–B-complex (IV) functionalized with gold nanodots
Biomimetics	Study of cell adhesion	Modified proteins (I-III) would enable the creation of biomimetic surfaces for studying cell adhesion at the nanometer scale
Nanotechnology	Nanoconstruction material	DcAvd-Cys (I) with a neutralized charge would enable the functionalization of self-assembling DNA constructs with thiol-reactive agents
Biophysical characterization	AFM force spectroscopy	DcAvd-Cys (I) could be covalently immobilized on a surface through maleimide coupling and used to study the properties of biotinylated molecules

6.2 Assembly of biomolecules

In this thesis, avidin proteins, DNA and chitosan were characterized and tailored using genetical or chemical modification strategies. These molecules were then used to build molecular assemblies involving non-covalent and covalent interactions.

6.2.1 Biomolecular complexes based on non-covalent interactions

The affinity of the C-terminal Brad-tag (II) towards the neighbouring binding-site of wt bradavidin was based on several hydrogen bonds and hydrophobic effects. This reversible, non-covalent interaction could find use in biochemical assays, for

example on a sensor surface, where the C-terminal Brad-tag could compete for biotinylated ligands, which have a weaker affinity than the Brad-tag. Biotinylated ligands of high-affinity would, instead, replace the Brad-tag in the binding site of wt bradavidin. Therefore, surfaces containing wt bradavidin could be used for the detection of high-affinity bionylated ligands. The C-terminally shortened core-bradavidin could find use in self-assembly applications, for example, core-bradavidin could be applied on biotinylated self-assembling DNA, and then Brad-tagged fusion proteins would assembly on top of the core-bradavidins.

The designed B–A–B-complex (IV) was based on the self-assembly of oligonucleotides through a non-covalent interaction. The advantage of self-assembly is the spontaneous adoption of a predetermined structure. However, the assembly of DNA is a reversible process, and therefore the complexes may dissociate at elevated temperatures or in other conditions of higher stringency, which may restrict their usability. Therefore, the stability of the B–A–B-complex was increased by ligating the adjacent 5' and 3' ends of oligonucleotides after the self-assembly. As was demonstrated by using biotinylated indefinite TX tiles, streptavidin will self-assemble to the biotinylated sites upon a simple incubation step and result in a functionalized complex capable of binding with other biotinylated molecules.

Chitosan–pDNA nanoparticles (V) were successfully formed by the electrostatic interactions between the positively charged chitosan and the negatively charged DNA. The advantage of the non-covalent technology is the ability to prepare complexes from DNA and chitosan without using covalent modification by agents that might alter the biocompatibility of the chitosan or damage the structure of the DNA, for example fragment it. The nature of the non-covalent interaction between chitosan and pDNA is dynamic and would thus enable the release of the intact pDNA *in vivo* after it had reached the nucleus.

6.2.2 Covalent modification of biomolecules

A chemically reactive thiol group was incorporated into the ligand-binding site of avidin and dcAvd by a single point mutation, S16C (I). The covalent modification of the free thiol-group of Avd(S16C) and dcAvd-Cys was shown to be efficient with maleimide, N-ethylmaleimide, N-maleoyl-β-alanine and a fluorescent maleimide (DY560-MI). As the introduced Cys16 in the ligand-binding site is unable to make disulfides between avidin subunits, the covalent modification does not require reduced conditions, and therefore buffer exchanges after chemical modification could be avoided. The covalent modification of the ligand-binding site with thiol-reactive agents increases the repertoire of molecules that could be

utilized in combination with avidin-biotin technology. The mutants Avd(S16C) and dcAvd-Cys were still able to bind biotin, but the affinity of Avd(S16C) was remarkably weaker than that of avidin, whereas dcAvd-Cys contained two low and two high-affinity binding sites.

In DEP trapping the non-specific physisorption of DNA to a gold electrode has been demonstrated to be quite low as DNA constructs without a thiol group diffused away from the electrodes after the trapping voltage was turned off (Tuukkanen et al. 2007). Therefore, thiol groups were included at the ends of *tiles B* of the self-assembling B–A–B-complex (IV) to make the construct immobilizable on gold-electrodes via chemical thiol-gold bonding (Herne & Tarlov 1997) in the trapping experiment. A similar technology has been utilized in previous studies to manipulate different sized dsDNA molecules (Tuukkanen et al. 2005, Tuukkanen et al. 2007) and DNA origami (Kuzyk et al. 2008). For molecular electronics components the contact with the electrode is essential, which could be guaranteed by using thiol-gold immobilization. The AFM analysis revealed that the trapping and immobilization of the B–A–B-complex between the electrodes was successful.

The targeting peptides were covalently joined to chitosan-pDNA nanoparticles (V) using maleimide and the NHS-functionalities of heterobifunctional crosslinker molecules to achieve binding to and internalization into the target cells. Because of the covalent attachment, the peptides will not detach from the particles in *in vivo* applications, although the pH and composition of the surrounding media may change substantially. The coupling method does not require expensive specialized functionalities and can therefore be applied to almost all peptides.

7 SUMMARY AND CONCLUSION

The aim in this doctoral thesis was to develop novel biomolecular tools and demonstrate their applicability. A bifunctional dual-chain avidin (dcAvd-Cys) was developed. DcAvd-Cys contains two ligand-binding domains in a polypeptide chain, one modified and the other resembling that of wt avidin. DcAvd-Cys assembles into a pseudotetramer closely resembling the tetrameric structure of wt avidin. In the modified site the S16C-mutation introduces a chemically active thiol group that can be covalently modified with thiol-reactive agents such as maleimides. The bifunctionality of dcAvd-Cys was demonstrated by FRET experiments with maleimidylated and biotinylated fluorescent labels. The option to covalently modify the binding sites with thiol-reactive agents enlarges the toolbox that can be used in combination with avidin. For example, dcAvd-Cys could be covalently immobilized through S16C-modified binding sites to a sensor surface and the other binding sites would be available for biotin binding.

The crystallographic structures of two bradavidins were solved and their properties were characterized. Some atypical behaviour was observed that has not been reported with previously characterized avidins. In the tetrameric wt bradavidin, the C-terminus acted as an intersubunit intrinsic ligand so that subunits I & III, and II & IV interacted with each other. The C-terminal amino acids were named the Brad-tag and the affinity towards the C-terminally shortened core-bradavidin was determined to be ~2.5×10^{-5} M. The feasibility of the Brad-tag was demonstrated by creating Brad-tag–EGFP fusion proteins that could be concentrated and separated from other proteins in cleared cellular lysates by core-bradavidin conjugated agarose beads. The determined affinity of the Brad-tag–EGFP fusion toward core-bradavidin was in the micromolar range. The Brad-tag would be a valuable addition to the existing affinity-tag technology.

Bradavidin II crystals (two apo and one biotin-complex) revealed a monomeric assembly. The further native mass spectrometry and DLS analysis indicated that bradavidin II was mostly monomeric at a low pH and a low concentration, but formed oligomers at an increasing pH, concentration and temperature. The weak oligomerization tendency of bradavidin II was accompanied by a biotin-binding affinity about five orders of magnitude weaker (K_d ~7×10^{-11} M) when compared

with wt avidin ($K_d \sim 6 \times 10^{-16}$ M). The knowledge about the structural and dynamic behavour of bradavidin II could be applied in the design and production of novel biotin-binding proteins. In addition, the weak oligomerization tendency of bradavidin II might be useful in fusion protein development.

The tremendous self-assembling property of DNA was utilized in designing a defined-sized triple crossover (TX) tile structure, where two different kinds of *tiles A* and *B* assembled into a complex of three tiles, the B–A–B-complex. DEP trapping was used to direct and immobilize the B–A–B-complex between gold nanoelectrodes via thiol-gold bonding. The ability to functionalize the complex was demonstrated by functionalizing similar linear biotinylated TX tile arrays with streptavidin. The conductivity of the B–A–B-complex measured by the DC and AC-IS methods was due to the ionized water molecules adsorbed into the DNA helices, whereas the direct conductivity of the B–A–B-complex was insignificant. Therefore, the structure may find use mostly as a scaffold material in molecular electronic devices for the patterning of other components such as gold nanodots etc.

The electrostatic interaction between the positively charged chitosan and the negatively charged DNA was utilized to create chitosan-DNA nanoparticles at different weight ratios. Nanoparticle formation was successful at several chitosan to pDNA weight ratios but at a ratio of 4:1, chitosan was able to couple with all of the DNA and also protect it from degradation by the PstI-restriction enzyme. These particles were functionalized with fluorescent labels and crosslinkers that enabled the attachment of targeting peptides. In cell culture trials the particles were internalized within the cells. However, the transfection efficiency was low.

In conclusion, this work produced modified avidin proteins, a self-assembling DNA-complex and chitosan-DNA nanoparticles using overlapping technologies. The produced biomolecules or biomolecular complexes could be valuable in a range of applications, for instance in bioactive biosensor surfaces, in protein purification or as gene delivery vectors, just to name a few. Moreover, the information gathered during the course of this thesis gives valuable insights for the future tailoring of biomolecules.

ACKNOWLEDGEMENTS

My warmest appreciation goes to my supervisors Vesa Hytönen and Markku Kulomaa. I thank Vesa for excellent guidance. Your enthusiasm towards science has taught me a lot of about doing scientific research. Thank you Markku your professional support and for providing a warm, pleasant working atmosphere. The work has been financially supported by the Tampere Graduate Program in Biomedicine and Biotechnology (TGPBB) and the Academy of Finland via project funding.

I wish to thank Juha Määttä for kind help with many research methods and Sampo Kukkurainen for structural modelling and for providing beautiful figures for publications. I thank my present and previous roommates: Tiia Koho, Jenita Pärssinen, Barbara Taskinen and Soili Lehtonen for the nice atmosphere, fruitful discussions and help with various problems. I am thankful for Ulla Kiiskinen, Niklas Kähkönen, Laura Kananen and Outi Väätäinen for excellent technical assistance. I would also like to thank all other members of the Molecular Biotechnology and Protein Dynamics groups: Tiina Riihimäki, Sanna Auer, Taina Viheriälä, Rolle Rahikainen, Latifeh Azizi, Sanna Pietikäinen, Magdaléna von Essen, Ville Hynninen, Chloe Thomson, and Anssi Nurminen, you have created a very pleasant working environment. During the years I have learned a lot when supervising a Master's Thesis and guiding summer students, and therefore I would like to thank Toni Grönroos, Henrik Hammarén, Markus Ojanen and Ilmari Tamminen.

I am grateful to my thesis committee members Minna Kellomäki, Jussi Toppari and Pasi Kallio for invaluable input to my thesis. I wish to thank my co-authors: Janne Jänis, Mikko Laitaoja, Tomi Airenne, Mark Johnson, Mikko Soikkeli, Veikko Linko, Seppo-Tapio Paasonen, Oded Livnah, Amit Meir, Elina Talvitie and Andrey Mikhailov, without your significant contribution this thesis could not have been finished. I warmly thank reviewers Mauri Kostiainen and Reijo Lahti for valuable comments and feedback to improve my thesis, and Helen Cooper for proofreading the English. In addition, I would like to thank all my other collaborators not already mentioned: Katri Paavilainen, Doris Pryjma, Maija Vihinen-Ranta, Teemu Ihalainen, Einari Niskanen, Kosti Tapio and Jarkko Valjakka.

I would like to thank my dear friends, my relatives and my family-in-law for all the support and encouragement during the years. I am grateful to my brother and my parents for your love and trust in me. Your help during the last couple of years has been priceless! Finally, my deepest gratitude goes to my dear husband Harri and our lovely son Toivo. You bring so much love, joy and happiness to my life. You are irreplaceable to me and therefore I dedicate this PhD thesis to both of you!

REFERENCES

Abzalimov, R.R., Bobst, C.E., Salinas, P.A., Savickas, P., Thomas, J.J. & Kaltashov, I.A. 2013, "Studies of pH-dependent self-association of a recombinant form of arylsulfatase A with electrospray ionization mass spectrometry and size-exclusion chromatography", *Analytical Chemistry,* vol. 85, no. 3, pp. 1591-1596.

Ahmed, M. & Narainhmed, R. 2010, "Cationic glycopolymers" in: Narain, R. (ed.), *Engineered Carbohydrate-Based Materials for Biomedical Applications: Polymers, Surfaces, Dendrimers, Nanoparticles, and Hydrogels,* Wiley, Hoboken, NJ, USA, pp. 143-165.

Airenne, K.J., Oker-Blom, C., Marjomaki, V.S., Bayer, E.A., Wilchek, M. & Kulomaa, M.S. 1997, "Production of biologically active recombinant avidin in baculovirus-infected insect cells", *Protein Expr Purif,* vol. 9, pp. 100-108.

Alberts, B., Johnson, A., Lewis, J., Raff, M., Roberts, K. & Walter, P. (eds.). 2002, *Molecular Biology of the Cell*, 4th edition, Garland Science, New York.

Aldaye, F.A., Lo, P.K., Karam, P., McLaughlin, C.K., Cosa, G. & Sleiman, H.F. 2009, "Modular construction of DNA nanotubes of tunable geometry and single- or double-stranded character", *Nature nanotechnology,* vol. 4, no. 6, pp. 349-352.

Aldaye, F.A., Palmer, A.L. & Sleiman, H.F. 2008, "Assembling materials with DNA as the guide", *Science (New York, N.Y.),* vol. 321, no. 5897, pp. 1795-1799.

Allen, J.P. 2009, *Biophysical Chemistry,* Wiley-Blackwell, Hoboken, NJ, USA.

American Chemical Society, 2013. Available: http://www.acs.org/content/acs/en/careers/whatchemistsdo/careers/biotechnology.html (accessed 2013, 11/22).

Andersen, E.S., Dong, M., Nielsen, M.M., Jahn, K., Lind-Thomsen, A., Mamdouh, W., Gothelf, K.V., Besenbacher, F. & Kjems, J. 2008, "DNA origami design of dolphin-shaped structures with flexible tails", *ACS nano,* vol. 2, no. 6, pp. 1213-1218.

Arakawa, T., Ejima, D., Li, T. & Philo, J.S. 2010, "The critical role of mobile phase composition in size exclusion chromatography of protein pharmaceuticals", *Journal of pharmaceutical sciences,* vol. 99, no. 4, pp. 1674-1692.

Arnau, J., Lauritzen, C., Petersen, G.E. & Pedersen, J. 2006, "Current strategies for the use of affinity tags and tag removal for the purification of recombinant proteins", *Protein expression and purification,* vol. 48, no. 1, pp. 1-13.

Aslan, F.M., Yu, Y., Mohr, S.C. & Cantor, C.R. 2005, "Engineered single-chain dimeric streptavidins with an unexpected strong preference for biotin-4-fluorescein", *Proceedings of the National Academy of Sciences of the United States of America,* vol. 102, no. 24, pp. 8507-8512.

Aydin, D., Hirscfeld-Warneken, V.C., Louban, I. & Spatz, J.P. 2012, "Micro- and Nanopatterning of Active Biomolecules and Cells" in: Textor, M. & Grandin, H.M. (eds.), *Intelligent Surfaces in Biotechnology: Scientific and Engineering Concepts, Enabling Technologies, and Translation to Bio-Oriented Applications,* Wiley, Hoboken, NJ, USA, pp. 291-319.

Baek, K., Yun, G., Kim, Y., Kim, D., Hota, R., Hwang, I., Xu, D., Ko, Y.H., Gu, G.H., Suh, J.H., Park, C.G., Sung, B.J. & Kim, K. 2013, "Free-standing, single-monomer-thicktwo-dimensionalpolymers through covalentself-assembly in solution", *Journal of American Chemical Society,* vol. 135, no. 17, pp. 6523-6528.

Balázs, N. & Sipos, P. 2007, "Limitations of pH-potentiometric titration for the determination of the degree of deacetylation of chitosan", *Carbohydrate Research,* vol. 342, no. 1, pp. 124-130.

Ball, M.P. DNA chemical structure, 2013. Available: http://commons.wikimedia.org/wiki/File:DNA_chemical_structure.svg# filelinks (accessed 2014, 01/02).

Baron, R. & McCammon, J.A. 2013, "Molecular recognition and ligand association", *Annual Review of Physical Chemistry,* vol. 64, pp. 151-175.

Barsoukov, E. & Macdonald, J.R. (eds.). 2005, *Impedance Spectroscopy: Theory, Experiment, and Applications*, 2nd edition, Wiley, Hoboken, NJ, USA.

Bayer, E.A., Ehrlich-Rogozinski, S. & Wilchek, M. 1996, "Sodium dodecyl sulfate-polyacrylamide gel electrophoretic method for assessing the quaternary state and comparative thermostability of avidin and streptavidin", *Electrophoresis,* vol. 17, pp. 1319-1324.

Bayer, E.A., Kulik, T., Adar, R. & Wilchek, M. 1995, "Close similarity among streptavidin-like, biotin-binding proteins from Streptomyces", *Biochimica et Biophysica Acta,* vol. 1263, pp. 60-66.

Becer, C.R., Hoogenboom, R. & Schubert, U.S. 2009, "Click Chemistry beyond Metal-Catalyzed Cycloaddition", *Angewandte Chemie International Edition,* vol. 48, no. 27, pp. 4900-4908.

Bensimon, A., Simon, A., Chiffaudel, A., Croquette, V., Heslot, F. & Bensimon, D. 1994, "Alignment and sensitive detection of DNA by a moving interface", *Science (New York, N.Y.),* vol. 265, no. 5181, pp. 2096-2098.

BioTechniques - Strep-tag® and One-STrEP-tag for Protein-protein Interaction Analysis, 2009. Available: http://www.biotechniques.com/protocols/Protein-protein_Interaction/Strep-tag-and-One-STrEP-tag-for-Protein-protein-Interaction-Analysis/biotechniques-115518.html (accessed 2013, 12/12).

Birac, J.J., Sherman, W.B., Kopatsch, J., Constantinou, P.E. & Seeman, N.C. 2006, "Architecture with GIDEON, a program for design in structural DNA

nanotechnology", *Journal of molecular graphics & modelling,* vol. 25, no. 4, pp. 470-480.

Björk, J., Hanke, F. & Stafström, S. 2013, "Mechanisms of halogen-based covalent self-assembly on metal surfaces", *Journal of the American Chemical Society,* vol. 135, no. 15, pp. 5768-5775.

Boehr, D.D., Nussinov, R. & Wright, P.E. 2009, "The role of dynamic conformational ensembles in biomolecular recognition", *Nature chemical biology,* vol. 5, no. 11, pp. 789-796.

Bosshard, H.R. 2001, "Molecular Recognition by Induced Fit: How Fit is the Concept?", *Physiology,* vol. 16, no. 4, pp. 171-173.

Brugnerotto, J., Lizardi, J., Goycoolea, F.M., Argüelles-Monal, W., Desbrières, J. & Rinaudo, M. 2001, "An infrared investigation in relation with chitin and chitosan characterization", *Polymer,* vol. 42, no. 8, pp. 3569-3580.

Carpino, L.A. & Han, G.Y. 1972, "9-Fluorenylmethoxycarbonyl amino-protecting group", *The Journal of organic chemistry,* vol. 37, no. 22, pp. 3404-3409.

Carroll, W.L. 1993, "Introduction to recombinant-DNA technology", *The American Journal of Clinical Nutrition,* vol. 58, no. 2 Suppl, pp. 249S-258S.

Carter, P. 1986, "Site-directed mutagenesis", *The Biochemical journal,* vol. 237, no. 1, pp. 1-7.

Chalker, J.M. & Davis, B.G. 2010, "Chemical mutagenesis: selective post-expression interconversion of protein amino acid residues", *Current opinion in chemical biology,* vol. 14, no. 6, pp. 781-789.

Chen, J.H. & Seeman, N.C. 1991, "Synthesis from DNA of a molecule with the connectivity of a cube", *Nature,* vol. 350, no. 6319, pp. 631-633.

Chitosan synthese, 2008. Available: http://commons.wikimedia.org/wiki/File: Chitosan_Synthese.svg#file (accessed 2014, 01/03).

Cobb, R.E., Si, T. & Zhao, H. 2012, "Directed evolution: an evolving and enabling synthetic biology tool", *Current opinion in chemical biology,* vol. 16, no. 3-4, pp. 285-291.

Committee on Biomolecular Materials and Processes 2008, *Inspired by Biology: From Molecules to Materials to Machines,* National Academies Press, Washington, DC, USA.

Corsi, K., Chellat, F., Yahia, L. & Fernandes, J.C. 2003, "Mesenchymal stem cells, MG63 and HEK293 transfection using chitosan-DNA nanoparticles", *Biomaterials,* vol. 24, no. 7, pp. 1255-1264.

Cronan, J.E.,Jr. 2001, "The biotinyl domain of Escherichia coli acetyl-CoA carboxylase. Evidence that the "thumb" structure id essential and that the domain functions as a dimer", *The Journal of biological chemistry,* vol. 276, no. 40, pp. 37355-37364.

Cronan, J.E.,Jr. & Reed, K.E. 2000, "Biotinylation of proteins in vivo: a useful posttranslational modification for protein analysis", *Methods in enzymology,* vol. 326, pp. 440-458.

Cuatrecasas, P. & Wilchek, M. 1968, "Single-step purification of avidine from egg white by affinity chromatography on biocytin-Sepharose columns", *Biochemical and biophysical research communications,* vol. 33, no. 2, pp. 235-239.

Di Marco, M., Shamsuddin, S., Razak, K.A., Aziz, A.A., Devaux, C., Borghi, E., Levy, L. & Sadun, C. 2010, "Overview of the main methods used to combine proteins with nanosystems: absorption, bioconjugation, and encapsulation", *International journal of nanomedicine,* vol. 5, pp. 37-49.

Diehl, F., Grahlmann, S., Beier, M. & Hoheisel, J.D. 2001, "Manufacturing DNA microarrays of high spot homogeneity and reduced background signal", *Nucleic acids research,* vol. 29, no. 7, pp. E38.

Douglas, S.M., Dietz, H., Liedl, T., Hogberg, B., Graf, F. & Shih, W.M. 2009a, "Self-assembly of DNA into nanoscale three-dimensional shapes", *Nature,* vol. 459, no. 7245, pp. 414-418.

Douglas, S.M., Marblestone, A.H., Teerapittayanon, S., Vazquez, A., Church, G.M. & Shih, W.M. 2009b, "Rapid prototyping of 3D DNA-origami shapes with caDNAno", *Nucleic acids research,* vol. 37, no. 15, pp. 5001-5006.

Einhauer, A. & Jungbauer, A. 2001, "The FLAG™ peptide, a versatile fusion tag for the purification of recombinant proteins", *Journal of Biochemical and Biophysical Methods,* vol. 49, no. 1–3, pp. 455-465.

Ellison, D., Hinton, J., Hubbard, S.J. & Beynon, R.J. 1995, "Limited proteolysis of native proteins: the interaction between avidin and proteinase K", *Protein Sci,* vol. 4, pp. 1337-1345.

Fairhead, M., Krndija, D., Lowe, E.D. & Howarth, M. 2014, "Plug-and-Play Pairing via Defined Divalent Streptavidins", *Journal of Molecular Biology,* vol. 426, no. 1, pp. 199-214.

Ferrari, F., Bonferoni, M.C., Rossi, S., Sandri, G. & Caramella, C.M. 2012, "Manufacture Techniques of Chitosan-Based Microparticles and Nanoparticles for Biopharmaceuticals" in: Sarmento, B. & das Neves, J. (eds.), *Chitosan-Based Systems for Biopharmaceuticals: Delivery, Targeting and Polymer Therapeutics,* 2nd edition, Wiley, Hoboken, NJ, USA, pp. 137-158.

Fischer, E. 1894, "Einfluss der Configuration auf die Wirkung der Enzyme", *Berichte der deutschen chemischen Gesellschaft,* vol. 27, no. 3, pp. 2985-2993.

Fu, J., Liu, M., Liu, Y. & Yan, H. 2012, "Spatially-interactive biomolecular networks organized by nucleic acid nanostructures", *Accounts of Chemical Research,* vol. 45, no. 8, pp. 1215-1226.

Fu, T.J. & Seeman, N.C. 1993, "DNA double-crossover molecules", *Biochemistry,* vol. 32, no. 13, pp. 3211-3220.

Fuchs, P., Breitling, F., Little, M. & Dübel, S. 1997, "Primary Structure and Functional scFv Antibody Expression of an Antibody Against the Human Protooncogen c-myc", *Hybridoma,* vol. 16, no. 3, pp. 227-233.

Gaj, T., Meyer, S.C. & Ghosh, I. 2007, "The AviD-tag, a NeutrAvidin/avidin specific peptide affinity tag for the immobilization and purification of

recombinant proteins", *Protein expression and purification,* vol. 56, no. 1, pp. 54-61.

García-Fuentes, L., Téllez-Sanz, R., Quesada-Soriano, I. & Barón, C. 2011, "Thermodynamics of Molecular Recognition by Calorimetry" in: Moreno-Pirajan, J.C. (ed.), *Thermodynamics - Physical Chemistry of Aqueous Systems eBook,* InTech, New York, NY, USA, pp. 1-26.

Gazit, E. 2007, *Plenty of Room For Biology at the Bottom: An Introduction to Bionanotechnology,* Imperial College Press, SGP.

Gell, C., Brockwell, D. & Smith, A. 2006, *Handbook of Single Molecule Fluorescence Spectroscopy,* Oxford University Press, UK, Oxford, GBR.

Germino, F.J., Wang, Z.X. & Weissman, S.M. 1993, "Screening for in vivo protein-protein interactions", *Proceedings of the National Academy of Sciences of the United States of America,* vol. 90, no. 3, pp. 933-937.

Gonzalez, M., Argarana, C.E. & Fidelio, G.D. 1999, "Extremely high thermal stability of streptavidin and avidin upon biotin binding", *Biomolecular engineering,* vol. 16, no. 1-4, pp. 67-72.

Goodman, R.P., Berry, R.M. & Turberfield, A.J. 2004, "The single-step synthesis of a DNA tetrahedron", *Chemical communications,* , no. 12, pp. 1372-1373.

Gradisar, H., Bozic, S., Doles, T., Vengust, D., Hafner-Bratkovic, I., Mertelj, A., Webb, B., Sali, A., Klavzar, S. & Jerala, R. 2013, "Design of a single-chain polypeptide tetrahedron assembled from coiled-coil segments", *Nature chemical biology,* vol. 9, no. 6, pp. 362-366.

Green, N.M. 1975, "Avidin", *Advances in Protein Chemistry,* vol. 29, pp. 85-133.

Gruber, H.J., Kada, G., Marek, M. & Kaiser, K. 1998, "Accurate titration of avidin and streptavidin with biotin-fluorophore conjugates in complex, colored biofluids", *Biochimica et Biophysica Acta,* vol. 1381, no. 2, pp. 203-212.

Gruber, H.J., Marek, M., Schindler, H. & Kaiser, K. 1997, "Biotin-fluorophore conjugates with poly(ethylene glycol) spacers retain intense fluorescence after binding to avidin and streptavidin", *Bioconjugate chemistry,* vol. 8, no. 4, pp. 552-559.

Häkkinen, H. 2012, "The gold-sulfur interface at the nanoscale", *Nature chemistry,* vol. 4, no. 6, pp. 443-455.

Halim, A.S., Keong, L.C., Zainol, I. & Rashid, A.H.A. 2012, "Biocompatibility and Biodegradation of Chitosan and Derivatives" in: Sarmento, B. & das Neves, J. (eds.), *Chitosan-Based Systems for Biopharmaceuticals: Delivery, Targeting and Polymer Therapeutics,* 2nd edition, Wiley, Hoboken, NJ, USA, pp. 57-74.

Halley, J.D. & Winkler, D.A. 2008, "Consistent concepts of self-organization and self-assembly", *Complexity,* vol. 14, no. 2, pp. 10-17.

Hejazi, R. & Amiji, M. 2003, "Chitosan-based gastrointestinal delivery systems", *Journal of controlled release: official journal of the Controlled Release Society,* vol. 89, no. 2, pp. 151-165.

Helppolainen, S.H., Määttä, J.A., Halling, K.K., Slotte, J.P., Hytönen, V.P., Jänis, J., Vainiotalo, P., Kulomaa, M.S. & Nordlund, H.R. 2008, "Bradavidin II from

Bradyrhizobium japonicum: a new avidin-like biotin-binding protein", *Biochim Biophys Acta,* vol. 1784, pp. 1002-1010.

Helppolainen, S.H., Nurminen, K.P., Määttä, J.A., Halling, K.K., Slotte, J.P., Huhtala, T., Liimatainen, T., Ylä-Herttuala, S., Airenne, K.J. & Närvänen, A. 2007, "Rhizavidin from Rhizobium etli: the first natural dimer in the avidin protein family", *Biochem J,* vol. 405, pp. 397-405.

Hermanson, G.T. 1996, *Bioconjugate Techniques,* Academic Press, San Diego, California, USA.

Herne, T.M. & Tarlov, M.J. 1997, "Characterization of DNA Probes Immobilized on Gold Surfaces", *Journal of the American Chemical Society,* vol. 119, no. 38, pp. 8916-8920.

Hilpert, K., Hansen, G., Wessner, H., Küttner, G., Welfle, K., Seifert, M. & Hohne, W. 2001, "Anti-c-myc antibody 9E10: epitope key positions and variability characterized using peptide spot synthesis on cellulose", *Protein Engineering Design and Selection,* vol. 14, no. 10, pp. 803-806.

Hochuli, E., Bannwarth, W., Dobeli, H., Gentz, R. & Stuber, D. 1988, "Genetic Approach to Facilitate Purification of Recombinant Proteins with a Novel Metal Chelate Adsorbent", *Nature Biotechnology,* vol. 6, no. 11, pp. 1321-1325.

Hochuli, E., Dobeli, H. & Schacher, A. 1987, "New metal chelate adsorbent selective for proteins and peptides containing neighbouring histidine residues", *Journal of chromatography,* vol. 411, pp. 177-184.

Hofmann, K., Wood, S.W., Brinton, C.C., Montibeller, J.A. & Finn, F.M. 1980, "Iminobiotin affinity columns and their application to retrieval of streptavidin", *Proceedings of the National Academy of Sciences of the United States of America,* vol. 77, no. 8, pp. 4666-4668.

Hoogenboom, H.R., Griffiths, A.D., Johnson, K.S., Chiswell, D.J., Hudson, P. & Winter, G. 1991, "Multi-subunit proteins on the surface of filamentous phage: methodologies for displaying antibody (Fab) heavy and light chains", *Nucleic Acids Research,* vol. 19, no. 15, pp. 4133-4137.

Hopp, T.P., Prickett, K.S., Price, V.L., Libby, R.T., March, C.J., Pat Cerretti, D., Urdal, D.L. & Conlon, P.J. 1988, "A Short Polypeptide Marker Sequence Useful for Recombinant Protein Identification and Purification", *Nature Biotechnology,* vol. 6, no. 10, pp. 1204-1210.

Howarth, M., Chinnapen, D.J., Gerrow, K., Dorrestein, P.C., Grandy, M.R., Kelleher, N.L., El-Husseini, A. & Ting, A.Y. 2006, "A monovalent streptavidin with a single femtomolar biotin binding site", *Nature methods,* vol. 3, no. 4, pp. 267-273.

Huang, Z., Hwang, P., Watson, D.S., Cao, L. & Szoka, F.C.,Jr 2009, "Tris-nitrilotriacetic acids of subnanomolar affinity toward hexahistidine tagged molecules", *Bioconjugate chemistry,* vol. 20, no. 8, pp. 1667-1672.

Hytönen, V.P., Hörhä, J., Airenne, T.T., Niskanen, E.A., Helttunen, K.J., Johnson, M.S., Salminen, T.A., Kulomaa, M.S. & Nordlund, H.R. 2006, "Controlling quaternary structure assembly: subunit interface engineering and crystal

structure of dual chain avidin", *Journal of Molecular Biology,* vol. 359, no. 5, pp. 1352-1363.

Hytönen, V.P., Laitinen, O.H., Airenne, T.T., Kidron, H., Meltola, N.J., Porkka, E., Hörhä, J., Paldanius, T., Määttä, J.A. & Nordlund, H.R. 2004, "Efficient production of active chicken avidin using a bacterial signal peptide in Escherichia coli", *Biochem J,* vol. 384, pp. 385-390.

Hytönen, V.P., Laitinen, O.H., Grapputo, A., Kettunen, A., Savolainen, J., Kalkkinen, N., Marttila, A.T., Nordlund, H.R., Nyholm, T.K., Paganelli, G. & Kulomaa, M.S. 2003, "Characterization of poultry egg-white avidins and their potential as a tool in pretargeting cancer treatment", *Biochem J,* vol. 372, pp. 219-225.

Hytönen, V.P., Nordlund, H.R., Hörhä, J., Nyholm, T.K., Hyre, D.E., Kulomaa, T., Porkka, E.J., Marttila, A.T., Stayton, P.S., Laitinen, O.H. & Kulomaa, M.S. 2005, "Dual-affinity avidin molecules", *Proteins,* vol. 61, no. 3, pp. 597-607.

Ishihara, M., Fujita, M., Kishimoto, S., Hattori, H. & Kanatani, Y. 2012, "Biological, Chemical, and Physical Compatibility of Chitosan and Biopharmaceuticals" in: Sarmento, B. & das Neves, J. (eds.), *Chitosan-Based Systems for Biopharmaceuticals: Delivery, Targeting and Polymer Therapeutics,* 2nd edition, Wiley, Hoboken, NJ, USA, pp. 93-106.

Jadzinsky, P.D., Calero, G., Ackerson, C.J., Bushnell, D.A. & Kornberg, R.D. 2007, "Structure of a thiol monolayer-protected gold nanoparticle at 1.1 A resolution", *Science,* vol. 318, no. 5849, pp. 430-433.

Jain, S. & Amiji, M. 2012, "Target-Specific Chitosan-Based Nanoparticle Systems for Nucleic Acid Delivery" in: Sarmento, B. & das Neves, J. (eds.), *Chitosan-Based Systems for Biopharmaceuticals: Delivery, Targeting and Polymer Therapeutics,* 2nd edition, Wiley, Hoboken, NJ, USA, pp. 277-300.

Janes, K.A., Calvo, P. & Alonso, M.J. 2001, "Polysaccharide colloidal particles as delivery systems for macromolecules", *Advanced Drug Delivery Reviews,* vol. 47, no. 1, pp. 83-97.

Jayakumar, R., Chennazhi, K.P., Muzzarelli, R.A.A., Tamura, H., Nair, S.V. & Selvamurugan, N. 2010, "Chitosan conjugated DNA nanoparticles in gene therapy", *Carbohydrate Polymers,* vol. 79, no. 1, pp. 1-8.

Jin, W., Lin, X., Lv, S., Zhang, Y., Jin, Q. & Mu, Y. 2009, "A DNA sensor based on surface plasmon resonance for apoptosis-associated genes detection", *Biosensors & bioelectronics,* vol. 24, no. 5, pp. 1266-1269.

Junttila, M.R., Saarinen, S., Schmidt, T., Kast, J. & Westermarck, J. 2005, "Single-step Strep-tag purification for the isolation and identification of protein complexes from mammalian cells", *Proteomics,* vol. 5, no. 5, pp. 1199-1203.

Kada, G., Falk, H. & Gruber, H.J. 1999, "Accurate measurement of avidin and streptavidin in crude biofluids with a new, optimized biotin-fluorescein conjugate", *Biochimica et Biophysica Acta,* vol. 1427, no. 1, pp. 33-43.

Ke, Y., Ong, L.L., Shih, W.M. & Yin, P. 2012, "Three-dimensional structures self-assembled from DNA bricks", *Science,* vol. 338, no. 6111, pp. 1177-1183.

Keefe, A.D., Wilson, D.S., Seelig, B. & Szostak, J.W. 2001, "One-step purification of recombinant proteins using a nanomolar-affinity streptavidin-binding peptide, the SBP-Tag", *Protein expression and purification,* vol. 23, no. 3, pp. 440-446.

King, N.P., Sheffler, W., Sawaya, M.R., Vollmar, B.S., Sumida, J.P., Andre, I., Gonen, T., Yeates, T.O. & Baker, D. 2012, "Computational design of self-assembling protein nanomaterials with atomic level accuracy", *Science (New York, N.Y.),* vol. 336, no. 6085, pp. 1171-1174.

Klumb, L.A., Chu, V. & Stayton, P.S. 1998, "Energetic roles of hydrogen bonds at the ureido oxygen binding pocket in the streptavidin-biotin complex", *Biochemistry,* vol. 37, no. 21, pp. 7657-7663.

Kokko, T., Kokko, L., Soukka, T. & Lövgren, T. 2007, "Homogeneous non-competitive bioaffinity assay based on fluorescence resonance energy transfer", *Analytica Chimica Acta,* vol. 585, no. 1, pp. 120-125.

Kolb, H.C., Finn, M.G. & Sharpless, K.B. 2001, "Click Chemistry: Diverse Chemical Function from a Few Good Reactions", *Angewandte Chemie (International ed. in English),* vol. 40, no. 11, pp. 2004-2021.

Kopetzki, E., Muller, R., Engh, R., Schmitt, U., Deger, A. & Brandstetter, H., 2002, "Recombinant inactive avidin mutants", US6391571 (B1).

Korndörfer, I.P. & Skerra, A. 2002, "Improved affinity of engineered streptavidin for the Strep-tag II peptide is due to a fixed open conformation of the lid-like loop at the binding site", *Protein science : a publication of the Protein Society,* vol. 11, no. 4, pp. 883-893.

Korpela, J.K., Kulomaa, M.S., Elo, H.A. & Tuohimaa, P.J. 1981, "Biotin-binding proteins in eggs of oviparous vertebrates", *Experientia,* vol. 37, pp. 1065-1066.

Koshland, D.E. 1958, "Application of a Theory of Enzyme Specificity to Protein Synthesis", *Proceedings of the National Academy of Sciences of the United States of America,* vol. 44, no. 2, pp. 98-104.

Kuzyk, A., Yurke, B., Toppari, J.J., Linko, V. & Törmä, P. 2008, "Dielectrophoretic trapping of DNA origami", *Small,* vol. 4, no. 4, pp. 447-450.

LaBean, T.H., Yan, H., Kopatsch, J., Liu, F., Winfree, E., Reif, J.H. & Seeman, N.C. 2000, "Construction, Analysis, Ligation, and Self-Assembly of DNA Triple Crossover Complexes", *Journal of the American Chemical Society,* vol. 122, no. 9, pp. 1848-1860.

Laitinen, O.H., Hytönen, V.P., Nordlund, H.R. & Kulomaa, M.S. 2006, "Genetically engineered avidins and streptavidins", *Cellular and molecular life sciences: CMLS,* vol. 63, no. 24, pp. 2992-3017.

Laitinen, O.H., Marttila, A.T., Airenne, K.J., Kulik, T., Livnah, O., Bayer, E.A., Wilchek, M. & Kulomaa, M.S. 2001, "Biotin induces tetramerization of a recombinant monomeric avidin. A model for protein-protein interactions", *The Journal of biological chemistry,* vol. 276, no. 11, pp. 8219-8224.

Laitinen, O.H., Nordlund, H.R., Hytönen, V.P., Uotila, S.T., Marttila, A.T., Savolainen, J., Airenne, K.J., Livnah, O., Bayer, E.A., Wilchek, M. &

Kulomaa, M.S. 2003, "Rational design of an active avidin monomer", *The Journal of biological chemistry,* vol. 278, no. 6, pp. 4010-4014.

Lamla, T. & Erdmann, V.A. 2004, "The Nano-tag, a streptavidin-binding peptide for the purification and detection of recombinant proteins", *Protein expression and purification,* vol. 33, no. 1, pp. 39-47.

Lata, S., Reichel, A., Brock, R., Tampé, R. & Piehler, J. 2005, "High-affinity adaptors for switchable recognition of histidine-tagged proteins", *Journal of the American Chemical Society,* vol. 127, no. 29, pp. 10205-10215.

Lavertu, M., Méthot, S., Tran-Khanh, N. & Buschmann, M.D. 2006, "High efficiency gene transfer using chitosan/DNA nanoparticles with specific combinations of molecular weight and degree of deacetylation", *Biomaterials,* vol. 27, no. 27, pp. 4815-4824.

Le Trong, I., Humbert, N., Ward, T.R. & Stenkamp, R.E. 2006, "Crystallographic analysis of a full-length streptavidin with its C-terminal polypeptide bound in the biotin binding site", *Journal of Molecular Biology,* vol. 356, no. 3, pp. 738-745.

Le, J.D., Pinto, Y., Seeman, N.C., Musier-Forsyth, K., Taton, T.A. & Kiehl, R.A. 2004, "DNA-Templated Self-Assembly of Metallic Nanocomponent Arrays on a Surface", *Nano Letters,* vol. 4, no. 12, pp. 2343-2347.

Lee, Y.S. 2011, *Self-Assembly and Nanotechnology Systems: Design, Characterization, and Applications,* Wiley, Hoboken, NJ, USA.

Li, H., LaBean, T.H. & Kenan, D.J. 2006, "Single-chain antibodies against DNA aptamers for use as adapter molecules on DNA tile arrays in nanoscale materials organization", *Organic & biomolecular chemistry,* vol. 4, no. 18, pp. 3420-3426.

Li, H., Park, S.H., Reif, J.H., LaBean, T.H. & Yan, H. 2004, "DNA-templated self-assembly of protein and nanoparticle linear arrays", *Journal of the American Chemical Society,* vol. 126, no. 2, pp. 418-419.

Li, Y. 2010, "Commonly used tag combinations for tandem affinity purification", *Biotechnology and applied biochemistry,* vol. 55, no. 2, pp. 73-83.

Lim, K.H., Huang, H., Pralle, A. & Park, S. 2013, "Stable, high-affinity streptavidin monomer for protein labeling and monovalent biotin detection", *Biotechnology and bioengineering,* vol. 110, no. 1, pp. 57-67.

Lin, C., Liu, Y. & Yan, H. 2009, "Designer DNA nanoarchitectures", *Biochemistry,* vol. 48, no. 8, pp. 1663-1674.

Lindoy, L.F., Richardson, C. & Clegg, J.K. 2012, "Bioinspired Self-Assembly I: Self-Assembled Structures" in: Swiegers, G. (ed.), *Bioinspiration and Biomimicry in Chemistry: Reverse-Engineering Nature,* Wiley, Somerset, NJ, USA, pp. 17-46.

Linko, V., Paasonen, S.T., Kuzyk, A., Törmä, P. & Toppari, J.J. 2009, "Characterization of the conductance mechanisms of DNA origami by AC impedance spectroscopy", *Small,* vol. 5, no. 21, pp. 2382-2386.

Liu, D., Park, S.H., Reif, J.H. & LaBean, T.H. 2004, "DNA nanotubes self-assembled from triple-crossover tiles as templates for conductive nanowires",

Proceedings of the National Academy of Sciences of the United States of America, vol. 101, no. 3, pp. 717-722.

Liu, Y., Lin, C., Li, H. & Yan, H. 2005, "Aptamer-Directed Self-Assembly of Protein Arrays on a DNA Nanostructure", *Angewandte Chemie International Edition,* vol. 44, no. 28, pp. 4333-4338.

Livnah, O., Bayer, E.A., Wilchek, M. & Sussman, J.L. 1993, "Three-dimensional structures of avidin and the avidin-biotin complex", *Proceedings of the National Academy of Sciences of the United States of America,* vol. 90, no. 11, pp. 5076-5080.

Lodish, H., Berk, A., Zipursky, S.L., Matsudaira, P., Baltimore, D. & Darnell, J. 2000, *Molecular Cell Biology,* 4th edn, W. H. Freeman, New York.

Love, J.C., Estroff, L.A., Kriebel, J.K., Nuzzo, R.G. & Whitesides, G.M. 2005, "Self-assembled monolayers of thiolates on metals as a form of nanotechnology", *Chemical reviews,* vol. 105, no. 4, pp. 1103-1169.

Luna, R.E., Akabayov, S.R., Ziarek, J.J. & Wagner, G. 2013, "Examining weak protein-protein interactions in start codon recognition via NMR spectroscopy", *The FEBS journal,* in press.

Ma, Z., Wu, X., Cao, M., Pan, W., Zhu, F., Chen, J. & Qi, Z. 2003, "Selection of trkB-binding peptides from a phage-displayed random peptide library", *Science in China. Series C, Life sciences / Chinese Academy of Sciences,* vol. 46, no. 1, pp. 77-86.

Määttä, J.A., Airenne, T.T., Nordlund, H.R., Jänis, J., Paldanius, T.A., Vainiotalo, P., Johnson, M.S., Kulomaa, M.S. & Hytönen, V.P. 2008, "Rational modification of ligand-binding preference of avidin by circular permutation and mutagenesis", *Chembiochem: a European journal of chemical biology,* vol. 9, no. 7, pp. 1124-1135.

Määttä, J.A., Eisenberg-Domovich, Y., Nordlund, H.R., Hayouka, R., Kulomaa, M.S., Livnah, O. & Hytönen, V.P. 2011, "Chimeric avidin shows stability against harsh chemical conditions – biochemical analysis and 3D structure", *Biotechnology and bioengineering,* vol. 108, no. 3, pp. 481-490.

Määttä, J., Helppolainen, S., Hytönen, V., Johnson, M., Kulomaa, M., Airenne, T. & Nordlund, H. 2009, "Structural and functional characteristics of xenavidin, the first frog avidin from Xenopus tropicalis", *BMC Structural Biology,* vol. 9, no. 1, pp. 63.

MacLaughlin, F.C., Mumper, R.J., Wang, J., Tagliaferri, J.M., Gill, I., Hinchcliffe, M. & Rolland, A.P. 1998, "Chitosan and depolymerized chitosan oligomers as condensing carriers for in vivo plasmid delivery", *Journal of controlled release : official journal of the Controlled Release Society,* vol. 56, no. 1-3, pp. 259-272.

Mansouri, S., Lavigne, P., Corsi, K., Benderdour, M., Beaumont, E. & Fernandes, J.C. 2004, "Chitosan-DNA nanoparticles as non-viral vectors in gene therapy: strategies to improve transfection efficacy", *European journal of pharmaceutics and biopharmaceutics: official journal of Arbeitsgemeinschaft fur Pharmazeutische Verfahrenstechnik e.V,* vol. 57, no. 1, pp. 1-8.

Mao, H.Q., Roy, K., Troung-Le, V.L., Janes, K.A., Lin, K.Y., Wang, Y., August, J.T. & Leong, K.W. 2001, "Chitosan-DNA nanoparticles as gene carriers: synthesis, characterization and transfection efficiency", *Journal of controlled release: official journal of the Controlled Release Society,* vol. 70, no. 3, pp. 399-421.

Mardyani, S., Jiang, W., Lai, J., Zhang, J. & Chan, W.C.W. 2004, "Bioinspired approaches to building nanoscale devices" in: Stroscio, M.A. & Dutta, M. (eds.), *Biological Nanostructures and Applications of Nanostructures in Biology: Electrical, Mechanical, & Optical Properties,* Kluwer Academic Publishers, Secaucus, NJ, USA, pp. 149-160.

Marek, M., Kaiser, K. & Gruber, H.J. 1997, "Biotin-pyrene conjugates with poly(ethylene glycol) spacers are convenient fluorescent probes for avidin and streptavidin", *Bioconjugate chemistry,* vol. 8, no. 4, pp. 560-566.

Marttila, A.T., Airenne, K.J., Laitinen, O.H., Kulik, T., Bayer, E.A., Wilchek, M. & Kulomaa, M.S. 1998, "Engineering of chicken avidin: a progressive series of reduced charge mutants", *FEBS letters,* vol. 441, no. 2, pp. 313-317.

Mattson, G., Conklin, E., Desai, S., Nielander, G., Savage, M.D. & Morgensen, S. 1993, "A practical approach to crosslinking", *Molecular biology reports,* vol. 17, no. 3, pp. 167-183.

Maune, H.T., Han, S.P., Barish, R.D., Bockrath, M., Iii, W.A., Rothemund, P.W. & Winfree, E. 2010, "Self-assembly of carbon nanotubes into two-dimensional geometries using DNA origami templates", *Nature nanotechnology,* vol. 5, no. 1, pp. 61-66.

Meir, A., Helppolainen, S.H., Podoly, E., Nordlund, H.R., Hytönen, V.P., Määttä, J.A., Wilchek, M., Bayer, E.A., Kulomaa, M.S. & Livnah, O. 2009, "Crystal structure of rhizavidin: insights into the enigmatic high-affinity interaction of an innate biotin-binding protein dimer", *Journal of Molecular Biology,* vol. 386, no. 2, pp. 379-390.

Meir, A., Bayer, E.A. & Livnah, O. 2012, "Structural Adaptation of a Thermostable Biotin-binding Protein in a Psychrophilic Environment", *Journal of Biological Chemistry,* vol. 287, no. 22, pp. 17951-17962.

Merten, J.A., Schultz, K.M. & Klug, C.S. 2012, "Concentration-dependent oligomerization and oligomeric arrangement of LptA", *Protein science : a publication of the Protein Society,* vol. 21, no. 2, pp. 211-218.

Meyer, S.C., Gaj, T. & Ghosh, I. 2006, "Highly selective cyclic peptide ligands for NeutrAvidin and avidin identified by phage display", *Chemical biology & drug design,* vol. 68, no. 1, pp. 3-10.

Michalet, X., Ekong, R., Fougerousse, F., Rousseaux, S., Schurra, C., Hornigold, N., van Slegtenhorst, M., Wolfe, J., Povey, S., Beckmann, J.S. & Bensimon, A. 1997, "Dynamic molecular combing: stretching the whole human genome for high-resolution studies", *Science,* vol. 277, no. 5331, pp. 1518-1523.

Mukhopadhyay, S. 2011, "Key Attributes of Nanoscale Materials and Special Functionalities Emerging from Them" in: Mukhopadhyay, S. (ed.), *Nanoscale*

Multifunctional Materials: Science and Applications, Wiley, Hoboken, NJ, USA, pp. 3-32.

Musheev, M.U., Kanoatov, M., Retif, C. & Krylov, S.N. 2013, "Stable DNA aggregation by removal of counterions", *Analytical Chemistry,* vol. 85, no. 21, pp. 10004-10007.

Muzzarelli, R.A.A. 2012, "Chemical and Technological Advances in Chitins and Chitosans Useful for the Formulation of Biopharmaceuticals" in: Sarmento, B. & das Neves, J. (eds.), *Chitosan-Based Systems for Biopharmaceuticals: Delivery, Targeting and Polymer Therapeutics,* 2nd edition, Wiley, Hoboken, NJ, USA, pp. 3-22.

Neet, K.E. & Koshland, D.E.,Jr 1966, "The conversion of serine at the active site of subtilisin to cysteine: a "chemical mutation"", *Proceedings of the National Academy of Sciences of the United States of America,* vol. 56, no. 5, pp. 1606-1611.

Nelson, D.L. & Cox, M.M. (eds.). 2000, *Lehninger Principles of Biochemistry*, 3rd edition, W.H. Freeman and Company, New York.

Niemeyer, C.M., Adler, M., Pignataro, B., Lenhert, S., Gao, S., Chi, L., Fuchs, H. & Blohm, D. 1999, "Self-assembly of DNA-streptavidin nanostructures and their use as reagents in immuno-PCR", *Nucleic acids research,* vol. 27, no. 23, pp. 4553-4561.

Niemeyer, C.M., Koehler, J. & Wuerdemann, C. 2002, "DNA-directed assembly of bienzymic complexes from in vivo biotinylated NAD(P)H:FMN oxidoreductase and luciferase", *Chembiochem: a European journal of chemical biology,* vol. 3, no. 2-3, pp. 242-245.

Niemeyer, C. 2000, "Self-assembled nanostructures based on DNA: towards the development of nanobiotechnology", *Curr Opin Chem Biol,* vol. 4, no. 6, pp. 609-618.

Nimesh, S., Thibault, M.M., Lavertu, M. & Buschmann, M.D. 2010, "Enhanced gene delivery mediated by low molecular weight chitosan/DNA complexes: effect of pH and serum", *Molecular biotechnology,* vol. 46, no. 2, pp. 182-196.

Nordlund, H.R., Hytönen, V.P., Hörhä, J., Määttä, J.A., White, D.J., Halling, K., Porkka, E.J., Slotte, J.P., Laitinen, O.H. & Kulomaa, M.S. 2005a, "Tetravalent single-chain avidin: from subunits to protein domains via circularly permuted avidins", *The Biochemical journal,* vol. 392, no. Pt 3, pp. 485-491.

Nordlund, H.R., Hytönen, V.P., Laitinen, O.H. & Kulomaa, M.S. 2005b, "Novel avidin-like protein from a root nodule symbiotic bacterium, Bradyrhizobium japonicum", *The Journal of biological chemistry,* vol. 280, no. 14, pp. 13250-13255.

Nordlund, H.R., Laitinen, O.H., Hytönen, V.P., Uotila, S.T., Porkka, E. & Kulomaa, M.S. 2004, "Construction of a dual chain pseudotetrameric chicken avidin by combining two circularly permuted avidins", *The Journal of biological chemistry,* vol. 279, no. 35, pp. 36715-36719.

Nwe, K. & Brechbiel, M.W. 2009, "Growing applications of "click chemistry" for bioconjugation in contemporary biomedical research", *Cancer biotherapy & radiopharmaceuticals,* vol. 24, no. 3, pp. 289-302.

Park, S.H., Barish, R., Li, H., Reif, J.H., Finkelstein, G., Yan, H. & Labean, T.H. 2005a, "Three-helix bundle DNA tiles self-assemble into 2D lattice or 1D templates for silver nanowires", *Nano letters,* vol. 5, no. 4, pp. 693-696.

Park, S.H., Yin, P., Liu, Y., Reif, J.H., LaBean, T.H. & Yan, H. 2005b, "Programmable DNA self-assemblies for nanoscale organization of ligands and proteins", *Nano letters,* vol. 5, no. 4, pp. 729-733.

Paumier, G., Ronan, P., NIH, Fijałkowski, A.J., Walker, J., Jones, M.D., Heal, T., Ruiz, M., Science Primer (National Center for Biotechnology Information), Liquid 2003, Nordmann. A. & The Tango! Desktop Project Comparison of various biological assemblies and technological devices, 2009. Available: http://en.wikipedia.org/wiki/Portal:Nanotechnology/Selected_image/13 (accessed 2013, 11/24).

Perbandt, M., Bruns, O., Vallazza, M., Lamla, T., Betzel, C. & Erdmann, V.A. 2007, "High resolution structure of streptavidin in complex with a novel high affinity peptide tag mimicking the biotin binding motif", *Proteins,* vol. 67, no. 4, pp. 1147-1153.

Philo, J.S. 2006, "Is any measurement method optimal for all aggregate sizes and types?", *The AAPS journal,* vol. 8, no. 3, pp. E564-71.

Pohl, H.A. 1978, *Dielectrophoresis: The Behavior of Neutral Matter in Nonuniform Electric Fields,* Cambridge University Press, Cambridge, UK.

Polgár, L. & Bender, M.L. 1966, "A New Enzyme Containing a Synthetically Formed Active Site. Thiol-Subtilisin1", *Journal of the American Chemical Society,* vol. 88, no. 13, pp. 3153-3154.

Privalov, P.L. 2012, *Microcalorimetry of Macromolecules: The Physical Basis of Biological Structures,* Wiley, Hoboken, NJ, USA.

Rapley, R. 2000, "Molecular biology and basic techniques" in: Wilson, K. & Walker, J. (eds.), *Principles and Techniques of Practical Biochemistry,* 5th edition, Cambridge University Press, Cambridge, United Kingdom, pp. 80-137.

Rhodes, D. & Klug, A. 1980, "Helical periodicity of DNA determined by enzyme digestion", *Nature,* vol. 286, no. 5773, pp. 573-578.

Rigaut, G., Shevchenko, A., Rutz, B., Wilm, M., Mann, M. & Seraphin, B. 1999, "A generic protein purification method for protein complex characterization and proteome exploration", *Nature biotechnology,* vol. 17, no. 10, pp. 1030-1032.

Riihimäki, T.A., Hiltunen, S., Rangl, M., Nordlund, H.R., Määttä, J.A., Ebner, A., Hinterdorfer, P., Kulomaa, M.S., Takkinen, K. & Hytönen, V.P. 2011, "Modification of the loops in the ligand-binding site turns avidin into a steroid-binding protein", *BMC biotechnology,* vol. 11, no. 64, pp. 1-11.

Rinaudo, M. 2012, "Physical Properties of Chitosan and Derivatives in Sol and Gel States" in: Sarmento, B. & das Neves, J. (eds.), *Chitosan-Based Systems for Biopharmaceuticals: Delivery, Targeting and Polymer Therapeutics,* 2nd edition, Wiley, Hoboken, NJ, USA, pp. 23-44.

Rosano, C., Arosio, P. & Bolognesi, M. 1999, "The X-ray three-dimensional structure of avidin", *Biomolecular engineering,* vol. 16, no. 1-4, pp. 5-12.

Ross, S.E., Carson, S.D. & Fink, L.M. 1986, "Effects of detergents on avidin-biotin interaction", *BioTechniques,* vol. 4, pp. 350-354.

Rothemund, P.W. 2006, "Folding DNA to create nanoscale shapes and patterns", *Nature,* vol. 440, no. 7082, pp. 297-302.

Rowe, L., Khoury, G.E. & Lowe, C.R. 2012, "Affinity Chromatography: Historical and Prospective Overview" in: Subramanian, G. (ed.), *Biopharmaceutical Production Technology,* Wiley, Somerset, NJ, USA, pp. 225-282.

Rozkiewicz, D.I., Ravoo, B.J. & Reinhoudt, D.N. 2010, "Immobilization and Patterning of Biomolecules on Surfaces" in: Rurack, K. & Martinez-Manez, R. (eds.), *Supramolecular Chemistry of Organic-Inorganic Hybrid Materials,* Wiley, Hoboken, NJ, USA, pp. 433-466.

Saeger, J., Hytönen, V.P., Klotzsch, E. & Vogel, V. 2012, "GFP's Mechanical Intermediate States", *PLoS ONE,* vol. 7, no. 10, pp. e46962.

Sardo, A., Wohlschlager, T., Lo, C., Zoller, H., Ward, T.R. & Creus, M. 2011, "Burkavidin: a novel secreted biotin-binding protein from the human pathogen Burkholderia pseudomallei", *Protein expression and purification,* vol. 77, no. 2, pp. 131-139.

Sarkar, G. & Sommer, S.S. 1990, "The "megaprimer" method of site-directed mutagenesis", *BioTechniques,* vol. 8, no. 4, pp. 404-407.

Schena, M., Shalon, D., Davis, R.W. & Brown, P.O. 1995, "Quantitative monitoring of gene expression patterns with a complementary DNA microarray", *Science,* vol. 270, no. 5235, pp. 467-470.

Schmidt, T.G., Koepke, J., Frank, R. & Skerra, A. 1996, "Molecular interaction between the Strep-tag affinity peptide and its cognate target, streptavidin", *Journal of Molecular Biology,* vol. 255, no. 5, pp. 753-766.

Seeman, N.C. 2010, "Structural DNA nanotechnology: growing along with Nano Letters", *Nano letters,* vol. 10, no. 6, pp. 1971-1978.

Selzer, T., Albeck, S. & Schreiber, G. 2000, "Rational design of faster associating and tighter binding protein complexes", *Nat Struct Mol Biol,* vol. 7, no. 7, pp. 537-541.

Sharma, J., Chhabra, R., Liu, Y., Ke, Y. & Yan, H. 2006, "DNA-Templated Self-Assembly of Two-Dimensional and Periodical Gold Nanoparticle Arrays", *Angewandte Chemie International Edition,* vol. 45, no. 5, pp. 730-735.

Shih, W.M., Quispe, J.D. & Joyce, G.F. 2004, "A 1.7-kilobase single-stranded DNA that folds into a nanoscale octahedron", *Nature,* vol. 427, no. 6975, pp. 618-621.

Sigurskjold, B.W. 2000, "Exact analysis of competition ligand binding by displacement isothermal titration calorimetry", *Analytical Biochemistry,* vol. 277, no. 2, pp. 260-266.

Singh, R.P., Choi, J., Tiwari, A. & Pandey, A.C. 2012, "Biomimetic Materials Toward Application of Nanobiodevices" in: Mishra, A.K., Turner, A.P.F. & Kobayashi, H. (eds.), *Intelligent Nanomaterials,* Wiley, Hoboken, NJ, USA, pp. 741-782.

Skerra, A. & Schmidt, T.G.M. 1999, "Applications of a peptide ligand for streptavidin: the Strep-tag", *Biomolecular engineering,* vol. 16, no. 1-4, pp. 79-86.

Sorlier, P., Denuzière, A., Viton, C. & Domard, A. 2001, "Relation between the Degree of Acetylation and the Electrostatic Properties of Chitin and Chitosan", *Biomacromolecules,* vol. 2, no. 3, pp. 765-772.

Strand, S.P., Lelu, S., Reitan, N.K., de Lange Davies, C., Artursson, P. & Varum, K.M. 2010, "Molecular design of chitosan gene delivery systems with an optimized balance between polyplex stability and polyplex unpacking", *Biomaterials,* vol. 31, no. 5, pp. 975-987.

Takakura, Y., Tsunashima, M., Suzuki, J., Usami, S., Kakuta, Y., Okino, N., Ito, M. & Yamamoto, T. 2009, "Tamavidins-novel avidin-like biotin-binding proteins from the Tamogitake mushroom", *FEBS J,* vol. 276, pp. 1383-1397.

Tanoue, R., Higuchi, R., Enoki, N., Miyasato, Y., Uemura, S., Kimizuka, N., Stieg, A.Z., Gimzewski, J.K. & Kunitake, M. 2011, "Thermodynamically controlled self-assembly of covalent nanoarchitectures in aqueous solution", *ACS nano,* vol. 5, no. 5, pp. 3923-3929.

Tapio, K. 2012, *Itsejärjestäytyvä DNA-kultananopartikkeli-rakenne yhden elektronin transistorina*, Jyväskylän yliopisto, Fysiikan laitos.

Taskinen, B., Zmurko, J., Ojanen, M., Kukkurainen, S., Parthiban, M., Määttä, J.A., Leppiniemi, J., Jänis, J., Parikka, M., Turpeinen, H., Rämet, M., Pesu, M., Johnson, M.S., Kulomaa, M.S., Airenne, T.T. & Hytönen, V.P. 2013, "Zebavidin - an avidin-like protein from zebrafish", *PloS one,* vol. 8, no. 10, pp. e77207.

Terpe, K. 2003, "Overview of tag protein fusions: from molecular and biochemical fundamentals to commercial systems", *Applied Microbiology and Biotechnology,* vol. 60, no. 5, pp. 523-533.

The Mfold Web Server, 1995. Available: http://mfold.rna.albany.edu/?q=mfold (accessed 2010, 12/13).

Thibault, M., Astolfi, M., Tran-Khanh, N., Lavertu, M., Darras, V., Merzouki, A. & Buschmann, M.D. 2011, "Excess polycation mediates efficient chitosan-based gene transfer by promoting lysosomal release of the polyplexes", *Biomaterials,* vol. 32, no. 20, pp. 4639-4646.

Tuukkanen, S., Kuzyk, A., Toppari, J.J., Häkkinen, H., Hytönen, V.P., Niskanen, E., Rinkiö, M. & Törmä, P. 2007, "Trapping of 27 bp - 8 kbp DNA and immobilization of thiol-modified DNA using dielectrophoresis", *Nanotechnology,* vol. 18, no. 29, pp. 295204.

Tuukkanen, S., Toppari, J.J., Hytönen, V.P., Kuzyk, A., Kulomaa, M.S. & Törmä, P. 2005, "Dielectrophoresis as a tool for nanoscale DNA manipulation", *International Journal of Nanotechnology,* vol. 2, no. 3, pp. 280-291.

Uchegbu, I.F., Dufès, C., Kan, P.L. & Schätzlein, A.G. 2009, "Polymers and Dendrimers for Gene Delivery in Gene Therapy" in: Templeton, N.S. (ed.), *Gene and Cell Therapy, Therapeutic Mechanisms and Strategies,* 3rd edition, CRC Press, Taylor and Francis Group, Boca Raton, FL, USA, pp. 321-339.

Uhlén, M. 2008, "Affinity as a tool in life science", *BioTechniques,* vol. 44, no. 5, pp. 649-654.

United States National Nanotechnology Initiative, 2014. Available: http://www.nano.gov/nanotech-101 (accessed 2014, 01/13).

Varadan, V.K., Chen, L. & Xie, J. 2009, *Nanomedicine: Design and Applications of Magnetic Nanomaterials, Nanosensors and Nanosystems,* Wiley, Chichester, Great Britain.

Wang, J.C. 1979, "Helical repeat of DNA in solution", *Proceedings of the National Academy of Sciences of the United States of America,* vol. 76, no. 1, pp. 200-203.

Watson, J.D. & Crick, F.H. 1953, "Molecular structure of nucleic acids; a structure for deoxyribose nucleic acid", *Nature,* vol. 171, no. 4356, pp. 737-738.

Wegner, G.J., Lee, H.J. & Corn, R.M. 2002a, "Characterization and optimization of peptide arrays for the study of epitope-antibody interactions using surface plasmon resonance imaging", *Analytical Chemistry,* vol. 74, no. 20, pp. 5161-5168.

Wegner, G.J., Lee, H.J. & Corn, R.M. 2002b, "Characterization and optimization of peptide arrays for the study of epitope-antibody interactions using surface plasmon resonance imaging", *Analytical Chemistry,* vol. 74, no. 20, pp. 5161-5168.

Wei, B., Dai, M. & Yin, P. 2012, "Complex shapes self-assembled from single-stranded DNA tiles", *Nature,* vol. 485, no. 7400, pp. 623-626.

Wei, B., Wang, Z. & Mi, Y. 2006, "Uniquimer: A de Novo DNA Sequence Generation Computer Software for DNA Self-assembly" in: Chengde, M. & Takashi, Y. (eds.), *DNA Computing, 12th International Meeting on DNA Computing, DNA12, Seoul, Korea, June 5-9, 2006, Revised Selected Papers,* Springer Berlin Heidelberg, Heidelberg, Germany, pp. 266-273.

Welch, M., Govindarajan, S., Ness, J.E., Villalobos, A., Gurney, A., Minshull, J. & Gustafsson, C. 2009, "Design Parameters to Control Synthetic Gene Expression in *Escherichia coli*", *PLoS ONE,* vol. 4, no. 9, pp. e7002.

Whitesides, G.M. & Grzybowski, B. 2002, "Self-assembly at all scales", *Science (New York, N.Y.),* vol. 295, no. 5564, pp. 2418-2421.

Wilchek, M. & Bayer, E.A. 1990, "Introduction to avidin-biotin technology", *Methods in enzymology,* vol. 184, pp. 5-13.

Wilchek, M., Bayer, E.A. & Livnah, O. 2006, "Essentials of biorecognition: the (strept)avidin-biotin system as a model for protein-protein and protein-ligand interaction", *Immunology letters,* vol. 103, no. 1, pp. 27-32.

Williams, S., Lund, K., Lin, C., Wonka, P., Lindsay, S. & Yan, H. 2009, "Tiamat: A Three-Dimensional Editing Tool for Complex DNA Structures" in: Goel, A., Simmel, F.C. & Sosik, P. (eds.), *DNA Computing, 14th International Meeting on DNA Computing, DNA 14, Prague, Czech Republic, June 2-9, 2008. Revised Selected Papers,* Springer Berlin Heidelberg, Heidelberg, Germany, pp. 90-101.

Winfree, E., Liu, F., Wenzler, L.A. & Seeman, N.C. 1998, "Design and self-assembly of two-dimensional DNA crystals", *Nature,* vol. 394, no. 6693, pp. 539-544.

Wingren, C. & Borrebaeck, C.A. 2007, "Progress in miniaturization of protein arrays-a step closer to high-density nanoarrays", *Drug discovery today,* vol. 12, no. 19-20, pp. 813-819.

Yan, H., Park, S.H., Finkelstein, G., Reif, J.H. & LaBean, T.H. 2003, "DNA-templated self-assembly of protein arrays and highly conductive nanowires", *Science,* vol. 301, no. 5641, pp. 1882-1884.

Yao, G. & Tan, W. 2004, "Molecular-beacon-based array for sensitive DNA analysis", *Analytical Biochemistry,* vol. 331, no. 2, pp. 216-223.

Yi, H., Wu, L.Q., Bentley, W.E., Ghodssi, R., Rubloff, G.W., Culver, J.N. & Payne, G.F. 2005, "Biofabrication with chitosan", *Biomacromolecules,* vol. 6, no. 6, pp. 2881-2894.

Yumioka, R., Sato, H., Tomizawa, H., Yamasaki, Y. & Ejima, D. 2010, "Mobile phase containing arginine provides more reliable SEC condition for aggregation analysis", *Journal of pharmaceutical sciences,* vol. 99, no. 2, pp. 618-620.

Zhang, D.Y., Hariadi, R.F., Choi, H.M. & Winfree, E. 2013, "Integrating DNA strand-displacement circuitry with DNA tile self-assembly", *Nature communications,* vol. 4, pp. 1965.

Zhang, D.Y. & Seelig, G. 2011, "Dynamic DNA nanotechnology using strand-displacement reactions", *Nature chemistry,* vol. 3, no. 2, pp. 103-113.

Zhang, Y. & Seeman, N.C. 1994, "Construction of a DNA-Truncated Octahedron", *Journal of the American Chemical Society,* vol. 116, no. 5, pp. 1661-1669.

Zhao, X. & Zhang, S. 2007, "Designer Self-Assembling Peptide Materials", *Macromolecular Bioscience,* vol. 7, no. 1, pp. 13-22.

Zheng, J., Birktoft, J.J., Chen, Y., Wang, T., Sha, R., Constantinou, P.E., Ginell, S.L., Mao, C. & Seeman, N.C. 2009, "From molecular to macroscopic via the rational design of a self-assembled 3D DNA crystal", *Nature,* vol. 461, no. 7260, pp. 74-77.

Zheng, J., Constantinou, P.E., Micheel, C., Alivisatos, A.P., Kiehl, R.A. & Seeman, N.C. 2006, "Two-Dimensional Nanoparticle Arrays Show the Organizational Power of Robust DNA Motifs", *Nano Letters,* vol. 6, no. 7, pp. 1502-1504.

Zhou, H.X. & Bates, P.A. 2013, "Modeling protein association mechanisms and kinetics", *Current opinion in structural biology,* vol. 23, pp. 887-893.

Zhu, H. & Snyder, M. 2003, "Protein chip technology", *Current opinion in chemical biology,* vol. 7, no. 1, pp. 55-63.

Zuker, M. 2003, "Mfold web server for nucleic acid folding and hybridization prediction", *Nucleic acids research,* vol. 31, no. 13, pp. 3406-3415.

APPENDIX

Appendix 1. Composition of fermentation medium and feed liquid.

Table 1. Composition of fermentation medium.

Fermentation medium		Trace metals stock solution	
Substance	**Amount**	**Substance**	**Amount**
$(NH_4)_2HPO_4$	2 g	$FeSO_4 \cdot 7\ H_2O$	10 g/l
KH_2PO_4	6.75 g	$CaCl_2 \cdot 2\ H_2O$	2 g/l
Citric acid	0.85 g	$CuSO_4 \cdot 5\ H_2O$	1 g/l
Yeast extract	2 g	$ZnSO_4 \cdot 7\ H_2O$	2.5 g/l
H_2O	Add to 1000 ml	$(NH_4)_6\ Mo_7O_{24} \cdot 4\ H_2O$	0.1 g/l
The following items were added after autoclaving:		$Na_2B_4O_7 \cdot 10\ H_2O$	0.23 g/l
$MgSO_4$ (0.5g/ml)	1.4 ml	HCl (37 %)	415 ml
Glucose (0.5 g/ml)	10 ml	H_2O	Add to 1000 ml
Glycerol	10 ml		
Trace metals stock solution	5 ml		
pH was adjusted to 6.8			

Table 2. Composition of feed liquid used in *E. coli* fermentation.

Substance	**Amount**
Glycerol	500 g
Yeast extract	100 g
$MgSO_4 \cdot 7\ H_2O$	7 g

OPEN ACCESS Freely available online

PLoS one

Bifunctional Avidin with Covalently Modifiable Ligand Binding Site

Jenni Leppiniemi[1], Juha A. E. Määttä[1], Henrik Hammaren[1], Mikko Soikkeli[1], Mikko Laitaoja[2], Janne Jänis[2], Markku S. Kulomaa[1], Vesa P. Hytönen[1]*

1 Institute of Medical Technology, University of Tampere and Tampere University Hospital, Tampere, Finland, **2** Department of Chemistry, University of Eastern Finland, Joensuu, Finland

Abstract

The extensive use of avidin and streptavidin in life sciences originates from the extraordinary tight biotin-binding affinity of these tetrameric proteins. Numerous studies have been performed to modify the biotin-binding affinity of (strept)avidin to improve the existing applications. Even so, (strept)avidin greatly favours its natural ligand, biotin. Here we engineered the biotin-binding pocket of avidin with a single point mutation S16C and thus introduced a chemically active thiol group, which could be covalently coupled with thiol-reactive molecules. This approach was applied to the previously reported bivalent dual chain avidin by modifying one binding site while preserving the other one intact. Maleimide was then coupled to the modified binding site resulting in a decrease in biotin affinity. Furthermore, we showed that this thiol could be covalently coupled to other maleimide derivatives, for instance fluorescent labels, allowing intratetrameric FRET. The bifunctional avidins described here provide improved and novel tools for applications such as the biofunctionalization of surfaces.

Citation: Leppiniemi J, Määttä JAE, Hammaren H, Soikkeli M, Laitaoja M, et al. (2011) Bifunctional Avidin with Covalently Modifiable Ligand Binding Site. PLoS ONE 6(1): e16576. doi:10.1371/journal.pone.0016576

Editor: Dafydd Jones, Cardiff University, United Kingdom

Received September 30, 2010; **Accepted** December 21, 2010; **Published** January 27, 2011

Funding: This work was supported by Tampere Graduate Program in Biomedicine and Biotechnology, the Academy of Finland [SA 121236, SA 115976] and the Finnish Funding Agency for Technology and Innovation [TEKES 40055/08]. The funders had no role in study design, data collection and analysis, decision to publish, or preparation of the manuscript.

Competing Interests: The authors have declared that no competing interests exist.

* E-mail: vesa.hytonen@uta.fi

Introduction

The extremely high affinity of avidin and streptavidin towards D-biotin ($K_d \approx 6 \times 10^{-16}$ M for avidin and $K_d \approx 4 \times 10^{-14}$ M for streptavidin) [1–3] is the reason why these proteins are widely applied in life sciences. Biotin occupies a structurally optimal cavity inside the eight-stranded beta barrel of (strept)avidin forming several hydrogen bonds with the protein [4–6]. Previous studies have indicated the importance of a particular set of residues in this interaction. However, removal of a single hydrogen-bonding residue weakened biotin binding to (strept)avidin only moderately [7–11]. Therefore, fairly radical mutations have to be applied in order to extinguish the biotin-binding activity of (strept)avidin as previously reviewed [2]. In another approach, biotin was chemically adjusted to increase its binding affinity, but with poor results [12]. Two studies reported rational engineering of streptavidin, where the ligand-binding specificity of mutant streptavidin was altered from biotin to its analog, 2-iminobiotin [13], or to biotin-4-fluorescein [14]. Avidin was also modified to improve the binding of 4′-hydroxyazobenzene-2-carboxylic acid (HABA) resulting in a change of several orders of magnitude in the binding affinity as compared to wild type (wt) avidin [15]. However, avidin could not be converted to favour binding of HABA over biotin. Overall, the site-directed modulation of the ligand-binding specificity of (strept)avidins towards ligands other than biotin or its derivatives appears to be challenging.

The independent control of individual binding sites within tetrameric (strept)avidin has been the motivation for numerous studies. A monovalent streptavidin tetramer with only one functional biotin binding site was reported [16]: The unmodified and modified monomers were combined in a denaturated state at a molar ratio of 1:3 before refolding. This method created a mixture of tetramers of different compositions from monovalency to tetravalency following isolation of the monovalent protein from the oligovalent forms. This laborious procedure could be avoided by genetically joining two or four modified subunits together into a polypeptide chain like in the dual chain and single chain avidins previously reported [17,18]. The same approach has since also been applied to streptavidin [14].

Dual chain avidin (dcAvd) is a subunit fusion of two different circularly permuted avidin monomers, circularly permuted avidin 5→4 (cpAvd5→4) and circularly permuted avidin 6→5 (cpAvd6→5) [17]. Two dcAvd subunits, both with two binding sites, form a dimer with four binding sites (Figure 1A). The subunits can independently be modified, making it possible to create avidins with altered binding sites, for instance for low-affinity and high-affinity binding of a ligand within a single protein molecule [7]. The use of a disulphide bridge ($I117C_{5\rightarrow4}$, numbering according to wt avidin) combined with a critical mutation ($V115H_{6\rightarrow5}$) in the interface between subunits [19] made it possible to develop dcAvds with defined quaternary structures [20]. DcAvd provides a scaffold that can be modified not only to alternate affinity for a ligand, but also to change specificity – in other words to favour another ligand molecule instead of biotin.

In order to overcome the challenge of modifying the extremely high biotin-binding affinity of (strept)avidin, we established a novel

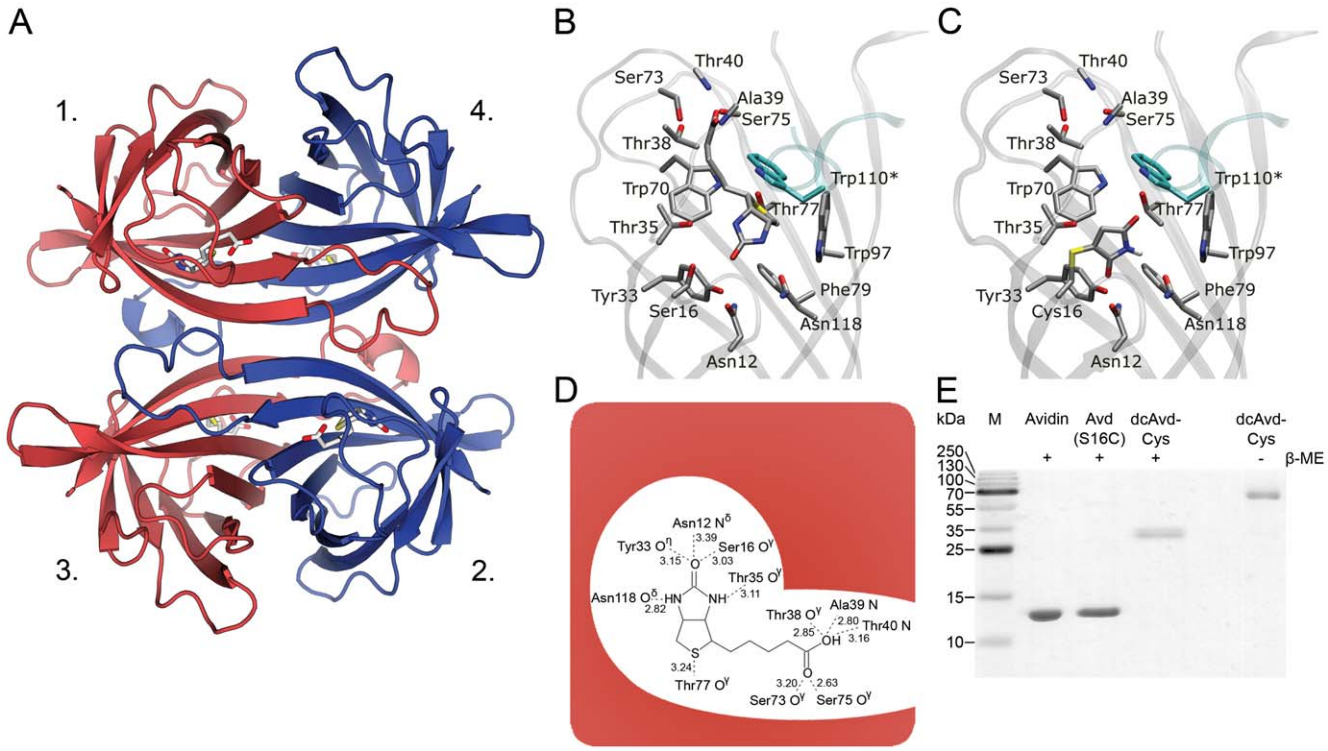

Figure 1. Avidin-ligand interaction. (**A**) Avidin tetramer (PDB 2AVI), with subunits numbered according to [5]. Subunits are coloured to red and blue according to dual chain avidin subunits; cpAvd5→4 are shown in red and cpAvd6→5 are shown in blue. (**B**) A cartoon model of wild type (wt) avidin (PDB 2AVI) showing the biotin-binding contact residues in sticks. Oxygen atoms are shown in red, nitrogens in blue, sulphurs in yellow, and carbon atoms in grey. The W110 residue from the neighboring subunit is highlighted in cyan. (**C**) The cartoon model of the maleimide-treated binding site of Avd(S16C) showing a thioether bond between Cys16 and maleimide. (**D**) A schematic of the hydrogen bonds between wt avidin and biotin. Bond lengths in ångströms are shown according to (PDB 2avi) [6]. (**E**) SDS-PAGE analysis of recombinant proteins shows high purity and correct molecular weights. In the presence (+) of the reducing agent β-mercaptoethanol (β-ME), Avidin, Avd(S16C) and dcAvd-Cys (more specifically dcAvd(I117$C_{5\rightarrow4}$S16C,V115$H_{6\rightarrow5}$)) exist as monomers of sizes ~14.5 kDa, ~14.5 kDa and ~30 kDa, respectively. DcAvd-Cys without (-) the reducing agent exists mainly in the form of a disulfide linked dimer, ~60 kDa. M, molecular weight marker.
doi:10.1371/journal.pone.0016576.g001

concept, in which a cysteine residue was introduced into the ligand binding site of avidin. The thiol group of the cysteine could then be covalently modified leading to the inhibition of biotin-binding. In addition, this allowed the selective covalent linking of thiol group reactive molecules to avidin. Furthermore, an avidin with two specific ligand-binding sites was created by applying the same modification to dcAvd.

Results

Serine 16 replaced by cysteine can be modified by maleimide

Serine 16 is positioned in the biotin-binding pocket of avidin and is hydrogen bonded to a ureido oxygen in biotin in the avidin-biotin complex (PDB 2AVI; Figure 1B,D). Our strategy was to replace serine 16 with a cysteine to introduce a thiol group to the polypeptide available for covalent bonding with small thiol-reactive molecules. Importantly, being located inside the binding pocket, the free thiol group is unable to form disulphide bond between another avidin subunit, which would lead to oligomeric assemblies [21], and therefore reducing conditions were not needed for protein handling. Cysteine 16 could then be modified by maleimide, which reacts specifically with thiol group in chemically mild conditions forming a stable thioether linkage (Figure 1C). Furthermore, Cys16 could be covalently coupled to other maleimide derivatives, as demonstrated here by linking a maleimide-activated fluorescent probe to dcAvd(I117$C_{5\rightarrow4}$S16C,V115$H_{6\rightarrow5}$), referred to as dcAvd-Cys from now on. DcAvd-Cys could be coupled to two different kinds of molecules, to thiol-reactive molecules as well as to biotinylated molecules.

We produced avidin and Avd(S16C) in *E. coli* cells and dcAvd-Cys in baculovirus infected Sf9 insect cells. This was followed by successful protein purification by one-step 2-iminobiotin affinity chromatography [22] indicating protein solubility and activity in the form of biotin binding. The purified proteins were of the correct size according to SDS-PAGE analysis (Figure 1E). Non-reducing SDS-PAGE showed the formation of a thioether between the dcAvd-Cys subunits (Figure 1E).

We used high-resolution electrospray ionization Fourier transform ion cyclotron resonance (ESI FT-ICR) mass spectrometry to confirm protein primary structures and to detect the efficiency of coupling maleimide into Avd(S16C). Figure 2 shows isotopically-resolved, charge-deconvoluted ESI FT-ICR mass spectra for wt avidin, Avd(S16C) and Avd(S16C) coupled with maleimide (MI). Based on the mass data, both wt avidin and Avd(S16C) had three additional amino acid residues (QTV) of the *B. avium* OmpA signal peptide in the N-terminus of the protein and contained an intramolecular disulfide bridge, Cys4–Cys83 (the theoretical masses are 14668.43 and 14684.41 Da for wt avidin and Avd(S16C), respectively). In addition, both proteins appeared in two different forms, separated by 17 Da, due to the partial cyclization of an N-terminal glutamine residue into the pyrroli-

done carboxylic acid (PCA) form (Figure 2A,B). No protein dimers or higher oligomers were detected, indicating the absence of C16-mediated tetramer crosslinking. We incubated a high molar excess of maleimide with Avd(S16C) to measure coupling efficiency with the free cysteine present in the protein structure. A mass spectrum of Avd(S16C) treated with maleimide (Figure 2C) consistently showed a mass increase of +97 Da, indicating the formation of a covalent thioether linkage, presumably with Cys16 (theoretical mass 14781.43 Da). The coupling efficiency appeared to be high since only a small amount of unreacted protein was present in the sample. We detected no other protein modifications upon the maleimide treatment. We obtained similar results when Avd(S16C) was treated with N-ethylmaleimide, another thiol-reactive maleimide derivative, showing nearly 100% coupling efficiency (data not presented). In contrast, treatment of wt avidin with maleimide or N-ethylmaleimide showed no reaction at all, as expected, indicating high specificity of the two reagents towards free thiol groups in these conditions.

To further verify the presence of the maleimide-coupled residue, wt avidin as well as Avd(S16C), with or without maleimide treatment, were digested in solution with trypsin (data presented as Table S1 in Supporting Information). The full sequence coverage was obtained, except in the case of Avd(S16C) (87%), represented by up to 20 specific tryptic peptides. Among the identified peptides for Avd(S16C) treated with maleimide, a peptide having a monoisotopic mass of 1947.8630 Da was observed, consistent with the maleimide conjugation into residues 10–26 (theoretical mass 1947.8567 Da). With untreated Avd(S16C), this peptide was absent, but a peptide having a monoisotopic mass of 1850.8512 Da was observed instead, corresponding to the uncoupled tryptic peptide 10–26. These results indicate that maleimide was effectively and specifically conjugated to the Cys16 residue in the modified Avd(S16C). The digestion data also confirmed the presence of intramolecular disulfide bridge (disulfide linked tryptic peptides 3–9+72–94 and 4–9+72–94) as well as the N-terminal PCA modification.

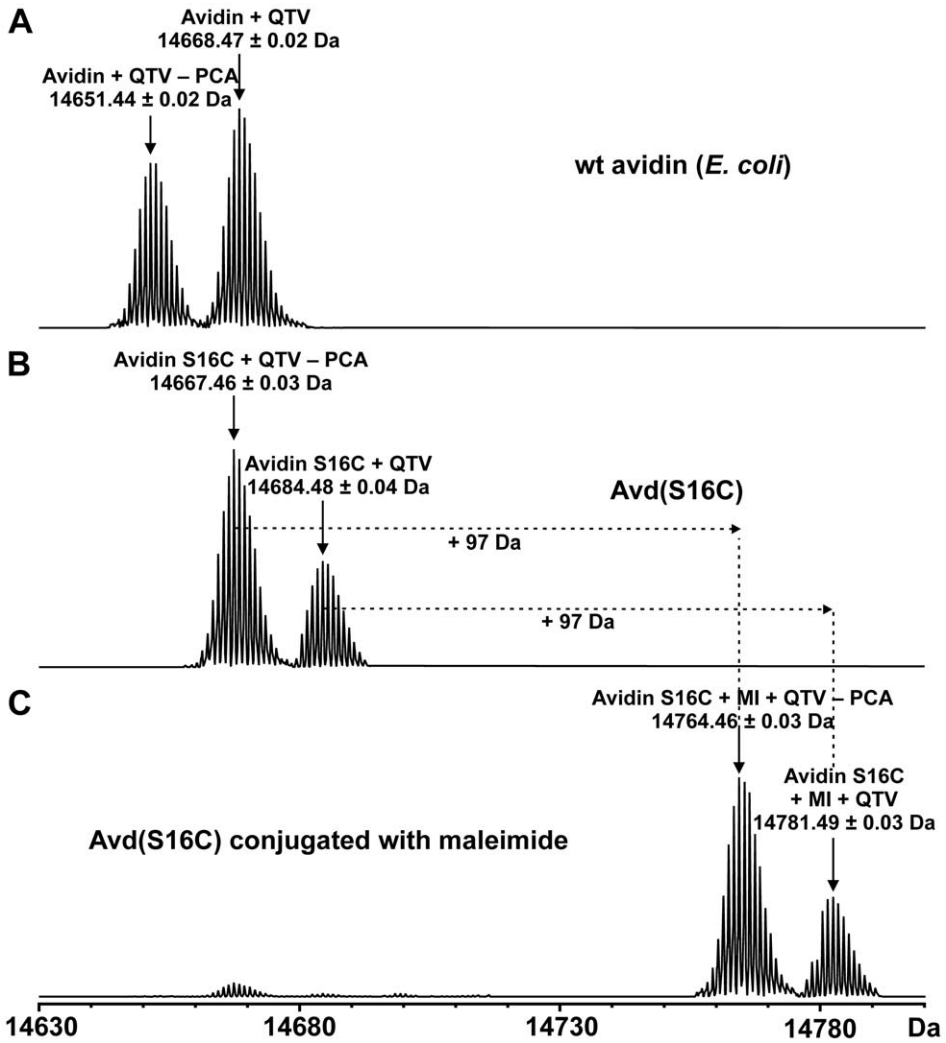

Figure 2. A charge-deconvoluted ESI FT-ICR mass spectra for avidin, Avd(S16C) and Avd(S16C) conjugated with maleimide. The mass spectra showed that both avidin (**A**) and Avd(S16C) (**B**) have three additional N-terminal amino acid residues (QTV) of the *B. avium* OmpA signal peptide and they both contain an intramolecular disulfide bridge (theoretical masses are 14668.43 and 14684.41 Da for avidin and Avd(S16C), respectively). The proteins appeared in two different forms separated by 17 Da due to the partial cyclization of an N-terminal glutamine residue into the pyrrolidone carboxylic acid (PCA) form. The mass spectrum of Avd(S16C) conjugated with maleimide (MI) (**C**) showed a mass increase of +97 Da, indicating a formation of a covalent thioether linkage with Cys16 (theoretical mass 14781.43 Da). The small amount of unreacted protein present in the sample indicated high coupling efficiency between maleimide and the cysteine-residue.
doi:10.1371/journal.pone.0016576.g002

The S16C mutation does not prevent biotin binding but decreases affinity to biotin

The thermal stability of Avd(S16C) in the absence of biotin was comparable to that of wt avidin (Table 1, see also Figure S1). However, the S16C mutation had a negative effect on the thermal stability of the quaternary structure of wt avidin in the presence of biotin, since the thermal transition temperature decreased about 20°C. This was expected, as the mutation was targeted to one of the key residues participating in ligand binding. Similarly to dcAvd(I117$C_{5\rightarrow4,}$V115$H_{6\rightarrow5}$), dcAvd-Cys was a monomer at room temperature (RT, 23±1°C) in the absence of biotin. The presence of biotin stabilized dcAvd-Cys, although it lost its pseudotetrameric structure at 60°C, which is about 20°C lower than the thermal transition temperature determined for dcAvd(I117$C_{5\rightarrow4,}$V115$H_{6\rightarrow5}$) [20].

As was stated above, Avd(S16C) efficiently bound to a 2-iminobiotin affinity matrix, which qualitatively suggested relatively high biotin-binding affinity. We analyzed the ligand binding properties of the modified avidins with a fluorescent biotin conjugate, BF560-biotin, by measuring the quenching of fluorescence after protein binding at RT. The quenching of fluorescence (Figure 3B) of wt avidin, Avd(S16C) and dcAvd-Cys were fairly equal, 66.5±1.3, 61.0±0.6 and 63.2±7.3% respectively, indicating that the S16C mutation had only a modest effect on the binding of the fluorescent biotin. However, after addition of free biotin, the recovery of fluorescence (Figure 3C) of Avd(S16C) was

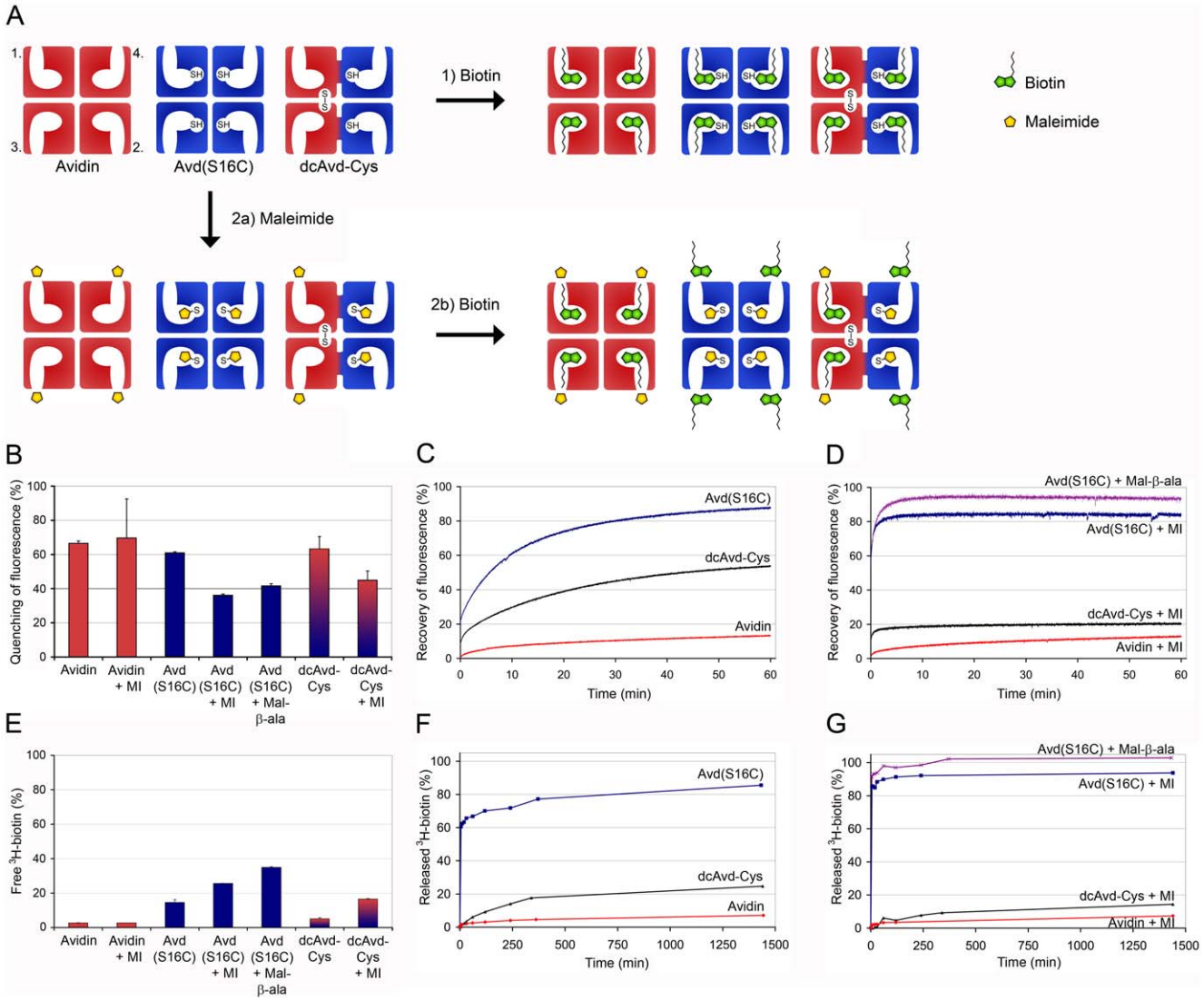

Figure 3. Biotin dissociation asays. (**A**) A schematic presentation of the four binding sites in avidin, Avd(S16C) and dcAvd(I117$C_{5\rightarrow4}$S16C,V115$H_{6\rightarrow5}$) (dcAvd-Cys). Biotin could bind to both of the S16C-mutated and unmodified binding sites (scheme 1). The biotin binding to Avd(S16C) and dcAvd-Cys could be inhibited with maleimide, which forms a covalent bond with a thiol group in the modified binding site (scheme 2 a,b). (**B**) The level of quenching of fluorescence of BF560-biotin after it was bound to protein indicated different biotin-binding abilities for different protein forms with or without chemical coupling to maleimide (MI) or to N-maleoyl-β-alanine (Mal-β-ala). The means for duplicate measurements are shown ± s.d. (**C**, **D**) The recovery of fluorescence of BF560-biotin after the addition of a 100-fold excess of free biotin indicates dissociation of the BF560-biotin-protein complex. (**E**) Proteins were incubated with ^{3}H-biotin and unbound ^{3}H-biotin was filtered and measured with a scintillation counter. Means of triplicate measurements are shown ± s.d. (**F, G**) The release of ^{3}H-biotin after addition of cold biotin measured at different time points.

doi:10.1371/journal.pone.0016576.g003

over 15-fold faster ($k_{diss} = 3.7\times10^{-4}$ s^{-1}) compared to wt avidin ($k_{diss} = 2.4\times10^{-5}$ s^{-1}), indicating an increase in the dissociation rate and thus decreased affinity to the conjugated biotin. After one hour the recovery of fluorescence was nearly 15% with avidin and 85% with Avd(S16C). When compared to that of the previously analyzed Avd(S16A) with its dissociation rate constant of 3.6×10^{-4} s^{-1} and fluorescence recovery of 74.5% after one hour [7], we can conclude that the mutations S16A and S16C affect the biotin-binding properties of avidin in a similar fashion. The recovery of fluorescence for dcAvd-Cys was slightly over 50% after one hour and the dissociation rate constant 1.3×10^{-4} s^{-1}, being thus five-fold faster than for wt avidin but three-fold slower than for Avd(S16C). Because the pseudotetrameric dcAvd-Cys has two S16C-modified and two unmodified binding sites, the result appears logical: dcAvd-Cys behaves like an independent combination of wt avidin and Avd(S16C).

We used ^{3}H-biotin to confirm the results we obtained for ligand binding with fluorescently labelled biotin. Incubation of ^{3}H-biotin with proteins at RT following filtering and scintillation counting of ^{3}H-biotin indicated differences in biotin-binding abilities. The results appeared logical, since wt avidin bound almost all of the ^{3}H-biotin and the amount of free ^{3}H-biotin was 2.7±0.1% (Figure 3E). The ^{3}H-biotin-binding ability of Avd(S16C) was somewhat reduced, since the amount of free biotin was 14.6±1.6%. The amount of unbound ^{3}H-biotin in the case of dcAvd-Cys was 5.1±0.6% indicating a slightly reduced ability to bind ^{3}H-biotin as compared to wt avidin. The release of the bound ^{3}H-biotin was measured after the addition a 1000-fold excess of cold biotin and the dissociation from Avd(S16C) ($k_{diss} = 6.4\times10^{-4}$ s^{-1}) approached 85% after 24 hours, and therefore, dissociation was increased nearly 18-fold as compared to wt avidin, which had released only 7% of the bound ^{3}H-biotin after 24 hours ($k_{diss} = 3.6\times10^{-5}$ s^{-1}) (Figure 3F). At 24 hours after addition of cold biotin the dissociation of the bound ^{3}H-biotin from dcAvd-Cys approached 25% and was nearly five-fold faster ($k_{diss} = 1.7\times10^{-4}$ s^{-1}) than from wt avidin.

According to both assays biotin dissociation was much faster from Avd(S16C) as compared to wt avidin. However, for dcAvd-Cys the results of the two assays differed slightly. A possible reason for this could be the structural differences of the used ligands. The fluorescent label itself is large compared to biotin and when attached to biotin via a linker, the label could affect biotin-binding properties. D-[8,9-^{3}H]-biotin with two tritiums, on the other hand, is structurally almost identical with natural D-biotin.

Blocking the biotin binding of avidins by coupling with maleimide

We coupled maleimide to the binding sites of the modified avidins (Figure 3A) and tested whether this had an effect on the biotin binding-affinity as determined by using fluorescently labelled BF560-biotin. Maleimide had no effect on the binding properties of wt avidin (Figure 3B). In contrast, maleimide coupled to Avd(S16C) disrupted the binding of fluorescent biotin, which was seen as a decrease in the quenching of fluorescence to 36.1±0.7%. The recovery of fluorescence after the addition of free biotin was rapid and most of the complexes were dissociated already after one minute from the beginning of the measurement (Figure 3D), indicating significant decrease in the affinity for biotin. Ser16 is located in the loop area of β-barrel of avidin and therefore it is possible that the loop may partly distort so that biotin may fit in the binding site, although maleimide is already covalently coupled to modified Cys16. Therefore, we were interested to know whether maleimide with an attached side group would prevent the binding of biotin to the modified site more efficiently. We selected N-maleoyl-β-alanine (Mal-β-ala), a maleimide with an attached three-carbon chain, and coupled it to Avd(S16C). However, the quenching of fluorescence did not decrease, although the recovery of fluorescence after the addition of free biotin was even faster in the case of Mal-β-ala than bare maleimide (Figure 3D) indicating that larger molecules can decrease the affinity of Avd(S16C) for biotin more efficiently.

The quenching of fluorescence of dcAvd-Cys coupled with maleimide was 45.0±5.3% (Figure 3B), which was an intermediate of the values measured for wt avidin and Avd(S16C). Therefore, it seems that maleimide was able to inhibit the binding of biotin to the cysteine-modified binding site in the cpAvd6→5 domain of the dcAvd-Cys. As a consequence, the remaining biotin-binding activity of dcAvd-Cys would depend mainly on the cpAvd5→4 domain, which closely resembles that of wt avidin [17,20]. The rapid burst (~10%) in the recovery of fluorescence just after the addition of free biotin was most probably mainly associated with the dissociation of fluorescent biotin from the cpAvd6→5 domain with the S16C modified binding site. The burst is followed by a slow phase of biotin dissociation from the cpAvd5→4 domain with an unmodified ligand-binding site. After an hour the recovery of fluorescence of dcAvd-Cys-MI was 26.3±7.8% suggesting that the cpAvd5→4 domain had a wt-like biotin-binding affinity.

Again, the biotin dissociation results were confirmed using ^{3}H-biotin (Figure 3E,G). Maleimide had no effect on the ability of wt avidin to bind or release ^{3}H-biotin, since the amount of unbound ^{3}H-biotin was 2.7±0.1% and the dissociation of the bound ^{3}H-biotin 24 hours after the addition of cold biotin was 7%. In contrast, maleimide significantly reduced the ability of Avd(S16C) to bind ^{3}H-biotin as the amount of unbound ^{3}H-biotin was 25.6±0.1%. Following the addition of a 1000-fold excess of cold biotin, Avd(S16C) rapidly released over 85% of the bound ^{3}H-biotin and during 24 hours the release exceeded 90%. Furthermore, Mal-β-ala decreased the ability of Avd(S16C) to bind ^{3}H-biotin, since the amount of free ^{3}H-biotin was 34.9±0.4% and following the addition of cold biotin the dissociation of the bound ^{3}H-biotin reached 100%. With dcAvd-Cys conjugated with maleimide, the amount of unbound ^{3}H-biotin was 16.5±0.3% and the addition of cold biotin led to dissociation of 15% of the bound biotin after 24 hours, showing a slight increase compared to wt avidin.

According to both dissociation assays coupling with maleimide increased the dissociation of BF560-biotin and ^{3}H-biotin from Avd(S16C), whereas the dissociation from dcAvd-Cys decreased in comparison to non-conjugated proteins. We believe that maleimide blocks most of the S16C-modified binding sites on dcAvd-Cys and the unmodified sites behave like the binding sites of wt avidin. We expect the coupling efficiency of dcAvd-Cys with maleimide to be high, as was in the case of Avd(S16C).

Dual chain avidin with two different ligands

In order to demonstrate the possibility of introducing new molecules to the cpAvd6→5 domain via a maleimide linker we performed a fluorescence resonance energy transfer (FRET) experiment. As a donor we used a fluorescent maleimide (MI) derivative, DY560-MI, which reacts with the introduced thiol group of Cys16 in the cpAvd6→5 domain forming a stable covalent thioether bond. The fluorescent biotin derivative, DY633-biotin acted as the acceptor occupying the unmodified biotin-binding site in the cpAvd5→4 domain. See Figure S2 for structures of DY560-MI and DY633-biotin. After exciting the complex with 560 nm, the DY560-MI was found to transfer energy to the DY633-biotin (Figure 4A). As a result, we saw quenching of the donor emission by 73% and increased acceptor emission (Figure 4C), suggesting the coexistence of both dyes in the same protein tetramers. When the

binding sites of the cpAvd5→4 domains were blocked with biotin before addition of DY633-biotin, the emission of the donor was quenched less than 13% (Figure 4D). The fluorescence spectra normalized according to the maximum fluorescence at 590 nm of dcAvd-Cys in the presence of both DY560-MI and DY633-biotin clearly indicated an increase in acceptor emission when the donor and the acceptor were bound to the same protein tetramer (Figure 4E). The increase in acceptor emission was insignificant when the unmodified binding sites were blocked with biotin before the FRET experiment (Figure 4D,E). According to previous studies the fluorescence of another biotin dye (DY630-biotin) increased two-fold after the addition of avidin [19]. Similarly, DY633-biotin also showed increased fluorescence emission accompanied by a slight shift in the emission maximum to the longer wavelength when bound to avidin or to dcAvd-Cys. Still, in the FRET experiments the increase in fluorescence was only about 10% (data not presented), since DY633 was excited at 559 nm, which is the wavelength of the DY560 excitation maximum. This increase alone did not explain the increase of the acceptor emission when both donor and acceptor were present.

The size of the avidin tetramer is about 50×50×40 Å and the distance between neighboring cpAvd5→4 to cpAvd6→5 (subunit one and subunit two, or subunit three and subunit four) biotin tails is roughly 20 Å (Figure 4B) as measured from the avidin 3D-structure (PDB 2AVI) using the VMD 1.8.7 program. The fluorescent labels used in the experiment have ten-atom (DY560-MI) and nine-atom (DY633-biotin) flexible linkers. Therefore, the theoretical maximal distance between labels attached to subunits one and two, or to subunits three and four (for clarification, see also the three-dimensional structure of avidin (Figure 1A), would be ~50 Å, although the structural features of avidin limit the maximal distance to around (30±10) Å in reality. In contrast, the distance between biotin tails bound to another cpAvd5→4 - cpAvd6→5 pair over the symmetry axis of a dcAvd molecule would be about 30 Å and with linkers (60±10) Å. Taken together, if both DY560-MI and DY630-biotin had been bound to subunits one and two, respectively, or to subunits three and four, FRET should have been very efficient. Therefore, our results suggest the binding of dyes to subunits one and four, or to subunits two and three. This assumption is supported by previous studies showing that the affinity towards biotinylated dyes decreases when more than two dyes are bound per molecule [23,24]. In other words, binding of DY560 equipped with a short linker might inhibit the binding of DY633-biotin to the neighboring binding site. This phenomenon known as anti-cooperative binding is described elsewhere [24].

The efficiency of bioconjugation was determined as the degree of labeling per tetramer (the measured absorbance data presented as Table S2 in Supporting Information). Labeling of wt avidin yielded no bound DY560-maleimides verifying the specificity of the reaction. The degree of labeling was 0.6±0.1 per dcAvd-Cys pseudotetramer. As a control, Avd(S16C) was also labeled with an identical protocol and the degree of labeling was found to be 0.6 per tetramer. We would have expected a higher bioconjugation efficiency, as results obtained by mass spectrometry suggested nearly complete conjugation of Avd(S16C) both with maleimide and N-ethylmaleimide. Thus the low conjugation efficiency may be associated with the non-optimized structure of linker between maleimide and the dye.

Discussion

A great number of studies performed during the past two decades have indicated that the biotin-binding pocket of (strept)avidin strongly favors its natural ligand, biotin, and it is thus difficult to develop novel ligands, which are not competed out by biotin [2]. Here we present a novel concept for engineering these biotin-binding proteins. A single point mutation S16C in the ligand-binding site of avidin generates an active thiol group, which can be chemically linked to, for example maleimide, as shown here. As a result, a targeted genetic engineering followed by a mild chemical treatment can now be used to control the activity of avidin. Introducing S16C mutation to dcAvd creates two modified binding sites per pseudotetramer. Both mutant sites can be controlled, while the two remaining binding sites resemble those of wt avidin (Figure 3A). The possibility to further modify both biotin binding sites in dcAvd independently provides new opportunities for creating tailored avidins for applications in bio- and nanotechnology. As demonstrated here, dcAvd-Cys can be used in FRET experiments with maleimide- and biotin-dyes (Figure 4). DcAvd-Cys might also prove to be a valuable building block for creating molecular arrangements, for example on sensor surfaces.

The positioning of Cys16 in the ligand-binding pocket of Avd(S16C) and dcAvd-Cys did not significantly affect protein folding, since the proteins could be produced with standard expression methods and the isolated proteins had normal oligomeric states according to an SDS-PAGE assay. However, replacing a serine residue in the biotin-binding pocket led to a modest decrease in biotin-binding affinity, resembling that of the previously introduced S16A mutation [7]. Importantly, the location of the introduced cysteine residue was selected so that it is not available for disulphide bonding between avidin subunits. This improves the usability of the protein since reducing agents and subsequent laborious buffer exchanges can be avoided.

The strategy used here could also be applied to the independent modification of binding sites in single chain avidin (scAvd), which has four binding sites in one polypeptide chain [18]. This would make it possible to create avidins with one to four active binding sites per tetramer, freely selecting the positioning of the active sites (Figure 5). The advantage of the Cys-based strategy described here is the wide availability of maleimide reagents, which enable production of tailored proteins to different purposes. In addition, a completely inactive binding site could be created, for example, by combining the mutations S16R [25] and N118M [15]. Furthermore, we have recently modified avidin by random mutagenesis to bind other small ligands. As a proof of principle, avidin was modified to bind testosterone (Paldanius et al. unpublished results). One may also envision an extension to the palette of chemicals used in this scheme. As was demonstrated earlier, Tyr33 in avidin can be specifically modified by tetranitromethane leading to reversible biotin binding [26]. Since it is possible to apply the mutation Y33F to avidin without severe loss in biotin-binding affinity, one could use this to introduce other specific chemical fingerprint to the subunits.

Finally, the properties of covalent and noncovalent binding are different. In the case of avidin, biotin binding can be considered a virtually irreversible reaction. However, if the bond is subjected to mechanical force, the bond lifetime can decrease substantially [27]. Therefore, the technology developed here offer great potential for novel technologies, such as atomic force microscopy (AFM) and molecular recognition force spectroscopy (MRFS), relying on extremely stable and specific molecular bonding.

Materials and Methods

Design, production and purification of recombinant proteins

The site-directed mutagenesis of the cDNA encoding avidin, cpAvd6→5 and cpAvd5→4 was performed by the QuikChange

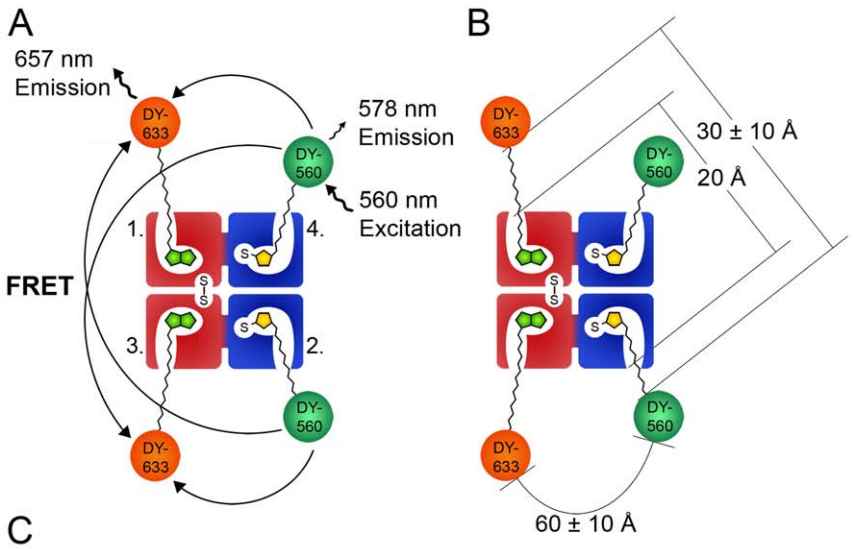
A
657 nm
Emission
DY-
633
578 nm
Emission
DY-
560
560 nm
Excitation
1.
4.
FRET
3.
2.
DY-
560
DY-
633
B
DY-
633
DY-
560
30 ± 10 Å
20 Å
DY-
560
DY-
633
60 ± 10 Å

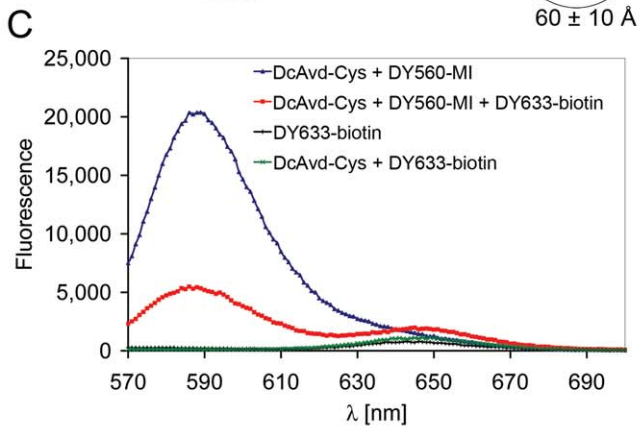
C
25,000
20,000
15,000
10,000
5,000
0
Fluorescence
DcAvd-Cys + DY560-MI
DcAvd-Cys + DY560-MI + DY633-biotin
DY633-biotin
DcAvd-Cys + DY633-biotin
570
590
610
630
650
670
690
λ [nm]

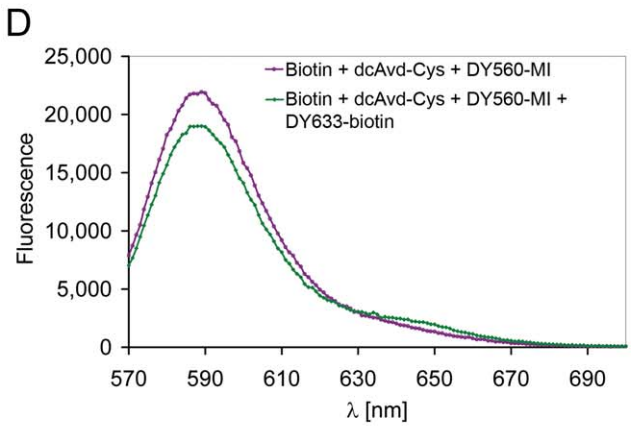
D
25,000
20,000
15,000
10,000
5,000
0
Fluorescence
Biotin + dcAvd-Cys + DY560-MI
Biotin + dcAvd-Cys + DY560-MI +
DY633-biotin
570
590
610
630
650
670
690
λ [nm]

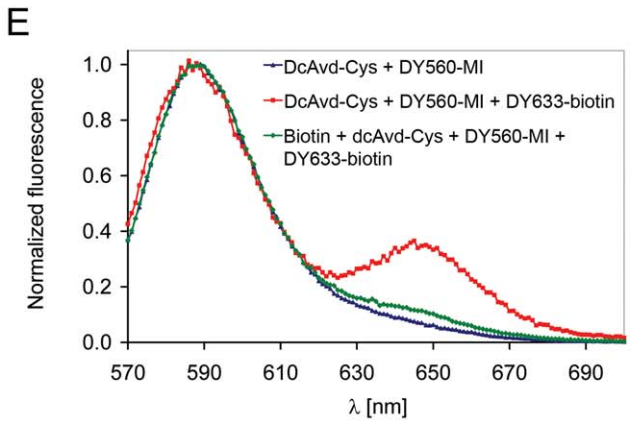
E
1.0
0.8
0.6
0.4
0.2
0.0
Normalized fluorescence
DcAvd-Cys + DY560-MI
DcAvd-Cys + DY560-MI + DY633-biotin
Biotin + dcAvd-Cys + DY560-MI +
DY633-biotin
570
590
610
630
650
670
690
λ [nm]

Figure 4. A FRET experiment with dcAvd-Cys. (**A**) A schematic of the FRET of the dcAvd-Cys. The DY560-maleimide (DY560-MI) acting as a FRET donor could be coupled to the Cys16-modified binding sites of dcAvd-Cys, whereas DY633-biotin acting as a FRET acceptor bound to the unmodified binding sites. (**B**) A schematic of the distances of the fluorescent labels attached to dcAvd-Cys. The distance between labels attached to the same side of the dcAvd-Cys molecule is limited by structural features of avidin to 30±10 Å. In contrast, the distance between the labels bound to another cpAvd5→4 - cpAvd6→5 pair over the symmetry axis of the avidin is ~60±10 Å. (**C, D**) Fluorescence intensity of dcAvd-Cys with a FRET donor and acceptor. The intensities are corrected for sample dilution. (**C**) After exciting the protein complex at 560 nm, the DY560-MI transfers energy to the DY633-biotin, which caused quenching of the donor emission and increased acceptor emission. When the DY633-biotin incubated with dcAvd-Cys or the DY633-biotin label alone was excited at 560 nm the complexes had a minimal fluorescence at 657 nm. (**D**) The quenching of the donor emission decreased when the unmodified binding sites of DcAvd-Cys were blocked with biotin before the addition of DY633-biotin. (**E**) The fluorescence spectra normalized according to the maximum fluorescence at 590 nm of dcAvd-Cys with donor and acceptor present clearly indicated acceptor emission as a consequence of FRET. The acceptor emission was minimal when unmodified binding sites were blocked with biotin before the addition of DY633-biotin indicating that FRET did not occur.
doi:10.1371/journal.pone.0016576.g004

(Stratagene, La Jolla, CA, USA) or megaprimer methods [28]. Sequences of primers used in PCR are shown in Table S3. To obtain efficient bacterial secretion the bacterial signal peptide OmpA from *Bordetella avium* was used in front of the Avd(S16C) sequence. The amplified PCR-product was extracted from an agarose gel and subcloned into the pET101/D-TOPO® vector according to the manufacturers instructions (Invitrogen, Carlsbad, CA, USA). Similarly, mutagenized forms of cpAvd5→4(I117C) and cpAvd6→5(S16C, V115H) were joined together by ligation and the complete dcAvd-Cys was subcloned into a pFastBac vector (Invitrogen). All constructs were confirmed by DNA sequencing (ABI PRISM 3100 Genetic Analyzer, Applied Biosystems).

Avidin and Avd(S16C) were produced in *E. coli* BL21-AI cells (Invitrogen) as described in detail earlier [29]. The pET101/D-based expression vectors were transformed into *E. coli* BL21-(AI) cells (Invitrogen). The fresh transformants were cultured in Lysogeny broth (LB) medium with supplements of 0.1% (w/v) glucose and 100 µg/ml ampicillin at 27°C with rotation at 220 rev/min. When culture reached OD_{600} 0.2–0.4 the protein expression was induced by adding 0.2% (w/v) L-arabinose and 1 mM IPTG. Cultivation was continued at 27°C an additional 18 hours before cells were collected by centrifugation (5000 g, 10 min, 4°C).

The Bac-To-Bac® baculovirus expression system (Invitrogen) was used to produce dcAvd-Cys as instructed by the manufacturer

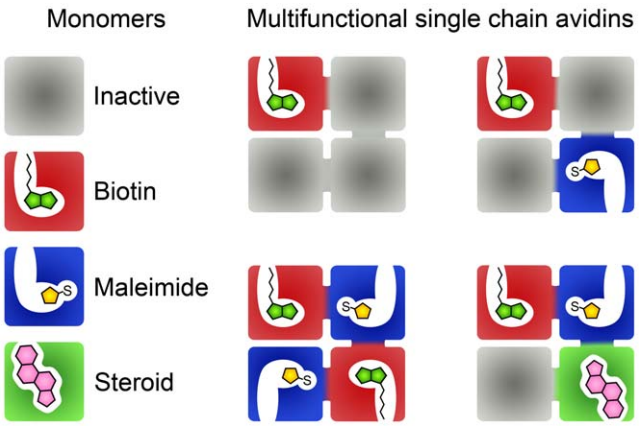

Figure 5. Strategies to selectively modify the binding sites of single chain avidin. Since all four binding sites are encoded by one polypeptide chain, each of them can be modified independently. A combination of the mutations S16R [25] and N118M [15] would lead to a completely inactive monomer, which could be useful in some experiments. In our previous experiments we have generated a steroid binding avidin as an example of an altered binding specificity (Paldanius et al. unpublished results).
doi:10.1371/journal.pone.0016576.g005

and as described in detail previously [22]. Briefly, the pFastBac construct was transformed into *E. coli* DH10Bac cells to generate a recombinant bacmid, which was purified and transfected into *Spodoptera frugiperda* Sf9 insect cells to generate a recombinant baculovirus. The primary baculovirus stock was further amplified for a larger scale production of recombinant dcAvd-Cys. Approximately 2×10^8 Sf9 cells were seeded to a final volume of 100 ml of HyClone SFX-Insect cell culture medium (Thermo Fisher Scientific, Waltham, MA, USA) without biotin in a 250 ml Erlenmayer flask. Recombinant viruses were added in ratio of 1:100 and transfected cells were cultured for three days at 28°C with rotation at 125 rev/min. The cells were pelleted by centrifugation (500 g, 10 min, RT).

All produced proteins were purified in a single step with a 2-iminobiotin affinity agarose column (Affiland S. A., Ans-Liege, Belgium). First, cell pellets from *E. coli* cultivations containing avidin and Avd(S16C) were suspended in 30 mM Tris-HCl buffer (pH 8) containing 2 mM EDTA and 20% sucrose. Then lysozyme was added to a final concentration of 2.5 µg/ml and cell lysates were incubated on ice for 30 minutes. After this, 50 mM Tris-HCl buffer (pH 8) containing 2 mM EDTA, 150 mM NaCl and 1% Triton X-100 was added and cells were sonicated two times for five min (50% duty cycle, 5 s on, 3 s off) on ice. This was followed by centrifugation (15 000 g, 30 min, 4°C) of the cell lysate, after which the supernatant was filtered and mixed with an equal volume of binding buffer (50 mM Na-carbonate buffer (pH 11) containing 1 M NaCl). The crude protein mixture was applied to 2-iminobiotin agarose (1 ml), which had previously been equilibrated with binding buffer. The obtained mixture was incubated for one hour on a rolling shaker at 4°C with subsequent centrifugation (500 g, 5 min, RT) and two washing steps with binding buffer. Finally, agarose was transferred to a column and proteins were eluted in one ml fractions with 50 mM sodium acetate buffer (pH 4) containing 100 mM NaCl.

The first steps of purification of dcAvd-Cys from insect cells differed from the steps described above for purifications from bacterial cells. First, the cell pellet from insect cell culture was suspended in 50 mM Tris-HCl (pH 8) buffer containing 2 mM EDTA, 150 mM NaCl and 1% Triton X-100. The obtained cell lysate was sonicated two times for five min (50% duty cycle, 1 s on, 1 s off) on ice. The steps following sonication were similar to those described above for avidin and Avd(S16C) purification.

Following purification all proteins were dialyzed against 50 mM Na-phosphate buffer (pH 7.0) containing 100 mM NaCl. The molecular masses of the proteins were analysed with 15% SDS-PAGE gel stained with Coomassie Brilliant Blue. Proteins were denaturated in SDS-PAGE sample buffer with or without a reducing agent (β-mercaptoethanol) by heating at 95°C for ten minutes. The protein concentrations were determined with a UV/Vis spectrophotometer (NanoDrop 1000 Spectrophotometer, Thermo Scientific, Wilmington, DE, USA) by measuring the

absorbance at 280 nm and using an extinction coefficient of 23615 $M^{-1}cm^{-1}$ for both avidin and Avd(S16C) monomers and 47355 $M^{-1}cm^{-1}$ for the dcAvd-Cys pseudodimer.

SDS-PAGE-based thermostability assay

Protein samples in the absence and in the presence of D-biotin (Fluka Chemie GmbH, Buchs, Switzerland) were acetylated *in vitro*. An equal volume of SDS-PAGE buffer with β-mercaptoethanol was added and the samples were heated to selected temperatures between RT and 100°C for 20 min. The oligomeric states of the proteins were analysed by 15% SDS-PAGE gel followed by Coomassie Brilliant Blue staining described in detail by Bayer and his coworkers [30].

Maleimide treatment

Maleimide (Sigma-Aldrich, St. Louis, MO, USA) as well as N-maleoyl-β-alanine (Mal-β-ala, Sigma-Aldrich) were dissolved in DMSO and added in a 100-fold molar excess to the protein solution in 50 mM Na-phosphate buffer (pH 7.0) containing 100 mM NaCl. The samples were incubated at RT for one hour.

Mass spectrometry

All mass spectrometric measurements were performed with a 4.7-T hybrid quadrupole–FT-ICR instrument (APEX-Qe™; Bruker Daltonics, Billerica, MA, USA), described in detail earlier [31]. Lyophilized avidins were dissolved in HPLC-grade water and desalted with PD-10 columns (Amersham Biosciences, Uppsala, Sweden), equilibrated in advance with 10 mM ammonium acetate buffer (pH 6.8). Desalted protein samples were further concentrated with Microcon (3-kDa cut-off) centrifugal filter devices (Millipore, Billerica, MA, USA). The samples (untreated or treated with maleimide) were further diluted with acetonitrile/water/acetic acid (49.5:49.5:1.0, v/v) solution and directly infused into the ESI source at a flow rate of 1.5 µL/min. Maleimide and N-ethylmaleimide (Sigma-Aldrich) were dissolved in HPLC-grade DMSO to a concentration of ~3 mM, mixed with avidins (ten-fold molar excess of maleimide) and subsequently incubated at RT for 15–30 min before measurements. In-solution trypsin digestion was performed by incubating 150 µl of a 10 µM avidin sample with 0.25 µl of 0.5 mg/ml trypsin (corresponding to ~1:40 w/w trypsin:protein ratio) in 10 mM ammonium acetate buffer (pH 6.8) for four hours at RT. The resulting peptide mixtures were diluted two-fold with acetonitrile/acetic acid (99:1, vv) and measured immediately. All mass values given in the text refer to the most abundant isotopic masses, either experimentally determined or theoretically calculated from the sequence-derived atomic compositions, unless otherwise stated.

Biotin dissociation assays

The biotin-binding properties of avidins were studied by dissociation assays using two different methods involving fluorescently labelled biotin (BF560-biotin™, ArcDia Ltd, Turku, Finland) and radioactive biotin ([8,9-^{3}H]biotin, PerkinElmer, Waltham, MA, USA). The measurements were performed at RT.

The fluorescence signal from unbound BF560-biotin™ in 3 ml (50 mM Na-phosphate buffer (pH 7.0) containing 650 mM NaCl) was measured for 300 seconds. This was followed by the addition of a two-fold molar excess of protein and the binding of the fluorescent biotin was detected for 300 seconds as quenching of the fluorescence. The fluorescence recovery was measured for one hour after the addition of a 100-fold molar excess of free D-biotin (Fluka Chemie GmbH). A QuantaMaster™ spectrofluorometer (Photon Technology International, Inc., Lawrenceville, NJ, USA) was used to excite the sample at 560 nm and to detect emission at 576 nm. Each measurement was performed twice.

Radioactive ^{3}H-biotin at a concentration of 10 nM was incubated overnight with a 50 nM subunit concentration of protein. The unbound ^{3}H-biotin was separated from the protein-ligand complex by centrifugal ultrafiltration through 30,000 MW cutoff filters (Vivaspin 500 centrifugal concentrators, Sigma-Aldrich). Measurements were performed in 50 mM Na-phosphate buffer (pH 7.0) containing 100 mM NaCl and 10 µg BSA per ml to prevent non-specific binding. To initiate the dissociation reaction, cold biotin was added to a final concentration of 50 µM and the released ^{3}H-biotin was separated from the protein-ligand complex at different time points by ultrafiltration. The radioactivity of the filtrate was analyzed in a Wallac 1410 liquid scintillation counter (Wallac Oy, Turku, Finland). Triplicates of each sample were measured at each time point.

The fraction of bound fluorescent or radioactive biotin at each time point and the dissociation rate constants (k_{diss}) were determined using the equation (1):

$$-k_{diss}t = \ln\left[\frac{(x_t - x)}{(x_t - x_0)}\right] = \ln(\textit{fraction bound}) \qquad (1)$$

where x_t is the total amount of fluorescent/radioactive ligand before the addition of protein, x is the free biotin at each time point and x_0 is the amount of free ligand in the presence of protein just before the addition of the competing biotin [11]. The first 500 s were omitted from the data to eliminate the effect of the fast initial-phase characteristic of the avidin-BF650-biotin™ interaction [7].

Fluorescence resonance energy transfer assay

The FRET donor DY560-maleimide (DY560-MI) (absorption/emission max: 559 nm/578 nm (in ethanol), molar extinction coefficient: 120.000 $M^{-1}cm^{-1}$) and the FRET acceptor DY633-biotin (absorption/emission max.: 637 nm/657 nm (in ethanol), molar extinction coefficient: 200.000 $M^{-1}cm^{-1}$) for this study were supplied by Dyomics GmbH (Jena, Germany).

Proteins in 50 mM Na-phosphate buffer (pH 7.0) containing 100 mM NaCl were incubated with a five-fold molar excess of DY560-MI for two hours at RT protected from light. The obtained protein-dye conjugate was separated from the free dye by dialysis. The absorption spectrum for the protein-dye conjugate was recorded with a PerkinElmer Lambda 35 UV/Vis spectrometer (PerkinElmer Life and Analytical Sciences) over the full wavelength range. The absorption maxima of the wavelengths 280 nm and 560 nm were used to calculate a dye/protein ratio (5) according to a formula derived from the Lambert-Beer law for the absorption maximum of the dye (2) and for the absorption maximum of the protein at 280 nm adjusted by a correction factor, *CF*, (4) contributed by the dye absorbance at 280 nm. The extinction coefficients used in the calculations were 94460 $M^{-1}cm^{-1}$ for the avidin and Avd(S16C) tetramers and 94710 $M^{-1}cm^{-1}$ for the dcAvd-Cys pseudotetramer.

$$c_{dye} = \frac{A_{\max}}{\varepsilon' \times l} \qquad (2)$$

ε' = molar extinction coefficient of the fluorescent dye

$$c_{prot} = \frac{A_{280} - (A_{\max} \times CF)}{\varepsilon \times l} \times DF \qquad (3)$$

DF, dilution factor.

$$CF = \frac{A_{280}(dye)}{A_{560}(dye)} \quad (4)$$

$$Dye/protein = \frac{c_{dye}}{c_{protein}} \quad (5)$$

A QuantaMaster™ spectrofluorometer (Photon Technology International, Inc., Lawrenceville, NJ, USA) was used to excite the sample at 559 nm and to detect the emission spectra from 570 nm to 700 nm. The measurements were performed at RT in a 50 mM Na-phosphate buffer (pH 7.0) containing 100 mM NaCl. First, the emission spectrum was measured for DY560-maleimide conjugated with dcAvd-Cys. This was followed by the addition of DY633-biotin, after which the emission spectrum showing the quenching of the donor emission and the increase of the acceptor emission was measured. As a control measurement the emission spectrum for DY633-biotin alone, and incubated with dcAvd-Cys without DY560-MI were measured. Finally, free biotin was incubated with dcAvd-Cys conjugated with DY560-maleimide and the emission was measured before and after the addition of DY633-biotin. The fluorescence intensities of the measured emission spectra were corrected for sample dilution. Moreover, the fluorescence spectra were normalized according to the maximum fluorescence of dcAvd-Cys in the presence of both DY560-MI and DY633-biotin at 590 nm to clearly indicate the occurrence of FRET when both labels were bound to the same protein tetramer.

Supporting Information

Figure S1 SDS-PAGE thermal stability analysis of avidin, Avd(S16C) and dcAvd-Cys without (−) and with (+) biotin. The transition temperature was determined after 20 minute heat treatment in the presence of SDS and β-mercaptoethanol followed by SDS-PAGE analysis. M, molecular weight marker.
(TIF)

Figure S2 Structures of fluorescent conjugates used in FRET experiment. (**A**) DY560-maleimide acting as a FRET donor and (**B**) DY633-biotin acting as a FRET acceptor.
(TIF)

Table S1 Trypsin digestion data for Avidin, Avd(S16C) and Avd(S16C) treated with maleimide. Three additional amino acid residues (QTV) originating from the *B. avium* OmpA signal peptide in the N-terminus of the protein are numbered to −3, −2 and −1. Among the identified peptides for Avd(S16C) treated with maleimide, a peptide having a monoisotopic mass of 1947.8630 Da was observed, consistent with the maleimide conjugation into residues 10–26 (highlighted in red). With untreated Avd(S16C), this peptide was absent, but a peptide having a monoisotopic mass of 1850.8512 Da was observed instead, corresponding to the uncoupled tryptic peptide 10–26 (highlighted in red).
(DOC)

Table S2 The degree of labeling per protein tetramer determined by measuring the absorbance at 280 nm and 560 nm for avidin, Avd(S16C), dcAvd-Cys, and for the label, DY560-maleimide (MI).
(DOC)

Table S3 Primers used in polymerase chain reactions (PCR).
(DOC)

Acknowledgments

We thank Ulla Kiiskinen and Soili Hiltunen for their excellent technical assistance and Sampo Kukkurainen for preparing picture of crystal structure of avidin. We also thank Dr. Jussi Toppari (NanoScience Center, University of Jyväskylä) for valuable comments.

Author Contributions

Conceived and designed the experiments: JL JAEM JJ VPH. Performed the experiments: JL HH MS ML JJ. Analyzed the data: JL JAEM ML JJ VPH. Contributed reagents/materials/analysis tools: JJ MSK VPH. Wrote the paper: JL JJ VPH.

References

1. Green NM (1975) Avidin. Adv Protein Chem 29: 85–133.
2. Laitinen OH, Hytönen VP, Nordlund HR, Kulomaa MS (2006) Genetically engineered avidins and streptavidins. Cell Mol Life Sci 63(24): 2992–3017.
3. Wilchek M, Bayer EA (1990) Introduction to avidin-biotin technology. Methods Enzymol 184: 5–13.
4. Hendrickson WA, Pahler A, Smith JL, Satow Y, Merritt EA, et al. (1989) Crystal structure of core streptavidin determined from multiwavelength anomalous diffraction of synchrotron radiation. Proc Natl Acad Sci U S A 86(7): 2190–2194.
5. Livnah O, Bayer EA, Wilchek M, Sussman JL (1993) Three-dimensional structures of avidin and the avidin-biotin complex. Proc Natl Acad Sci U S A 90(11): 5076–5080.
6. Eisenberg-Domovich Y, Hytönen VP, Wilchek M, Bayer EA, Kulomaa MS, et al. (2005) High-resolution crystal structure of an avidin-related protein: Insight into high-affinity biotin binding and protein stability. Acta Crystallogr D 61: 528–538.
7. Hytönen VP, Nordlund HR, Hörhä J, Nyholm TK, Hyre DE, et al. (2005) Dual-affinity avidin molecules. Proteins 61(3): 597–607.
8. Marttila AT, Hytönen VP, Laitinen OH, Bayer EA, Wilchek M, et al. (2003) Mutation of the important tyr-33 residue of chicken avidin: Functional and structural consequences. Biochem J 369(Pt 2): 249–254.
9. Hyre DE, Le Trong I, Freitag S, Stenkamp RE, Stayton PS (2000) Ser45 plays an important role in managing both the equilibrium and transition state energetics of the streptavidin-biotin system. Protein Sci 9(5): 878–885.
10. Freitag S, Chu V, Penzotti JE, Klumb LA, To R, et al. (1999) A structural snapshot of an intermediate on the streptavidin-biotin dissociation pathway. Proc Natl Acad Sci U S A 96(15): 8384–8389.
11. Klumb LA, Chu V, Stayton PS (1998) Energetic roles of hydrogen bonds at the ureido oxygen binding pocket in the streptavidin-biotin complex. Biochemistry 37(21): 7657–7663.
12. Dixon RW, Radmer RJ, Kuhn B, Kollman PA, Yang J, et al. (2002) Theoretical and experimental studies of biotin analogues that bind almost as tightly to streptavidin as biotin. J Org Chem 67(6): 1827–1837.
13. Reznik GO, Vajda S, Sano T, Cantor CR (1998) A streptavidin mutant with altered ligand-binding specificity. Proc Natl Acad Sci U S A 95(23): 13525–13530.
14. Aslan FM, Yu Y, Mohr SC, Cantor CR (2005) Engineered single-chain dimeric streptavidins with an unexpected strong preference for biotin-4-fluorescein. Proc Natl Acad Sci U S A 102(24): 8507–8512.
15. Määttä JA, Airenne TT, Nordlund HR, Jänis J, Paldanius TA, et al. (2008) Rational modification of ligand-binding preference of avidin by circular permutation and mutagenesis. Chembiochem 9(7): 1124–1135.
16. Howarth M, Chinnapen DJ, Gerrow K, Dorrestein PC, Grandy MR, et al. (2006) A monovalent streptavidin with a single femtomolar biotin binding site. Nat Methods 3(4): 267–273.
17. Nordlund HR, Laitinen OH, Hytönen VP, Uotila ST, Porkka E, et al. (2004) Construction of a dual chain pseudotetrameric chicken avidin by combining two circularly permuted avidins. J Biol Chem 279(35): 36715–36719.
18. Nordlund HR, Hytönen VP, Hörhä J, Määttä JA, White DJ, et al. (2005) Tetravalent single-chain avidin: From subunits to protein domains via circularly permuted avidins. Biochem J 392(Pt 3): 485–491.
19. Nordlund HR, Hytönen VP, Laitinen OH, Uotila STH, Niskanen EA, et al. (2003) Introduction of histidine residues into avidin subunit interfaces allows pH-dependent regulation of quaternary structure and biotin binding. FEBS Letters 555(3): 449–454.
20. Hytönen VP, Hörhä J, Airenne TT, Niskanen EA, Helttunen KJ, et al. (2006) Controlling quaternary structure assembly: Subunit interface engineering and crystal structure of dual chain avidin. J Mol Biol 359(5): 1352–1363.
21. Hytönen VP, Nyholm TK, Pentikäinen OT, Vaarno J, Porkka EJ, et al. (2004) Chicken avidin-related protein 4/5 shows superior thermal stability when

compared with avidin while retaining high affinity to biotin. J Biol Chem 279(10): 9337–9343.
22. Airenne KJ, Oker-Blom C, Marjomäki VS, Bayer EA, Wilchek M, et al. (1997) Production of biologically active recombinant avidin in baculovirus-infected insect cells. Protein Expr Purif 9: 100–108.
23. Gruber HJ, Kada G, Marek M, Kaiser K (1998) Accurate titration of avidin and streptavidin with biotin-fluorophore conjugates in complex, colored biofluids. Biochim Biophys Acta 1381(2): 203–212.
24. Kada G, Falk H, Gruber HJ (1999) Accurate measurement of avidin and streptavidin in crude biofluids with a new, optimized biotin-fluorescein conjugate. Biochim Biophys Acta 1427(1): 33–43.
25. Kopetzki E, Muller R, Engh R, Schmitt U, Deger A, et al. (2002) Recombinant Inactive avidin mutants. (US6391571 (B1)) Patent.
26. Morag E, Bayer EA, Wilchek M (1996) Reversibility of biotin-binding by selective modification of tyrosine in avidin. Biochem J 316(Pt 1): 193–199.
27. Evans E (2001) Probing the relation between force-lifetime-and chemistry in single molecular bonds. Annu Rev Biophys Biomol Struct 30: 105–128.
28. Sarkar G, Sommer SS (1990) The "megaprimer" method of site-directed mutagenesis. BioTechniques 8(4): 404–407.
29. Hytönen VP, Laitinen OH, Airenne TT, Kidron H, Meltola NJ, et al. (2004) Efficient production of active chicken avidin using a bacterial signal peptide in Escherichia Coli. Biochem J 384: 385–390.
30. Bayer EA, Kulik T, Adar R, Wilchek M (1995) Close similarity among streptavidin-like, biotin-binding proteins from Streptomyces. Biochim Biophys Acta 1263: 60–66.
31. Helppolainen SH, Määttä JA, Halling KK, Slotte JP, Hytönen VP, et al. (2008) Bradavidin II from Bradyrhizobium japonicum: A new avidin-like biotin-binding protein. Biochim Biophys Acta 1784: 1002–1010.

Bifunctional Avidin with Covalently Modifiable Ligand Binding Site

Jenni Leppiniemi[1], Juha A. E. Määttä[1], Henrik Hammaren[1], Mikko Soikkeli[1], Mikko Laitaoja[2], Janne Jänis[2], Markku S. Kulomaa[1], Vesa P. Hytönen[1]

1 Institute of Medical Technology, University of Tampere and Tampere University Hospital, Tampere, Finland,
2 Department of Chemistry, University of Eastern Finland, Joensuu, Finland

Table 1. Thermal stability of the avidin proteins.

Protein	T_r – biotin (ºC)	T_r + biotin (ºC)
Avidin	55	95
Avd(S16C)	60	75
dcAvd(I117C$_{5\rightarrow4,}$V115H$_{6\rightarrow5}$)	ND[a]	80[a]
dcAvd-Cys	ND[b]	60

The transition temperature of proteins without (-) and with (+) biotin was determined by heating samples in the presence of SDS and 2-mercaptoethanol for 20 minutes, followed by SDS-PAGE analysis. Biotin was added prior to heat treatment and the sample was incubated for 5 minutes before heating.

[a] From Hytönen *et al*. [20].

[b] The transition temperature could not be determined because the protein appeared as a diffuse band already at room temperature. At temperatures above 40 ºC, the protein was almost totally monomeric.

Supporting Information

Bifunctional Avidin with Covalently Modifiable Ligand Binding Site

Jenni Leppiniemi[1], Juha A. E. Määttä[1], Henrik Hammaren[1], Mikko Soikkeli[1], Mikko Laitaoja[2], Janne Jänis[2], Markku S. Kulomaa[1], Vesa P. Hytönen[1]

1 Institute of Medical Technology, University of Tampere and Tampere University Hospital, Tampere, Finland,
2 Department of Chemistry, University of Eastern Finland, Joensuu, Finland

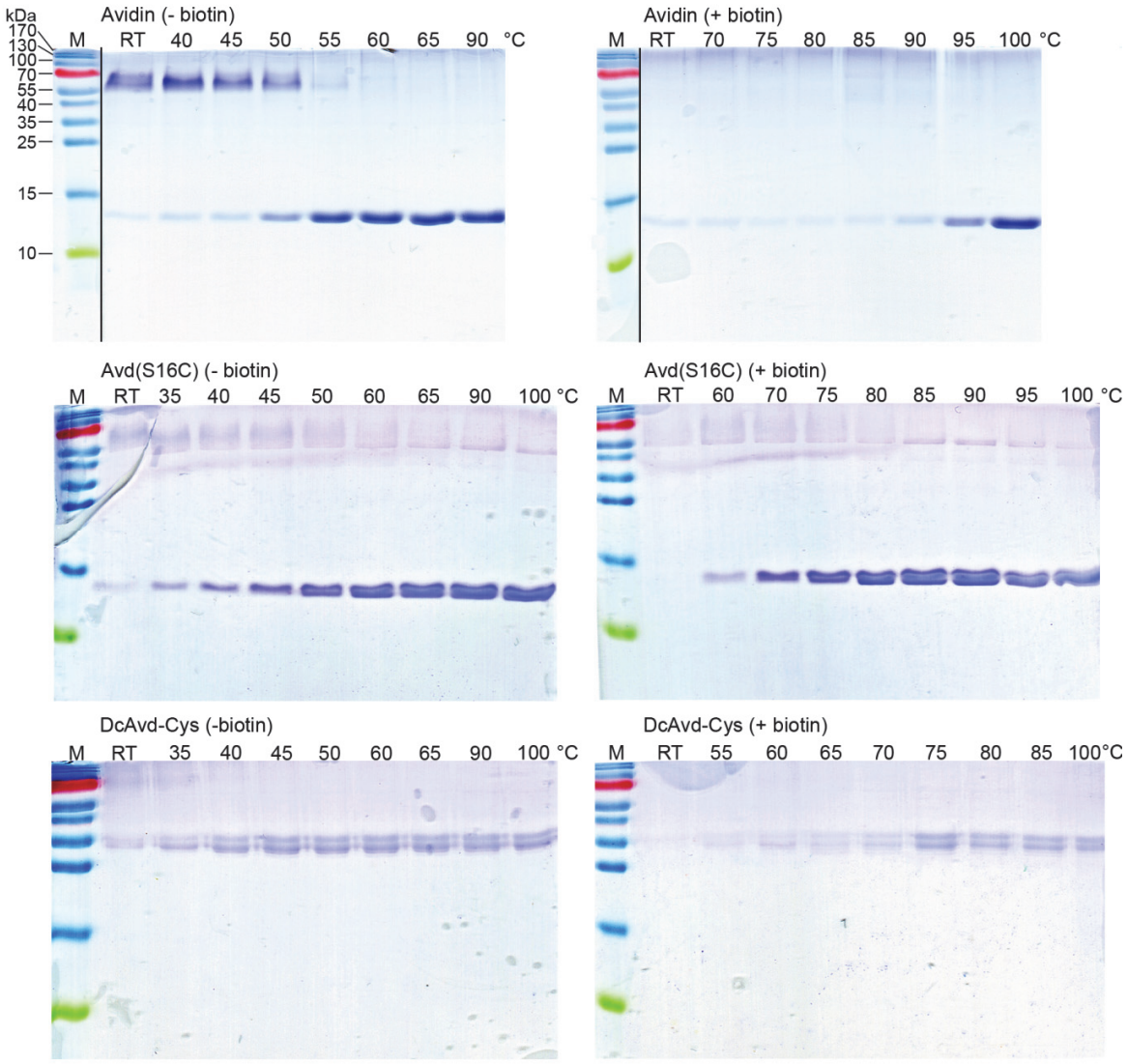

Figure S1. SDS-PAGE thermal stability analysis of avidin, Avd(S16C) and dcAvd-Cys without (−) and with (+) biotin. The transition temperature was determined after 20 minute heat treatment in the presence of SDS and β-mercaptoethanol followed by SDS-PAGE analysis. M, molecular weight marker.

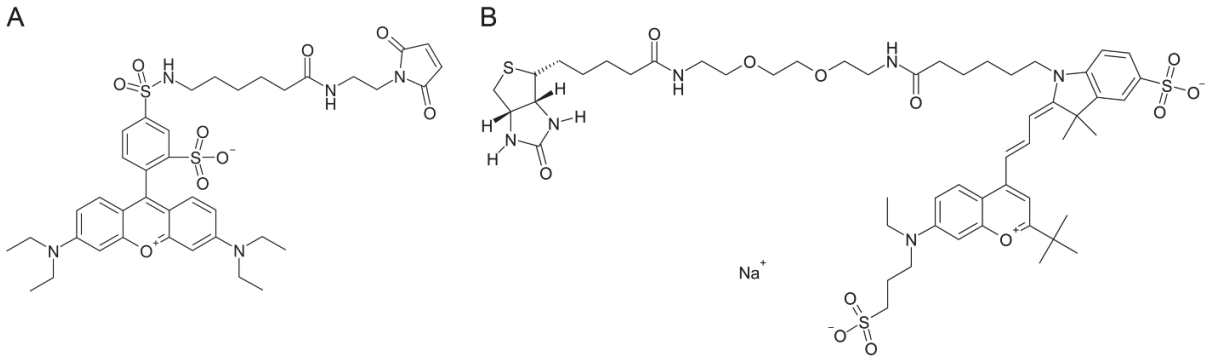

Figure S2. Structures of fluorescent conjugates used in FRET experiment. (**A**) DY560-maleimide acting as a FRET donor and (**B**) DY633-biotin acting as a FRET acceptor.

Table S1. Trypsin digestion data for Avidin, Avd(S16C) and Avd(S16C) treated with maleimide. Three additional amino acid residues (QTV) originating from the *B. avium* OmpA signal peptide in the N-terminus of the protein are numbered to −3, −2 and −1. Among the identified peptides for Avd(S16C) treated with maleimide, a peptide having a monoisotopic mass of 1947.8630 Da was observed, consistent with the maleimide conjugation into residues 10–26 (highlighted in red). With untreated Avd(S16C), this peptide was absent, but a peptide having a monoisotopic mass of 1850.8512 Da was observed instead, corresponding to the uncoupled tryptic peptide 10–26 (highlighted in red).

Avidin

Peptides identified without modifications:

Experimental (Da)	Theoretical (Da)	Deviation (ppm)	From...to	Sequence
504.2557	504.2544	2.6	125...128	TQKE
537.3259	537.3235	4.5	-3...2	QTVAR
773.4424	773.4395	3.7	123...128	LRTQKE
786.4561	786.4600	-5.0	88...94	NGKEVLK
818.4478	818.4473	0.6	95...100	TMWLLR
918.5328	918.5287	4.5	115...122	VGINIFTR
1234.5467	1234.5466	0.1	101...111	SSVNDIGDDWK
1424.7092	1424.7088	0.3	60...71	TQPTFGFTVNWK
1437.7264	1437.7212	3.6	46...58	ESPLHGTQNTINK
1562.7338	1562.7325	0.8	101...114	SSVNDIGDDWKATR
1593.8230	1593.8223	0.4	46...59	ESPLHGTQNTINKR
1834.8643	1834.8632	0.6	10...26	WTNDLGSNMTIGAVNSR
2001.9907	2001.9895	0.6	27...45	GEFTGTYITAVTATSNEIK
3218.6813	3218.6796	0.5	101...128	SSVNDIGDDWKA...INIFTRLRTQKE
3421.7046	3421.7001	1.3	27...58	GEFTGTYITAVT...SPLHGTQNTINK
3577.8032	3577.8012	0.6	27...59	GEFTGTYITAVT...PLHGTQNTINKR
2442.1222	2442.1195	1.1	4...9 + 72...87	CSLTGK + FSESTTVFTGQCFIDR (Ox)
3210.5698	3210.5689	0.3	4...9 + 72...94	CSLTGK + FSESTTVFTGQCFIDRNGKEVLK (Ox)
3338.6621	3338.6639	-0.5	3...9 + 72...94	KCSLTGK + FSESTTVFTGQCFIDRNGKEVLK

Peptides identified with modifications:

556.2972	556.2969	0.5	-3...2	PCA-QTVAR

Sequence coverage 100%

Avd(S16C)

Peptides identified without modifications:

Experimental (Da)	Theoretical (Da)	Deviation (ppm)	From...to	Sequence
573.3261	573.3235	4.5	-3...2	QTVAR
773.4401	773.4395	0.8	123...128	LRTQKE
786.4566	786.4600	-4.3	88...94	NGKEVLK
818.4482	818.4473	1.1	95...100	TMWLLR
918.5299	918.5287	1.3	115...122	VGINIFTR
1234.5474	1234.5466	0.6	101...111	SSVNDIGDDWK
1424.7099	1424.7088	0.8	60...71	TQPTFGFTVNWK
1437.7228	1437.7212	1.1	46...58	ESPLHGTQNTINK
1562.7349	1562.7325	1.5	101...114	SSVNDIGDDWKATR
1593.8236	1593.8223	0.8	46...59	ESPLHGTQNTINKR
1850.8512	1850.8403	5.9	10...26	WTNDLGCNMTIGAVNSR
2001.9918	2001.9895	1.1	27...45	GEFTGTYITAVTATSNEIK
2438.1157	2438.1141	0.7	4...26	CSLTGKWTNDLGCNMTIGAVNSR (Ox)
2456.1374	2456.1246	5.2	4...9 + 10...26	CSLTGK + WTNDLGCNMTIGAVNSR (Ox)
2566.2090	2566.2090	0.0	3...26	KCSLTGKWTNDLGCNMTIGAVNSR (Ox)
2584.2325	2584.2196	5.0	3...9 + 10...26	KCSLTGK + WTNDLGCNMTIGAVNSR (Ox)
3218.7015	3218.6796	6.8	101...128	SSVNDIGDDWKA...INIFTRLRTQKE
3421.7070	3421.7001	2.0	27...58	GEFTGTYITAVT...SPLHGTQNTINK
3577.8054	3577.8054	0.0	27...59	GEFTGTYITAVT...PLHGTQNTINKR

Peptides identified with modifications:

556.2974	556.2969	0.9	-3...2	PCA-QTVAR
684.3928	684.3919	1.3	-3...3	PCA-QTVARK

Sequence coverage 87% (missing residues 72-87, including Cys83)

Avd(S16C)+maleimide

Peptides identified without modifications:

Experimental (Da)	Theoretical (Da)	Deviation (ppm)	From...to	Sequence
773.4404	773.4395	1.2	123...128	LRTQKE
818.4484	818.4473	1.3	95...100	TMWLLR
918.5302	918.5287	1.6	115...122	VGINIFTR
1234.5477	1234.5466	0.9	101...111	SSVNDIGDDWK
1424.7103	1424.7088	1.1	60...71	TQPTFGFTVNWK
1437.7232	1437.7212	1.4	46...58	ESPLHGTQNTINK
1562.7356	1562.7325	2.0	101...114	SSVNDIGDDWKATR
1593.8254	1593.8223	1.9	46...59	ESPLHGTQNTINKR
2001.9926	2001.9895	1.5	27...45	GEFTGTYITAVTATSNEIK
3421.7092	3421.7001	2.7	27...58	GEFTGTYITAVT...SPLHGTQNTINK
3577.8068	3577.8012	1.6	27...59	GEFTGTYITAVT...PLHGTQNTINKR
3210.5718	3210.5698	0.6	4...9 + 72...94	CSLTGK + FSESTTVFTGQCFIDRNGKEVLK (Ox)
3218.6867	3218.6796	2.2	101...128	SSVNDIGDDWKA...INIFTRLRTQKE
3338.6648	3338.6639	0.3	3...9 + 72...94	KCSLTGK + FSESTTVFTGQCFIDRNGKEVLK (Ox)

Peptides identified with modifications:

556.2977	556.2969	1.4	-3...2	PCA-QTVAR
1947.8630	1947.8567	3.2	10...26	WTNDLGCNMTIGAVNSR + **maleimide**

Sequence coverage 100%

Table S2. The degree of labeling per protein tetramer determined by measuring the absorbance at 280 nm and 560 nm for avidin, Avd(S16C), dcAvd-Cys, and for the label, DY560-maleimide (MI).

Sample	Avidin	Avd(S16C)	dcAvd-Cys	DY560-MI
Absorbance at 280 nm	0.027	0.183	0.169	0.119
Absorbance at 560 nm	0	0.117	0.111	0.570
Dilution factor	3	1	1	10
Correction factor				0.209
ε [M^{-1} cm^{-1}]	94460[a]	94460[a]	94710[b]	120000
$c_{protein\ tetramer}$ [M]	8.6×10^{-7}	1.7×10^{-6}	1.5×10^{-6}	
c_{dye} [M]	0	9.7×10^{-7}	9.3×10^{-7}	
Degree of labeling	0	0.6	0.6	

[a] For tetramer
[b] For pseudotetramer

Table S3. Primers used in polymerase chain reactions (PCR).

Primer	Sequence
5' Avd	5'-CACCATGAACAAACCCTCCAAATTCGCTCTGC-3'
3' Avd	5'-TTACTCCTTCTGTGTGCG-3'
S16C.1	5'-GACCAACGATCTGGGCTGCAACATGACCATCGG-3'
S16C.2	5'-CCGATGGTCATGTTGCAGCCCAGATCGTTGGTC-3'

OPEN ACCESS Freely available online

PLoS one

Structure of Bradavidin – C-Terminal Residues Act as Intrinsic Ligands

Jenni Leppiniemi[1,2], Toni Grönroos[1,2], Juha A. E. Määttä[1,2], Mark S. Johnson[3], Markku S. Kulomaa[1,2], Vesa P. Hytönen[1,2], Tomi T. Airenne[3]*

1 Institute of Biomedical Technology, University of Tampere, Tampere University Hospital, Tampere, Finland, **2** BioMediTech, Tampere, Finland, **3** Department of Biosciences, Biochemistry, Åbo Akademi University, Tykistökatu, Turku, Finland

Abstract

Bradavidin is a homotetrameric biotin-binding protein from *Bradyrhizobium japonicum*, a nitrogen fixing and root nodule-forming symbiotic bacterium of the soybean. Wild-type (wt) bradavidin has 138 amino acid residues, whereas the C-terminally truncated core-bradavidin has only 118 residues. We have solved the X-ray structure of wt bradavidin and found that the C-terminal amino acids of each subunit were uniquely bound to the biotin-binding pocket of an adjacent subunit. The biotin-binding pocket occupying peptide (SEKLSNTK) was named ''Brad-tag'' and it serves as an intrinsic stabilizing ligand in wt bradavidin. The binding of Brad-tag to core-bradavidin was analysed by isothermal titration calorimetry and a binding affinity of ~25 μM was measured. In order to study the potential of Brad-tag, a green fluorescent protein tagged with Brad-tag was prepared and successfully concentrated from a bacterial cell lysate using core-bradavidin-functionalized Sepharose resin.

Citation: Leppiniemi J, Grönroos T, Määttä JAE, Johnson MS, Kulomaa MS, et al. (2012) Structure of Bradavidin – C-Terminal Residues Act as Intrinsic Ligands. PLoS ONE 7(5): e35962. doi:10.1371/journal.pone.0035962

Editor: Andreas Hofmann, Griffith University, Australia

Received November 16, 2011; **Accepted** March 26, 2012; **Published** May 4, 2012

Funding: This work was supported by the Academy of Finland [projects 115976 and 121236], ISB (National Graduate School in Informational and Structural Biology), TGPBB (Tampere Graduate Program in Biomedicine and Biotechnology), the Institute of Biomedical Technology, the Foundation of Åbo Akademi (Centre of Excellence in Cell Stress and Aging), the Sigrid Jusélius Foundation, the Competitive Research Funding of the Tampere University Hospital [Grants 9M019 and 9M042], and the Joe, Pentti and Tor Borg Memorial Fund. The authors acknowledge support by the European Community - Research Infrastructure Action under the FP6 ''Structuring the European Research Area'' Programme and FIRI infrastructure support for structural biology from the Academy of Finland. Biocenter Finland is acknowledged for the infrastructure support. The funders had no role in study design, data collection and analysis, decision to publish, or preparation of the manuscript.

Competing Interests: The authors have declared that no competing interests exist.

* E-mail: tomi.airenne@abo.fi

Introduction

Chicken egg-white avidin and its eukaryotic and prokaryotic homologs, known collectively as avidins, are proteins that have extreme affinity towards D-biotin (K_d ~10^{-15} M for chicken avidin) [1–3]. Eukaryotic avidins exist in the eggs of e.g. birds, reptilia and amphibians [4–7], whereas prokaryotic avidins have been isolated from a few bacterial species: *Streptomyces avidinii* (streptavidin) [8], *Bradyrhizobium japonicum* (bradavidin and bradavidin II) [9,10], *Rhizobium etli* (rhizavidin) [11] and *Burkholderia pseudomallei* (burkavidin) [12]. Avidins are known to be homotetrametric proteins, with the exception rhizavidin, which is a homodimer in its native form [11]. Due to the high-affinity interaction with D-biotin, avidins are widely applied in life sciences as well as in bio- and nanotechnology [13–15].

The best-studied avidins are the mature forms of chicken avidin and streptavidin. In the chicken egg-white, only the 28 amino acid signal peptide is removed from the full-length polypeptide chain to form the mature avidin protein (residues 1–128) [1], whereas several different cleavage products have been detected for streptavidin [16]. Streptavidin has been expressed as a recombinant protein with and without signal peptide [17,18]. The most stable truncated form of streptavidin is the so-called core streptavidin, which contains residues 13–139 but still retains extremely high affinity towards D-biotin K_d ~10^{-15} M [16]. Full-length wild-type (wt) streptavidin is expressed as a polypeptide of 159 residues. Interestingly, C-terminal residues 150–153 (Asn150-Gly151-Asn152-Pro153) of wt streptavidin fold back into the biotin-binding site in each monomer [19], thereby competing with the binding of at least low-affinity biotinylated macromolecules [16,20].

Bradavidin is a tetrameric biotin-binding protein structurally and functionally resembling chicken avidin and other avidins. The gene encoding bradavidin was identified in *B. japonicum*, a nitrogen fixing and root nodule-forming symbiotic bacterium of the soybean [9]. Full-length, wt bradavidin has 138 amino acid residues, whereas the C-terminally truncated core form (core-bradavidin) has 118 amino acid residues [9]. Although bradavidin shares structural and functional similarities with other avidins, the percentage of amino acid sequence identity between the core regions of bradavidin and chicken avidin or streptavidin is only about 30%. As an additional indication of uniqueness, bradavidin has been proven to be immunologically different from chicken avidin and streptavidin [9]. Moreover, bradavidin has an acidic pI value (6.3 for wt bradavidin and 4.1 for core-bradavidin [9]) whereas mature chicken avidin (pI ~10 [1]) is a basic protein. This property may allow the use of bradavidin instead of chicken avidin in applications disturbed by the charge-driven, non-specific binding of chicken avidin [21,22].

In this study, we have determined the crystal structure of full-length, wt bradavidin at 1.8 Å resolution. Inspired by the X-ray structure, C-terminal residues occupying the biotin-binding pocket of wt bradavidin were evaluated as an affinity tag (Brad-tag) by using a synthetic peptide and by producing a fusion protein of enhanced green fluorescent protein (EGFP) and the Brad-tag. The binding of Brad-tag to core-bradavidin and other biotin-binding proteins were characterized using isothermal titration calorimetry (ITC) and its effect on the stability of bradavidin was determined by differential scanning calorimetry (DSC).

Results

The X-ray Structure of Bradavidin Reveals Unique Features

Wild-type bradavidin and core-bradavidin were produced in the periplasmic space of *E. coli* in an active form, essentially as previously described [9]. Bottle cultures (typical protein yields were around 1–5 mg/L) and a pilot-scale fermentor (yields of 3–7 mg/L) were used for protein expression. The isolated proteins were homogeneous and of high purity by SDS-PAGE analysis (data not shown).

In order to help understand the molecular details behind the functional properties of bradavidin, the 3D structure of wt bradavidin was solved. We tried to crystallize wt bradavidin in the absence and presence of biotin, and in the presence of an azo dye HABA (4-hydroxyazobenzene-2-carboxylic acid, also called 2-(4′-hydroxybenzene)azobenzoic acid) in the hope that the dye would bind to the biotin-binding site. However, the protein crystallized only in the presence of HABA, but we could not identify HABA in the final structure. Orthorhombic crystals with a homotetramer in the asymmetric unit were obtained (for structure determination details, see Table 1). Each subunit I-IV (numbering according to [23]) of wt bradavidin had the overall β-barrel shape typical of avidins. A long C-terminal tail protruded from the closed-ends of the barrels and extended into the ligand-binding sites of the neighbouring subunits, serving as an intrinsic, intersubunit ligand (named Brad-tag; see below). More specifically, C-terminal residues of subunit I bound within the biotin-binding pocket of subunit III (and *vice versa*), and similar reciprocal interactions took place between subunits II and IV. These interactions uniquely anchored the 'two dimers' of the tetramer (a dimer of dimers) to each other (Figure 1A). This kind of intersubunit interaction has not been reported for any known member of the avidin family and thus provides an example of the utilization of an oligopeptide from adjacent subunits as an intrinsic ligand. In the X-ray structure of the T7-tagged wt streptavidin, C-terminal residues 150–153 also occupy the biotin-binding site [19], however, the extended C-terminus and the ligand-binding pocket into which it folds is formed by a single polypeptide chain (intrasubunit ligand). The overall intrinsic ligand-binding architecture is therefore clearly different in bradavidin and in streptavidin (Figure 1).

Even though the quaternary structure of wt bradavidin resembles the known structures of avidins (Figure 1A), some of the secondary structure elements and loops, especially those in the close proximity to either the N- or C-terminal residues, differ noticeably in comparison to other avidins (Figures 1B, 1C, 2). For example, the first five amino acids of wt bradavidin have different spatial locations in comparison to wt streptavidin or chicken avidin. Residue Trp5 of bradavidin is located in a key position and helps determine the unique conformation of the N-terminus: the Trp5 side chain is located in a hydrophobic pocket created by residues that include Val3, Trp7, Ile17, Ile27, Leu51, Phe20, Leu118 and Leu119; the side-chain nitrogen atom of Trp5 is hydrogen bonded to the carbonyl oxygen of Asp115, too. Residues 1–3 of wt bradavidin interact with residues 17–20 of the β2-strand and the adjacent L2,3-loop. Additionally, the side-chain oxygen atom of Asn4 is hydrogen bonded to the backbone nitrogen atom of Asp115, located at the beginning of the C-terminal extension. Unique structural features of the C-terminus of wt bradavidin are seen beginning with residues directly following β-strand 8, and extending through the adjacent short 3/10-helix and then turning towards and entering the neighbouring subunit (Figure 1D). Ala128 and Gly129 are the first residues clearly leaving the original subunit and form a linker between the original (e.g. subunit I) and the neighbouring subunit (e.g. subunit III), whereas the terminal residues 130–138 are part of the neighbouring subunit. Together, the N- and C-terminal residues have a clear effect on determining the shape of the fold of wt bradavidin. In bradavidin, the L4,5-loop and the L6,7-loop of one subunit seem to be adapted to pack and guide the C-terminal extension towards the neighbouring subunit and the L7,8-loop of neighbouring subunit contributes to the conformation of the C-terminus, too (Figure 1D). Several of the β-strands, i.e. strands 1, 6 and 8, also differ in their spatial arrangements (length and/or orientation) in comparison to chicken avidin and streptavidin. Moreover, analysis of the surface of the bradavidin structure identified bradavidin-specific characteristics (Figure S1).

Subunit Interfaces of Bradavidin

In a previous study we found that bradavidin in the presence of biotin was structurally less stable when compared to either chicken avidin or streptavidin [9]. Avidins gain stability via oligomerization [24,25] and the subunit-interfaces play a significant role in determining their stability. Consequently, the subunit-subunit contacts of bradavidin were carefully examined.

Four tyrosine residues (Tyr90), one from each subunit, are located in the center of the bradavidin tetramer (Figure 3), and they are likely to play a major role in the assembly and stability of the tetramer. Structural water molecules in the vicinity (2.6–2.8 Å) of the hydroxyl groups support the idea that hydrogen bonds together with ring stacking stabilize the tetramer.

In bradavidin, there are eight residues (Trp89, Tyr90, Leu91, Trp99, Asn100, Ile102, Ser103 and Ala104) having non-hydrogen atoms within 4 Å of each other at the interface of subunits I and II. Ile102, Ser103 and Ala104 form the core of the I-II interface and, together with Tyr90 and Asn100, are the most characteristic residues of the I-II subunit interface (Figure S2). Of these residues, only an isoleucine equivalent to Ile102 of bradavidin is found in one other known avidin structure, rhizavidin [11]. Interactions among residues (102–104) of the I-II interface include conventional hydrogen bonds between the backbone oxygen atom of Ile102 and the backbone nitrogen atom of Ala104– these backbone interactions are well conserved within the avidin family. A weak hydrogen bond (C-H$^{\cdots}$O; [26,27]) between the side-chain oxygen atom of Ser103 and the Cα atom of Asn100 was also seen. Moreover, the Cη atom of Trp89 is at a distance of 3.6 Å, and thus able to form a weak hydrogen bond (C–H$^{\cdots}$O) with the backbone oxygen atom of Trp99. Both Trp89 and Trp99 are well conserved within the avidin family, including chicken avidin and streptavidin, and are known to line the biotin-binding pocket. Leu91 of bradavidin is also well conserved and its side chain is involved in van der Waals interactions with the side chain of Trp99. The side chain of Tyr90 is in van der Waals contact with the side-chain atom of Ala104.

The core of the I-III subunit interface of wt bradavidin is formed by Gln86, Leu88, Tyr90, Ala104 and Ala106 (Figure S2),

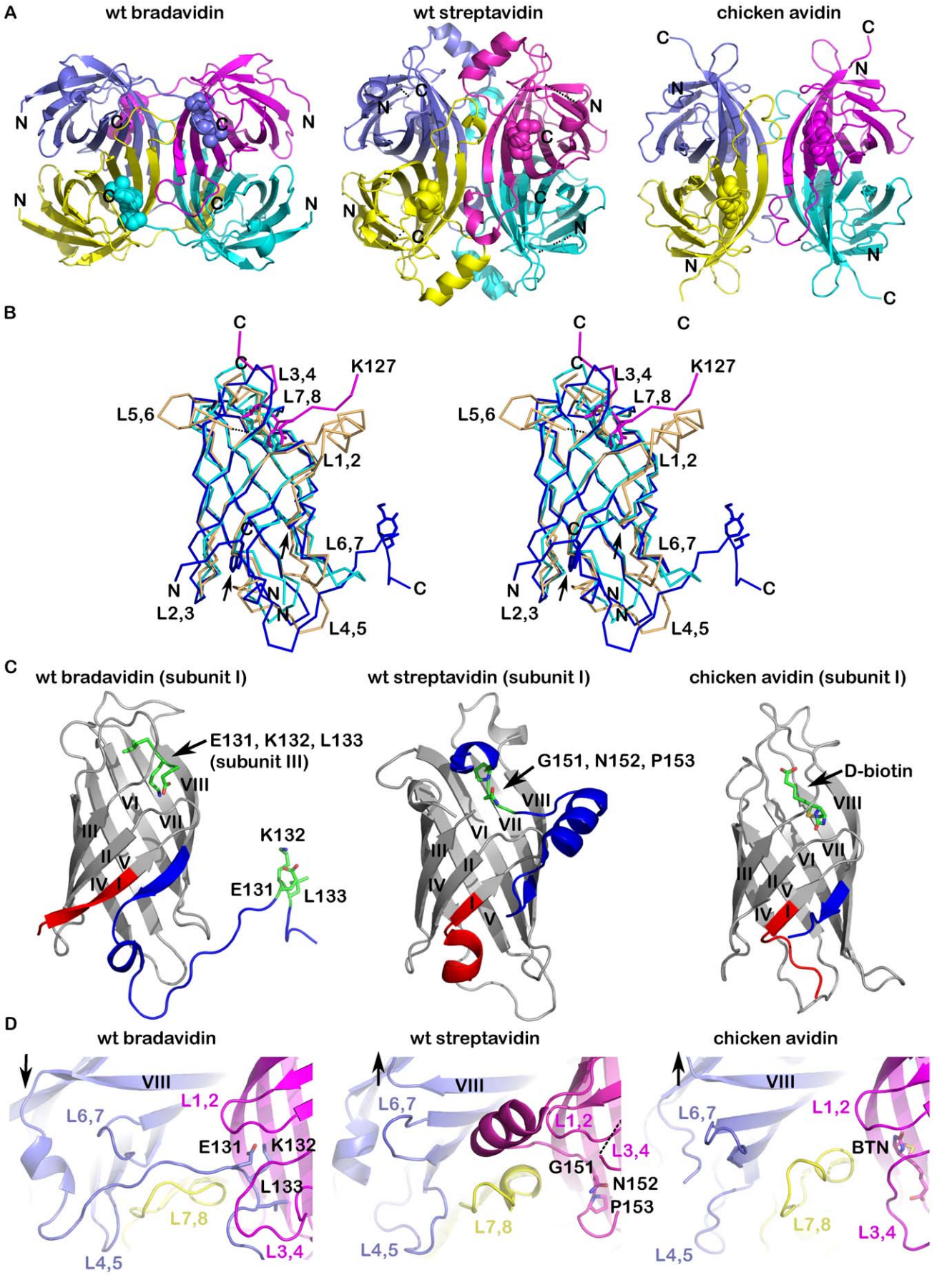
A
wt bradavidin
wt streptavidin
chicken avidin
B
K127
L3,4
L7,8
L5,6
L1,2
L6,7
L2,3
L4,5
C
wt bradavidin (subunit I)
wt streptavidin (subunit I)
chicken avidin (subunit I)
E131, K132, L133
(subunit III)
G151, N152, P153
D-biotin
D
wt bradavidin
wt streptavidin
chicken avidin
BTN

Figure 1. Structure comparison of wt bradavidin, wt streptavidin [PDB: 2BC3] and chicken avidin [PDB: 1AVD]. (**A**) Cartoon models of tetrameric proteins. Subunits are shown in different colors as follows: I (blue), II (cyan), III (magenta) and IV (yellow). The key biotin-binding pocket occupying residues (wt bradavidin and wt streptavidin) and biotin (chicken avidin) are shown as spheres. The N- and C-termini are indicated by letters. (**B**) Superimposition of the Cα traces of subunits I of wt bradavidin (blue), wt streptavidin (orange) and chicken avidin (cyan). The Cα trace for C-terminal residues starting from Lys127 of subunit III of wt bradavidin is shown, too. The ligand-binding site occupying residues Glu131-Leu133 of wt bradavidin and Gly151-Pro153 of wt streptavidin, and the biotin ligand of avidin, are shown as sticks. The left and right arrows pinpoint the N- and C-terminal sites, respectively, were major differences are seen between the proteins. Trp5 (left arrow) of wt bradavidin is shown as sticks. The N- and C-termini are indicated and loops are numbered. (**C**) Monomeric cartoon models. The N-terminus and C-terminus of each protein are indicated in red and blue, respectively, the colouring starting from equal positions in all proteins. The key residues occupying the biotin-binding site are shown as sticks. (**D**) Loop design. Colouring of subunits are as in (A) and representation of the key residues as in (C). The arrow pinpoints the varying beginnings of the L7,8-loops in the three structures. The L3,4-loop of the wt streptavidin structure is not fully visible (dashed line).
doi:10.1371/journal.pone.0035962.g001

which are all poorly conserved in the avidin family. For example, Gln86, Leu88, Tyr90, Ala104 and Ala106 in bradavidin are in chicken avidin (and streptavidin) Lys94 (Asn105), Met96 (Gln107), Leu98 (Leu109), Val115 (Val125) and Ile117 (His127). The nitrogen atom of the Gln86 side chain of subunit I is hydrogen bonded with the carbonyl oxygen atom of Ala106 of subunit III (and vice versa), and the Cβ atoms of Ala106 of subunits I and III are in van der Waals contact with each other. Weak van der Waals interactions between the side chain of Leu88 and the atoms of Ala104 are apparent, too. Tyr90 of subunit I is within hydrogen-bonding distance (2.8 Å) of Tyr90 of subunit III. The C-terminal residues 129–137, containing the residues of the Brad-tag, are also involved in I-III subunit interactions but these residues are described separately below.

Table 1. X-ray structure determination statistics for wt bradavidin [PDB: 2Y32].

Cell parameters	
Space group	$P2_12_12_1$
Unit cell:	
a, b, c (Å)	46.7, 84.9, 120.3
α, β, γ (°)	90, 90, 90
Data collection[a]	
Wavelength (Å)	1.04192
Beamline	I911–2 (MAX-lab, Lund)
Detector	MarCCD
Resolution (Å)b	25–1.78 (1.78–1.88)
Unique observations[b]	46670 (6955)
I/sigma[b]	18.0 (5.9)
R_{factor} (%)[b]	9.0 (42.4)
Completeness[b]	100 (100)
Redundancy[b]	9.6 (9.6)
Refinement	
R_{work} (%)[c]	14.4
R_{free} (%)[c]	18.2
Monomers (asymmetric unit)	4
Protein atoms	4115
Solvent atoms	680
R.m.s.d:	
Bond lengths (Å)	0.014
Bond angles (°)	1.4

[a]The numbers in parenthesis refer to the highest resolution bin.
[b]From XDS [53].
[c]From Refmac 5 [57] using TLS [71] & restrained refinement.
doi:10.1371/journal.pone.0035962.t001

The I-IV subunit interface of bradavidin involves 47 amino acid residues (4 Å probe using non-hydrogen atoms) and is stabilized by a large number of non-covalent interactions. In comparison to known avidin structures, the I–IV subunit interface of bradavidin is also distinctive. In addition to the central Tyr90 and the C-terminal Brad-tag, the I–IV subunit interface is stabilized by van der Waals interactions and hydrogen bonding of e.g. the side chain of Trp50 with the atoms of residues Gly46, Thr48, Ser63, Val64 and Asn65, and the side chain of the well-conserved Gln78 is uniquely packed against residues of the L7,8-loop, and Trp99 of this loop is part of the ligand-binding site.

All in all, tetrameric wt bradavidin is stabilized by a large set of non-covalent intersubunit interactions, many of which are unique to bradavidin within the members of the avidin family. However, the decreased thermal stability of bradavidin suggests that the subunit interfaces of wt bradavidin are less optimal for maintaining the tetrameric stability as in chicken avidin or streptavidin.

The Ligand-binding Site of wt Bradavidin has an Intrinsic Ligand

The C-terminal extension of each subunit in wt bradavidin reaches out and occupies the ligand-binding site of an adjacent subunit, serving as an intrinsic, intersubunit ligand. Namely, residues 130-138 of subunits I and II respectively occupy the ligand-binding pocket of subunits III and IV, and vice versa (Figure 1). In comparison to chicken avidin [PDB: 1AVD; [28]] or wt streptavidin [PDB: 2BC3; with a T7-tag], the ligand-binding site of wt bradavidin is rich in novel features. For example (see Figure 4A), the C-terminus (Ser130-Lys137) of subunit I has two consecutive turns mimicking the shape of an S letter (“S-shaped”) and embedding between Ser13, Tyr31 and Asn33-Asp40 (L3,4-loop) of the neighbouring subunit III on one side and, on the other side, Trp99 of a third subunit (IV). The binding pocket (III) is lined by Asn9, Tyr11, Phe66, Ser71, Thr73, Trp75, Trp89, Leu91 and Asp107 and the L3,4-loop is stabilized by an intrasubunit disulfide bond between Cys39 and Cys69, similar to rhizavidin [29]. In general, the C-terminus causes the opening or widening of the ligand-binding pocket of wt bradavidin in a manner not observed for any other known avidin structure. The binding of the C-terminal extension of bradavidin is stabilized by a number of non-covalent interactions and several structural water molecules are found in close proximity of the binding site (Figure 4A).

Glu131, Lys132 and Leu133 of wt bradavidin insert deepest into the ligand-binding pocket of the adjacent subunit. When superimposed with chicken avidin [PDB: 1AVD], it is evident that residues 131-133 occupy the site equivalent to the biotin-binding site of avidin (Figure S3). The Leu133 side chain matches the location of the carboxylate end of biotin, whereas the side chain of Lys132 fills the space occupied by the bicyclic ring system (2′-keto-3,4-imidazolidotetrahydrothiophene moiety)

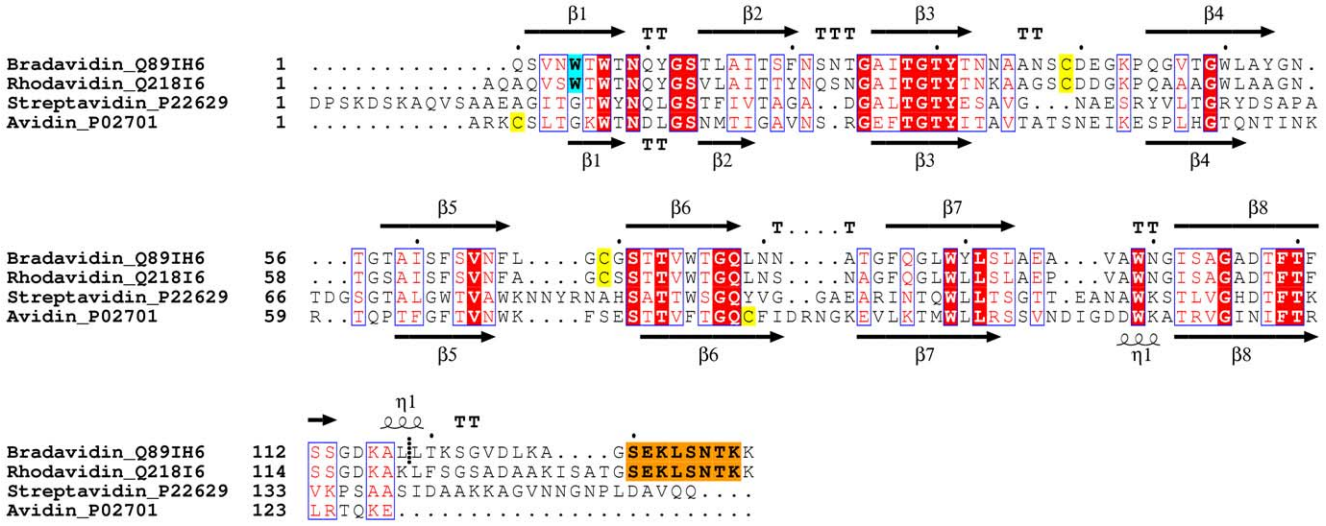

Figure 2. Sequence alignment of wt bradavidin, rhodavidin, streptavidin and chicken avidin. The UniProt [70] accession numbers are shown after the names of the sequences. The Brad-tag sequence is highlighted with orange background, cysteine residues with yellow and the tryptophan residue important for the N-terminus of wt bradavidin with cyan. The secondary structures of wt bradavidin (from the structure reported here) and chicken avidin (from [PDB: 1AVD]) are shown. The truncation site for core-bradavidin is between Leu118 and Leu119 and is shown by a short, vertical dashed line. The conserved residues are indicated by the default colouring scheme of the ESPript program. TT, β-turn; TTT, α-turn; and η1, 3/10-helix. The structural alignment was created in Bodil [66] and the picture using ESPript [68].
doi:10.1371/journal.pone.0035962.g002

of biotin. Glu131 stabilizes the local structure, and especially, the side-chain conformation of Lys132 (Figure S4). With respect to the wt streptavidin structure [PDB: 2BC3], Leu133 superposes with Pro153, whereas the side chain of Lys132 overlaps with Gly151. Even though some of the residues lining the ligand-binding site of bradavidin, avidin and streptavidin are identical in sequence and are structurally conserved (Figure 4B), the binding mode of Glu131-Lys132-Leu133 is different from that seen for Gly151-Asn152-Pro153 in the wt streptavidin structure and for biotin in the avidin structure (Figures 4, S3). This is due to the two-layered, "S-shaped" conformation of the C-terminus of bradavidin, the terminus entering into a neighbouring subunit (Figures 1, 4). Moreover, the side-chain nitrogen atom of K132 is stabilized by several hydrogen bonds; interaction of K132 (NZ atom) with the side-chain oxygen atoms of Y31, D107 and E131 are possible; Y31 and D107 are from a different subunit (Figure S4).

To get an idea how biotin would bind to the presumed ligand-binding site of wt bradavidin and how it would affect to the conformation of the C-terminus, we tried to co-crystallize wt bradavidin with biotin. However, we did not get any crystals with biotin. Therefore, selected residues lining the biotin-binding site of chicken avidin [PDB: 1AVD] were superimposed with the equivalent residues of wt bradavidin (Figure 4B). We left out the C-terminal residues (Brad-tag) of wt bradavidin from the structural comparison because of two reasons: 1) the C-terminus is very likely to undergo major conformational changes due to biotin binding, changes that would require heavy computations to give reasonable predictions (beyond this study); and 2) direct contacts between the C-terminal residues and biotin are not likely to occur. Our structural comparison suggests that the L3,4-loop of wt bradavidin, and especially the residues Ala35-Ser38 of it, should undergo a major conformational change for efficient biotin binding, whereas most of the other residues (i.e. not in the L3,4-loop) lining the presumed biotin-binding site of wt bradavidin have conformations close to those seen in chicken avidin and are hence likely to undergo only minor conformational changes due to biotin binding. In conclusion, most of the

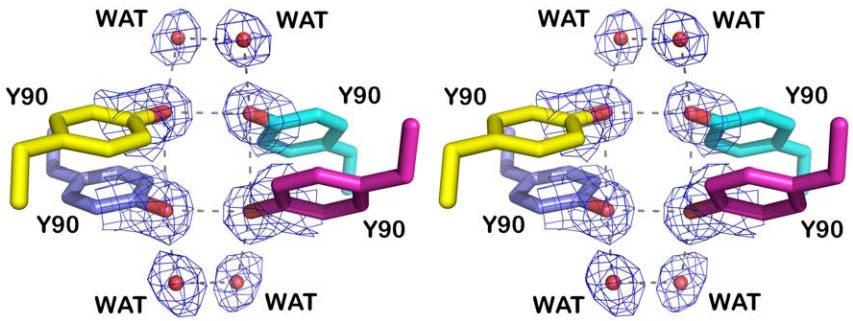

Figure 3. Four tyrosine residues at the intersection of all four subunit interfaces in bradavidin. A stereo view. The tyrosine residues are shown as stick models with different colouring for the different subunits (subunit I, blue; II, cyan; III, magenta; and IV, yellow). Structural water molecules are shown as red spheres. Electron density map (a weighted 2FO-FC map; sigma level 1) around the water molecules and the side chain oxygen atoms of Tyr90 is shown in blue. Putative hydrogen bonds are indicated with grey dashes.
doi:10.1371/journal.pone.0035962.g003

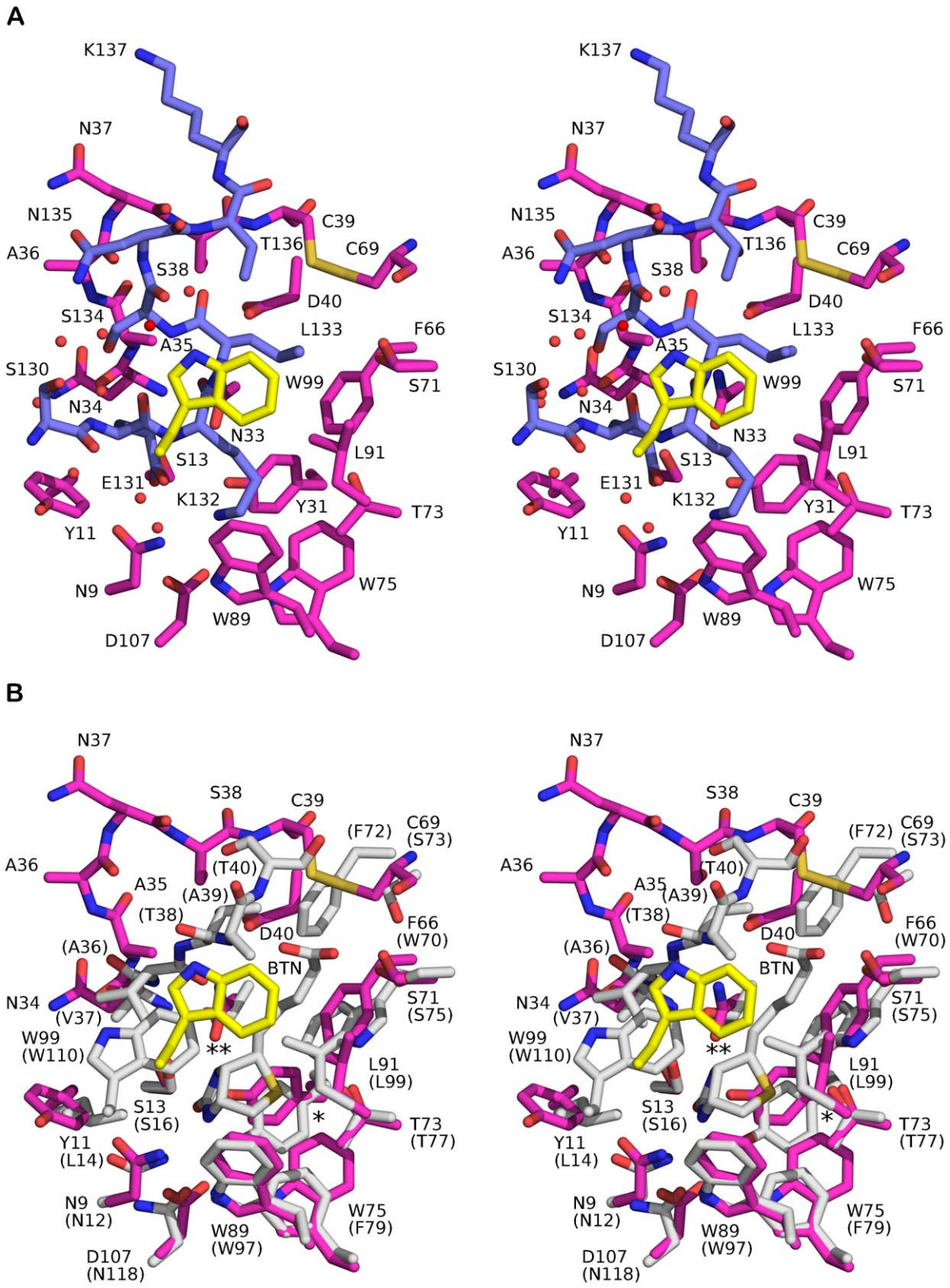

Figure 4. Stick model (stereo view) of the ligand-binding site of wt bradavidin. (**A**) The carbon atoms of the Brad-tag sequence (subunit I) are shown in blue and the residues around the Brad-tag sequence in magenta (subunit III) and yellow (subunit IV). Structural water molecules near the Brad-tag sequence are shown as red spheres. (**B**) Superimpositioning of the ligand-binding site of wt bradavidin and chicken avidin [PDB: 1AVD]. Colouring for wt bradavidin as in (A); the carbon atoms of residues of chicken avidin are shown in grey. The residues Asn12, Leu14, Ser16, Tyr33, Trp70, Ser73, Ser75, Thr77, Phe79, Trp97, Leu99 and Asn118 of chicken avidin were superimposed to the equivalent residues Asn9, Tyr11, Ser13,

Tyr31, Phe66, Cys69, Ser71, Thr73, Trp75, Trp89, Leu91 and Asp107 of wt bradavidin. For clarity, the Brad-tag sequence is not shown. For chicken avidin, the residue numbers are shown in brackets. BTN, biotin; *, Tyr31 (Tyr33); **, Asn33 (Thr35).
doi:10.1371/journal.pone.0035962.g004

interactions seen between chicken avidin and biotin [PDB: 1AVD] are probably also seen in wt bradavidin when in complex with biotin.

Several peptide tags binding to the biotin-binding site of avidin, and particularly to streptavidin, have been reported (Table 2), and X-ray structures are known for the Strep-tag [PDB: 1RST], Strep-tagII [PDB: 1RSU, 1KL3/5] and Nano-tag [PDB: 2G5L] streptavidin complexes. However, the binding modes of these tags are clearly different from that seen for bradavidin (Figure S5). For example, the peptide backbone of Strep-tag [30], Strept-tag II [30,31] and Nano-tag [32] have a 3_{10}-helical conformation, whereas the C-terminus of wt bradavidin is a combination of two consecutive turns.

Isothermal Titration Calorimetry Reveals Moderate Affinity between Brad-tag and Core-bradavidin

We used isothermal titration calorimetry (ITC) to determine the affinity between core-bradavidin and a synthetically produced Brad-tag (SEKLSNTK), and found that the binding enthalpy of Brad-tag to core-bradavidin was temperature dependent (Figure 5, Table 3). At 15°C, the enthalpy was found to be positive (1.1±0.2 kcal/mol, Figure $5A_1$) indicating endothermic binding, whereas a negative binding enthalpy (–4.4±0.3 kcal/mol, Figure $5C_1$) was observed for core-bradavidin titrated with Brad-tag at 40°C, indicating the exothermic nature of binding. At 25°C, the binding enthalpy was negligible (Figure $5B_1$) most likely because the measurement was performed close to the transition temperature between the exothermic and endothermic binding mode. The calculated dissociation constant (K_d) was 25 μM at 15°C and 26 μM at 40°C but could not be determined at 25°C.

We could not determine the K_d of D-biotin for core-bradavidin, as the measurement exceeded the sensitivity limit of ITC ($K_d < 10^{-9}$ M). However, ITC titration provided the enthalpy and stoichiometry of the binding. The highly negative binding enthalpies (–15.9±0.1, –20.1±0.1, and –26.4±0.1 kcal/mol at 15, 25 and 40°C, Figures $5A_3$, B_3, C_3, respectively) indicated the exothermic nature of biotin binding and were in accordance with our earlier observations with rhizavidin [11] and avidin [33]. The average of the calculated stoichiometries of binding at different temperatures was 0.78±0.23/subunit, suggesting 1:1 binding of Brad-tag to core-bradavidin subunits. In a competitive binding assay, core-bradavidin was first saturated with Brad-tag followed by a second titration with biotin (Figures $5A_2$, B_2, C_2). At 15°C, the measured enthalpy (–17.3±0.1 kcal/mol) was more negative in the competitive binding assay than in the non-competitive assay, because core-bradavidin was saturated with Brad-tag (positive enthalpy) before titration with biotin (Figure 5D). At 25°C, the enthalpies for competitive and non-competitive binding of biotin differed only by 0.4 kcal/mol; the enthalpy measured for the binding of Brad-tag to core-bradavidin was close to zero at this temperature. At 40°C, the competitive biotin titration resulted in less negative enthalpy (–21.4±0.1 kcal/mol) than the non-competitive binding. The sum of the measured binding enthalpy of core-bradavidin titrated with Brad-tag and the enthalpy of the competitive titration with biotin was almost equal to the binding enthalpy of core-bradavidin titrated with biotin only.

Avidin, streptavidin and rhizavidin were titrated with Brad-tag at 40°C (Figure S6) in order to study the specificity of Brad-tag towards core-bradavidin. No sign of interaction was observed, indicating that Brad-tag is specific for core-bradavidin.

Table 2. Summary of different avidin-binding peptide tags.

Tag	Sequence (residues)	Size (kDa)	Receptor	K_d	PDB entry	References
Avi-tag	DRATPY (6)	0.72	Avidin, NeutrAvidin	28 μM 12 μM	[a]	[72]
AviD-tag	Divalent DRATPY (6+spacer+6)	1.44+spacer	Avidin, NeutrAvidin	[a]	[a]	[73]
Nano-tag$_{15}$	fMDVEAWLGAR VPLVET (formyl-Met+15)	1.81	Streptavidin	4 nM	[a]	[74]
Nano-tag$_9$	fMDVEAWLGAR (formyl-Met+9)	1.18	Streptavidin	17 nM	[a]	[74]
Nano-tag	fMDVEAWL (formyl-Met+6)	0.89	Streptavidin	<20 nM	2G5L	[32]
Strep-tag	AWRHPQFGG (9)	1.06	Streptavidin	37 μM	1RST	[30]
Strep-tag II	WSHPQFEK (8)	1.06	Streptavidin SA mutant 1 i.e. StrepTactin SA mutant 2	72 μM 1 μM 1 μM	1RSU 1KL3 1KL5	[30,31,75]
SBP-tag	MDEKTTGWRG GHVVEGLAGE LEQLRARLEH HPQGQREP (38)	4.31	Streptavidin	2.5 nM	[a]	[76]
Brad-tag	SEKLSNTK (8)	0.91	Core-bradavidin	25 μM		This study

[a]Not available.
doi:10.1371/journal.pone.0035962.t002

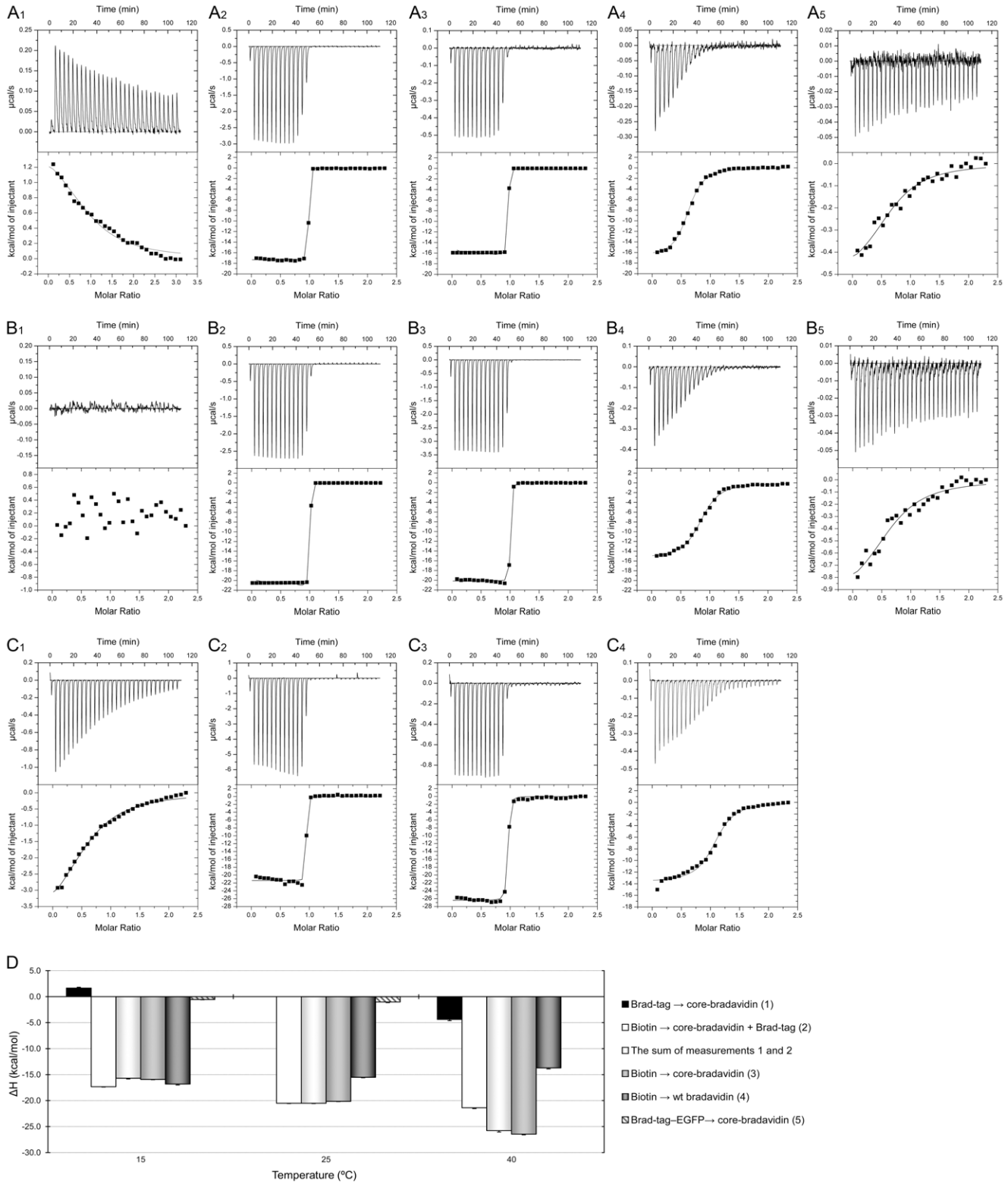

Figure 5. ITC analysis of ligand binding. Thermograms of measurements performed at three different temperatures (**A**) 15°C, (**B**) 25°C and (**C**) 40°C are shown. At each temperature, core-bradavidin was first titrated with Brad-tag (1), followed by competitive titration with biotin (2). As a control measurement, core-bradavidin was titrated with biotin only (3). In order to prove that the intrinsic Brad-tag decreases the affinity towards biotin, wt bradavidin was also titrated with biotin (4). In addition, core-bradavidin was titrated with Brad-tag–EGFP at 15 and 25°C (5). (**D**) Comparison of the binding enthalpies of all measurements at different temperatures. Brad-tag had a clear effect on the binding enthalpy of the competitive titration with biotin at 15°C (endothermic Brad-tag binding) and 40°C (exothermic Brad-tag binding). At 25°C, the enthalpy of competitive titration was equal to that of titration with biotin only (no detectable binding of Brad-tag to core-bradavidin).
doi:10.1371/journal.pone.0035962.g005

Table 3. Thermodynamic parameters of ligand binding analyzed by ITC.

Cell		Syringe		T	ΔH	-TΔS	ΔG	K_d	n
Contents	$c_{initial}$	Contents	$c_{initial}$						
	[mM]		[mM]	[°C]	[kcal mol^{-1}]	[kcal mol^{-1}]	[kcal mol^{-1}]	[M]	
Core-bradavidin	0.073	Brad-tag	0.985	15	1.7±0.2	–7.7	–6.1	$2.5\pm0.5\times10^{-5}$	0.94
Brad-tag/core-bradavidin	0.169/0.06	Biotin	0.6	15	–17.3±0.0	ND[a]	ND[a]	$<10^{-9}$	0.95
Core-bradavidin	0.01	Biotin	0.1	15	–15.9±0.1	ND[a]	ND[a]	$<10^{-9}$	0.93
Core-bradavidin	0.015	Brad-tag–EGFP	0.15	15	–0.5±0.1	–6.8	–7.3	$2.8\pm0.8\times10^{-6}$ [b]	0.68 [b]
wt Bradavidin	0.01	Biotin	0.1	15	–16.8±0.2	8.1	–8.7	$2.7\pm0.2\times10^{-7}$	0.61
Core-bradavidin	0.05	Brad-tag	0.25	25	ND[c]	ND[c]	ND[c]	ND[c]	ND[c]
Brad-tag/core-bradavidin	0.043/0.041	Biotin	0.4	25	–20.5±0.1	ND[a]	ND[a]	$<10^{-9}$	0.97
Core-bradavidin	0.05	Biotin	0.5	25	–20.1±0.1	ND[a]	ND[a]	$<10^{-9}$	0.98
Core-bradavidin	0.015	Brad-tag–EGFP	0.15	25	–1.0±0.1	–6.5	–7.5	$3.1\pm1.0\times10^{-6}$ [b]	0.68 [b]
wt Bradavidin	0.01	Biotin	0.1	25	–15.5±0.1	6.6	–8.9	$3.0\pm0.2\times10^{-7}$	0.85
Core-bradavidin	0.1	Brad-tag	1	40	–4.4±0.3	–2.2	–6.6	$2.6\pm0.3\times10^{-5}$	0.62
Brad-tag/core-bradavidin	0.172/0.083	Biotin	0.8	40	–21.4±0.1	ND[a]	ND[a]	$<10^{-9}$	0.91
Core-bradavidin	0.01	Biotin	0.1	40	–26.4±0.1	ND[a]	ND[a]	$<10^{-9}$	0.93
wt Bradavidin	0.01	Biotin	0.1	40	–13.7±0.2	4.3	–9.4	$2.6\pm0.4\times10^{-7}$	1.08

[a]K_d could not be determined as it exceeded the sensitivity limit of ITC.
[b]A rough estimate because the noise level in thermogram was relatively high.
[c]Could not be determined.
doi:10.1371/journal.pone.0035962.t003

C-terminal Extension Stabilizes wt Bradavidin and Inhibits Biotin Binding

ITC analysis revealed a clearly reduced biotin-binding affinity for wt bradavidin ($K_d \sim 2.8\times10^{-7}$ M) compared to core-bradavidin ($K_d < 10^{-9}$ M) (Figure 5, Table 3). This indicates that the C-terminal extension of bradavidin competes with biotin for the ligand-binding site, which is in agreement with the structure of wt bradavidin. The exothermic binding was detected as highly negative enthalpies (–16.8±0.2, –15.5±0.1, and –13.7±0.2 kcal/mol at 15, 25 and 40°C; Figures 5A$_4$, B$_4$, C$_4$, respectively). At 40°C, we observed a two-phase binding-curve and the non-linear least-squares fit was not perfect over the first three titration steps, increasing the error in the binding enthalpy. One possible explanation for this could be that the C-terminus becomes more flexible at 40°C due to increased thermal motion.

Differential scanning calorimetry (DSC) was used to study the heat-induced unfolding of core-bradavidin and wt bradavidin. The melting temperatures (T_m) for core-bradavidin in the absence and in the presence of biotin were 73.2±0.3°C and 97.9±0.2°C. For wt bradavidin, the T_m value without biotin was 96.2±0.1°C, and 101.7±0.1°C with biotin. These results further indicate that the C-terminal extension (including the Brad-tag) can serve as an intrinsic ligand and stabilize wt bradavidin, since the melting temperatures of wt bradavidin with and without biotin were quite similar. No peaks were seen in the second heating scan of DSC analysis, indicating irreversible unfolding, which is typical for avidin proteins.

Feasibility of Brad-tag as Affinity Tag

In order to study the potential of Brad-tag as an affinity tag, we designed four different fusion proteins with EGFP as described in Figure 6A. The recombinant Brad-tag–EGFP fusion proteins were produced in *E. coli* and their expression was analyzed by immunoblotting, where Brad-tag–EGFP and Brad-tag–EGFP–His-tag were clearly recognized by an antibody against GFP (Figure 6B). In contrast, the signal from C-terminally tagged EGFPs was negligible, indicating that proteins were not produced efficiently. Shorter protein forms were also seen in the lysates corresponding to C-terminally tagged EGFPs, possibly resulting from proteolytic cleavage. The spectrofluorometric analysis of cellular lysates, however, confirmed that the C-terminally tagged EGFPs were expressed (Figure 6C).

To find out whether the Brad-tag would prove functional in protein purification, core-bradavidin was conjugated to a sepharose resin. As a first experiment, Ni-NTA purified Brad-tag–EGFP–His-tag fusion protein was loaded onto the core-bradavidin-conjugated resin, which concentrated the fusion protein (Figure 7A). In contrast, a resin saturated previously with free biotin had no concentrating effect showing that biotin can efficiently prevent Brad-tag–core-bradavidin interaction. As a second experiment, we also studied whether Brad-tag–EGFP could be purified from cleared cellular lysates with core-bradavidin-conjugated resin. First, cleared cellular lysates were incubated with resin, and then the resin was washed with the binding buffer, which quite rapidly (~5–10 column volumes) led to dissociation of the bound protein. The protocol still made it possible to separate Brad-tagged EGFP from other proteins of the

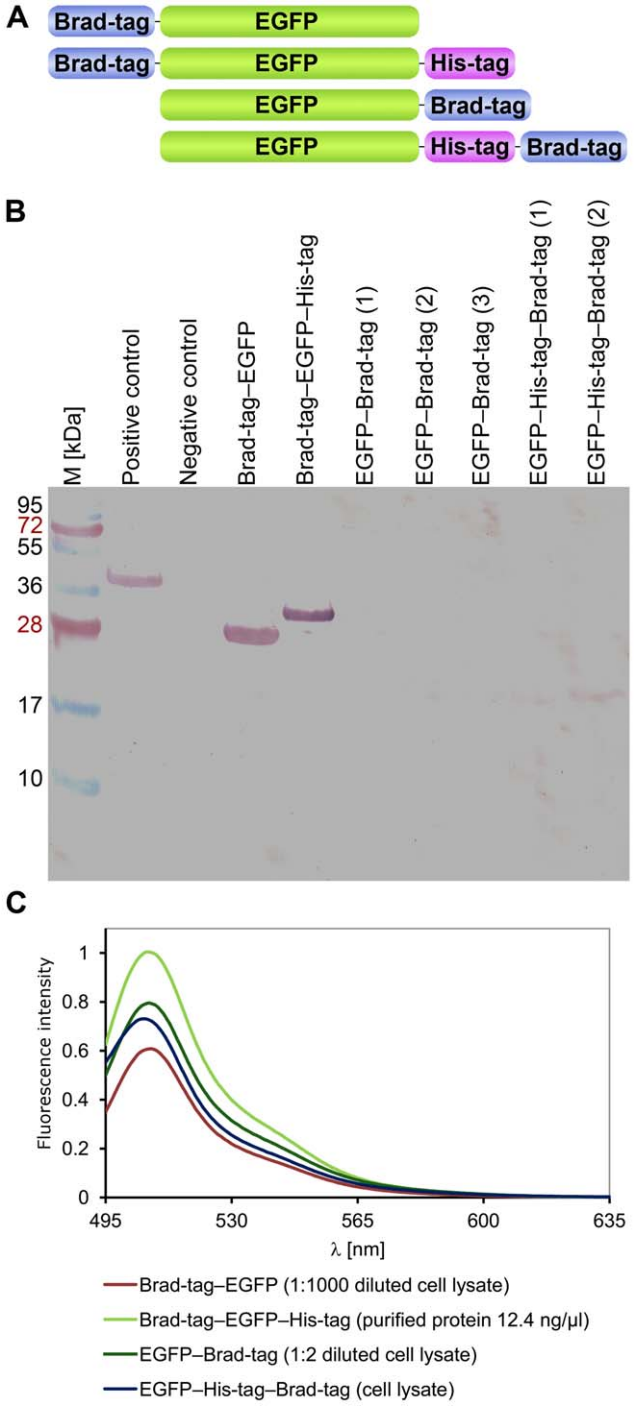

Figure 6. Brad-tag–EGFP fusion proteins. (**A**) Four different Brad-tag–EGFP fusion protein constructs were used in the current study. Brad-tag was positioned at the N- or C-terminus of the fusion proteins. A His-tag was also included in two of the constructs directly after the sequence of EGFP. (**B**) Immunoblot analysis using antibody against GFP was used to evaluate the quality and amount of tagged EGFPs. Biotinylated–EGFP was used as a positive control (Vikholm-Lundin et al, unpublished) and core-bradavidin as a negative control. Numbers in brackets indicate different protein productions. Molecular weight markers (M, kDa) are indicated on the left. (**C**) The fluorescence spectra measured for purified Brad-tag–EGFP–His-tag (12.4 ng/µl) and clarified cellular lysates of other Brad-tag–EGFP constructs.
doi:10.1371/journal.pone.0035962.g006

cell lysate as verified by SDS-PAGE (Figure 7B). Moreover, the emission spectrum of the isolated Brad-tag–EGFP protein strongly resembled that of free EGFP indicating that the tag did not affect the conformation of EGFP (Figure 7C).

In order to further study the functionality of Brad-tag, we performed ITC analysis using Brad-tag–EGFP and core-bradavidin. Here, slightly negative binding enthalpies (–0.5±0.1 at 15°C and –1.0±0.1 kcal/mol at 25°C) were detected, indicating exothermic binding. However, the noise level in the thermograms (Figures $5A_5$, B_5) was relatively high because of low protein concentrations, and therefore, the non-linear least-squares fit only gave a very rough estimate of the K_d : $\sim 3.0 \times 10^{-6}$ M (Table 3).

Specificity of Brad-tag Binding

The specificity of core-bradavidin binding to Brad-tag was studied using a biolayer interferometry biosensor ForteBio Octet RED384. Anti-Penta-HIS biosensors were functionalized with Brad-tag–EGFP–His-tag fusion protein showing efficient binding (Figure 8A, shift ~1 nm). The Brad-tag-functionalized sensors were then incubated in the presence of different avidin proteins. At a protein concentration of 0.06 mg/ml, only core-bradavidin showed clear binding to the sensor surface, whereas wt bradavidin, avidin, streptavidin or rhizavidin were not distinguishable from a sample with plain buffer (Figure 8A). We noticed dissociation of Brad-tag–EGFP–His-tag from the sensor surface, and therefore the buffer sample was subtracted from the other measured data to better illustrate the binding reaction (Figure 8B).

To further prove the specificity of the binding (Figure S7), we exposed the Brad-tag–EGFP–His-tag functionalized sensor to solutions containing higher protein concentrations as follows: core-bradavidin (0.5 mg/ml), wt bradavidin (1.2 mg/ml), chicken avidin (1.8 mg/ml), streptavidin (1.7 mg/ml) and rhizavidin (2.0 mg/ml). Core-bradavidin showed a strong binding response (shift 1.2 nm, Figure S7A), and chicken avidin showed a small response (shift 0.13 nm; Figure S7A). However, further control measurements revealed that chicken avidin bound equally well to plain anti-Penta-HIS biosensors (shift ~0.35 nm, Figure S7D). This was not surprising, as avidin is a highly basic protein (pI ~10) [1], and has in numerous previous studies been shown to bind non-specifically on different materials. Interestingly though, the binding of chicken avidin to both sensor types could be inhibited in the presence of free biotin, which seems to be the case also for chicken avidin–DNA interaction [34]. Core-bradavidin also showed some binding to non-functionalized anti-Penta-HIS sensors (shift ~0.45 nm; Figure S7D), but this binding was not dependent on the presence of biotin. Importantly, core-bradavidin showed no binding to the Brad-tag–EGFP–His-tag-functionalized surface in the presence of biotin (Figure S7C), thus proving the specificity of the assay. We also confirmed the specificity of the binding by coating the anti-penta-HIS surface with His-tagged EYFP (Hytönen, Saeger & Vogel unpublished). Neither core-bradavidin nor chicken avidin showed binding to this surface (data not shown).

Discussion

We recently characterized a novel biotin-binding protein from the symbiotic bacterium *B. japonicum*, and named the protein bradavidin. It resembles chicken avidin and streptavidin in terms of the biotin-binding properties, but has different immunological properties [9]. This property could be beneficial for development of clinical applications, where bradavidin could be used instead of avidin or streptavidin. In the original study, the evaluation of the biotin-binding properties of bradavidin was carried out by

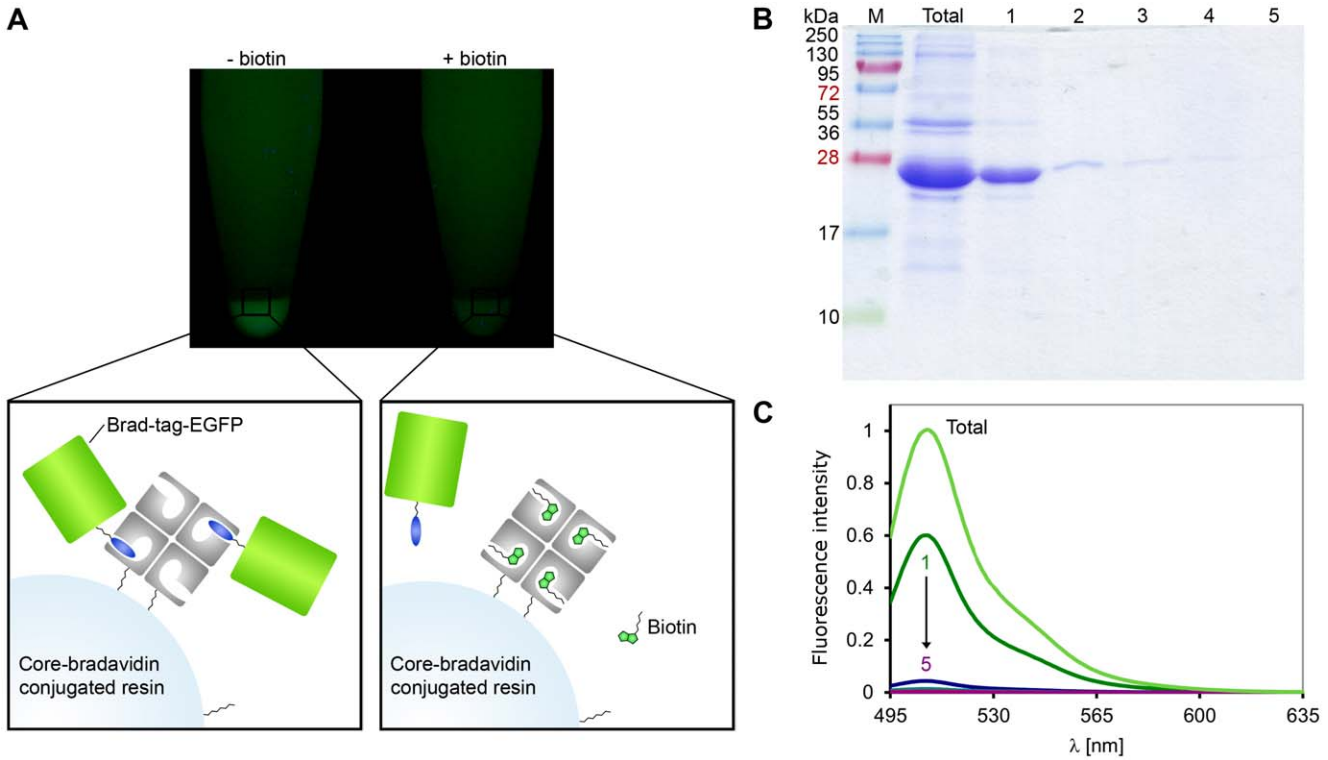

Figure 7. Purification of EGFP fusion protein using N-terminal Brad-tag. (**A**) Photograph of Brad-tag–EGFP–His-tag bound to core-bradavidin resin under UV-light. First, core-bradavidin was coupled by amine groups to the terminal NHS carboxylates of the linkers (resin–NH–$(CH_2)_5$–COONHS). Then, Brad-tag–EGFP–His-tag (prepurified with Ni-NTA column) was incubated with the functionalized resin and the resin was pelleted. In the absence (–) of biotin Brad-tag–EGFP–His-tag concentrates on the resin pellet. The presence (+) of free biotin inhibits the binding. Stoichiometry and the size of compounds in the schematic figure are only speculative. (**B**) SDS-PAGE analysis of the protein purification experiment for cellular lysates of N-Brad-tag–EGFP-C. Cleared cellular lysate (total) was incubated with core-bradavidin resin. Then the resin was washed with buffer (50 mM Tris-HCl, 100 mM NaCl, pH 7.5) and samples 1 to 5 were eluted. Molecular weight markers (M, kDa) are indicated on the left. (**C**) The fluorescence spectra measured for cleared cellular lysate (total) and eluted samples 1 to 5 from the protein purification experiment for Brad-tag–EGFP.
doi:10.1371/journal.pone.0035962.g007

measuring the dissociation rate constants (k_{diss}) of biotin analogues [9], and the dissociation rate determined at 30°C by radioactive [^{3}H]-biotin was very similar for core-bradavidin (k_{diss} 1.9×10^{-4} s^{-1}) and wt bradavidin (k_{diss} 2.9×10^{-4} s^{-1}), but faster than for avidin (k_{diss} 1.3×10^{-7} s^{-1}, extrapolated from the data published in [35]) and streptavidin (k_{diss} 9.0×10^{-6} s^{-1} extrapolated from the data published in [36]). In contrast, at 50°C, both core-bradavidin and wt bradavidin were just as extreme fluorescent biotin conjugate binders as streptavidin, whereas avidin showed a clearly faster dissociation rate [9]. These experiments led to the conclusion that bradavidin and core-bradavidin do not significantly differ in their ligand-binding properties. However, recent experiments with 1,4,7,10-tetraazacyclododecane-1,4,7,10-tetraacetic acid (DOTA)-conjugated biotin revealed a much lower binding affinity for wt bradavidin in comparison to core-bradavidin (Hytönen and Petronzelli, unpublished results).

In the current study, we solved the X-ray structure of wt bradavidin in order to better understand the function of the full-length protein at structural level. We also conducted ITC experiments both with wt bradavidin and core-bradavidin, which indeed did reveal the lower affinity of wt bradavidin towards biotin in comparison to core-bradavidin. These findings complete our understanding of the ligand-binding properties of wt bradavidin, showing that the C-terminal extension lowers the association rate of the ligand, whereas the extension has no important effect for the dissociation phase, at least in the case of biotin and fluorescently-labelled biotin (Bf560-biotin) [9].

Wt bradavidin has a β-barrel fold typical for avidins. The overall structure of wt bradavidin revealed clear similarities to the known structures of avidins but also unique structural features like the C-terminal extension (see below) and the four Tyr90 residues packing tightly to each other in the center of the tetramer. Tyrosine residues are also found in the subunit interfaces of some known avidin structures, for example in the subunit I-III interface of the AVR4/5 structure [37], but not in the center of the tetramer as in bradavidin (Figure 3). Many of the loops and β-strands of bradavidin also have distinctive structural properties, such as conformation or length. This is especially true for the β-strands and loops near or in contact with the termini of the protein (Figure 1).

Wt bradavidin was crystallized in the presence of HABA, but the azo-dye ligand was not present in the final structure. Instead, the C-terminal amino acids Ser130-Lys137 of each subunit of wt bradavidin folded into the ligand-binding site of the neighbouring subunit (Figure 1). The C-terminal amino acids (SEKLSNTK) were named "Brad-tag" and the affinity of this peptide to core-bradavidin and to other avidins was measured using ITC. We found that Brad-tag binds to core-bradavidin with an affinity (~25 μM) comparable to that measured between the original Strep-tag and streptavidin [30] (Table 2). Similarly to the binding of other known peptide tags to different avidins (Table 2), the

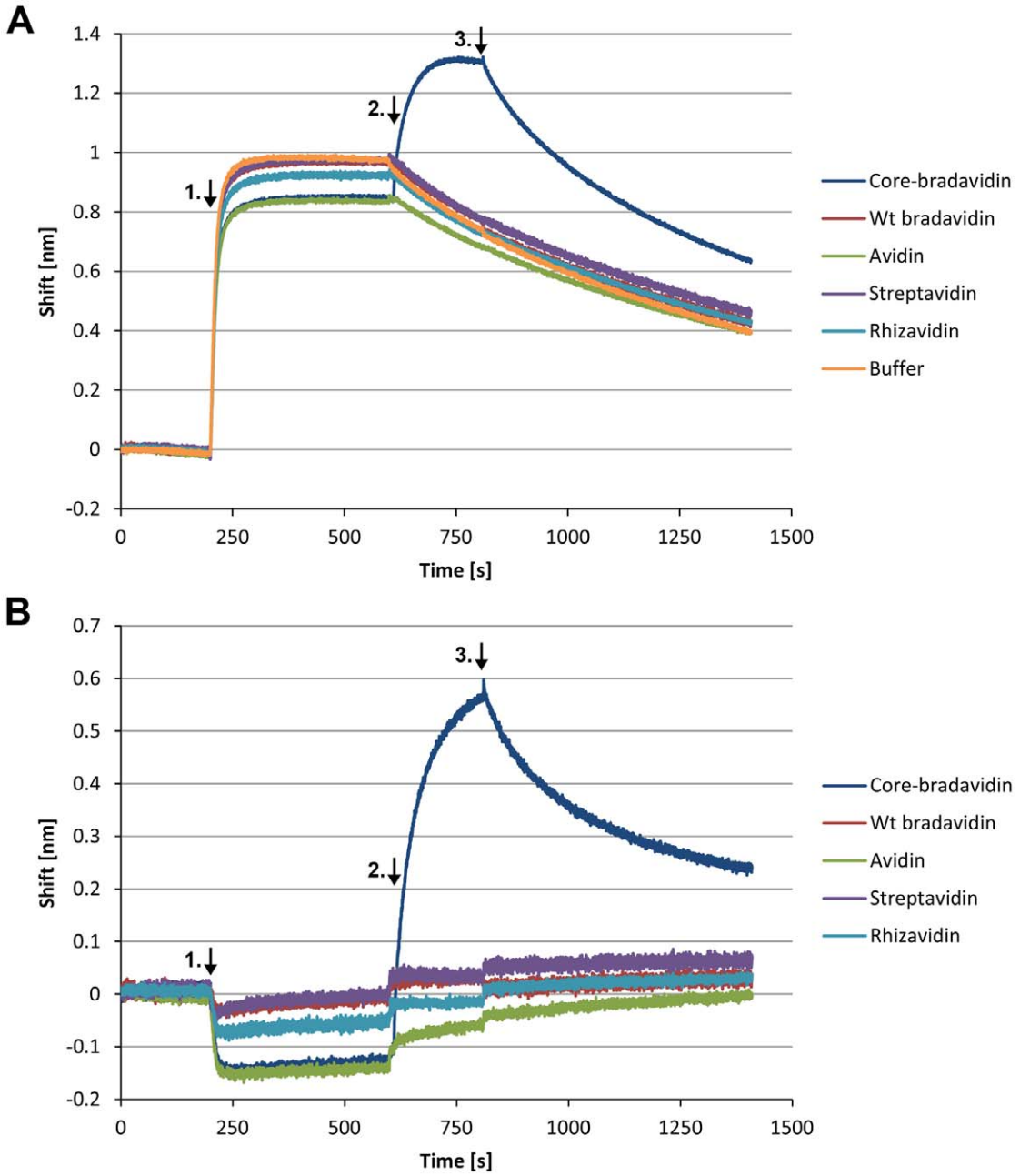

Figure 8. Specificity of core-bradavidin binding to Brad-tag analyzed by biolayer interferometry. (**A**) Anti-Penta-HIS biosensors were functionalized with Brad-tag–EGFP–His-tag fusion protein (step 1, arrow in the graph). After a brief wash (10 s) in measurement buffer, biosensors were incubated with a series of different avidin proteins at concentration of 0.06 mg/ml (step 2). Sample without any avidin protein was used as a negative control (buffer). Finally, biosensors were exposed to the measurement buffer leading to dissociation of the bound core-bradavidin proteins (step 3). (**B**) The measured raw data for buffer is subtracted from the raw data of different proteins.
doi:10.1371/journal.pone.0035962.g008

binding of Brad-tag, according to ITC and biosensor analysis, was specific for bradavidin. In ITC analysis, Brad-tag did not interact with other biotin-binding proteins that were analysed, including chicken avidin, streptavidin and rhizavidin. Biosensor analysis initially showed that chicken avidin may have some affinity for surface-immobilized Brad-tagged EGFP. However, our control experiments suggest that this interaction is likely to be non-specific, typical for highly basic avidin. In order to demonstrate that Brad-tag could find use in biotechnological applications, we showed that Brad-tag could be used to concentrate Brad-tag–EGFP protein from cleared cellular lysate. However, the affinity is not yet high enough for efficient purification of fusion proteins and needs to be improved by using mutagenesis or other methods. In our opinion, Brad-tag has potential to be an additional tool within the avidin-biotin technology platform, resembling e.g. Strep-tag [38], a peptide that binds to the ligand-binding site of streptavidin, and Strep-tag II that binds with higher affinity ($K_d \approx 1$ μM) to an engineered version of streptavidin (streptactin [18]; Table 2).

Our preliminary amino acid sequence comparison of wt bradavidin and its homolog from *Rhodopseudomonas palustris* (Q21816; named rhodavidin [39]) revealed that Trp5, important for the unique conformation of the N-terminus of wt bradavidin, is found at an equivalent position in the sequence of rhodavidin. The high overall similarity for these two proteins (76% sequence identity; Figure 2) indicates potentially similar tertiary structures. More interestingly, the C-terminal Brad-tag sequence (GSEKLSNTK) was found at the C-terminus of rhodavidin but not, to our knowledge, in any other known sequence of the avidin protein family. This suggests a similar mechanism for bradavidin and rhodavidin for the use of the Brad-tag sequence and the question arises as to the biological significance of this sequence. Unfortunately, this is not known yet, although it is clear from our results that the C-terminal extension especially affects the binding of large biotinylated ligands. It has earlier been suggested that the C-terminal residues of the T7-tagged wt streptavidin would compete with weakly bound ligands for the binding site, not least for the reason that the local concentrations of the intrinsic ligands are high [16,19,20]. Analogously to wt bradavidin and wt streptavidin, the C-terminal residues of rhodavidin most probably also contribute to the ligand-binding preferences. Because of the much lower affinity for large biotinylated ligands, such as the endogenous biotin carboxyl carrier protein, one could speculate that the biological role of both bradavidin and rhodavidin could be to selectively bind free biotin and, hence, protect the cellular machinery of the host cell. One could also envision the utilization of the ligand-binding preferences of wt bradavidin in biochemical assays.

Even though the biological role of the extended C-termini of wt bradavidin and wt streptavidin may be the same, the structural implementation differs: in wt bradavidin each C-terminus reaches and interacts with the biotin-binding site of the neighbouring subunit (intrinsic, intersubunit ligand), whereas in T7-tagged wt streptavidin the C-terminus interact with the ligand binding site of the same subunit (intrinsic, intrasubunit ligand). The binding mode of the C-termini of wt bradavidin and T7-tagged wt streptavidin is different, too. In wt bradavidin, the key residues for binding to the biotin-binding site are Glu131, Lys132 and Leu133, whereas those of wt streptavidin are Gly151, Asn152 and Pro153 [19]. Moreover, the T7-tag replaces the 13 N-terminal residues of wt streptavidin but no electron density was observed for the tag in the crystal structure [PDB: 2BC3]. Hence, the role of the N-terminus for the structure of wt streptavidin is not fully clear. However, the structure of wt bradavidin reported here shows that the very first N-terminal residues are a unique part of the extended β1-strand; interactions with the first residues after the last β-strand, the β8-strand, affect the folding of the C-terminus, too (Figures 1B, 2).

The ITC-determined dissociation constants (K_d) for Brad-tag to core-bradavidin were 25 μM at 15°C and 26 μM at 40°C. We also studied the characteristics of the interaction between Brad-tag and core-bradavidin by biosensor sandwich assay. Even though this technique was not optimal for accurate determination of the binding constants due to the leakage of the His-tagged protein from the surface (Figure 8A), the 1:1 binding model fitted to the buffer-subtracted data (Figure 8B) yielded a value of K_d in the micromolar range, which is in good agreement with our ITC-analysis data (Table 3). All in all, the determined dissociation constants were of the same order of magnitude as that for the original Strep-tag to streptavidin ($K_d = 37$ μM). Although limited, the strength of the Strep-tag-streptavidin interaction was found to be sufficient for affinity purification [30]. The Strep-tag was functional only when attached to the C-terminus of a fusion partner, whereas Brad-tag was functional only at the N-terminus, based on findings made for only one protein, namely EGFP. The terminus-independent affinity tag, Strep-tag II, has also been reported and was discovered by screening a designed peptide array of 400 sequences, but the tag showed lower affinity to streptavidin ($K_d \approx 72$ μM) than the original Strep-tag [30]. In order to improve the affinity of Strep-tag II, Voss & Skerra (1997) subjected streptavidin to random mutagenesis resulting in increased affinity ($K_d \approx 1$ μM) [18]. Our novel crystal structure of wt bradavidin provides the basis for improving the Brad-tag–core-bradavidin pair, for example, to increase the affinity and other binding properties by rational mutagenesis of core-bradavidin and/or by redesigning the tag.

Several affinity tags have been developed and are widely used in recombinant fusion proteins, e.g. to aid protein purification from crude cell lysates [40,41] or as tools for probing molecular functions [42]. Affinity tags include a variety of molecules from polypeptides to proteins [40] and several of them bind to avidin, neutravidin or streptavidin (summarized in Table 2). Brad-tag and core-bradavidin utilizing technology would be a valuable addition to this toolbox. Since each tag-based strategy has both advantages and disadvantages, there is a constant need to develop alternative tag-based strategies. These combined with the existing ones may be needed to develop novel methodologies suitable for studies of protein complexes and assemblies. For example, one may envision tagging of several different proteins being an efficient approach to characterize complicated molecular arrangements, such as focal adhesions [43]. On the other hand, by creating circular permutants of bradavidin [44], we could produce bradavidin mutants that would bind more than one type of ligand simultaneously. Moreover, layer-by-layer construction of novel architectures through biological interactions, including avidin-biotin, is an evolving area in the field of optical and electrochemical biosensing [45], where the Brad-tag–core-bradavidin pair could also be used.

In summary, wt bradavidin is a unique member of the avidin protein family having a C-terminal extension, which enters and occupies the ligand-binding site of the neighbouring subunit. The isolated binding epitope has potential to be used as an affinity tag in the field of bio(nano)technology including detection and purification methods as well as construction of novel biomaterials for biosensing and other purposes.

Materials and Methods

Protein Expression and Purification

The construction of core-bradavidin and wt bradavidin containing pBVboostFG vectors is described earlier [9]. For Brad-tag–EGFP fusion proteins, the pHis–EGFP plasmid [46, Saeger, Hytönen & Vogel, unpublished] was used as a template in PCR, and primers contained the Brad-tag sequence (Table S1). The amplified PCR-products were extracted from an agarose gel and subcloned into the pET101/D-TOPO® vector according to the manufacturer's instructions (Invitrogen, Carlsbad, CA, USA). All constructs were confirmed by DNA sequencing (ABI PRISM 3100 Genetic Analyzer, Applied Biosystems).

Core-bradavidin and wt bradavidin were produced in the periplasmic space of *E. coli* BL21-AI cells (Invitrogen) in an active form, as previously described in detail [47]. Similarly, Brad-tag–EGFP fusion proteins were produced in the periplasm of *E. coli* BL21 Star™(DE3) cells (Invitrogen). The pET101/D-based expression vectors were transformed into *E. coli* Star™(DE3) or BL21-AI cells. Fresh transformants were cultured using an orbital shaker with continuous shaking at 28°C in Lysogeny broth (LB)

medium, supplemented with 100 μg/ml ampicillin and 0.1% (w/v) glucose for core-bradavidin, 7 μg/ml gentamycin and 0.1% (w/v) glucose for wt bradavidin, and 100 μg/ml ampicillin for Brad-tag–EGFP fusion proteins. When the culture reached an OD_{600} of 0.5, the protein expression was induced by adding 1 mM IPTG (and 0.2% (w/v) L-arabinose for core-bradavidin and wt bradavidin). For Brad-tag–EGFP fusion proteins, bottle cultivation was continued overnight at 28°C, and cells were then collected by centrifugation (4000 g, 10 min, 4°C). For core-bradavidin and wt bradavidin, the pilot-scale fermentation was made with a Labfors Infors 3 (Infors HT, Bottmingen, Switzerland), using the pO_2 (DO-stat) controlled fed-batch protocol that has been described in detail elsewhere [48].

Core-bradavidin and wt bradavidin were purified in a single step using 2-iminobiotin affinity chromatography (Affiland S. A., Ans-Liege, Belgium) [49]. First, 50 g of cells (wet weight) pelleted from *E. coli* fermentation were suspended in binding buffer (50 mM Na-carbonate, pH 11, containing 1 M NaCl). The suspension was homogenized twice using an EmulsiFlex C3 homogenizator (Avestin Inc., Ottawa, Canada) using homogenizing pressure of 15 000–18 000 psi. After this, cell lysates were centrifuged (15 000 g, 30 min, 4°C). The supernatant was filtered and the pH was measured, and when necessary, adjusted to 10.5 using 10 M NaOH. The crude protein mixture was applied to 2-iminobiotin agarose, which had previously been equilibrated with the binding buffer. This mixture was incubated for one hour on a rolling shaker at 4°C with subsequent centrifugation (3000 g, 10 min, RT) and two washing steps with the binding buffer. Finally, the agarose was transferred to a column and the protein was eluted in one ml fractions with 0.1 M acetic acid (pH 3).

Brad-tag–EGFP fusion proteins containing a His-tag were purified using Ni-NTA metal-affinity chromatography (Qiagen GmbH, Hilden, Germany). First, cells from 500 ml cultivation volume were suspended in lysis buffer (50 mM NaH_2PO_4, 300 mM NaCl, 10 mM imidazole, pH 8). Lysozyme (one mg per 100 ml) was added and the cells were sonicated for 5 min (30% duty cycle, 5 s on, 3 s off) on ice. The cellular debris was pelleted by centrifugation (15 000 g, 30 min, 4°C) and the supernatant was filtered using a 0.2 μm filter cloth. Ni-NTA agarose was equilibrated with lysis buffer before mixing with the cleared cellular lysate. The resulting mixture was incubated on a rolling shaker for one hour at 4°C. After this, the mixture was transferred to a column and washed three times with 20 ml of lysis buffer and again three times with 20 ml of wash buffer (50 mM NaH_2PO_4, 300 mM NaCl, 20 mM imidazole, pH 8). Finally, the protein was eluted in one ml fractions with elution buffer (50 mM NaH_2PO_4, 300 mM NaCl, 250 mM imidazole, pH 8).

Brad-tag–EGFP fusion proteins without a His-tag were purified with core-bradavidin agarose (see below). To prepare the clarified lysate, the cell pellets were suspended in 50 mM Tris-HCl, 100 mM NaCl, pH 7.5. Lysozyme was added to a final concentration of 10 mg/l and the mixture was sonicated and filtered similarly as above.

The purity of all proteins was studied by SDS-PAGE. Cell lysates and eluted proteins were denaturated by heating at 95°C for ten minutes in SDS-PAGE sample buffer containing a reducing agent (β-mercaptoethanol). Samples were run on 15% SDS-PAGE and the gel was stained with Coomassie Brilliant Blue. The amount of EGFP fusion proteins were further investigated by immunoblot analysis. Proteins blotted onto nitrocellulose were detected by incubating with a primary antibody against GFP (Anti-GFP Epitope Tag Polyclonal Antibody, Thermo Scientific) at a 1:2000 dilution. This was followed by incubation with a secondary antibody - alkaline phosphatase (AP) conjugate (anti-rabbit IgG-AP, Sigma) at a 1:30000 dilution. Finally, AP was reacted with 5-bromo-4-chloro-3-indolyl phosphate (BCIP) and nitro-blue tetrazolium (NBT) to yield a coloured precipitate.

The protein concentration was determined with a UV/Vis spectrophotometer (NanoDrop 1000 Spectrophotometer, Thermo Scientific, Wilmington, DE, USA) by measuring the absorbance at 280 nm and using an extinction coefficient of 39085 $M^{-1}cm^{-1}$ for core-bradavidin and 20525 $M^{-1}cm^{-1}$ for EGFP fusion proteins containing Brad-tag and the His-tag.

Purification of Brad-tag–EGFP Fusion Proteins with Immobilized Core-bradavidin Resin

Core-bradavidin was coupled to NHS-activated resin through amine coupling. First, 4.5 ml of core-bradavidin (0.93 mg/ml) in coupling buffer (10 mM $NaHCO_3$, 0.9% NaCl (w/v), pH 7.5) was coupled to Sepharose™ 4 fast flow, NHS-4FF (Affiland, Liège, Belgium). Five ml of resin suspended in isopropanol was centrifuged (3000 g, 10 min, 4°C) and washed twice with 15 ml of cold distilled water and centrifuged again (3000 g, 10 min, 4°C). The supernatant was removed and the protein was added to the resin. The suspension was incubated on a rolling shaker overnight at 4°C followed by incubation on a rolling shaker for one hour at room temperature (RT, 21±1°C). The resin was then centrifuged 3200 g, 10 min, at RT and the supernatant was removed. The protein concentration of the supernatant was measured in order to estimate the amount of resin-bound protein. Next, the resin was washed three times with 14 ml of 10 mM $NaHCO_3$, 0.9% NaCl (w/v), pH 7.5, followed by washing three times with 14 ml of PBS buffer, pH 4.0, and again three times with 14 ml of PBS buffer, pH 8.0. Finally, the resin was washed once with 14 ml of PBS buffer, pH 7.4, and stored at 4°C.

Core-bradavidin resin (0.2 ml) was washed with binding buffer (50 mM Tris-HCl, 100 mM NaCl, pH 7.5). Purified Brad-tag–EGFP–His-tag or cleared cellular lysate containing Brad-tag–EGFP was added to the resin and the mixture was incubated on a rolling shaker for one hour at 4°C. After this, the resin was transferred to a column and washed ten times with one ml of binding buffer and again ten times with one ml of wash buffer (50 mM Tris-HCl, 1 M NaCl, pH 7.5). Finally, the protein was eluted in one ml fractions with the elution buffer (50 mM Na-carbonate, 1 M NaCl, pH 11). All fractions were collected and the sample tubes were photographed under UV-light to visualize the elution profile. Samples of fractions were analyzed by 15% SDS-PAGE and the gel stained with Coomassie Brilliant Blue.

To estimate whether the EGFP fusion proteins were concentrated on the resin, 100 μl of the core-bradavidin resin was mixed with 900 μl of binding buffer in the absence and presence of biotin (77 μM). Then, 100 μl of Brad-tag–EGFP–His-tag fusion protein (125 μM) was added and samples were incubated using an orbital shaker with continuous shaking for 10 min. The resin was pelleted by incubation without shaking for 10 min and the sample tubes were photographed under UV-light.

EGFP fusion protein expression and purification were verified by fluorescence. A QuantaMaster™ spectrofluorometer (Photon Technology International, Inc., Lawrenceville, NJ, USA) was used to excite the sample at 485 nm and to detect the emission spectra from 495 nm to 635 nm. The measurements were performed at RT in 50 mM Tris-HCl, 100 mM NaCl, pH 7.5. The emission spectrum of the buffer was subtracted as the baseline.

Crystallization and X-ray Structure Determination of Wild Type Bradavidin

Suitable conditions for crystallization of bradavidin were found using the Classics™ (Nextal Biotechnology) screen, the vapour diffusion method and sitting drops (1–2 µl) on 96 well plates (Corning Inc.). The protein solution (~0.4 mg/ml) contained 50 mM sodium acetate (pH 4). Saturated solution of an azo dye HABA (<10 mg/ml) was added to the protein solution in 1:10 (v/v) ratio, respectively, before crystallization. Bar-like crystals of a typical size of 0.2×0.05×0.05 mm were used for data collection. The crystals were formed at 22°C using 0.7 µl of well solution containing 25% (w/v) PEG 4000, 0.17 M ammonium acetate and 0.08 M sodium acetate (pH 4.6), and 0.8 µl of the protein solution.

X-ray diffraction data were collected at the MAX-lab beam line I911-2 (Lund, Sweden) equipped with a MarCCD detector. The crystal was cryoprotected by adding 0.7 µl of 4 M sodium formate to the crystallization drop just prior to flash-freezing in a 100 K liquid nitrogen stream (Oxford Cryosystem). The collected data was originally processed with Mosflm (7.0.3) [50] using the iMosflm (0.6.1) GUI and scaled with Scala of the CCP4 program suite [51] using the CCP4i GUI [52], and later reprocessed with XDS [53] (see Table 1 for X-ray structure determination statistics).

The initial phase information for structure factors was obtained using the molecular replacement program Phaser [54] within the CCP4i GUI [52]. Multiple search models and ensembles were tested before a solution could be found, finally using homology models as a search ensemble. Shortly, three tetrameric homology models were produced using Modeller [55] of Discovery Studio 2.1 (Accelrys Software Inc.). A structural alignment (data not shown) of the core sequence of bradavidin (Uniprot Q89IH6) and the sequences from X-ray structures of avidin [PDB: 1AVD], streptavidin [PDB: 1MK5] and xenavidin [PDB: 2UYW], respectively, was used for modelling. The models (one model per template structure) were structurally aligned using Pymol [56] and their N- and C-termini were trimmed based on visual checking of the models. Monomers of the aligned structures were then used as a search ensemble in Phaser (two monomers were searched) giving an initial solution with TFZ = 8.5 and LGG = 80 in space group $P2_12_12_1$. The initial, incomplete dimeric model of bradavidin was refined using Refmac5 [57] resulting in an $R_{factor} = 0.513$, $R_{free} = 0.536$ and FOM = 0.297 and then used as a search model for the next round of Phaser, where two dimers were searched giving a solution with TFZ = 13.5 and LGG = 246. Refinement of the solution, *i.e.* a tetrameric model of bradavidin, resulted in an $R_{factor} = 0.449$, $R_{free} = 0.482$ and FOM = 0.477. This model was used then, again, as a search model in Phaser now yielding a solution with TFZ = 20.7 and LGG = 320. The model was manually edited/rebuilt using Coot [58] and refined with Refmac5 ($R_{factor} = 0.420$, $R_{free} = 0.456$ and FOM = 0.546) before rebuilding the whole structure with ARP/wARP (starting from an existing model; v. 6.1.1) [59–61], finally giving a model of bradavidin that could be finished through further cycles of refinement with Refmac5 and modification/rebuilding with Coot. Solvent atoms and other non-protein atoms were added to the model either with the automatic procedure of ARP/wARP or Coot, or manually in Coot. Few cycles of the refinement in the middle of the structure building was done also with the software suite Phenix [62]. We could not solve the structure without the step-by-step procedure used for molecular replacement described above.

The final structure of wt bradavidin was validated using the inbuilt tools of Coot [58], and using MolProbity [63] of the Phenix software suite [62], before deposition to the Protein Data Bank [64,65] with PDB entry code 2Y32. The data collection and structure determination statistics are summarized in Table 1.

Isothermal Titration Calorimetry

The affinity of core-bradavidin towards Brad-tag or D-biotin was measured by isothermal titration calorimetry (ITC). We also analyzed binding between wt bradavidin and D-biotin. The synthetic Brad-tag, SEKLSNTK, was ordered from GenScript (Piscataway, NJ, USA). The purified core-bradavidin or wt bradavidin was dialyzed against 50 mM sodium phosphate (pH 7.0) buffer containing 100 mM NaCl, and Brad-tag and D-biotin were directly dissolved in the same buffer. Samples were degassed with stirring for 5 min and heated to a temperature of 0.5 degrees lower than the measurement temperature by MicroCal™ ThermoVac. The measurements were performed at 15, 25 or 40°C in an isothermal titration calorimetry VP-ITC MicroCalorimeter (GE Healthcare, MicroCal, Northampton, MA, USA) with 10 µl titration aliquots of ligands (Brad-tag, biotin or Brad-tag–EGFP–His-tag) in 30 repeated additions at intervals of 200 s using constant stirring speed 440 rpm. The data were analyzed with Microcal Origin 7.0 (MicroCal LLC, Northampton, MA, USA) software. The observed reaction heats were corrected by subtracting the heat of dilution caused by the titration of the ligand alone into buffer. K_a, ΔH and n (stoichiometry per subunit) were obtained through non-linear least-squares fit of the corrected reaction heats for each titration step.

Differential Scanning Calorimetry

The unfolding temperatures of core-bradavidin and wt bradavidin were analyzed by MicroCal™ VP-Capillary DSC System (GE Healthcare, MicroCal, Northampton, MA, USA). Before analysis, the samples were dialyzed against 50 mM sodium phosphate (pH 7.0) buffer containing 100 mM NaCl. The proteins were then diluted to a final concentration of 15 µM. Samples were degassed with stirring for 5 min at 20°C by MicroCal™ ThermoVac. Thermograms were recorded from 20°C to 135°C using scan rate of 120°C/hour. Two parallel measurements of each sample were analysed and each of them were scanned twice. The measurements were conducted in the absence and in the presence of biotin using ~3:1 molar ratio of biotin:protein subunit. Microcal Origin 7.0 software was used for data analysis.

Biolayer Interferometry

Specificity of core-bradavidin binding to Brad-tag–EGFP–His-tag fusion protein was analyzed by biolayer interferometry using ForteBio Octet RED384 instrument (FortéBio, Menlo Park, CA, USA). The instrument was controlled by using Data Acquisition 7.0 software (FortéBio). First, the baseline for anti-Penta-HIS biosensors (FortéBio) in measurement buffer containing 50 mM sodium phosphate (pH 7.0) and 100 mM NaCl was recorded for 200 s. Then, Brad-tag–EGFP–His-tag (0.03 mg/ml) was attached to sensors with 400 s incubation. Following a 10-second washing step in the measurement buffer, the biosensors were moved to a solution containing core-bradavidin (0.06 mg/ml) for 200 s. As a control, 0.06 mg/ml solutions of wt bradavidin, avidin, streptavidin or rhizavidin were studied. Finally, biosensors were exposed to the measurement buffer and the dissociation of bound proteins was measured for 600 s.

The experiment described above was repeated using higher protein concentrations and a slightly longer incubation times: Brad-tag–EGFP–His-tag (0.03 mg/ml) was bound to sensors for 700 s. After washing, the biosensors were then used to study binding of core-bradavidin (0.5 mg/ml), wt bradavidin (1.2 mg/

ml), avidin (1.8 mg/ml), streptavidin (1.7 mg/ml) and rhizavidin (2.0 mg/ml) for 200 s. The dissociation of bound proteins in buffer was followed for 1900 s. As a negative control, Brad-tag–EGFP–His-tag coated biosensors, prepared as described above, were incubated in a solution containing core-bradavidin (0.5 mg/ml) and avidin (1.8 mg/ml) in the presence of biotin (3.2 mM for core-bradavidin and 13 mM for avidin). Another control experiment was carried out by using His-tagged EYFP with terminal cysteine residues (Hytönen, Saeger & Vogel unpublished) for the functionalization of the anti-penta-HIS sensors, followed by incubation with various avidins. Yet another control experiment was carried out where plain anti-penta-HIS biosensors were exposed to core-bradavidin (0.5 mg/ml) and chicken avidin (1.8 mg/ml) both in the absence and presence of biotin (3.2 mM for core-bradavidin and 13 mM for avidin). The measurement parameters were as follows: measurement temperature 30°C, stirring speed 1000 rpm and the distance of the tip from the surface 4 mm. Black 96-well plates (Greiner Bio-One GmbH, Frickenhausen, Germany) were used for the biosensor analyses, 1:1 Langmuir binding model was fitted to the buffer-subtracted binding curve by using Data Analysis 7.0 software (FortéBio). For preparation of the graphs, the raw data was exported from the instrument and processed with MS Excel.

Miscellaneous Methods

The structure-based sequence alignment was done using Malign of the Bodil software, a modular, multi-platform software package for biomolecular visualization and modeling [66,67]. ESPript [68] was used for visualization of the sequence alignment. PyMOL (The PyMOL Molecular Graphics System, Version 1.3, Schrödinger, LLC) was used to create all the figures relating to structural representations. ABPS plugin of PyMOL (MG Lerner and HA Carlson. APBS plugin for PyMOL, 2006, University of Michigan, Ann Arbor) was used for electropotential calculations – alternative rotamers were excluded from the calculations. Inkscape 0.47 [69] was used to edit the figures related to structural representations.

Supporting Information

Figure S1 Surface properties of wt bradavidin (reported here [PDB: 2Y32]) and T7-tagged wt streptavidin [PDB: 2BC3]. Electropotential maps were calculated using the APBS plugin (MG Lerner and HA Carlson, APBS plugin for PyMOL, 2006, University of Michigan, Ann Arbor) of PyMOL (The PyMOL Molecular Graphics System, Version 1.3, Schrödinger, LLC). Default settings were used and alternative conformers were excluded from the calculations. The views rotated 90 degrees around the x-axis (x90) and y-axis (y90) are also shown.
(TIF)

Figure S2 Subunit interfaces of wt bradavidin and avidin. The subunit I-II interface (**A**) and subunit I-III interface (**B**) for wt bradavidin [PDB: 2Y32] (left) and avidin [PDB: 1VYO] (right) are shown. The residues participating to the subunit-subunit interaction are shown as sticks and the carbon atoms coloured as follow: subunit I, blue; II, cyan; and III, magenta.
(TIF)

Figure S3 Superimposition of the ligand-binding pocket occupying residues of wt bradavidin and wt streptavidin [PDB: 2BC3]. Stereo view. A biotin molecule of chicken avidin structure [PDB: 1AVD] is also shown for the comparison of equivalent moieties. Stick models are shown with colouring of the carbon atoms as follows: wt bradavidin, blue; wt streptavidin, magenta; biotin, white.
(TIF)

Figure S4 Hydrogen bonding of the side chain nitrogen atom of K132. A stick model (stereo view) is shown. The carbon atoms of residues from subunit I are shown in blue and from subunit III in magenta. Electron density map (a weighted 2FO-FC map; sigma level 1) around the residues is shown in blue and the putative hydrogen bonds with yellow dashes.
(TIF)

Figure S5 Structural comparison of peptide tags binding to the ligand-binding site of wt bradavidin and streptavidin. Carbon atoms of wt bradavidin and streptavidin are shown in blue and green, respectively. The PDB entry codes are shown in brackets.
(TIF)

Figure S6 Brad-tag titrations to control proteins by ITC. Thermograms of measurements performed at 40°C for (**A**) avidin, (**B**) streptavidin and (**C**) rhizavidin are shown. No detectable binding of Brad-tag to these proteins is seen.
(TIF)

Figure S7 Interaction between various avidin proteins and Brad-tag analyzed by biolayer interferometry. (**A**) Anti-Penta-HIS biosensors were coated with Brad-tag–EGFP–His-tag fusion protein (step 1, arrow in the graph). After a brief wash (10 s) in measurement buffer, biosensors were incubated with a series of different proteins: core-bradavidin (0.5 mg/ml), wt bradavidin (1.2 mg/ml), avidin (1.8 mg/ml), streptavidin (1.7 mg/ml) and rhizavidin (2.0 mg/ml) and a buffer as a control (step 2). Binding of core-bradavidin was detected and a slight increase in the signal for avidin as well. Finally, biosensors were exposed to buffer and the bound proteins started to dissociate (step 3). (**B**) The measured raw data for buffer is subtracted from the raw data measured for different proteins. (**C**) As a control measurement, core-bradavidin (0.5 mg/ml) and chicken avidin (1.8 mg/ml) were measured in the presence of biotin (3.2 mM for core-bradavidin and 13 mM for avidin). The data where the effect of the used measurement buffer is subtracted is shown. (**D**) As another control measurement, core-bradavidin (0.5 mg/ml) and chicken avidin (1.8 mg/ml) in the absence and presence of biotin (3.2 mM for core-bradavidin and 13 mM for avidin) were incubated with plain anti-penta-HIS biosensors.
(TIF)

Table S1 Sequences of primers used in PCR reactions.
(DOC)

Acknowledgments

We thank Ulla Kiiskinen, Soili Hiltunen and Ilmari Tamminen for their excellent technical assistance. We would like to thank the staff at the MAX-lab beam lines I711 and I911 for excellent support. We also thank Dr. Fiorella Petronzelli, Sigma-tau, Pomezia, Italy for helpful discussions.

Author Contributions

Conceived and designed the experiments: JL VPH TTA. Performed the experiments: JL TG TTA. Analyzed the data: JL TG JAEM VPH TTA. Contributed reagents/materials/analysis tools: MSJ MSK VPH TTA. Wrote the paper: JL TG JAEM MSJ MSK VPH TTA.

References

1. Green NM (1975) Avidin. Adv Protein Chem 29: 85–133.
2. Wilchek M, Bayer EA (1990) Introduction to avidin-biotin technology. Methods Enzymol 184: 5–13.
3. Laitinen OH, Hytönen VP, Nordlund HR, Kulomaa MS (2006) Genetically engineered avidins and streptavidins. Cell Mol Life Sci 63: 2992–3017.
4. Korpela JK, Kulomaa MS, Elo HA, Tuohimaa PJ (1981) Biotin-binding proteins in eggs of oviparous vertebrates. Experientia 37: 1065–1066.
5. Määttä J, Helppolainen S, Hytönen V, Johnson M, Kulomaa M, et al. (2009) Structural and functional characteristics of xenavidin, the first frog avidin from xenopus tropicalis. BMC Structural Biology 9: 63.
6. Laitinen OH, Hytönen VP, Ahlroth MK, Pentikäinen OT, Gallagher C, et al. (2002) Chicken avidin-related proteins show altered biotin-binding and physicochemical properties as compared with avidin. Biochem J 363: 609–617.
7. Hytönen VP, Laitinen OH, Grapputo A, Kettunen A, Savolainen J, et al. (2003) Characterization of poultry egg-white avidins and their potential as a tool in pretargeting cancer treatment. Biochem J 372: 219–225.
8. Chaiet L, Wolf FJ (1964) The properties of streptavidin, a biotin-binding protein produced by streptomycetes. Arch Biochem Biophys 106: 1–5.
9. Nordlund HR, Hytönen VP, Laitinen OH, Kulomaa MS (2005) Novel avidin-like protein from a root nodule symbiotic bacterium, bradyrhizobium japonicum. J Biol Chem 280: 13250–13255.
10. Helppolainen SH, Määttä JA, Halling KK, Slotte JP, Hytönen VP, et al. (2008) Bradavidin II from bradyrhizobium japonicum: A new avidin-like biotin-binding protein. Biochim Biophys Acta 1784: 1002–1010.
11. Helppolainen SH, Nurminen KP, Määttä JA, Halling KK, Slotte JP, et al. (2007) Rhizavidin from rhizobium etli: The first natural dimer in the avidin protein family. Biochem J 405: 397–405.
12. Sardo A, Wohlschlager T, Lo C, Zoller H, Ward TR, et al. (2011) Burkavidin: A novel secreted biotin-binding protein from the human pathogen burkholderia pseudomallei. Protein Expr Purif 77: 131–139.
13. Lesch HP, Kaikkonen MU, Pikkarainen JT, Ylä-Herttuala S (2010) Avidin-biotin technology in targeted therapy. Expert Opin Drug Deliv 7: 551–564.
14. Wilchek M, Bayer EA, Livnah O (2006) Essentials of biorecognition: The (strept)avidin-biotin system as a model for protein-protein and protein-ligand interaction. Immunol Lett 103: 27–32.
15. Zhou M, Ghosh I (2007) Quantum dots and peptides: A bright future together. Biopolymers 88(3): 325–339.
16. Sano T, Pandori MW, Chen X, Smith CL, Cantor CR (1995) Recombinant core streptavidins. A minimum-sized core streptavidin has enhanced structural stability and higher accessibility to biotinylated macromolecules. J Biol Chem 270: 28204–28209.
17. Schmidt TG, Skerra A (1994) One-step affinity purification of bacterially produced proteins by means of the "strep tag" and immobilized recombinant core streptavidin. J Chromatogr A 676: 337–345.
18. Voss S, Skerra A (1997) Mutagenesis of a flexible loop in streptavidin leads to higher affinity for the strep-tag II peptide and improved performance in recombinant protein purification. Protein Eng 10: 975–982.
19. Le Trong I, Humbert N, Ward TR, Stenkamp RE (2006) Crystallographic analysis of a full-length streptavidin with its C-terminal polypeptide bound in the biotin binding site. J Mol Biol 356: 738–745.
20. Bayer EA, Ben-Hur H, Hiller Y, Wilchek M (1989) Postsecretory modifications of streptavidin. Biochem J 259: 369–376.
21. Marttila AT, Laitinen OH, Airenne KJ, Kulik T, Bayer EA, et al. (2000) Recombinant NeutraLite avidin: A non-glycosylated, acidic mutant of chicken avidin that exhibits high affinity for biotin and low non-specific binding properties. FEBS Lett 467: 31–36.
22. Rosebrough SF, Hartley DF (1996) Biochemical modification of streptavidin and avidin: In vitro and in vivo analysis. J Nucl Med 37: 1380–1384.
23. Livnah O, Bayer EA, Wilchek M, Sussman JL (1993) Three-dimensional structures of avidin and the avidin-biotin complex. Proc Natl Acad Sci U S A 90: 5076–5080.
24. Hytönen VP, Määttä JA, Nyholm TK, Livnah O, Eisenberg-Domovich Y, et al. (2005) Design and construction of highly stable, protease-resistant chimeric avidins. J Biol Chem 280: 10228–10233.
25. Nordlund HR, Hytönen VP, Laitinen OH, Uotila STH, Niskanen EA, et al. (2003) Introduction of histidine residues into avidin subunit interfaces allows pH-dependent regulation of quaternary structure and biotin binding. FEBS Letters 555: 449–454.
26. Derewenda ZS, Lee L, Derewenda U (1995) The occurrence of C-H…O hydrogen bonds in proteins. J Mol Biol 252: 248–262.
27. Denessiouk KA, Johnson MS (2003) "Acceptor-donor-acceptor" motifs recognize the watson-crick, hoogsteen and sugar "donor-acceptor-donor" edges of adenine and adenosine-containing ligands. J Mol Biol 333: 1025–1043.
28. Pugliese L, Coda A, Malcovati M, Bolognesi M (1993) Three-dimensional structure of the tetragonal crystal form of egg-white avidin in its functional complex with biotin at 2.7 A resolution. J Mol Biol 231: 698–710.
29. Meir A, Helppolainen SH, Podoly E, Nordlund HR, Hytönen VP, et al. (2009) Crystal structure of rhizavidin: Insights into the enigmatic high-affinity interaction of an innate biotin-binding protein dimer. J Mol Biol 386: 379–390.
30. Schmidt TG, Koepke J, Frank R, Skerra A (1996) Molecular interaction between the strep-tag affinity peptide and its cognate target, streptavidin. J Mol Biol 255: 753–766.
31. Korndörfer IP, Skerra A (2002) Improved affinity of engineered streptavidin for the strep-tag II peptide is due to a fixed open conformation of the lid-like loop at the binding site. Protein Sci 11: 883–893.
32. Perbandt M, Bruns O, Vallazza M, Lamla T, Betzel C, et al. (2007) High resolution structure of streptavidin in complex with a novel high affinity peptide tag mimicking the biotin binding motif. Proteins 67: 1147–1153.
33. Määttä JA, Airenne TT, Nordlund HR, Jänis J, Paldanius TA, et al. (2008) Rational modification of ligand-binding preference of avidin by circular permutation and mutagenesis. Chembiochem 9: 1124–1135.
34. Niederhauser B, Siivonen J, Määttä JA, Jänis J, Kulomaa MS, et al. (2012) DNA family shuffling within the chicken avidin protein family - A shortcut to more powerful protein tools. J Biotechnol 157: 38–49.
35. Hytönen VP, Määttä JA, Kidron H, Halling KK, Hörhä J, et al. (2005) Avidin related protein 2 shows unique structural and functional features among the avidin protein family. BMC Biotechnol 5: 28.
36. Klumb LA, Chu V, Stayton PS (1998) Energetic roles of hydrogen bonds at the ureido oxygen binding pocket in the streptavidin-biotin complex. Biochemistry 37: 7657–7663.
37. Eisenberg-Domovich Y, Hytönen VP, Wilchek M, Bayer EA, Kulomaa MS, et al (2005) High-resolution crystal structure of an avidin-related protein: Insight into high-affinity biotin binding and protein stability. Acta Crystallogr D 61: 528–538.
38. Schmidt TG, Skerra A (1993) The random peptide library-assisted engineering of a C-terminal affinity peptide, useful for the detection and purification of a functional ig fv fragment. Protein Eng 6: 109–122.
39. Sardo A, Wohlschlager T, Lo C, Zoller H, Ward TR, et al. (2011) Burkavidin: A novel secreted biotin-binding protein from the human pathogen burkholderia pseudomallei. Protein Expr Purif 77: 131–139.
40. Terpe K (2003) Overview of tag protein fusions: From molecular and biochemical fundamentals to commercial systems. Appl Microbiol Biotechnol 60: 523–533.
41. Gräslund S, Nordlund P, Weigelt J, Hallberg BM, Bray J, et al. (2008) Protein production and purification. Nat Methods 5: 135–146.
42. Xie H, Guo XM, Chen H (2009) Making the most of fusion tags technology in structural characterization of membrane proteins. Mol Biotechnol 42: 135–145.
43. Byron A, Humphries JD, Bass MD, Knight D, Humphries MJ (2011) Proteomic analysis of integrin adhesion complexes. Sci Signal 4: pt2.
44. Nordlund HR, Laitinen OH, Hytönen VP, Uotila ST, Porkka E, et al. (2004) Construction of a dual chain pseudotetrameric chicken avidin by combining two circularly permuted avidins. J Biol Chem 279: 36715–36719.
45. Takahashi S, Sato K, Anzai JI (2011) Layer-by-layer construction of protein architectures through avidin-biotin and lectin-sugar interactions for biosensor applications. Anal Bioanal Chem 402: 1749–1758.
46. Farres J, Rechsteiner MP, Herold S, Frey AD, Kallio PT (2005) Ligand binding properties of bacterial hemoglobins and flavohemoglobins. Biochemistry 44: 4125–4134.
47. Hytönen VP, Laitinen OH, Airenne TT, Kidron H, Meltola NJ, et al. (2004) Efficient production of active chicken avidin using a bacterial signal peptide in Escherichia coli. Biochem J 384: 385–390.
48. Määttä JA, Eisenberg-Domovich Y, Nordlund HR, Hayouka R, Kulomaa MS, et al. (2011) Chimeric avidin shows stability against harsh chemical conditions – biochemical analysis and 3D structure. Biotechnol Bioeng 108: 481–490.
49. Hofmann K, Wood SW, Brinton CC, Montibeller JA, Finn FM (1980) Iminobiotin affinity columns and their application to retrieval of streptavidin. Proc Natl Acad Sci USA 77: 4666–4668.
50. Leslie AGW (1992) Recent changes to the MOSFLM package for processing film and image plate data. Joint CCP4+ESF-EAMCB News-Letter on Protein Crystallography (No. 26).
51. Collaborative Computational Project, Number 4 (1994) The CCP4 suite: Programs for protein crystallography. Acta Crystallogr D Biol Crystallogr 50: 760–763.
52. Potterton E, Briggs P, Turkenburg M, Dodson E (2003) A graphical user interface to the CCP4 program suite. Acta Crystallogr D Biol Crystallogr 59: 1131–1137.
53. Kabsch W (1993) Automatic processing of rotation diffraction data from crystals of initially unknown symmetry and cell constants. J Appl Crystallogr 26: 795–800.
54. McCoy AJ, Grosse-Kunstleve RW, Adams PD, Winn MD, Storoni LC, et al. (2007) Phaser crystallographic software. J Appl Crystallogr 40: 658–674.
55. Sali A, Blundell TL (1993) Comparative protein modelling by satisfaction of spatial restraints. J Mol Biol 234: 779–815.
56. Schrödinger L (2010) The PyMOL molecular graphics system, version 1.3.
57. Murshudov GN, Vagin AA, Dodson EJ (1997) Refinement of macromolecular structures by the maximum-likelihood method. Acta Crystallogr D Biol Crystallogr 53: 240–255.
58. Emsley P, Cowtan K (2004) Coot: Model-building tools for molecular graphics. Acta Crystallogr D Biol Crystallogr 60: 2126–2132.

59. Lamzin VS, Wilson KS (1993) Automated refinement of protein models. Acta Crystallogr D Biol Crystallogr 49: 129–147.
60. Perrakis A, Morris R, Lamzin VS (1999) Automated protein model building combined with iterative structure refinement. Nat Struct Biol 6: 458–463.
61. Langer G, Cohen SX, Lamzin VS, Perrakis A (2008) Automated macromolecular model building for X-ray crystallography using ARP/wARP version 7. Nat Protoc 3: 1171–1179.
62. Adams PD, Grosse-Kunstleve RW, Hung LW, Ioerger TR, McCoy AJ, et al. (2002) PHENIX: Building new software for automated crystallographic structure determination. Acta Crystallogr D Biol Crystallogr 58: 1948–1954.
63. Davis IW, Leaver-Fay A, Chen VB, Block JN, Kapral GJ, et al. (2007) MolProbity: All-atom contacts and structure validation for proteins and nucleic acids. Nucleic Acids Res 35: W375–83.
64. Berman HM, Westbrook J, Feng Z, Gilliland G, Bhat TN, et al. (2000) The protein data bank. Nucleic Acids Res 28: 235–242.
65. Berman HM, Battistuz T, Bhat TN, Bluhm WF, Bourne PE, et al. (2002) The protein data bank. Acta Crystallogr D Biol Crystallogr 58: 899–907.
66. Lehtonen JV, Still DJ, Rantanen VV, Ekholm J, Björklund D, et al. (2004) BODIL: A molecular modeling environment for structure-function analysis and drug design. J Comput Aided Mol Des 18: 401–419.
67. Bodil (2012) website. Available: http://users.abo.fi/bodil/. Accessed 2012 April 1.
68. Gouet P, Courcelle E, Stuart DI, Metoz F (1999) ESPript: Analysis of multiple sequence alignments in PostScript. Bioinformatics 15: 305–308.
69. Inkscape website (2012) Available: http://www.inkscape.org. Accessed 2012 April 1.
70. Uniprot website (2012) Available: http://www.uniprot.org. Accessed 2012 April 1.
71. Winn MD, Isupov MN, Murshudov GN (2001) Use of TLS parameters to model anisotropic displacements in macromolecular refinement. Acta Crystallogr D Biol Crystallogr 57: 122–133.
72. Meyer SC, Gaj T, Ghosh I (2006) Highly selective cyclic peptide ligands for NeutrAvidin and avidin identified by phage display. Chem Biol Drug Des 68: 3–10.
73. Gaj T, Meyer SC, Ghosh I (2007) The AviD-tag, a NeutrAvidin/avidin specific peptide affinity tag for the immobilization and purification of recombinant proteins. Protein Expr Purif 56: 54–61.
74. Lamla T, Erdmann VA (2004) The nano-tag, a streptavidin-binding peptide for the purification and detection of recombinant proteins. Protein Expr Purif 33: 39–47.
75. Skerra A, Schmidt TGM (1999) Applications of a peptide ligand for streptavidin: The strep-tag. Biomol Eng 16: 79–86.
76. Keefe AD, Wilson DS, Seelig B, Szostak JW (2001) One-step purification of recombinant proteins using a nanomolar-affinity streptavidin-binding peptide, the SBP-tag. Protein Expr Purif 23: 440–446.

Supporting Information

Structure of Bradavidin – C-Terminal Residues Act as Intrinsic Ligands

Jenni Leppiniemi[1,2], Toni Grönroos[1,2], Juha A. E. Määttä[1,2], Mark S. Johnson[3], Markku S. Kulomaa[1,2], Vesa P. Hytönen[1,2], Tomi T. Airenne[3*]

1 Institute of Biomedical Technology, University of Tampere, Tampere University Hospital, Tampere, Finland,
2 BioMediTech, Tampere, Finland,
3 Department of Biosciences, Biochemistry, Åbo Akademi University, Tykistökatu, Turku, Finland

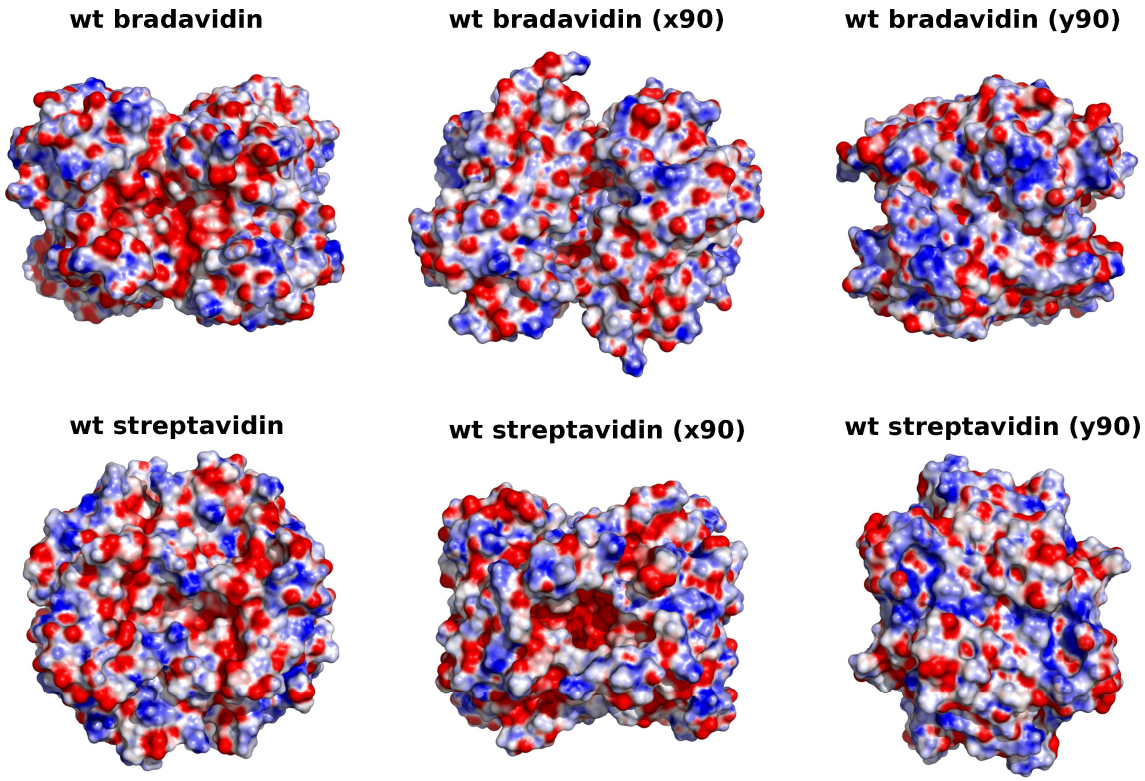

Figure S1. Surface properties of wt bradavidin (reported here [PDB: 2Y32]) and T7-tagged wt streptavidin [PDB: 2BC3]. Electropotential maps were calculated using the APBS plugin (MG Lerner and HA Carlson, APBS plugin for PyMOL, 2006, University of Michigan, Ann Arbor) of PyMOL (The PyMOL Molecular Graphics System, Version 1.3, Schrödinger, LLC). Default settings were used and alternative conformers were excluded from the calculations. The views rotated 90 degrees around the x-axis (x90) and y-axis (y90) are also shown.

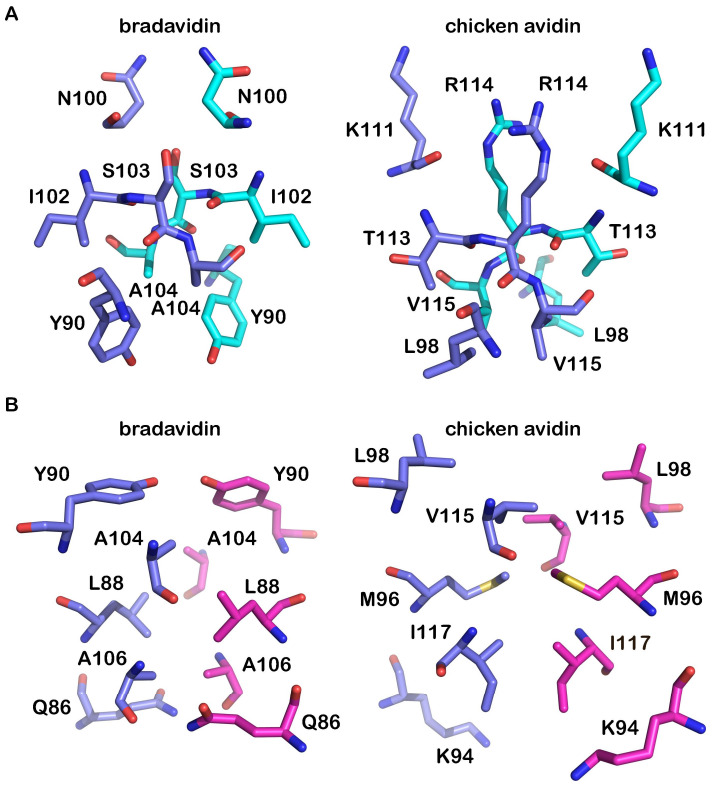

Figure S2. Subunit interfaces of wt bradavidin and avidin. The subunit I-II interface (A) and subunit I-III interface (B) for wt bradavidin [PDB: 2Y32] (left) and avidin [PDB: 1VYO] (right) are shown. The residues participating to the subunit-subunit interaction are shown as sticks and the carbon atoms coloured as follow: subunit I, blue; II, cyan; and III, magenta.

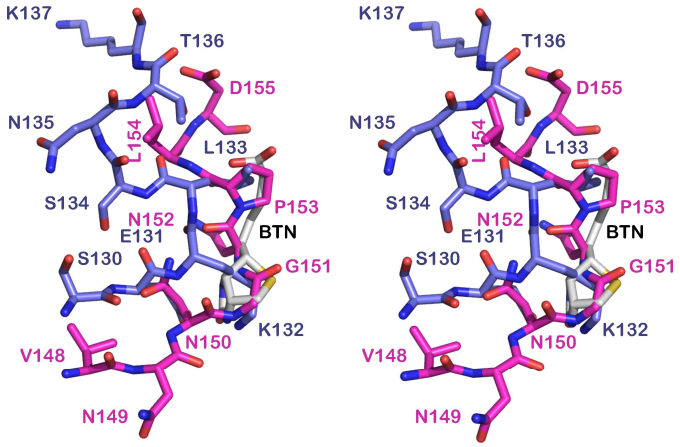

Figure S3. Superimposition of the ligand-binding pocket occupying residues of wt bradavidin and wt streptavidin [PDB: 2BC3]. Stereo view. A biotin molecule of chicken avidin structure [PDB: 1AVD] is also shown for the comparison of equivalent moieties. Stick models are shown with colouring of the carbon atoms as follows: wt bradavidin, blue; wt streptavidin, magenta; biotin, white.

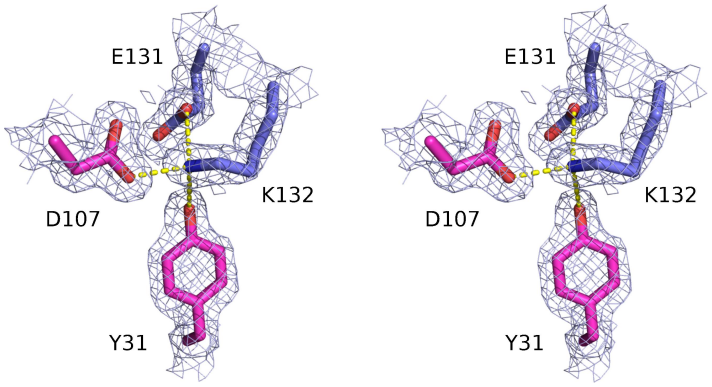

Figure S4. Hydrogen bonding of the side chain nitrogen atom of K132. A stick model (stereo view) is shown. The carbon atoms of residues from subunit I are shown in blue and from subunit III in magenta. Electron density map (a weighted 2FO-FC map; sigma level 1) around the residues is shown in blue and the putative hydrogen bonds with yellow dashes.

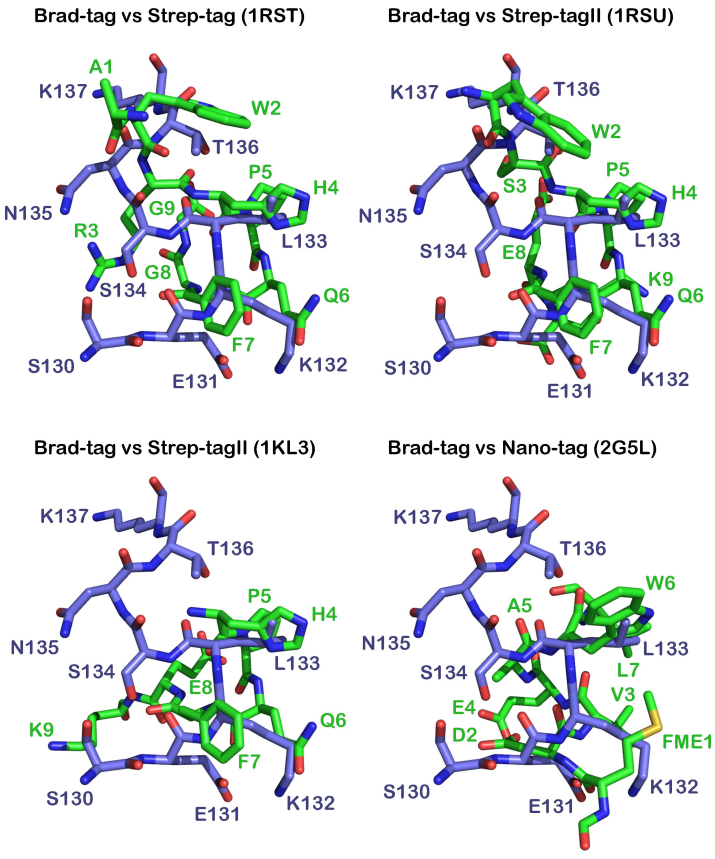

Figure S5. Structural comparison of peptide tags binding to the ligand-binding site of wt bradavidin and streptavidin. Carbon atoms of wt bradavidin and streptavidin are shown in blue and green, respectively. The PDB entry codes are shown in brackets.

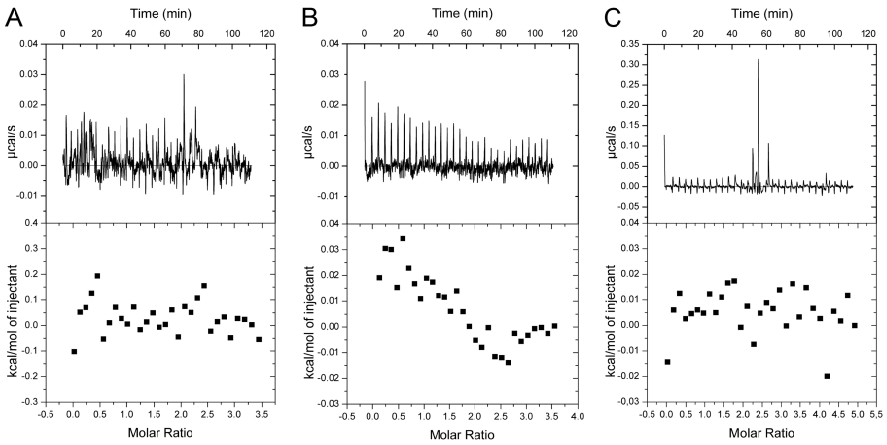

Figure S6. Brad-tag titrations to control proteins by ITC. Thermograms of measurements performed at 40°C for (A) avidin, (B) streptavidin and (C) rhizavidin are shown. No detectable binding of Brad-tag to these proteins is seen.

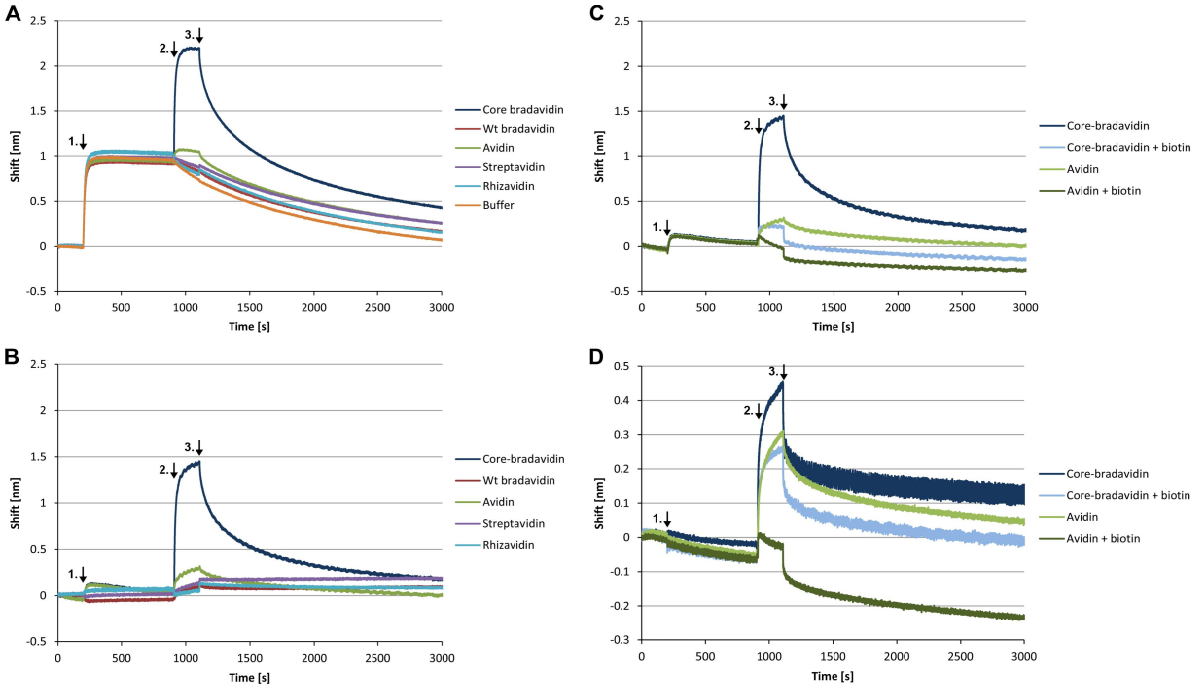

Figure S7. Interaction between various avidin proteins and Brad-tag analyzed by biolayer interferometry. (A) Anti-Penta-HIS biosensors were coated with Brad-tag–EGFP–His-tag fusion protein (step 1, arrow in the graph). After a brief wash (10 s) in measurement buffer, biosensors were incubated with a series of different proteins: core-bradavidin (0.5 mg/ml), wt bradavidin (1.2 mg/ml), avidin (1.8 mg/ml), streptavidin (1.7 mg/ml) and rhizavidin (2.0 mg/ml) and a buffer as a control (step 2). Binding of core-bradavidin was detected and a slight increase in the signal for avidin as well. Finally, biosensors

were exposed to buffer and the bound proteins started to dissociate (step 3). (B) The measured raw data for buffer is subtracted from the raw data measured for different proteins. (C) As a control measurement, core-bradavidin (0.5 mg/ml) and chicken avidin (1.8 mg/ml) were measured in the presence of biotin (3.2 mM for core-bradavidin and 13 mM for avidin). The data where the effect of the used measurement buffer is subtracted is shown. (D) As another control measurement, core-bradavidin (0.5 mg/ml) and chicken avidin (1.8 mg/ml) in the absence and presence of biotin (3.2 mM for core-bradavidin and 13 mM for avidin) were incubated with plain anti-penta-HIS biosensors.

Table S1. Sequences of primers used in PCR reactions.

Primer	Sequence
5' Brad-tag_GFP	5'-CACCATGTCA GAAAAACTGT CAAATACAAA AAGCAAGGGC GAGGAG-3'
5' GFP	5'-CACCATGAGC AAGGGCGAGG AG-3'
3' GFP_Stop	5'-TCAAGTGATC CCGGCGGC-3'
3' GFP	5'-AGTGATCCCG GCGGC-3'
3' GFP_Brad-tag_Stop	5'-TCATTTTGTA TTTGACAGTT TTTCTGAAGT GATCCCGGCG GC-3'
3' GFP_6xHis_Brad-tag_Stop	5'-TTATCATTTT GTATTTGACA GTTTTTCTGA ATGGTGATGG TGATGATGAC CGGTAC-3'

THE PROTEIN SOCIETY

The highly dynamic oligomeric structure of bradavidin II is unique among avidin proteins

Jenni Leppiniemi,[1,2] Amit Meir,[3] Niklas Kähkönen,[1,2] Sampo Kukkurainen,[1,2] Juha A. Määttä,[1,2] Markus Ojanen,[1,2] Janne Jänis,[4] Markku S. Kulomaa,[1,2] Oded Livnah,[3] and Vesa P. Hytönen[1,2,5]

[1]Institute of Biomedical Technology, University of Tampere and Tampere University Hospital, FI-33014 Tampere, Finland

[2]BioMediTech, Tampere, Finland

[3]The Alexander Silberman Institute of Life Sciences and The Wolfson Centre for Applied Structural Biology, The Hebrew University of Jerusalem, Jerusalem 91904, Israel

[4]Department of Chemistry, University of Eastern Finland, FI-80101 Joensuu, Finland

[5]Fimlab Laboratories, Tampere, Finland

Received 4 March 2013; Revised 5 April 2013; Accepted 6 May 2013
DOI: 10.1002/pro.2281
Published online 10 May 2013 proteinscience.org

Abstract: Bradavidin II is a biotin-binding protein from *Bradyrhizobium japonicum* that resembles chicken avidin and bacterial streptavidin. A biophysical characterization was carried out using dynamic light scattering, native mass spectrometry, differential scanning calorimetry, and isothermal titration calorimetry combined with structural characterization using X-ray crystallography. These observations revealed that bradavidin II differs from canonical homotetrameric avidin protein family members in its quaternary structure. In contrast with the other avidins, bradavidin II appears to have a dynamic (transient) oligomeric state in solution. It is monomeric at low protein concentrations but forms higher oligomeric assemblies at higher concentrations. The crystal structure of bradavidin II revealed an important role for Phe42 in shielding the bound ligand from surrounding water molecules, thus functionally replacing the L7,8 loop essential for tight ligand binding in avidin and streptavidin. This bradavidin II characterization opens new avenues for oligomerization-independent biotin-binding protein development.

Keywords: ligand binding; oligomeric state; dynamic structure; structural cooperativity

Introduction

Avidin and streptavidin are the workhorses of the life sciences. These biotin-binding proteins are used in numerous applications and their structures and functions have been widely studied (for review, see Refs. 1 and 2). Avidin was originally isolated from chicken egg white, whereas streptavidin is a structurally and functionally analogous protein that was isolated from the bacterium *Streptomyces avidinii*.[3] Recent studies have revealed there are several other avidins that functionally resemble (strept)avidin. Of these proteins, bradavidin,[4] rhizavidin,[5]

Abbreviations: AVR2, avidin-related protein 2; AVR4, avidin-related protein 4; DSC, differential scanning calorimetry; DLS, dynamic light scattering; DMSO, dimethyl sulfoxide; FT-ICR, Fourier transform ion cyclotron resonance; ITC, isothermal titration calorimetry; L1,2, loop between beta strands 1 and 2; MS, mass spectrometry; RMSD, root-mean-square deviation; T_m, transition midpoint of thermal denaturation

Additional Supporting Information may be found in the online version of this article.

Grant sponsor: Academy of Finland, Pirkanmaa Hospital District, Sigrid Jusélius Foundation, and the Tampere Graduate Program in Biomedicine and Biotechnology (TGPBB).

*Correspondence to: Vesa Hytönen, BioMediTech, Biokatu 6, FI-33520 Tampere, Finland. E-mail: vesa.hytonen@uta.fi

shwanavidin,[6] xenavidin,[7] tamavidin 2,[8] and chicken avidin-related proteins 2 (AVR2)[9] and 4 (AVR4)[10] have been structurally characterized, and the majority share similarities with (strept)avidin and consist of eight-strand beta barrels assembled into tetramers.

Avidins are characterized as beta-barrel proteins with a high affinity to biotin (with a K_d in the pM to fM range). Their high ligand-binding affinity is based on a perfect structural complementarity between the protein and biotin ligand (also known as vitamin H), high number of hydrogen bonds, and ligand-binding site architecture. Avidins are relatively thermostable, and some are also resistant to proteases and harsh chemical conditions, so they are widely used in life science applications. All avidins characterized to date, with the exceptions of rhizavidin[11] and shwanavidin,[6] use residues from two adjacent subunits in ligand recognition. Therefore, although biotin binding to avidin is noncooperative in nature,[12] ligand binding and the protein's oligomeric state are interdependent properties in avidins. Tetrameric avidins may be not optimal as fusion partners or labeling purposes, because oligomerization of the fusion partner may change its biological function and oligomerization in general leads to avidity effects. In addition, oligomerization increases molecular weight of the fusion protein. Therefore, in many applications, monomeric avidins could be beneficial. The oligomericity of (strept)avidin has been genetically manipulated by applying mutations to its subunit interfaces (for example, see Refs. [13] and [14]). The outcomes of these studies have typically produced proteins with relatively low biotin affinities, and the engineered proteins have also been found to be less thermostable than wild-type proteins. A promising recent study has shown that monomeric streptavidin with relatively high affinity to biotin and increased thermostability can be obtained via genetic engineering.[15] Importantly, nature appears to offer good alternatives to avidin and streptavidin in relation to oligomeric states, with naturally dimeric rhizavidin and shwanavidin as good examples.

This study describes the three-dimensional (3D) structure and biophysical analysis of bradavidin II, which is a biotin-binding protein derived from *Bradyrhizobium japonicum* that resembles other avidins in its primary sequence (Fig. 1). Bradavidin I and II are both from the genome of *B. japonicum*. They share only low sequence identity (34% as calculated by NCBI blastp), whereas majority of the residues associated with ligand binding are conserved in both of the proteins. Bradavidin I has been found to structurally resemble canonical avidin members.[4] Now, for the first time, we report a highly dynamic oligomeric state for an avidin family member. Biophysical analyses suggest that bradavidin II is monomeric at low protein concentrations but forms transient oligomers (mainly dimers and trimers) at higher protein concentrations. Structural X-ray crystallography analysis revealed the assembly of bradavidin II subunits to be a loosely packed tetramer in which the canonical interactions between subunits of tetrameric avidin family members (chicken avidin, streptavidin, bradavidin, etc.) are missing, and the relative orientation between the subunits is unique. The bradavidin II structural information presented here sheds new light on tight ligand binding and may enable the design of more sophisticated biotin binders with better control over protein oligomeric states.

Results

Protein production

Initial attempts to crystallize bradavidin II by following Helppolainen *et al.*[16] were unsuccessful. All resulting crystals showed poor diffraction. To increase protein yield and quality, novel protein batches were produced with a fermentor by fed-batch protocol as described.[17] Following 2-iminobiotin purification, two protein forms were detected by SDS-PAGE analysis. To further identify these protein forms, the protein sample was analyzed using high-resolution Fourier transform ion cyclotron resonance (FT-ICR) mass spectrometry (MS). We detected 12.5 and 16.1 kDa protein forms, with the latter representing protein accompanied by extra residues from the expression vector and resolved by MS/MS experiments (for details, see Supporting Information Fig. S1). To resolve the problem described above, a second stop codon was added to the expression vector and homogenous 12.5-kDa protein was obtained after 2-iminobiotin affinity chromatography purification with yield of more than 10 mg pure protein per liter of bacterial culture.

The structure of bradavidin II

Bradavidin II was crystallized and solved in three forms (two apo and one biotin complex) (Table I). All three bradavidin II forms displayed the typical tertiary structure of the avidin family, which consists of eight antiparallel β-strands forming a β-barrel. The asymmetric units of all crystal forms contained one (apo Form-A, resolution 1.9 Å), two (apo Form-B, resolution 1.7 Å), or four (biotin complex, resolution 1.75 Å) monomers, none of which resembled any common avidin canonical dimer or tetramer arrangements, even during symmetry operations, suggesting the presence of a monomer in a crystalline state. In practice, structural alignment of bradavidin II structures with tetrameric avidins such as chicken avidin (PDB 2AVI and 1VYO) or streptavidin (PDB 1STP) or dimeric avidins such as rhizavidin (PDB 3EW2) and shwanavidin (PDB 3SZJ) clearly show that the interface contacts between subunits are not present

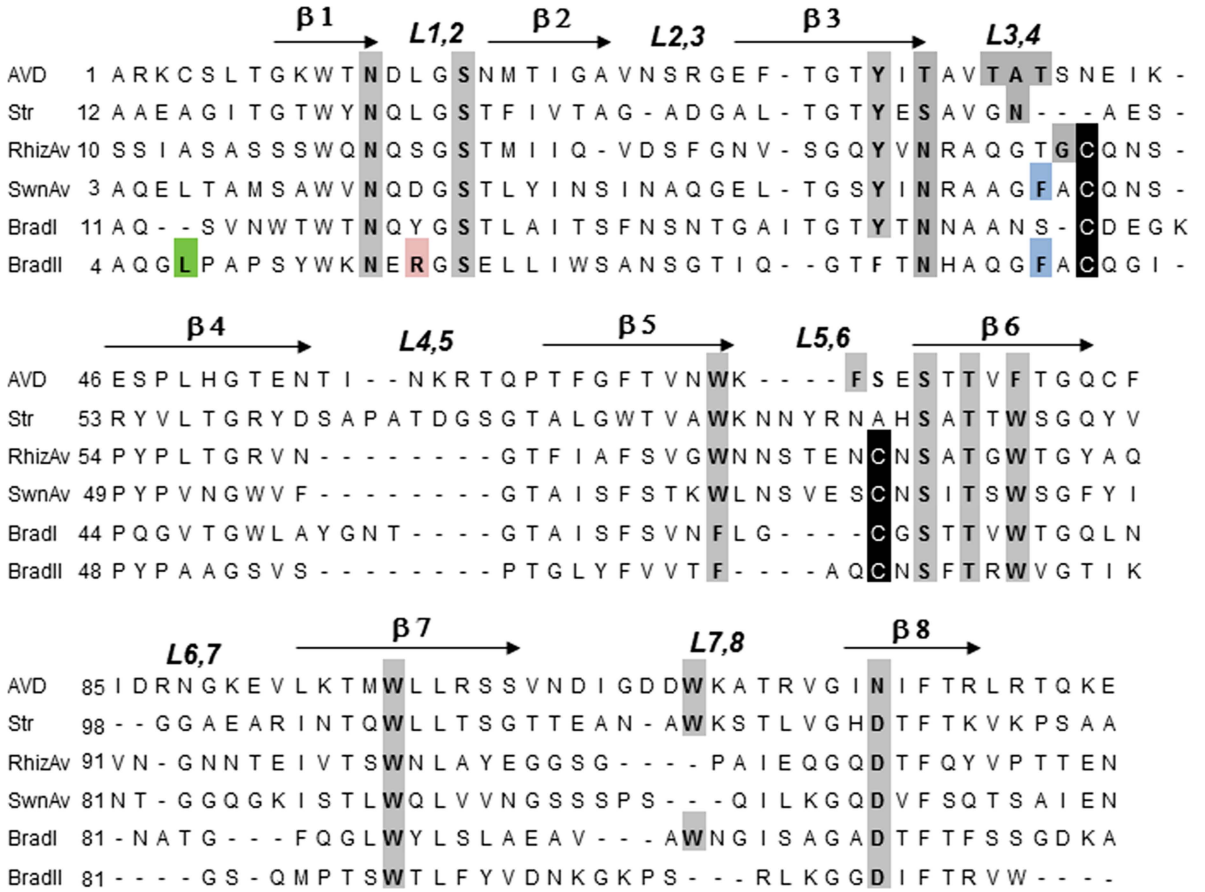

Figure 1. Sequence alignment. The bradavidin II sequence is aligned with the following previously characterized avidins: AVD, chicken avidin; Str, streptavidin from *Streptomyces avidinii*; RhizAv, rhizavidin from *Rhizobium etli*; SwnAv, shwanavidin from *Shewanella denitrificans*; BradI, bradavidin I from *Bradorhizobium japonicum*; BradII, bradavidin II. The residues in close contact with biotin are highlighted in gray and bolded. Cysteine residues corresponding to disulfides close to the biotin-binding site are shaded with black. The Phe residues unique to bradavidin II and shwanavidin are shaded with light blue. The first residue within the resolved 3D structure of bradavidin II is shaded with green. Arg17 appears functionally important as discussed in Figure 2 and is therefore shaded red. The secondary structure elements are shown according to bradavidin II. [Color figure can be viewed in the online issue, which is available at wileyonlinelibrary.com.]

in bradavidin II. Bradavidin II is a relatively short protein consisting of only 115 amino acids [this number includes three N-terminal residues (QTV) from the ompA signal peptide used in protein expression[18]], making it the smallest known member of the avidin family. Some strand-connecting loops are relatively short (Fig. 1), and although in most avidins there is only a single β-turn to connect strands β1 and β2, in bradavidin II there are five β-turns (L1,2, L4,5, L5,6, L6,7, and L7,8) among the seven loops. In addition, L5,6 exhibits a unique short helical segment with Cys-69 in the disulfide bridge to connect with L3,4. The L3,4 loop, which is critical for biotin binding, has the same size as most avidins. In this context, the L3,4 in bradavidin II maintains remarkable sequence and conformational similarity with that of shwanavidin.[6] Like the dimeric avidins, bradavidin II lacks a Trp residue from L7,8, which is critical for the protein's high affinity to biotin and oligomeric integrity in tetrameric avidins,[19,20] also demonstrated earlier by mutagenesis.[13,21] A disulfide bridge connecting Cys-44 and Cys-69 to L3,4 and L5,6, respectively, is available in bradavidin II, rhizavidin,[5] and shwanavidin.[6] In addition, bradavidin II has a phenylalanine in its L3,4 loop (Phe-42) at an identical position to the phenylalanine of shwanavidin, which was shown to compensate for the lack of Trp from L7,8[6] (Fig. 2, see also Fig. 1).

The biotin-binding site

The biotin-binding site in bradavidin II shares many features with other dimeric and tetrameric avidins, which consist of conserved hydrophobic and polar residues (Fig. 1). The L3,4 loop of most avidin apo forms exhibits flexibility or open conformations. Two molecules are available in the asymmetric unit of crystal Form-B, in which L3,4 adopts two distinct conformations [Fig. 3(A)]. The open conformation leaves the biotin-binding site completely exposed to solvent, whereas the binding site in the closed form is completely sealed. The segment in L3,4 loop N-

Table I. *Data Collection and Refinement Statistics*

Bradavidin II	Apo Form-A	Apo Form-B	Biotin complex
ESRF beamline	ID 14-4	ID29	ID23-1
Wavelength (Å)	0.93	0.98	0.97
Space group	C2	P1	C2
Unit cell parameters (Å)	a = 62.1, b = 46.1, c = 47.2, β = 116.7°	a = 34.8, b = 46.1, c = 46.4, α = 106.6°, β = 106.9°, γ = 106.8°	a = 119.1, b = 95.4, c = 49.9, β = 113.6°
Resolution range (Å) (outer resolution shell)	42.17–1.9 (1.93–1.9)	40.66–1.7 (1.73–1.70)	71.8–1.75 (1.78–1.75)
Unique reflections	9133	23,010	51,302
Redundancy	3.1	2.2	3.5
R_{sym} (I)[a]	6.1 (56.0)	8.3 (27.2)	7.1 (75.4)
Completeness	96.4 (87.3)	86.0 (83.6)	99.8 (99.9)
I/σ	22.1 (2.0)	16.0 (2.4)	20.0 (1.76)
Number of protein atoms	829	1662	3420
Number of ligand atoms	—	—	64
Number of solvent atoms	27	135	404
R-factor	0.236	0.211	0.19
R-free[b]	0.272	0.256	0.235
B-factor			
Protein	33.96	26.01	21.7
Biotin	—	—	18.4
Solvent	44.26	37.66	37.6
RMSD			
Bond length	0.014	0.014	0.016
Bond angle	1.71	1.69	1.75
Ramachandran			
Favored	94.2	90.4	89.4
Allowed	5.8	9.6	10.6
Generously allowed	0.0	0.0	0.0
Disallowed	0.0	0.0	0.0

[a] $R_{sym}(I) = \sum |I - < I > | / \sum I$.
[b] Test set consists of 5% for all data.

terminal to the disulfide bridge (residues 38–43) displays different conformations, whereas the remainder of the loop exhibits an almost identical conformation in the resolved structures (Fig. 3). Thus, it can be concluded that L3,4 is flexible in solution and its crystal structures have discrete open and closed loops. The L3,4 loop exhibits a closed conformation in apo Form-A like that of Form-B.

In the biotin complex [Fig. 3(B)], the ligand forms a network of polar interactions with bradavidin II as in all other avidins. The main difference is a lack of conserved Tyr from the β3, which was replaced by Phe-35 in bradavidin II (Fig. 4). Previous studies have shown that this residue contributes to the biotin-binding affinity of chicken avidin[22] and streptavidin,[23] but is not essential for high affinity. The L3,4 loop adopts a closed conformation, as in all four asymmetric unit monomers, and forms two conserved H-bond interactions, one with the biotin ureido nitrogens and one with the carboxylate oxygens (Fig. 4). In addition to polar interactions, biotin resides in a hydrophobic box formed by four aromatic residues including Trp-75, Trp-90, Phe-66, and Phe-42. Moreover, the disulfide bridge also interacts with biotin, which phenomenon is known to be present in rhizavidin and shwanavidin.[5,6] A unique feature that was not observed in prior avidin studies is the presence of Arg-17 in L1,2 and its contribution to the biotin-binding site (Fig. 2). The side chain of Arg-17 extends toward the biotin molecule and forms a polar interaction with Asp-106 (the latter forms an H-bond interaction with biotin, see Fig. 4). In addition, the side chain of Arg-17 also seals the biotin-binding site from the side of the bicyclic ring (Fig. 2).

Bradavidin II shows a relatively high affinity to biotin

Previous studies revealed that bradavidin II tightly binds to biotin and has a dissociation rate constant comparable with those of other avidins, such as rhizavidin[11] and bradavidin,[24] but significantly higher than those measured for avidin and streptavidin.[16] However, the biotin-binding affinity was not quantitatively determined. As in a previous study,[16] we found the direct determination of biotin-binding affinity to be impossible with isothermal titration calorimetry (ITC), because the affinity exceeded the upper limit of the method. Therefore, we used competitive ITC[25] to more precisely determine the affinity by first injecting desthiobiotin into the sample cell, followed by biotin injection. This analysis was performed with a range of competing desthiobiotin

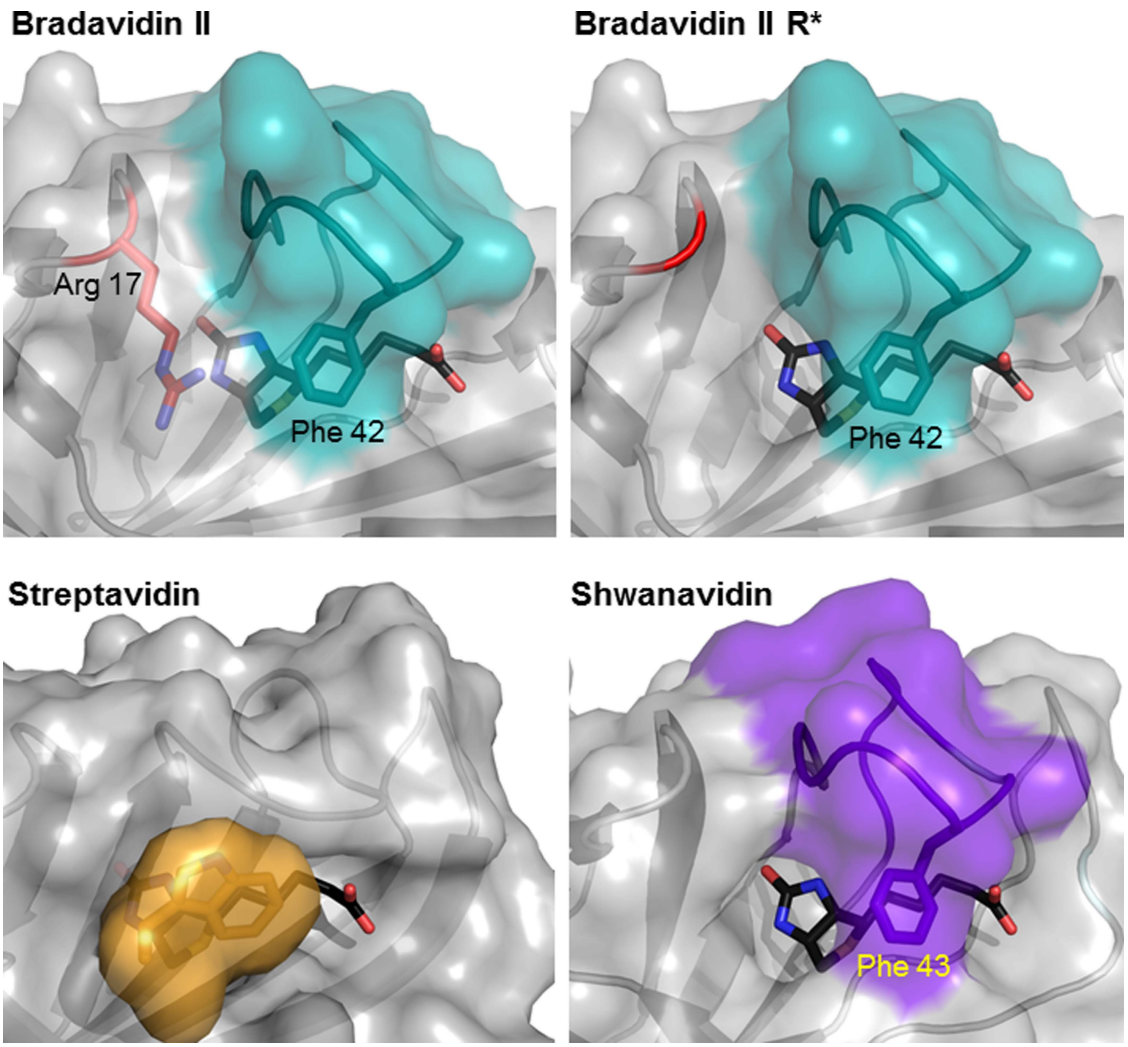

Figure 2. Biotin availability in the binding site. Surface presentation of the biotin-complexed bradavidin II (upper left), bradavidin II ΔR-17 (modeled R*, upper right), streptavidin (bottom, left), and shwanavidin (bottom, right). In streptavidin, the Trp-120 (shown in orange) from an adjacent monomer caps the biotin molecule in its binding pocket, almost completely leaving the carboxylate partially available to solvent. In bradavidin II and shwanavidin, the Trp is not available because of the oligomeric state and is compensated by a Phe (Phe-43 in purple and Phe-42 in dark cyan for shwanavidin and bradavidin II, respectively), thereby sealing biotin in its binding site. In bradavidin II, Arg-17 from the L1,2 β-turn provides an additional element in biotin solvent unavailability. Removing R-17 (*in silico*) now termed ΔR-17 results in a binding site that is more available to solvent, similar to that as in shwanavidin. [Color figure can be viewed in the online issue, which is available at wileyonlinelibrary.com.]

ligand concentrations. The competitive ITC revealed a $K_d = 1.2 \pm 0.2 \times 10^{-7} M$ for the bradavidin II–desthiobiotin complex, and the displacement of 500 μM desthiobiotin by biotin revealed a $K_d = 6.6 \pm 1.5 \times 10^{-11} M$ for the bradavidin II–biotin complex (Table II; Fig. 5). The K_d and ΔH values over the range of desthiobiotin concentrations are shown in Supporting Information Table S1.

Bradavidin II has lower thermal stability relative to other avidins

The thermal stability of bradavidin II was studied by using a differential scanning calorimeter (DSC). Protein samples were analyzed by varying the protein concentration and pH. Unfortunately, the experiments at pH 7 were not successful, most likely because the protein aggregated (see below for further analyses). In contrast, the experiments at pH 3 and pH 5 were more successful, although extended storage at pH 5 led to protein precipitation. Precipitated proteins were observed already after 1 week storage at pH 5 buffer at 4°C with the naked eye. Dimethyl sulfoxide (DMSO) (1%) was found to slower the precipitation. However, precipitated proteins were observed after 2 weeks storage also in the presence of 1% DMSO at pH 5. Partially reversible unfolding was observed at a pH of 3 in the presence of biotin (Fig. 6). The addition of 3× excess molar biotin significantly stabilized the protein, which is an indication of high ligand-binding affinity as well as a characteristic of avidins[1] (Table III). We found no significant differences in the transition midpoints of thermal

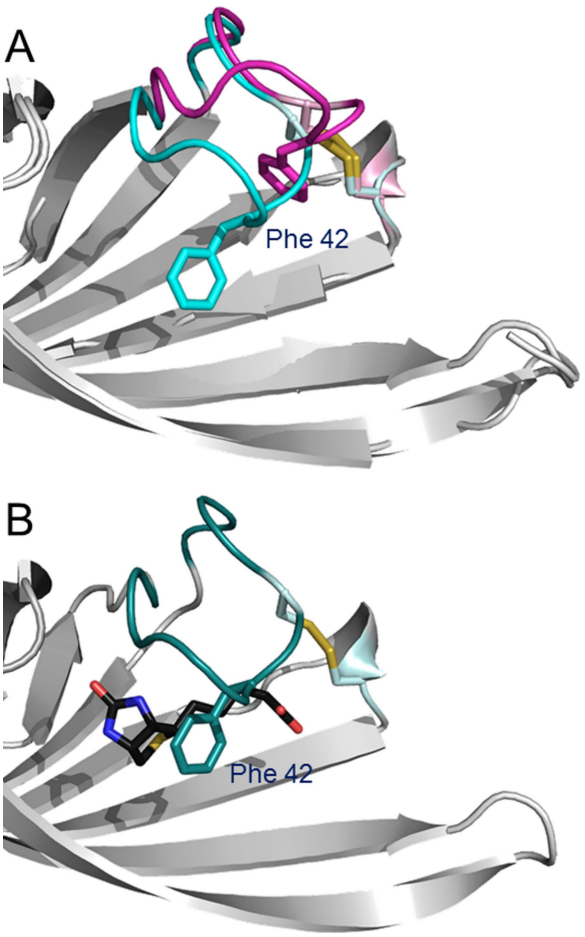

Figure 3. The biotin-binding site of apo (top) and biotin-complexed (bottom) bradavidin II. For the apo bradavidin II the L3,4 loop adopts two distinct conformations as observed in the Form-B crystals. These open (magenta) and closed (cyan) conformations depict the flexibility of the L3,4 loop. The L3,4 loop in the biotin complex form adopts a closed conformation similar to the conformation observed in the apo form. A Phe-42 contributed by the L3,4 forms hydrophobic interactions with biotin, resulting in almost complete ligand unavailability to the solvent. [Color figure can be viewed in the online issue, which is available at wileyonlinelibrary.com.]

denaturation (T_m) along the range of protein concentrations in the absence of the ligand. In contrast, T_m was found to be slightly dependent on the protein concentration in the presence of the ligand (Table III).

The oligomeric state of bradavidin II is dependent on protein concentration and pH

To study the oligomeric state of bradavidin II, the hydrodynamic radii of bradavidin II samples were analyzed by dynamic light scattering (DLS), and molecular weight estimates were calculated with a globular protein standard curve from the DLS instrument manufacturer (Malvern Instruments, Worcestershire, UK). In addition to determining the hydrodynamic radius at a fixed temperature, we also studied the behavior of the protein sample during heating with a temperature range of 20–90°C.

Bradavidin II oligomeric state was found to be concentration dependent. A monomer-oligomer transition was observed at low pH (0.5*M* acetic acid, pH 3) when the protein concentration was varied from 0.2 to 3.8 mg/mL [Fig. 7(C)]. Representative size distribution graphs are shown in Supporting Information Figure S2. At a low concentration (0.4 mg/mL), the protein was mostly monomeric and heat denaturation did not induce protein aggregation (Supporting Information Table S2). Oligomers were detected at a higher protein concentration (1 mg/mL), and protein aggregated at increasing temperatures with a transition temperature at 50°C. However, biotin stabilized the protein and affected its behavior after thermal unfolding; no aggregation was observed at 90°C even at a protein concentration of 1 mg/mL (Supporting Information Table S2). This finding suggests that thermal unfolding leads to aggregation at a lower temperature range, but biotin makes it possible to bypass this range, and thermal denaturation at high temperatures (DSC experiments, Table III) yields soluble denatured molecules that can refold upon cooling with the help of biotin (Fig. 6).

The oligomeric state of bradavidin II was also found to be dependent on pH. Oligomeric species were detected at room temperature and a pH of 5 (50 m*M* sodium phosphate and 100 m*M* NaCl), and when the temperature was increased [Fig. 7(B)]. As expected, the presence of biotin stabilized the

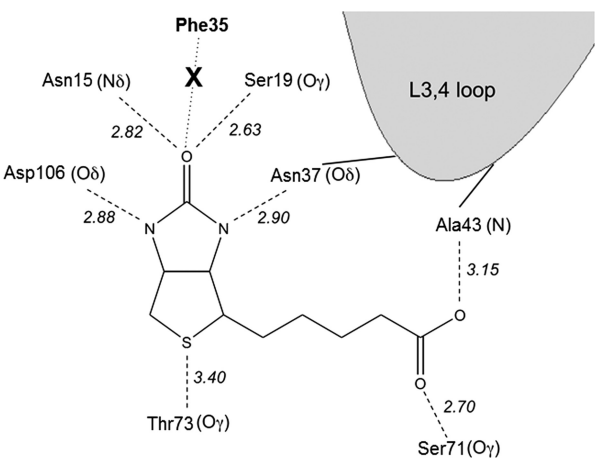

Figure 4. Schematic representation of the hydrogen-bond interactions of bradavidin II with biotin. In principle, biotin forms the canonical network of H-bond interactions as observed in other known avidins. In this context, the biotin carboxylate forms two interactions (one oxygen each) with Ala-43 N and Ser-71 Oγ. The biotin ureido ring exhibits a cardinal difference that was not previously observed. The conserved Tyr residue in all other avidins (from strand β3) is replaced by Phe-35 in bradavidin II, so the conserved avidin H-bond interaction with ureido oxygen is lacking. The remaining interactions with the bicyclic ring system remain identical.

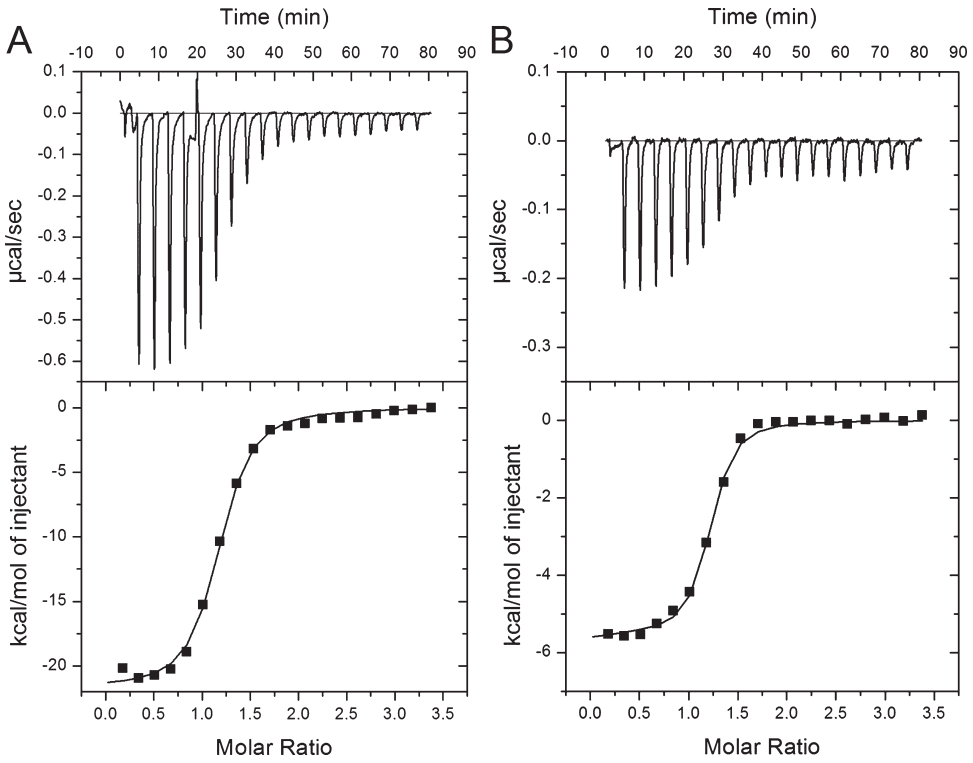

Figure 5. Isothermal titration calorimetry analysis for ligand binding. (A) Bradavidin II was titrated with desthiobiotin, which revealed a moderate affinity with a $K_d = 1.2 \pm 0.2 \times 10^{-7} M$. (B) To determine binding affinity for bradavidin II–biotin complex, biotin was titrated into a sample containing a mixture of desthiobiotin (500 μM) and bradavidin II (5 μM). This analysis revealed a high-affinity interaction of $K_d = 6.6 \pm 1.5 \times 10^{-11} M$. The original data are shown in the upper panels and the integrated heats for each injection in the lower panel are shown together with the fit.

protein, and the onset of aggregation was detected at higher temperatures when compared with samples devoid of biotin (Table III). However, biotin could not prevent temperature-induced protein aggregation at pH 5, as seen at a pH of 3. We observed increased thermal stability of bradavidin when pH was raised from pH 3 to pH 5 (Table III). This is not surprising, because pH 3 could be considered already quite harsh condition. Further increment in pH did not cause further stabilization of the protein. This may be caused by two different reasons: first, bradavidin II appears to form loose oligomers at neutral pH. It is possible that these oligomers accelerate protein unfolding at elevated temperature, thus causing decrease in the thermal stability. Second, it is possible that the protein has optimal thermal stability at mildly acidic pH.

DLS experiments performed at pH 7 (50 mM sodium phosphate and 100 mM NaCl) revealed mostly aggregated species [Fig. 7(A)] with protein concentrations of 0.4 or 1.0 mg/mL, which was not surprising, because the precipitation was visually observable. Therefore, we carried out additional experiments at a pH of 7 with a lower protein concentration (0.25 mg/mL), which also revealed large protein assemblies, the majority of which were dissolved with a slight increase in temperature. Aggregation was observed after heating the sample further, and biotin was found to increase the transition temperature (Supporting Information Table S2) as in the pH 3 and pH 5 treatments. Overall, the poor solubility of bradavidin II at pH 7 makes it challenging to characterize its oligomeric behavior in this condition.

Table II. *Isothermal Titration Calorimetry Analysis for Biotin and Desthiobiotin Binding to Bradavidin II*

Protein	Ligand	$K_a \pm$ SD ($\times 10^9 M^{-1}$)	$K_d \pm$ SD ($\times 10^{-9} M$)	$\Delta H \pm$ SD (kcal/mol)	ΔS (cal/mol/K)
Bradavidin II	Desthiobiotin	0.008 ± 0.001	123.5 ± 14.6	−21.7 ± 0.3	−37.8
Bradavidin II	Biotin	N.D.[a]	N.D.	−26.5 ± 0.4	N.D.
Bradavidin II–desthiobiotin	Biotin (competitive)	15.2 ± 0.4	0.066 ± 0.015	−23.1 ± 0.1	−27.1

The analysis was carried out at a pH of 3 at 40°C.
[a] The binding constant could not be determined because of a high binding affinity exceeding the capability of the instrument.

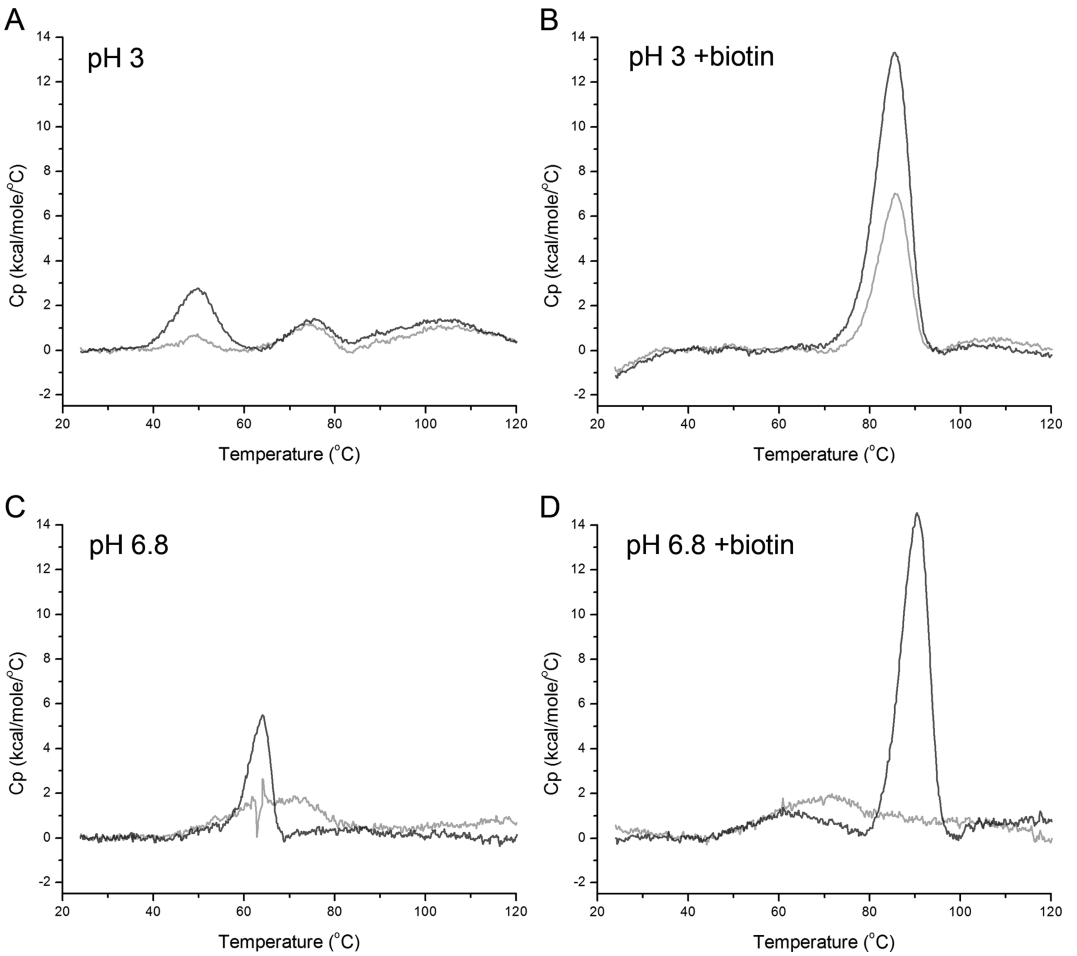

Figure 6. Thermal stability of bradavidin II. Differential scanning calorimetry scans of bradavidin II (0.4 mg/mL) in 0.5*M* acetic acid (pH 3) and in ammonium acetate (pH 6.8) containing 0.1% DMSO. The first heating scan (dark gray line) and rescan (gray line) of bradavidin II are shown both in the absence of biotin (A, C) and in the presence of biotin (B, D).

We also used native MS to characterize the oligomericity of bradavidin II as a function of protein concentration (Fig. 8). Native MS is a powerful tool for studying protein quaternary structure in solution because different oligomeric states are directly separated and quantified. All experiments were performed in 25 m*M* ammonium acetate (pH 6.8), and the protein concentration was varied from 0.25 to 1 mg/mL. Bradavidin II was mainly monomeric at a concentration of 0.25 mg/mL, with a small amount of dimeric protein. At higher concentrations, increasing amounts of higher oligomeric forms (mainly dimers and trimers) were observed. The protein was mostly trimeric at a concentration of 1 mg/mL, but other oligomers (up to a tetramer) were also observed. These results are consistent with the DLS data acquired at pH 3. No protein aggregation was observed in the 25 m*M* ammonium acetate buffer pH 6.8 used for native MS up to the highest concentration (1 mg/mL) as determined by visual inspection. The biotin efficiently complexed with bradavidin II with expected stoichiometries, indicating a high binding affinity. However, biotin did not cause significant changes in oligomeric distribution (data not shown). In accordance with these findings, DLS experiments performed in 25 m*M* ammonium acetate buffer pH 6.8 mainly revealed proteins with hydrodynamic radii of 2.24–2.66 nm (with estimated molecular weights of 22.3–33.3 kDa) within a protein concentration range of 0.2–0.6 mg/mL [see Fig. 7(A) corresponding to 0.4 mg/mL]. No radical changes in the average particle size were observed (hydrodynamic radius 2.38–3.19 nm) after 1 week of storage at +4°C, which indicates that the proteins are more soluble in this buffering system than in sodium phosphate buffer. DSC analysis revealed similar transition midpoint temperatures for thermal unfolding at pHs of 5 and 3, and thermal unfolding was found to be irreversible both in the absence and presence of biotin (Fig. 6).

Bradavidin II oligomeric state was also assessed by using SDS-PAGE method described by Bayer *et al.*[26] Only monomeric forms of bradavidin II were observed in both of the temperatures (20 and 80°C) studied and addition of biotin had no effect on the oligomeric state (Supporting Information Fig. S3).

Table III. *The Unfolding Temperatures (T_m) of Bradavidin II in the Absence and Presence of Threefold Molar Excess of Biotin Analyzed by Differential Scanning Calorimetry*

	T_m (°C)	
Condition used	−Biotin	+Biotin
pH 3, 0.2 mg/mL	50.9 ± 1.4	83.9 ± 0.7
pH 3, 0.4 mg/mL	50.3 ± 1.1	84.6 ± 0.8
pH 3, 0.6 mg/mL	50.3 ± 0.9	85.2 ± 1.3
pH 5, 0.2 mg/mL	66.5	90.4
pH 5, 0.4 mg/mL	66.3	93.2
pH 5, 0.6 mg/mL	66.5	85.7[a]
pH 6.8, 0.2 mg/mL	62.4	88.4
pH 6.8, 0.4 mg/mL	63.3	90.0
pH 6.8, 0.6 mg/mL	63.7	90.9

[a] A weak second peak corresponding to apo form was observed (T_m = 67.2°C), most likely indicating the presence of protein forms not accessible to biotin (aggregates).

Comparative analysis was carried out for chicken avidin variant, which appeared as monomer only when heated to 80°C in the absence of biotin, as expected. Chicken avidin tetramers were not visible in the Coomassie-stained gel, and therefore we silver stained the gel (Supporting Information Fig. S3b). The silver-stained gel further confirmed the absence of any oligomeric species of bradavidin II. Essentially, the same results were obtained without chemical acetylation of bradavidin II, but the sample treated at 20°C in the presence of biotin showed more diffuse band (data not shown), most probably because of high isoelectric point (theoretical pI 9.34).

Discussion

Bradavidin II resembles other avidins in terms of primary structure and shares certain special sequence characteristics with rhizavidin, shwanavidin, and bradavidin (Fig. 1). Therefore, we were interested in structurally characterizing this protein. Although the 3D structure revealed the tetrameric assembly of the asymmetric unit in the presence of biotin, the assembly differs from the tetramers of other avidins and lacks the majority of key subunit interactions conserved in other avidin protein family members, suggesting a monomeric or transient oligomeric structure for bradavidin II. In agreement with this structural hypothesis, biophysical characterization revealed relatively low thermal stability and a highly dynamic oligomeric state, which was found to be strongly dependent on the environment.

Tight biotin–avidin binding has been widely observed, and high ligand-binding affinity is thought to be closely associated with avidin oligomerization. In terms of protein structure, oligomeric assembly not only refers to interactions between ligand and protein subunits but also contributes to the protein function, for example, by shielding the ligand from surrounding water. In practice, a deuterium-hydrogen exchange between chicken avidin and the surrounding solution radically decreases when biotin is bound, indicating global communication between the avidin and its ligand.[27] It has also been observed that ligand binding significantly thermally stabilizes the oligomeric structure of avidin family members.

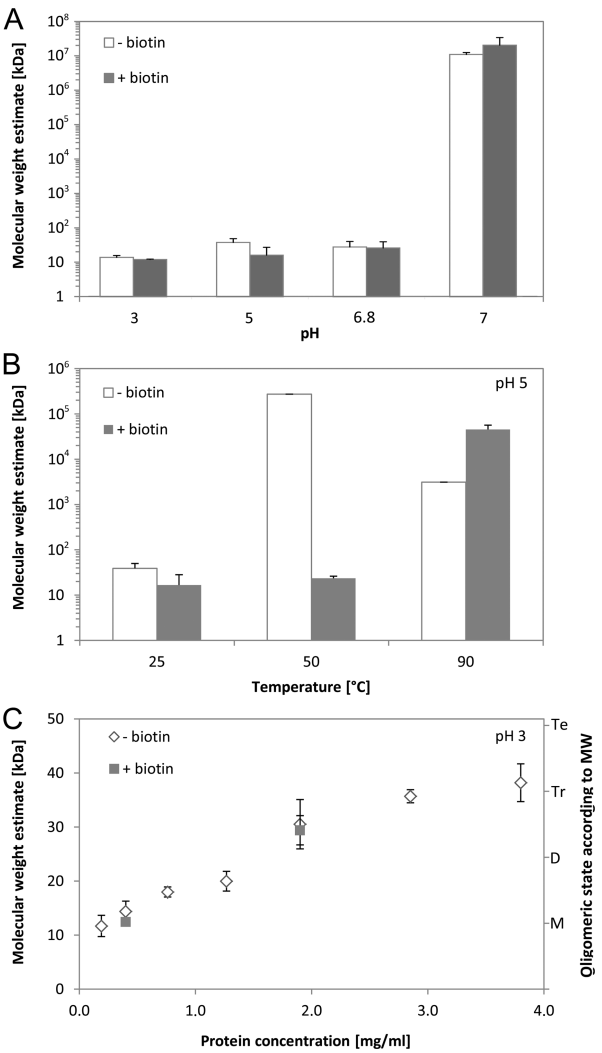

Figure 7. Oligomeric state of bradavidin II under different conditions. The molecular weight estimates of bradavidin II were analyzed by DLS. Bradavidin II was analyzed in the absence (−) and presence (+) of biotin in 0.5*M* acetic acid containing 0.1% DMSO (pH 3), in 50 m*M* sodium phosphate buffer containing 100 m*M* NaCl and 0.1% DMSO (pH 5), in 25 m*M* ammonium acetate containing 0.1% DMSO (pH 6.8), and in 50 m*M* sodium phosphate buffer containing 100 m*M* NaCl (pH 7). (A) The oligomeric state of bradavidin II (0.4 mg/mL) was analyzed at different conditions. (B) The oligomeric state of bradavidin II (0.4 mg/mL) at pH 5 varies at different temperatures. (C) At pH 3, the oligomeric state of bradavidin II increases at increasing protein concentration, both in the absence and presence of biotin. M indicates monomer (12.24 kDa), D indicates dimer (24.48 kDa), Tr indicates trimer (36.72 kDa), and Te indicates tetramer (48.96 kDa).

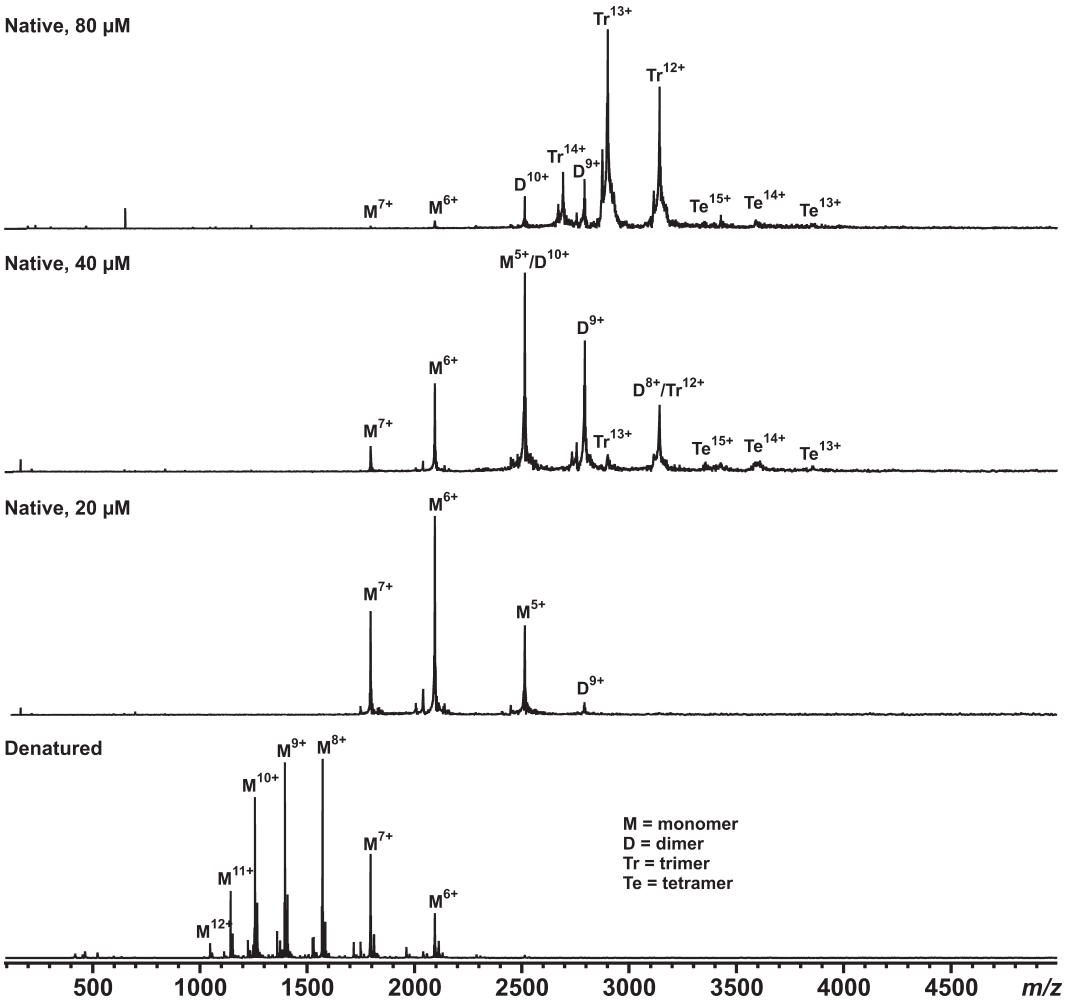

Figure 8. FTICR-MS analysis of bradavidin II. Native MS experiments reveal heterogenic distribution of oligomeric species, the higher order oligomers being more abundant at high protein concentrations. Experiments performed under denaturing conditions show purely a monomeric protein species with a molecular weight of 12569.42 Da, which is close to the expected molecular weight of Bradavidin II of 12569.42 Da (see also Supporting Information Fig. S1). Different peaks were assigned to oligomeric species and labeled in the figure as follows: M = monomer, D = dimer, Tr = Trimer, and Te = tetramer. The charge state of each species is shown.

From this perspective, it is surprising that there are avidins capable of tight biotin binding without canonical oligomericity (tetrameric quaternary assembly). The first examples of these proteins were rhizavidin and shwanavidin, which exhibited dimeric quaternary structures. This bradavidin II study appears be the first discovery of a natural avidin without a clearly defined oligomeric state, and the monomers are therefore functionally independent. We found it challenging to biophysically characterize bradavidin II because of its atypical behavior in several assays. For instance, we were not able to determine the protein's characteristics by gel filtration chromatography, and the poor solubility of the protein at neutral and basic pH in phosphate-based buffers also complicated its analysis.

A primary concern was to find what makes bradavidin II capable of tightly binding with biotin. First, the hydrogen bond network between the protein and its ligand (Fig. 4) was quite well conserved when compared with other avidins (Fig. 1), the only exception being the tyrosine residue in all other avidin loop L3,4s (Tyr-33 in chicken avidin), which is replaced by phenylalanine in bradavidin II. Second, the protein has a disulfide bridge, judged by MS and X-ray analyses, to stabilize the L3,4, which is a highly mobile loop in several other avidins. Disulfide apparently decreases mobility, and therefore makes it possible to more efficiently shield the bound ligand. Interestingly, rhizavidin, shwanavidin, and bradavidin I share this structural moiety with bradavidin II (Fig. 1). Third, bradavidin II appears to have a unique mechanism to compensate for the absence of the well-conserved Trp residue, which contributes to the biotin binding from the adjacent subunit in chicken avidin (Trp-110), streptavidin (Trp-120), and in other tetrameric avidins. In addition to phenylalanine 42, which is also found in

shwanavidin,[6] bradavidin II contains arginine 17, which helps to bury biotin in the surrounding solvent.

Ligand-binding analysis by ITC revealed exothermic binding both in the case of biotin and desthiobiotin. Both analyses had an entropic contribution against binding, but the effect was more pronounced in the case of desthiobiotin (Table II). This finding could be explained by the less rigid structure of desthiobiotin in solution relative to biotin, although both of them were virtually immobile when bound to protein. When compared with chicken avidin's extremely tight binding to biotin (K_d = 10^{-15}–$10^{-16}M$),[28,29] the biotin-binding affinity of bradavidin II decreased by more than 1000-fold. Previous studies indicated that the dissociation rate constant measured by displacing radioactive biotin associated with bradavidin II is significantly higher than that of chicken avidin.[16] Thus, it is clear that a more rapid dissociation rate provides an explanation for the decrease in bradavidin II biotin-binding affinity relative to avidin and streptavidin. An earlier study revealed binding affinities of $1 \times 10^{-12}M$ and $5 \times 10^{-13}M$ for avidin–desthiobiotin interaction at pHs of 4 and 7, respectively.[28] Therefore, the ligand-binding affinity decrease of bradavidin II in desthiobiotin relative to avidin (~100,000-fold) appears to be larger than that of biotin.

The oligomeric state of bradavidin II was found to be highly dependent on solution conditions (pH, temperature, and ionic composition). When exposed to neutral pH in sodium phosphate buffer, the protein started to form large complexes and precipitated (Fig. 7). When the pH was decreased to 5, the protein stayed in solution, but it aggregated during extended storage. Bradavidin II showed good solubility at a pH of 3. DLS experiments performed at pH 3 (0.5M acetic acid) indicated that the protein hydrodynamic radius increased with increasing protein concentrations, suggesting concentration-dependent oligomerization (Fig. 7). Native MS experiments performed in 25 mM ammonium acetate (pH 6.9) indicated increasing amounts of protein dimers, trimers, and tetramers in solution with an increasing protein concentration (Fig. 8). These findings are in agreement with the crystal structures, which indicated loose protein packing into tetrameric assemblies and ultimately did not resemble canonical avidin

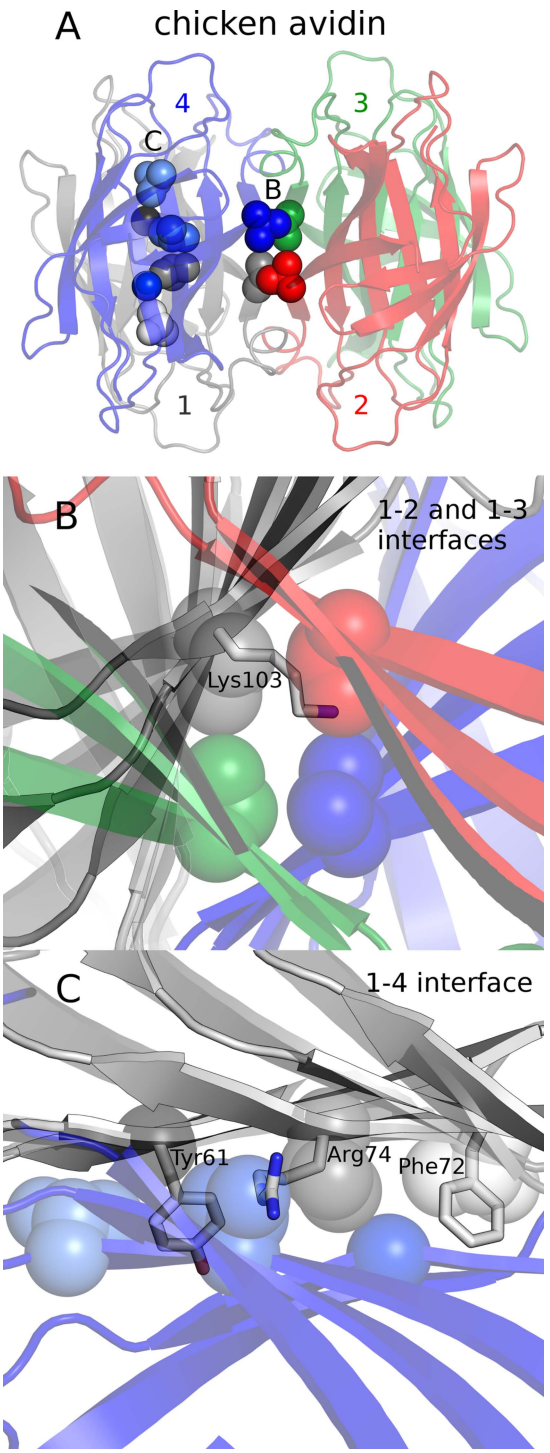

Figure 9.

Figure 9. Structural comparison of bradavidin II to chicken avidin. (A) Cartoon presentation of chicken avidin tetramer PDB 1VYO[33] with certain key residues in its 1-2/1-3 and 1-4 interfaces highlighted as VdW spheres. (B) Comparison of bradavidin II to avidin 1-2/1-3 interface. Bradavidin II structure superimposed with one of the subunits of avidin (gray subunit 1). Avidin Val115 residues are shown as spheres, and bradavidin II Lys103 as sticks. This analysis highlights the incompetence of bradavidin II to maintain the canonical 1-2/1-3 subunit interface structure seen in chicken avidin. (C) Comparison to avidin 1-4 interface. Bradavidin II residues Phe72, Tyr61, and Arg74 are shown in stick representation and labeled. Three hydrophobic avidin residues from two different subunits are shown as follows: white, Thr76 from subunit 1; light gray, Gly65 from subunit 1; gray, Val78 from subunit 1; light blue, Thr76 from subunit 4; blue, Gly65 from subunit 4; and dark blue, Val78 from subunit 4. Again, bradavidin II appears not to have conserved residues at these positions. [Color figure can be viewed in the online issue, which is available at wileyonlinelibrary.com.]

tetramers. The absence of oligomers was also judged by SDS-PAGE-based method (Supporting Information Fig. S3). The behavior of bradavidin is unique within avidin family, but other proteins have shown examples of concentration- and pH-dependent oligomerization. Arylsulfatase has been shown to form dimers in neutral and basic conditions but converts to octameric state in the mildly acidic environment.[30] Similar to bradavidin 2, this protein was found challenging to study using size-exclusion chromatography. LptA is a periplasmic lipopolysaccharide transport protein from *Escherichia coli*. This protein was studied using SEC-LS method, which indicated concentration-dependent oligomerization in a concentration range of 0–80 μM studied.[31] Unfortunately, we have not found explanation for the discrepancy between the gel filtration analysis results obtained by Helppolainen *et al*. and those observed in this study. It is possible that the 58.4-kDa form observed by Helppolainen *et al*. is somehow associated with the leaky stop codon.

We found the thermal unfolding characteristics of bradavidin II to be atypical among the avidins. To our knowledge, all avidins characterized so far experience irreversible thermal unfolding. Bradavidin II instead demonstrated a largely reversible thermal unfolding at a pH of 3 in the presence of biotin (Fig. 6). We believe that this phenomenon is associated with the oligomerization properties of bradavidin II. Protein refolding is a much simpler reaction if the protein has no oligomeric structure or only weak interactions between subunits. Successful oligomeric protein refolding might require assistance in shielding the hydrophobic protein–protein interfaces to cause rapid aggregation, whereas monomers can unfold and refold independently. SDS has been known to prevent streptavidin aggregation after thermal unfolding,[32] which supports this model.

Another important question is why bradavidin II does not form tetramers or dimers such as those of other avidin family members. We used the previously determined X-ray structure of chicken avidin (1VYO)[33] and positioned the bradavidin II structure by using avidin as a template (Fig. 9). A clear sign of a potentially important obstacle relative to the canonical avidin assembly was noted in the residue corresponding to Val115 in chicken avidin [Fig. 9(A,B)]. This residue forms extensive hydrophobic contacts in the center of the avidin tetramer and the corresponding residue in bradavidin II is a lysine 103, which is clearly incompatible with the role of valine. A lysine residue was also found at this position in shwanavidin, which is reportedly a dimer.[6] Finally, rhizavidin, which is also a dimeric avidin-like protein, has a glutamine at this site (Ref. [11], see also Fig. 1). Moreover, a closer look into the 1-4 dimer interface [Fig. 9(A,C)] explains why bradavidin II does not form a stable dimer, unlike rhizavidin and shwanavidin. Hydrophobic contacts are formed by a row of tiny residues of Thr76, Gly65, and Val78 in the chicken avidin 1-4 dimer. In bradavidin II, these residues are replaced by Phe72, Tyr61, and Arg74, which would cause clashes in an avidin-like pairing between subunits.

In conclusion, bradavidin II has an atypical 3D structure for a member of the avidin protein family, with no clear signs of oligomeric assembly into a well-defined quaternary structure. This finding was supported by biophysical analyses, which showed oligomeric state variations to be dependent on the protein concentration and solution conditions. DSC data showed that the protein has quite efficient refolding capacity after heat-induced unfolding at low pH. Although the ligand-binding affinity determined for bradavidin II ($K_d = 6.6 \pm 1.5 \times 10^{-11} M$) was not as high as in well-known streptavidin and chicken avidin, bradavidin II can be characterized as an avidin family member. The structural properties of bradavidin II may assist protein engineers in creating modified biotin-binding proteins with characteristics suitable for life science applications. Because of its weak oligomerization tendency, bradavidin II could be a better candidate for developing fusion partners for large proteins than chicken avidin or streptavidin.

Materials and Methods

Protein production and purification

Bradavidin II was expressed with a pET101/D expression plasmid. The original signal peptide of the protein was replaced with an ompA secretion signal as described in previous works.[16,18] A second stop codon was added by standard molecular biology methods to the expression construct used in the previous study[16] to ensure an end product of the correct size. Bradavidin II protein was produced in *E. coli* BL21-AI cells in a 7.5-L fermentor (Labfors Infors 3, Infors AG, Bottmingen, Switzerland) using the fed-batch mode as previously described,[17] and the resulting cell mass was collected by centrifugation and lysed with a homogenizator (Avestin Emulsiflex-C3, Avestin, Ottawa, ON, Canada). The lysate was clarified by centrifugation and subjected to 2-iminobiotin affinity chromatography (Affiland, Liége, Belgium). Protein was eluted with 0.5M acetic acid and verified as pure and homogenous by SDS-PAGE and MS.

Bradavidin II crystallization, data collection, and structure solution

Apo bradavidin II crystals were obtained by microbatch method at 20°C. A 1-μL drop contained equal amounts of 3.9 mg/mL protein in 0.5M acetic acid (pH 3) mixed with 30% PEG 4000, 0.2M $MgCl_2$, and 0.1M Tris-HCl (pH 8.5). Cube-shaped crystals appeared within a week and reached a final size of 0.05 mm within 2 weeks. A different batch with rod-

shaped crystals was obtained by combining 3.4 mg/mL protein with 0.12*M* magnesium formate. Diffraction parameters were improved later by the addition of 0.1*M* NaBr. A bradavidin II–biotin complex was obtained by incubating the protein with 5 μL of saturated *d*-biotin solution (1.5 mg biotin in 1 mL of 0.5*M* acetic acid) for 0.5 h at 4°C. Crystals from this complex were obtained by microbatch method at 20°C. A 1-μL drop contained equal amounts of 3.9 mg/mL protein–biotin complex in 0.5*M* acetic acid (pH 3) mixed with 10% PEG 20K, 2% 1,4 dioxane, and 0.1*M* bicine (pH 9). Hexagon-shaped crystals appeared within 1 month. Another crystallization condition was applied by mixing the bradavidin II–biotin complex in a reservoir containing 20% PEG 3350 and 0.1*M* sodium citrate (pH 3.5). Crystals appeared within 5 days and reached their final sizes within 14 days. Before freezing, apo crystal forms were briefly suspended in a cryoprotectant solution containing 25% glycerol and crystallization solution. Biotin complex crystals were suspended in crystallization solution containing 25% ethylene glycol.

Crystallographic data for apo bradavidin II Form-A were collected at the European Synchrotron Radiation Facility (ESRF), Grenoble, France at beamline ID14-4. The data were collected from a single crystal at 100 K using an Oxford Cryosystem Cryostream cooling device (as were all data described below) on an ADSC Q315 CCD detector. The crystal belonged to monoclinic space group C2 with cell parameters a = 62.1 Å, b = 46.01 Å, c = 47.2 Å, and β = 116.7 (Table I). All data were indexed, integrated, and scaled using the HKL2000 suite.[34]

The Form-A structure was solved by molecular replacement using PHASER[35,36] and implemented in the CCP4 suite. Search models included the monomer from a Swiss-Model[37,38] bradavidin II homology model derived from the structure of rhizavidin (PDB code 3EW1 with 47% sequence similarity).[5] Matthew's coefficient indicated the presence of one bradavidin II molecule in the asymmetric unit (V_M = 2.32 Å^3/Da, 47% solvent content). The resulting PHASER solution at a resolution range of 40.0–3.5 Å gave a monomer in the asymmetric unit. The structure was initially refined using the rigid body protocol in REFMAC,[39] resulting in an R-value of 48.7% and R-free of 49.6%. The structure was further refined with REFMAC5 via the restrained refinement mode at a resolution range of 42.17–1.9 Å, and solvent molecules were added with ARP/wARP.[40] After several iterative cycles of refinement and model building with Coot,[41] the R-value and R-free reached final values of 23.6 and 27.2%, respectively (Table I). The final model contained 827 protein atoms and 27 solvent molecules (Table I).

Additional data were collected for the apo bradavidin II displaying different symmetry (designated at Form-B) at the ESRF ID-29 beamline on a PILATUS 6M pixel detector at 100 K. Crystals from the triclinic P1 space group with cell parameters a = 34.77 Å, b = 46.12 Å, c = 46.45 Å, α = 106.59°, β = 106.92°, and γ = 106.82° exhibited somewhat better resolution (1.7 Å) than the Form-A (Table I). The structure of the Form-B triclinic bradavidin II was solved by PHASER using the bradavidin II refined Form-A monomer as the search model at a resolution range of 40–3.5 Å. The solution indicated the presence of two bradavidin II monomers in the asymmetric unit with a V_M value of 2.83 Å^3/Da and 56.6% solvent. The structure was initially refined in a similar protocol for the Form-A apo bradavidin II. The rigid body refinement resulted in an R-value of 31.9% and R-free of 33.6% at a resolution range of 40–3.5 Å. The structure was further refined at a resolution range of 40–1.7 Å, resulting in a final R-value of 21.1% and R-free of 25.5% after the addition of water molecules using ARP/wARP. The final model contained 1662 protein atoms and 135 solvent molecules (Table I).

Crystallographic data for the bradavidin II–biotin complex data were collected at ESRF ID-29 on an ADSC Q315 CCD detector. The crystals belonged to monoclinic space group C2 with cell parameters a = 119.01 Å, b = 95.43 Å, c = 49.95 Å, and β = 113.6° (Table I). The structure of the biotin complex was solved by PHASER (50–4 Å) using the bradavidin II refined monomer as the search model. The solution indicated the presence of four bradavidin II monomers in an asymmetric unit (V_M = 2.96 Å^3/Da, 58.4% solvent). The structure was further refined at a resolution range of 71.8–1.75 Å, resulting in a final R-value of 19.2% and R-free of 23.7% (Table I). Electron density maps clearly indicated the presence of biotin molecules in the corresponding binding sites, which were fitted with Coot.[41] The final model contained 3429 protein atoms, 404 solvent atoms, and 64 biotin atoms (Table I). The structures were deposited in the RCSB-PDB database with the following access codes: Bradavidin II apo Form-A, 4GGR; Bradavidin II apo Form-B, 4GGT; and Bradavidin II biotin-complex, 4GGZ.

Biophysical characterization

A MicroCal VP-Capillary DSC (GE Healthcare Life Sciences, Microcal, Northampton, MA) was used to determine the unfolding temperature (T_m) of bradavidin II. Samples were analyzed in 0.5*M* acetic acid (pH 3) and in 50 m*M* sodium phosphate buffer containing 100 m*M* NaCl (pH 5). It was not possible to perform the analysis in 50 m*M* sodium phosphate buffer containing 100 m*M* NaCl (pH 7) because of sample aggregation difficulties. However, we were able to perform DSC analysis using a 25 m*M* ammonium acetate buffer at pH 6.8. The measurements were conducted in the absence and presence of biotin using a 3:1 molar ratio of biotin per bradavidin II subunit. A scanning rate of 2°C/min was used

and the experiment was performed by running a temperature scan from 20 to 130°C. A small amount of DMSO (0.1%) was included to make the biotin soluble at a low pH. The data were analyzed using Microcal Origin 7.0 software.

The protein hydrodynamic radius was determined by DLS with a Zetasizer Nano ZS (Malvern Instruments, Worcestershire, UK). Six parallel measurements were carried out for each sample (100 μL) at 25°C. The molecular weight of the protein was estimated from the hydrodynamic radius using a globular protein standard curve from the manufacturer. A molecular weight of 12.24 kDa was used as the M_w of the monomer for determining the protein oligomeric state.

All mass spectrometric experiments were performed with a 12-T APEX-Qe FT-ICR instrument (Bruker Daltonics, Billerica, MA) equipped with an Apollo-II electrospray ion source. All protein samples were buffer-exchanged with 10 m*M* ammonium acetate (pH 6.8) before analysis. The samples were further diluted with acetonitrile/water/acetic acid (49.5:49.5:1.0, v/v) for denaturing MS or 25 m*M* ammonium acetate (pH 6.9) for native MS experiments. All ion source parameters (temperature and voltage settings) were optimized to maintain weak protein–protein interactions and all other instrument parameters were adjusted to maximize ion transmission at m/z 1500–4000. The instrument was operated and the data were processed and analyzed with Bruker XMASS 7.0.8 software. To calculate the neutral (most abundant isotopic or average) masses for each oligomeric protein form, mass spectra were charge-deconvoluted with a dedicated Tcl script.

A DLS thermal scanning experiment was performed by gradually increasing the sample temperature with a Peltier element embedded within the Zetasizer Nano ZS instrument. These experiments were carried out in a quartz cuvette (Hellma 104-QS, Hellma GmbH & Co. KG, Müllheim, Germany) in 300-μL samples. The temperature was raised from 20 to 90°C in 5°C steps, and the sample was incubated for 5 min at each temperature before measurement. The resulting data were analyzed by plotting the molecular weight estimate and deriving the count rate over the temperature.

ITC was performed with a Microcal VP-ITC (GE Healthcare, Life Sciences, Microcal, Northampton, MA). The measurements were completed in 0.5*M* acetic acid (pH 3) at 40°C. Samples were degassed before analysis by stirring for 5 min at 39.5°C in a MicroCal ThermoVac. First, 5 μ*M* bradavidin II was titrated with 15-μL aliquots of 75 μ*M* desthiobiotin solution, and the result was analyzed by using the "one sites of binding" method in Microcal Origin 7.0. A competitive ITC was performed for a mixture of 5 μ*M* bradavidin II in the presence of excess desthiobiotin (15, 75, 150, 200, 300, and 500 μ*M*) and 75 μ*M* biotin was injected in 15-μL aliquots into the mixture of bradavidin II and desthiobiotin. The resulting data were analyzed using the "competitive binding" method included in the data analysis software package provided by the manufacturer. This method, displacement ITC, is based on the protocol described by Sigurskjold and it allows to determine the binding isotherm of a ligand that is competitively inhibited in its binding to a protein with identical and independent binding sites. The injection reaction heats were integrated using Microcal Origin 7.0 and nonlinear least-squares fitting was used to obtain K_a, ΔH, and n.[25]

The oligomeric state of bradavidin II and chicken avidin variant with lowered isoelectric point (Niederhauser *et al*., unpublished) was studied by using thermal treatment in the presence of SDS, but in the absence of reducing agent using the method described earlier.[26] Before analysis, the proteins were chemically acetylated to decrease their isoelectric point using sulfo-NHS acetate (Pierce). The protein samples were treated for 20 min in SDS in the presence or absence of biotin. Then, the oligomeric state was analyzed using SDS-PAGE stained using Coomassie blue or with silver. PageRuler Plus Prestained Protein Ladder (Thermo Scientific) was used as molecular weight standard.

Acknowledgment

The authors thank Ulla Kiiskinen, Soili Lehtonen, and Ritva Romppanen for their support with the experiments.

References

1. Laitinen OH, Hytönen VP, Nordlund HR, Kulomaa MS (2006) Genetically engineered avidins and streptavidins. Cell Mol Life Sci 63:2992–3017.
2. Laitinen OH, Nordlund HR, Hytönen VP, Kulomaa MS (2007) Brave new (strept)avidins in biotechnology. Trends Biotechnol 25:269–277.
3. Green NM (1990) Avidin and streptavidin. Methods Enzymol 184:51–67.
4. Leppiniemi J, Grönroos T, Määttä JA, Johnson MS, Kulomaa MS, Hytönen VP, Airenne TT (2012) Structure of bradavidin-C-terminal residues act as intrinsic ligands. PLoS One 7:e35962.
5. Meir A, Helppolainen SH, Podoly E, Nordlund HR, Hytönen VP, Määttä JA, Wilchek M, Bayer EA, Kulomaa MS, Livnah O (2009) Crystal structure of rhizavidin: insights into the enigmatic high-affinity interaction of an innate biotin-binding protein dimer. J Mol Biol 386:379–390.
6. Meir A, Bayer EA, Livnah O (2012) Structural adaptation of a thermostable biotin-binding protein in a psychrophilic environment. J Biol Chem 287:17951–17962.
7. Määttä J, Helppolainen S, Hytönen V, Johnson M, Kulomaa M, Airenne T, Nordlund H (2009) Structural and functional characteristics of xenavidin, the first frog avidin from *Xenopus tropicalis*. BMC Struct Biol 9:63.
8. Takakura Y, Tsunashima M, Suzuki J, Usami S, Kakuta Y, Okino N, Ito M, Yamamoto T (2009) Tamavidins—novel avidin-like biotin-binding proteins from the Tamogitake mushroom. FEBS J 276:1383–1397.

9. Hytönen VP, Määttä JA, Kidron H, Halling KK, Hörhä J, Kulomaa T, Nyholm TK, Johnson MS, Salminen TA, Kulomaa MS, Airenne TT (2005) Avidin related protein 2 shows unique structural and functional features among the avidin protein family. BMC Biotechnol 5:28.
10. Eisenberg-Domovich Y, Hytönen VP, Wilchek M, Bayer EA, Kulomaa MS, Livnah O (2005) High-resolution crystal structure of an avidin-related protein: insight into high-affinity biotin binding and protein stability. Acta Crystallogr D Biol Crystallogr 61:528–538.
11. Helppolainen SH, Nurminen KP, Määttä JA, Halling KK, Slotte JP, Huhtala T, Liimatainen T, Ylä-Herttuala S, Airenne KJ, Närvänen A (2007) Rhizavidin from *Rhizobium etli*: the first natural dimer in the avidin protein family. Biochem J 405:397–405.
12. Jones ML, Kurzban GP (1995) Noncooperativity of biotin binding to tetrameric streptavidin. Biochemistry (NY) 34:11750–11756.
13. Laitinen OH, Nordlund HR, Hytönen VP, Uotila ST, Marttila AT, Savolainen J, Airenne KJ, Livnah O, Bayer EA, Wilchek M, Kulomaa MS (2003) Rational design of an active avidin monomer. J Biol Chem 278: 4010–4014.
14. Lim KH, Huang H, Pralle A, Park S (2011) Engineered streptavidin monomer and dimer with improved stability and function. Biochemistry 50:8682–8691.
15. Lim KH, Huang H, Pralle A, Park S (2013) Stable, high-affinity streptavidin monomer for protein labeling and monovalent biotin detection. Biotechnol Bioeng 110:57–67.
16. Helppolainen SH, Määttä JA, Halling KK, Slotte JP, Hytönen VP, Jänis J, Vainiotalo P, Kulomaa MS, Nordlund HR (2008) Bradavidin II from *Bradyrhizobium japonicum*: a new avidin-like biotin-binding protein. Biochim Biophys Acta 1784:1002–1010.
17. Määttä JA, Eisenberg-Domovich Y, Nordlund HR, Hayouka R, Kulomaa MS, Livnah O, Hytönen VP (2011) Chimeric avidin shows stability against harsh chemical conditions—biochemical analysis and 3D structure. Biotechnol Bioeng 108:481–490.
18. Hytönen VP, Laitinen OH, Airenne TT, Kidron H, Meltola NJ, Porkka E, Hörhä J, Paldanius T, Määttä JA, Nordlund HR (2004) Efficient production of active chicken avidin using a bacterial signal peptide in *Escherichia coli*. Biochem J 384:385–390.
19. Livnah O, Bayer EA, Wilchek M, Sussman JL (1993) Three-dimensional structures of avidin and the avidin-biotin complex. Proc Natl Acad Sci USA 90:5076–5080.
20. Freitag S, Le Trong I, Chilkoti A, Klumb LA, Stayton PS, Stenkamp RE (1998) Structural studies of binding site tryptophan mutants in the high-affinity streptavidin-biotin complex. J Mol Biol 279:211–221.
21. Sano T, Cantor CR (1995) Intersubunit contacts made by tryptophan 120 with biotin are essential for both strong biotin binding and biotin-induced tighter subunit association of streptavidin. Proc Natl Acad Sci USA 92:3180–3184.
22. Marttila AT, Hytönen VP, Laitinen OH, Bayer EA, Wilchek M, Kulomaa MS (2003) Mutation of the important Tyr-33 residue of chicken avidin: functional and structural consequences. Biochem J 369:249–254.
23. Hyre DE, Le Trong I, Freitag S, Stenkamp RE, Stayton PS (2000) Ser45 plays an important role in managing both the equilibrium and transition state energetics of the streptavidin-biotin system. Protein Sci 9:878–885.
24. Nordlund HR, Hytönen VP, Laitinen OH, Kulomaa MS (2005) Novel avidin-like protein from a root nodule symbiotic bacterium, *Bradyrhizobium japonicum*. J Biol Chem 280:13250–13255.
25. Sigurskjold BW (2000) Exact analysis of competition ligand binding by displacement isothermal titration calorimetry. Anal Biochem 277:260–266.
26. Bayer EA, Ehrlich-Rogozinski S, Wilchek M (1996) Sodium dodecyl sulfate-polyacrylamide gel electrophoretic method for assessing the quaternary state and comparative thermostability of avidin and streptavidin. Electrophoresis 17:1319–1324.
27. Celej MS, Montich GG, Fidelio GD (2004) Conformational flexibility of avidin: the influence of biotin binding. Biochem Biophys Res Commun 325:922–927.
28. Green NM (1975) Avidin. Adv Protein Chem 29:85–133.
29. Hytönen VP, Nyholm TK, Pentikäinen OT, Vaarno J, Porkka EJ, Nordlund HR, Johnson MS, Slotte JP, Laitinen OH, Kulomaa MS (2004) Chicken avidin-related protein 4/5 shows superior thermal stability when compared with avidin while retaining high affinity to biotin. J Biol Chem 279:9337–9343.
30. Abzalimov RR, Bobst CE, Salinas PA, Savickas P, Thomas JJ, Kaltashov IA (2013) Studies of pH-dependent self-association of a recombinant form of arylsulfatase A with electrospray ionization mass spectrometry and size-exclusion chromatography. Anal Chem 85:1591–1596.
31. Merten JA, Schultz KM, Klug CS (2012) Concentration-dependent oligomerization and oligomeric arrangement of LptA. Protein Sci 21:211–218.
32. Waner MJ, Navrotskaya I, Bain A, Oldham ED, Mascotti DP (2004) Thermal and sodium dodecylsulfate induced transitions of streptavidin. Biophys J 87:2701–2713.
33. Repo S, Paldanius TA, Hytönen VP, Nyholm TK, Halling KK, Huuskonen J, Pentikäinen OT, Rissanen K, Slotte JP, Airenne TT (2006) Binding properties of HABA-type azo derivatives to avidin and avidin-related protein 4. Chem Biol 13:1029–1039.
34. Otwinowski Z, Minor W (1997) Processing of X-ray diffraction data collected in oscillation mode. Methods Enzymol 276:307–326.
35. McCoy AJ, Grosse-Kunstleve RW, Adams PD, Winn MD, Storoni LC, Read RJ (2007) Phaser crystallographic software. J Appl Cryst 40:658–674.
36. Zwart PH, Afonine PV, Grosse-Kunstleve RW, Hung LW, Ioerger TR, McCoy AJ, McKee E, Moriarty NW, Read RJ, Sacchettini JC, Sauter NK, Storoni LC, Terwilliger TC, Adams PD (2008) Automated structure solution with the PHENIX suite. Methods Mol Biol 426:419–435.
37. Arnold K, Bordoli L, Kopp J, Schwede T (2006) The SWISS-MODEL workspace: a web-based environment for protein structure homology modelling. Bioinformatics 22:195–201.
38. Kiefer F, Arnold K, Kunzli M, Bordoli L, Schwede T (2009) The SWISS-MODEL Repository and associated resources. Nucleic Acids Res 37:D387–D392.
39. Vagin AA, Steiner RA, Lebedev AA, Potterton L, McNicholas S, Long F, Murshudov GN (2004) REFMAC5 dictionary: organization of prior chemical knowledge and guidelines for its use. Acta Crystallogr D Biol Crystallogr 60:2184–2195.
40. Morris RJ, Perrakis A, Lamzin VS (2003) ARP/wARP and automatic interpretation of protein electron density maps. Methods Enzymol 374:229–244.
41. Emsley P, Cowtan K (2004) Coot: model-building tools for molecular graphics. Acta Crystallogr D Biol Crystallogr 60:2126–2132.

ELECTRONIC SUPPLEMENTARY MATERIAL

The highly dynamic oligomeric structure of bradavidin II is unique among avidin proteins

Jenni Leppiniemi[1,2], Amit Meir[3], Niklas Kähkönen[1,2], Sampo Kukkurainen[1,2], Juha A. Määttä[1,2], Markus Ojanen[1,2], Janne Jänis[4], Markku S. Kulomaa[1,2], Oded Livnah[3] and Vesa P. Hytönen[1,2,5,*]

[1] Institute of Biomedical Technology, FI-33014 University of Tampere and Tampere University Hospital, Finland

[2] BioMediTech, Tampere, Finland

[3] Hebrew University of Jerusalem, The Alexander Silberman Institute of Life Sciences and The Wolfson Centre for Applied Structural Biology, The Hebrew University of Jerusalem, Jerusalem 91904, Israel

[4] Department of Chemistry, University of Eastern Finland, FI-80101 Joensuu, Finland

[5] Fimlab laboratories, Tampere, Finland

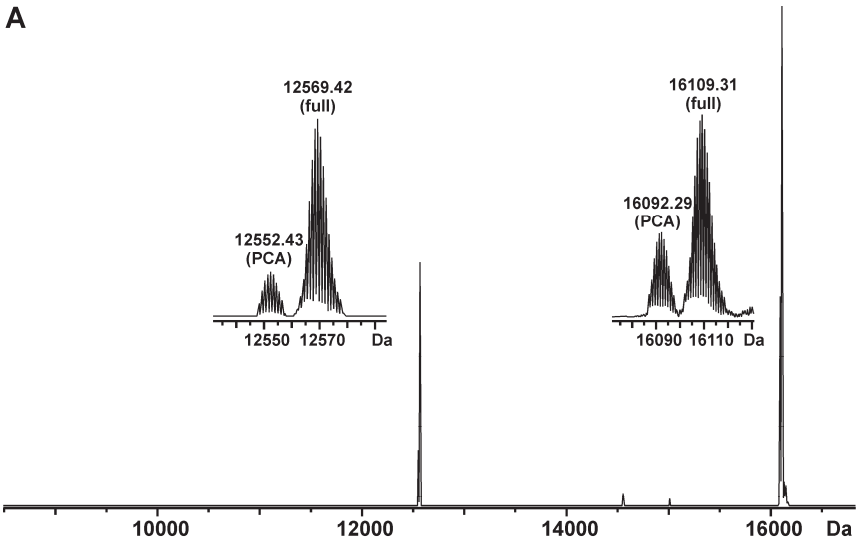

B

```
Bradavidin II-short (115 res., 12569.20 Da)
QTVEAMAQGLPAPSYWKNERGSELLIWSANSGTIQGTFTNHAQGFACQGIPYPAAGSVSPTGLYFVVT
FAQCNSFTRWVGTIKGSQMPTSWTLFYVDNKGKPSRLKGGDIFTRVW


Bradavidin II-long (extended+His-tag) (147 res., 16109.23 Da)
QTVEAMAQGLPAPSYWKNERGSELLIWSANSGTIQGTFTNHAQGFACQGIPYPAAGSVSPTGLYFVVT
FAQCNSFTRWVGTIKGSQMPTSWTLFYVDNKGKPSRLKGGDIFTRVWKGELNSKLEGKPIPNPLLGLD
STRTGHHHHHH
```

Figure S1. (**A**) **Deconvoluted ESI FT-ICR mass spectrum of bradavidin II.** The protein expressed with the original expression plasmid (only one stop codon) contained two protein forms (with the most abundant isotopic masses of 12569.42 and 16109.32 Da,) because of the additional 32 C-terminal amino acid residues from the expression vector construct (pET101/D), resulting in a bypass of the stop codon. The expected protein forms (full) were also accompanied by minor protein forms due to the cyclisation of the N-terminal glutamine to its pyrrolidone carboxylic acid (PCA; -17 Da) form. Adding a second stop codon to the expression vector resulted in the complete disappearance of the long protein forms (data not shown). (**B**) Sequences of the two detected protein forms.

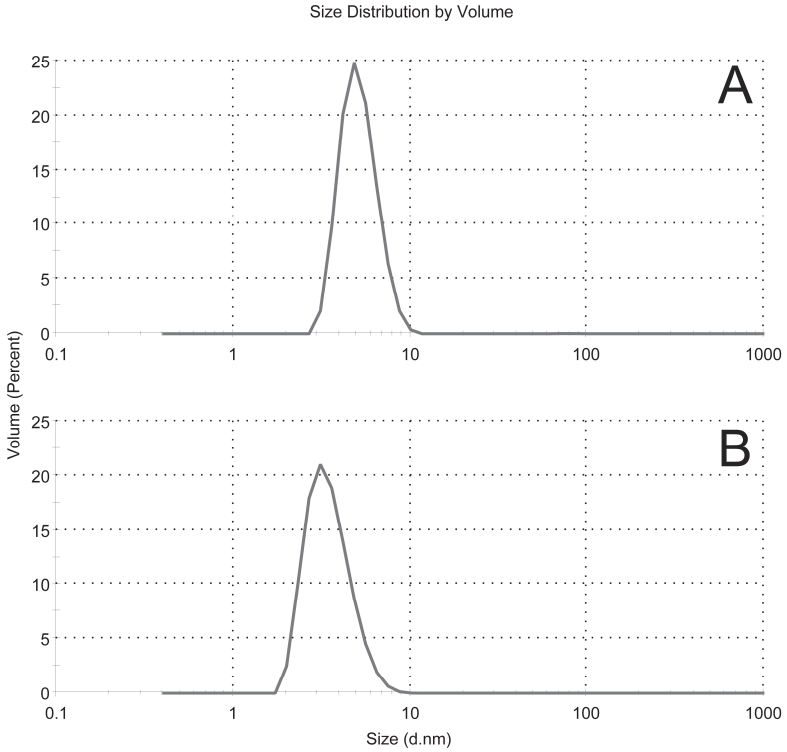

Figure S2. Size distribution of Bradavidin II determined by dynamic light scattering. (**A**) Bradavidin II at concentration of 3.8 mg/ml was analyzed in 0.5 M acetic acid (pH 3). 100% of the particles (by volume) were observed in a population with average particle diameter 5.21 nm. Polydispersity index was 0.188, indicating quite monodisperse particles. (**B**) Bradavidin II at concentration of 0.38 mg/ml was analyzed in 0.5 M acetic acid (pH 3). 100% of the particles (by volume) were observed in a population with average particle diameter 3.55 nm. Polydispersity index was 0.581, indicating relatively polydisperse particle sample.

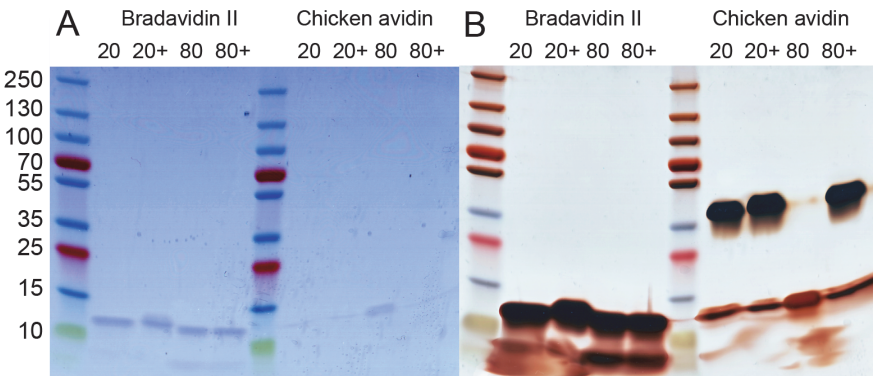

Figure S3. Determination of the oligomeric state by nondenaturing SDS-PAGE. (**A**) Bradavidin II and chicken avidin variant with lowered isoelectric point (Niederhauser et al., unpublished) were subjected to assessment of oligomeric state by using thermal treatment in the presence of SDS, but in the absence of reducing agent. Prior to analysis, the proteins were chemically acetylated to decrease their isoelectric point using sulfo-NHS acetate (Thermo Scientific). The protein samples were treated for 20 minutes in SDS in the presence or absence of biotin (the samples with biotin are indicated by (+) in the Figure 3) at 20°C or at 80°C. Then, the proteins were analyzed using SDS-PAGE and stained using coomassie blue. The molecular weight ladder used was PageRuler Plus Prestained Protein Ladder (Thermo Scientific) and the molecular weights of the ladder bands are indicated in the figure. (**B**) The gel showed in (A) with silver staining.

Table S1. Thermodynamic parameters of biotin binding to bradavidin II determined by competitive ITC. Desthiobiotin was used as a competitive ligand with the indicated concentrations.

[Desthiobiotin]	K_a±SD (x 10^9 M^{-1})	K_d±SD (x10^{-9} M)	ΔH±SD (cal/mol)
15	3.3±0.5	0.30±0.05	-26610±60
75	4.4±1.1	0.23±0.06	-23500±73
150	10.3±1.7	0.10±0.02	-23620±51
200	9.7±2.1	0.10±0.03	-23780±81
300	15.0±2.7	0.07±0.02	-24510±103
500	15.2±3.5	0.07±0.02	-23070±85

Table S2. Onset of protein aggregation during thermal scanning. Transition temperatures were determined at three different protein concentrations at three pH conditions with a dynamic light scattering instrument. The transition temperature is defined as an increase in scattering intensity (derived count rate [kcps]). Bradavidin II was analysed in the absence and presence of biotin in 0.5 M acetic acid (pH 3) containing 0.1% DMSO, in 50 mM Na-phosphate buffer containing 100 mM NaCl and 0.1% DMSO (pH 5), and in 50 mM Na-phosphate buffer containing 100 mM NaCl (pH 7).

Protein concentration (mg/ml)	**Transition temperature (°C)**					
	pH 3		**pH 5**		**pH 7**	
	(-Biotin)	**(+Biotin)**	**(-Biotin)**	**(+Biotin)**	**(-Biotin)**	**(+Biotin)**
0.25	NM	NM	NM	NM	45	65
0.4	-	-	50	75	ND	ND
1.0	50	-	-	-	NM	NM

NM = not measured

ND = could not be determined reliably as protein was heavily aggregated

- = no clear transition identified

Nanotechnology **22** (2011) 275610 (7pp) doi:10.1088/0957-4484/22/27/275610

Defined-size DNA triple crossover construct for molecular electronics: modification, positioning and conductance properties

Veikko Linko[1,3,4], Jenni Leppiniemi[2,3], Seppo-Tapio Paasonen[1,3], Vesa P Hytönen[2] and J Jussi Toppari[1]

[1] Nanoscience Center, Department of Physics, University of Jyväskylä, PO Box 35, FIN-40014, Finland
[2] Institute of Biomedical Technology, University of Tampere and Tampere University Hospital, FIN-33014, Finland

E-mail: veikko.linko@jyu.fi

Received 28 September 2010, in final form 19 April 2011
Published 25 May 2011
Online at stacks.iop.org/Nano/22/275610

Abstract
We present a novel, defined-size, small and rigid DNA template, a so-called B–A–B complex, based on DNA triple crossover motifs (TX tiles), which can be utilized in molecular scale patterning for nanoelectronics, plasmonics and sensing applications. The feasibility of the designed construct is demonstrated by functionalizing the TX tiles with one biotin–triethylene glycol (TEG) and efficiently decorating them with streptavidin, and furthermore by positioning and anchoring single thiol-modified B–A–B complexes to certain locations on a chip via dielectrophoretic trapping. Finally, we characterize the conductance properties of the non-functionalized construct, first by measuring DC conductivity and second by utilizing AC impedance spectroscopy in order to describe the conductivity mechanism of a single B–A–B complex using a detailed equivalent circuit model. This analysis also reveals further information about the conductivity of DNA structures in general.

S Online supplementary data available from stacks.iop.org/Nano/22/275610/mmedia

(Some figures in this article are in colour only in the electronic version)

1. Introduction

A variety of components for bionanotechnology devices are available, offering a broad range of functions. Yet the most crucial part in the realization of powerful multicomponent nanodevices is to find a suitable scaffold for the patterning of molecular components, and secondly to position these constructs on a chip in a controllable way. With respect to the first criterion, DNA has been proven to be a very flexible and promising molecule, mostly due to its superior self-assembly properties [1]. During recent years many DNA-based self-assembled templates and constructs have been introduced: grids [2], chains [3, 4], lattices [5], double (DX) and triple crossover (TX) tiles [6, 7], DNA nanotubes [8, 9], structurally dynamic 3D DNA assemblies [10] and two- and three-dimensional DNA origamis [11, 12], of which the latter are maybe the most versatile scaffolds owing to their controlled size and the possibility of non-periodic patterning. However, the fundamental question about the best possible template is highly ambiguous and non-trivial, since there does not exist a single indicator for that. One has to consider many issues, such as size of the template, electrical properties, stability, fabrication yield (templates utilizing longer strands or complicated structures are harder to fabricate), possibilities for further functionalization and integration to other substances etc. Lately, the usefulness

[3] These authors contributed equally to this work.
[4] Author to whom any correspondence should be addressed.

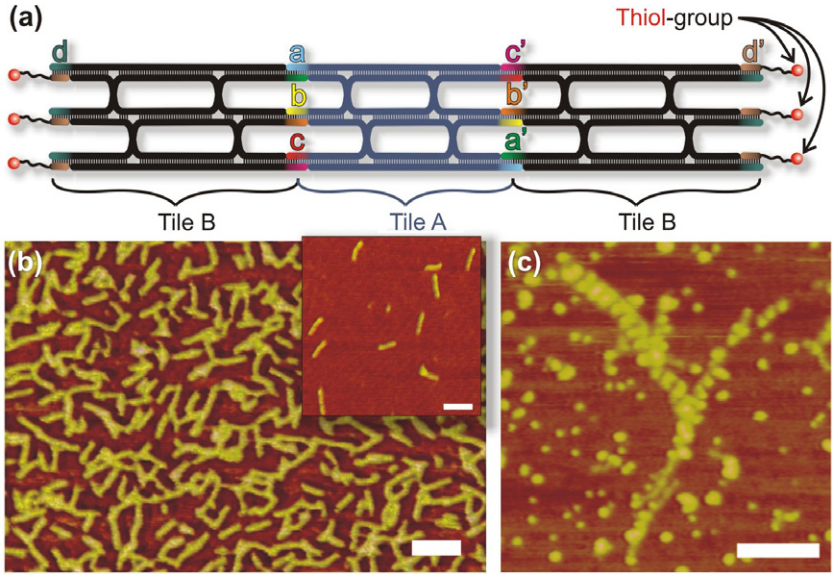

Figure 1. TX tile construct and its modification. (a) Schematic picture of the B–A–B-complex. The tiles are conjugated together via the sticky end pairing (a–a′, b–b′ and c–c′). The thiol-modified strands d′ are paired to the B tiles via sticky ends d. (b) AFM images of TX tile constructs dried on a mica surface. The scale bars are 100 nm. (c) AFM image of biotin–TEG functionalized TX tile chains decorated with streptavidin. The scale bar is 100 nm.

of DNA origami as a 'nanobreadboard' has been tested; the anchorage of origamis to certain locations on the substrates [13–15] and the utilization of the structures as templates for various components have been successfully demonstrated [16–20]. In addition, the electrical properties of triangular [21] and rectangular DNA origamis [22] have been investigated. However, in the conventional fabrication process of DNA origami the length of the scaffold strand limits the size of the object, and in some applications a smaller DNA template could be necessary.

In this paper, we present a relatively small but rigid and stable DNA template, which is based on the triple crossover motifs (TX tiles). The structure has a well-defined size, i.e. $\sim 10 \times 60$ nm^2, unlike previously reported TX-tile-based assemblies which were only able to form infinite linear or two-dimensional arrays [7, 23]. We demonstrate the feasibility of our concept by both positioning and immobilizing single thiol-modified and ligated TX tile constructs between nanoelectrodes by means of dielectrophoretic trapping, and additionally by decorating similar biotinylated TX tiles with streptavidin. Furthermore, since this kind of template could be used as a molecular scale circuit board, its electrical properties are of great concern. In general, the topic of DNA conductivity is still highly controversial [24]. Thus, we characterized the electrical conductivity of the immobilized constructs by utilizing alternating-current impedance spectroscopy (AC-IS) and detailed equivalent circuit modeling [22].

The TX tile constructs studied here differ from the DNA origamis mainly by being seamless, much shorter and smaller, and thus the conductance properties between these might differ significantly. Consequently, the results obtained in the current work, contrasted with those obtained earlier for the rectangular DNA origami, revealed further information about the conductivity of the origami. The comparison confirmed that the observed (Ohmic) conductivity in a humid environment is mostly due to adsorbed water molecules in the DNA helix, claiming the electronic conductance through base pairs to be negligible.

2. Results and discussion

2.1. TX tile construct

All the DNA-based self-assembled structures mentioned above are primarily based on the helical structure of the double stranded DNA (dsDNA) and are thus held together by the same forces, i.e. mainly by the hydrogen bonds between the bases, but also secondary stabilizing forces like the dipole–dipole and van der Waals interactions [25, 1]. In addition, counterions (in our case Na^+, Mg^{2+}) and water molecules that surround the DNA affect the conformation of dsDNA and thus the helices that form the structure. Also, it is possible that the binding of the ions inside the inter-helix gaps between the neighboring parallel helices in the structures is somewhat different from the binding of the ions to individual dsDNA molecules. For this reason the conductance properties of the DNA structures may differ from those of dsDNA molecules, as discussed in sections 2.4 and 2.5.

The TX tiles used in this work were designed so that only a finite-size complex of tile B–tile A–tile B (see figures 1(a) and (b)) was able to assemble instead of infinite array as in the earlier designs. To achieve this, first only three different kinds of eight nucleotide (nt) long sticky ends were symmetrically used in tile A, i.e. a, b, c (see the color codes of sticky ends in figure 1(a)), so that tile A could be rotated by 180° still having the sticky ends at the same orientation in both ends. Accordingly, tile B had complementary sticky ends a′, b′ and c′ at one end. The sticky ends d (12 nt) at the other end of

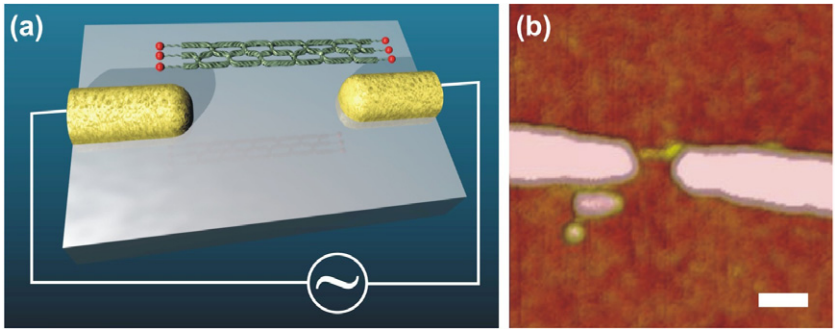

Figure 2. Dielectrophoretic trapping of TX tile constructs. (a) Schematic view of the trapping. (b) AFM image of a trapped and immobilized single construct in between the gold nanoelectrodes. The scale bar is 50 nm.

tile B had an identical sequence and therefore they could all be assembled with complementary strands d′ containing thiol groups at the 5′ end. The thiol-modifications were added to tile B for the purpose of the forthcoming immobilization of the constructs to the gold electrodes via S–Au bonding. Secondly, the sticky ends were designed to start at the same horizontal location in each helix, which enabled tiles B to be assembled to both ends of tile A. Third, tile A has 16 base pairs between crossover points, corresponding to 1.5 turns of B-DNA double helices, enabling the same natural orientation for helices when tile B is assembled to either sides of tile A.

The design of the exact sequences within the TX tiles was based on biotinylated DNA triple crossover motifs used in [23, 26], but without biotinylated hairpin loops in our design. The full design with the exact sequence maps is presented in the supplementary data (available at stacks.iop.org/Nano/22/275610/mmedia). The length of the full tile B–tile A–tile B (B–A–B) complex, with three thiol groups attached to both ends, is 167 bases, which corresponds to 15.9 full turns of DNA double helices. In addition, to help the B–A–B complex sustain its form during the forthcoming dielectrophoretic trapping, the individual components were covalently coupled by using a kinase–ligase procedure [27].

2.2. DEP trapping of TX tile constructs

For the controlled positioning of the thiol-modified B–A–B complexes, we used an AC dielectrophoresis (AC-DEP) trapping technique [13, 22, 28]. The trapping field was produced by applying an AC voltage of 1.2–1.5 V at a frequency of 11 MHz between two fingertip-type gold nanoelectrodes (fabricated by e-beam lithography on a SiO_2 substrate) with widths of 30–50 nm and a gap between them of 45–55 nm (figures 2(a) and (b)). About 10 μl of spin-filtered solution containing B–A–B-complexes was pipetted on the chip and the trapping voltage was applied for 3–5 min. A low-conductivity HEPES/NaOH-based buffer, pH $\sim$ 7, was used during the trapping and the concentration of the B–A–B complexes was 1–10 nM. After that, the sample was gently washed with the same buffer and water, and finally the trapping results were verified by atomic force microscopy (AFM) imaging (Veeco, Dimension 3100). For the conductivity measurements we only chose samples which contained just one intact and properly aligned structure (DNA duplexes of the structure oriented parallel to the electrodes) in the gap region as shown in figure 2(b).

2.3. Functionalization of TX tiles

The TX tile complexes described here could be used as a platform to assemble other substances, for example gold nanoparticles or proteins. To demonstrate this we fabricated similar TX tiles, now with biotinylated hairpins and capable of forming infinite arrays, and decorated them with streptavidin. The same kind of biotinylated TX tiles [23] and 4×4 tiles [29] have been previously decorated with streptavidin, but here we demonstrated a new functionalization of the reported TX tiles [23] having, instead of two biotins in the hairpin, only one biotin with 15-atom flexible triethylene glycol (TEG) spacer to optimize the (strept)avidin binding. Previous studies have claimed that two biotins are needed to enable tight binding of streptavidin to DNA [23, 29]. However, most of the studies have been carried out by utilizing short linker between DNA and biotin, and the length of the linker is known to be an important factor in tight biotin binding [30, 31]. Streptavidin assembly to the TX tiles functionalized with one biotin–TEG was successful, as can be seen from AFM studies (figure 1(c)). The same approach could be applied to functionalize our B–A–B complex.

2.4. DC-conductivity of TX tile constructs

After the trapping of the B–A–B complexes, DC conductivities of the samples were measured first in a dry environment, i.e. relative humidity (RH) $\sim$5%, and then in a moist chamber with RH = 90% corresponding to the level (15 water molecules per nucleotide [32]) at which the DNA should be in its natural B-form (at least 13 water molecules per nucleotide required [33]).

In the dry conditions samples containing TX tile constructs were insulating with resistances of the order of TΩ, similar to the rectangular DNA origamis measured in a previous work [22]. Instead, at RH = 90% the samples showed almost linear IV curves with resistances of $\sim$20 GΩ when the DC voltage was swept between -0.3 and 0.3 V (with the resistance dropping a bit, to $\sim$15 GΩ, above 0.2 V) (see figure 3(a)). The hysteresis in the IV curves

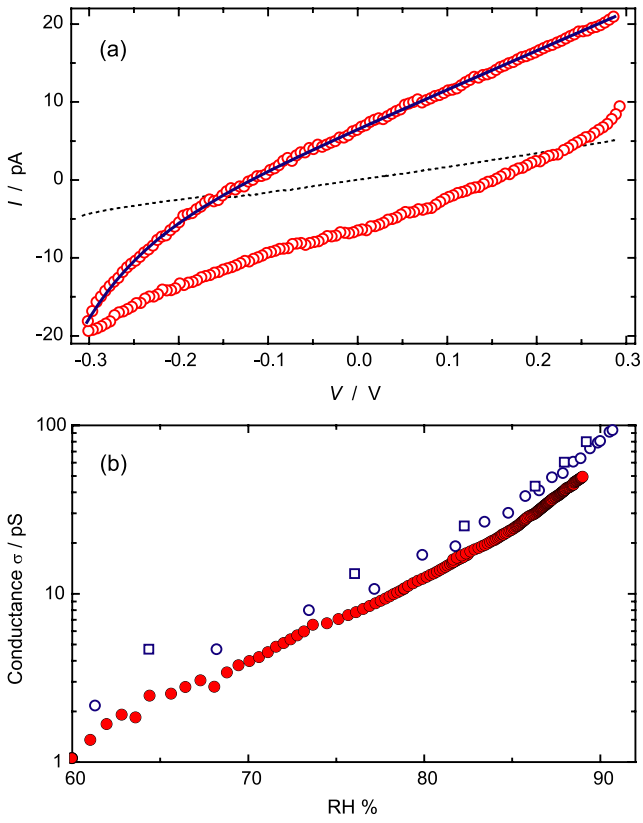

Figure 3. (a) IV curve measured for a control sample (dashed black line) and a sample containing a single B–A–B complex (open red circles) at RH = 90%. The hysteretic behavior of the TX tile sample is due to enhanced charging at the high humidity as shown by fitting a linear IV dependency with charging effects included to the data (solid blue line). The resistance of the TX tile construct yielded by the fitting is 20 GΩ. (b) The conductivity of a control sample (red dots) and two B–A–B complex samples (open blue circles and squares) as a function of relative humidity.

at high humidity is due to enhanced charging effects by the increased ionic mobility, and it is not present in the measurements done in the dry environment. The hysteresis can be taken into account as shown in figure 3(a) by fitting a linear IV dependency with the charging effect included to the measured data (more details in supplementary data available at stacks.iop.org/Nano/22/275610/mmedia). These results were compared to measured control samples, which underwent similar DEP trapping including the washing procedures but without any DNA in the trapping buffer. The control samples produced linear IV curves with larger resistances of ∼30 GΩ or more (figure 3(a)).

As a comparison, in previous studies of the DC conductivity of a rectangular DNA origami (same trapping buffer, same RH), origami samples showed linear IV characteristics (∼10 GΩ) between −0.2 and 0.2 V, but the resistance was clearly reduced above 0.2 V (∼2 GΩ), which is assumed to be a threshold voltage for some water related redox reaction at the electrodes [22]. The reason for the difference is quite obvious: firstly, a stretch of DNA nucleotides can adsorb only a certain number of water molecules at a given RH level [32], and secondly, the number of nucleotides is very different in the TX tile construct consisting of ∼1000 nt and the DNA origami having about 14 000 nt. Thus, the total quantity of adsorbed water molecules in a TX tile construct is much smaller than in a DNA origami, and in addition the permittivities of the formed water layers surrounding the structures can be quite distinct from each other. By comparing this information with the different resistance values and the shapes of the IV curves, it can be directly deduced that the ionized water molecules are the main charge carriers in DC [22, 34–37].

Conductivity analysis with different humidity levels also proposed a significant role for water in charge transport. The conductivity of the TX tile constructs and the control samples was not significantly increased although the RH was slowly raised from 5% to ∼60%. However, when the RH was above 60%, the conductivity increased almost exponentially as a function of RH (see figure 3(b)). This is in agreement with the results reported in [35–37], where a water-dominated charge-transfer mechanism has been proposed. The exponential enhancement of the conductivity as a function of RH can be explained by the increasing number of water molecules adsorbed to the structure and to the substrate, and also by the increasing permittivity of the formed water layer [34, 35]. In addition, since the conductivity is strongly enhanced by humidity, hole hopping as a major charge-transfer mechanism (reduced conductivity with increasing humidity) can be ruled out [38].

2.5. AC conductivity of TX tile constructs

The DC measurement indicates only that the water molecules have a crucial effect on the conductivity process, but it hides the information about other conductivity mechanisms. Thus, AC impedance spectroscopy was applied for further analysis of the electrical conductivity and characterization of its nature. The measurements were carried out similarly as in [22] with an AC excitation of 50 mV_{rms} (zero DC-offset) and frequencies ranging from 0.01 Hz to 100 kHz. All the actual AC-IS measurements were performed at the same RH = 90% as the DC measurements.

In order to compare and fully characterize the AC response of the TX tile construct, first the dry and empty sample, i.e. only the nanoelectrodes, was measured to find out the geometric self-capacitance and the leakage current of the measurement setup (see table 1, more details in supplementary data available at stacks.iop.org/Nano/22/275610/mmedia). Second, the AC responses of the control samples (similar samples to those stated in the previous paragraph) were investigated at RH = 90%. The Cole–Cole plot of a typical control sample (3 in total) and the fitted equivalent circuit model are shown in figures 4(a) and (b), respectively. The equivalent circuit model was the same as in [22], i.e. a modified Randles circuit, where an additional diffusive element W_{diff} (Warburg impedance $Z_W = 1/[W(i\omega)^{1/2}]$, where ω is the angular frequency of the signal) was added in parallel to the series resistance R_s [22, 39]. This parallel combination is called Z_s and it describes the area between electrodes, i.e. the resistance of 'electrolyte' and the diffusive element due to ions migrating and diffusing

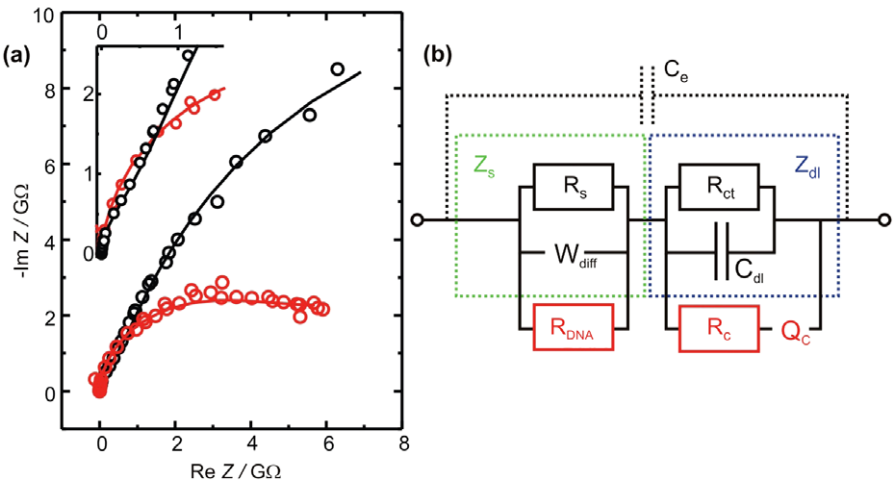

Figure 4. AC impedance spectroscopy. (a) Cole–Cole plots and data fittings of a control sample (black circles and black solid curve, respectively) and a typical sample containing a single TX tile construct in the gap (red circles and red solid curve). (b) Equivalent circuit models of a control sample (black components) and a DNA sample (black and red components). C_e is the measured self-capacitance of the electrodes. R_s represents the small current through the 'electrolyte' and W_{diff} describes the diffusion of the ions on the SiO_2 surface. Parallel combination of W_{diff} and R_s forms the series impedance Z_s (green) and in series with this there is a double-layer impedance Z_{dl} (blue) comprising the double-layer capacitance, C_{dl} and current through it, R_{ct}. R_{DNA} describes the resistance of the TX tile construct and R_c together with Q_c the contact impedances between the construct, linker and electrodes.

Table 1. Results from the fittings of the equivalent circuits of an empty dry sample, a typical control sample and a TX tile construct sample (control and TX are the same samples as in figure 4(a)). The values in parentheses are not fitted but fixed based on the fitting of the dry and empty sample or the control sample.

Sample	$R_s/R_{s\|DNA}$ (GΩ)	W_{diff} ($ps^{1/2}$ Ω^{-1})	C_{dl} (pF)	R_{ct} (GΩ)	R_c (GΩ)	Q_c (ns^{n_Q} Ω^{-1})	n_Q	R_e (TΩ)	C_e (pF)
Dry	—	—	—	—	—	—	—	0.3	6.8
Control	1.3	13	26	26	—	—	—	(0.3)	(6.8)
TX	0.9	29	1.8	(26)	1.5	0.13	0.3	(0.3)	(6.8)

along the SiO_2 surface. The other block, Z_{dl}, in series with Z_s, is a so-called double-layer part, which comprises a double-layer capacitance C_{dl} (formed by ions on the electrode–'electrolyte' interface) and the charge-transfer resistance R_{ct} (charge moving through the double layer) [22, 39]. According to the fittings, the resistance of the 'electrolyte' was typically ∼1–4 GΩ and the charge-transfer resistance 20–30 GΩ (table 1). The sum of these two resistors roughly corresponds to the observed DC resistance and the high resistance of the charge-transfer process through the double layer explains the poor DC conductivity.

Finally, the samples containing the B–A–B complex (three in total) were measured with AC-IS and compared to the control samples. As can be seen from figure 4(a), the Cole–Cole plot of a typical sample is quite similar to the control, except for the low frequency tail, which differs significantly. The observed behavior can be described by the equivalent circuit of the control combined with three additional elements (see figure 4(b)). Most importantly, these components include R_{DNA}, the resistance of the TX tile construct, which is located in parallel to Z_s. The two remaining components R_c (resistor) and Q_c (constant phase element, CPE, $Z_{CPE} = 1/[Q(i\omega)^n]$) together describe the modification of the double layer and thus appear in parallel to Z_{dl} (for more details see [22]).

This particular model can be exploited to get information about the conductivity mechanisms of the TX tile constructs similar to the DNA origamis earlier [22]. The main difference between these structures is the smaller overall size and the seamlessness of the TX tile construct. In addition, the linker molecules (hexanethiols) of the designed B–A–B complex have a lower resistance [40] than the longer linkers (hexanethiol and single-stranded DNA spacer [22]) used in the DNA origami design. The preceding facts lead to the conclusion that if the electronic conductivity through the bases is relevant, the B–A–B complex should show higher conductivity than the DNA origami (resistance ≈ 70 MΩ at RH = 90% [22]). However, our results show that for the B–A–B-complex $R_{s\|DNA}$, a parallel combination of R_s and R_{DNA}, is typically ∼1–2 G Ohm, which is only about half of R_s of the control (see also table 1), indicating that the conductivity through a single TX tile construct is lower than that measured for the origami. This implies, that in the same way as the presence of DNA enhances diffusivity of ions along the construct (W_{diff} is increased; see table 1) via gathered water molecules, the observed Ohmic [22] conductivity ($R_{s\|DNA} < R_s$) for both the B–A–B complex and origami is just due to enhancement of the conductivity of the 'electrolyte'. These effects are only more pronounced in the case of DNA origami since they can bind more water molecules and ions than TX tile constructs, which is also visible as a higher diffusion in the case of origamis, i.e. W_{diff} for the origami ∼1000 $ps^{1/2}$ Ω^{-1} [22] and W_{diff} for the TX tile construct ∼30 $ps^{1/2}$ Ω^{-1}. Altogether,

the observed conductivity should thus be strongly dependent on the size of the DNA structure in question, which agrees well with our measurements. In addition, the results are in agreement with those of [32], where the observed AC conductivity of DNA is reported to be mainly caused by water molecules. For more details see supplementary data (available at stacks.iop.org/Nano/22/275610/mmedia).

3. Experimental section

3.1. TX tile construct fabrication and ligation

The majority of the DNA sequences were adopted from previously published structures [23, 26] and modified to our needs. The change of sequence symmetry and undesired complementarity was minimized by using the M-fold web server [41, 42]. Complexes were formed in TAE Mg^{2+} buffer (40 mM Tris (pH 7.6), 1 mM EDTA, 19 mM acetic acid, 12.5 mM magnesium acetate) and T4 polynucleotide kinase (New England Biolabs) was used to add phosphates to the 5′ end of each DNA strand (PAGE- or HPLC-purified, Biomers GmbH, Ulm, Germany), except for the 5′thiol-modified strand (HPLC-purified, Integrated DNA Technologies, Coralville, IA, USA). Each strand was modified separately using T4 polynucleotide kinase with T4 DNA ligase buffer and the strands were incubated for 1 h at 37 °C. To achieve an appropriate concentration of each tile, the T4 kinase-modified strands were mixed by using a two-fold number of strands that form tile B (B strands) compared to strands forming tile A (A strands). In addition, a three-fold number of 5′thiol-modified strands compared to B strands were used in order to hybridize them with each sticky end d of the tile B. Complexes were formed by heating the mixture up to 90 °C and cooling it down to 20 °C at a rate of 0.01 °C s^{-1} in a PCR-machine (Biometra GmbH, Goettingen, Germany). After annealing, complexes were ligated using T4 DNA ligase (New England Biolabs) to make the complexes more stable for the DEP trapping. The mixture was incubated for 2 h in the dark at a room temperature and stored at 4 °C afterward. The theoretical concentration of obtained complexes was 0.29 μM of A strands (tile A) and 0.58 μM of B strands (tile B). Detailed sequences of the DNA strands used and the details of biotin functionalization are presented in the supplementary data (available at stacks.iop.org/Nano/22/275610/mmedia).

3.2. Nanoelectrode preparation

Nanoelectrodes were fabricated using standard electron beam lithography and evaporation of metal (1–2 nm of Ti followed by 15–20 nm Au) on top of a silicon oxide surface in an ultrahigh vacuum (UHV) chamber. Residues of the resist (PMMA) from the lift-off were removed by an oxygen plasma flash in a reactive ion etcher, which also made the SiO_2 surface hydrophilic for the DEP trapping.

3.3. Dielectrophoretic trapping

The annealing buffer of TX tile constructs was changed to the buffer with lower conductivity in a spin-filtering process (details in the supplementary data available at stacks.iop.org/Nano/22/275610/mmedia). DEP trapping was carried out in a low-conductivity HEPES/MgAc-based buffer: 6.5 mM HEPES, 1 mM MgAc, and ∼2 mM NaOH to adjust pH to 7 ($\sigma \approx 300$ μS cm^{-1}). Immediately after the trapping, samples were washed six times with 50 μl of 3 mM HEPES/2 mM NaOH buffer (pH $\approx$ 7) to reduce the concentration of Mg^{2+} ions. Finally, the samples were gently rinsed three times with 100 μl of distilled water and dried by nitrogen flow. The control samples also underwent DEP, except without any DNA in the buffer, and they were washed similarly to the samples with a TX tile construct in the gap.

3.4. Electrical measurements

DC measurements were performed by sweeping a battery powered bias voltage between −0.3 and 0.3 V while measuring the current and voltage by a computer equipped with DAQ card (National Instruments PXI-1031) via DL-Instruments 1211 current preamplifier and DL-Instruments 1201 voltage preamplifier. For the AC-IS measurements the same preamplifiers and two Stanford Research 830 lock-in amplifiers, controlled through a GBIP connection by a computer running a homemade LabVIEW AC-IS program, were used. All the electrical measurements were carried out in a room shielded from electromagnetic interference with optical isolation between the setup and the computer.

The ambient condition of the samples during the measurements was controlled by placing them in a humidity-tight chamber with a small constant flow of either dry nitrogen or deionized water vapor. By adjusting the flow the RH could be precisely tuned and kept constant. RH and temperature were continuously measured by a Honeywell HIH-3602-A humidity sensor. More details are available in the supplementary data (available at stacks.iop.org/Nano/22/275610/mmedia).

4. Conclusion

We have demonstrated the fabrication of a novel self-assembled defined-size TX tile DNA complex which can be incorporated into molecular electronic devices especially as a scaffold. The fabricated B–A–B complexes were guided to certain locations by dielectrophoretic trapping and immobilized between gold nanoelectrodes via thiol linkers. We have also demonstrated that the developed structure can be functionalized and that a single biotinylation is efficient in the attachment of streptavidin to DNA if a long linker is used. The conductivity of the trapped TX tiles was analyzed by AC impedance spectroscopy and found to be small enough for one to build almost any kind of electrical device without having to take the scaffold into account. Furthermore, by comparing the AC-IS studies of the TX tile complex and DNA origami, one can deduce the observed Ohmic conductivity being mostly due to the water molecules adsorbed to DNA helices and thus scaling as a function of the size of the DNA construct, i.e. the direct electronic conductivity via base pairs is negligible in most practical constructs. Overall, the developed technology provides a toolbox for the next generation of DNA-based nanodevices.

Acknowledgments

The authors thank T Ihalainen, E Niskanen, K Tapio, J Ylänne and M Vihinen-Ranta (Nanoscience Center, University of Jyväskylä) for help with biolab facilities and imaging. Financial support from the Academy of Finland (projects 218182, 130900 and 115976) is acknowledged. VL thanks the Finnish Academy of Science and Letters (Väisälä Foundation), the Finnish Cultural Foundation (Central Finland Regional Fund), the Finnish Foundation for Technology Promotion (TES) and the National Doctoral Programme in Nanoscience (NGS-NANO). JL thanks the Tampere Graduate Program in Biomedicine and Biotechnology (TGPBB).

References

[1] Seeman N C 2003 *Nature* **421** 427–31
Seeman N C 2010 *Nano Lett.* **10** 1971–8
[2] Sha R, Liu F and Seeman N C 2002 *Biochemistry* **41** 5950–5
[3] Mao C, Sun W and Seeman N C 1999 *J. Am. Chem. Soc.* **121** 5437–43
[4] Aldaye F A and Sleiman H F 2007 *J. Am. Chem. Soc.* **129** 4130–1
[5] Winfree E, Liu F, Wenzler L A and Seeman N C 1998 *Nature* **394** 539–44
[6] Li X, Yang X, Qi J and Seeman N C 1996 *J. Am. Chem. Soc.* **118** 6131–40
[7] LaBean T H, Yan H, Kopatsch J, Liu F, Winfree E, Reif J H and Seeman N C 2000 *J. Am. Chem. Soc.* **122** 1848–60
[8] Liu D, Park S H, Reif J H and LaBean T H 2004 *Proc. Natl Acad. Sci. USA* **101** 717–22
[9] Lo P K, Karam P, Aldaye F A, McLaughlin C K, Hamblin G D, Cosa G and Sleiman H F 2010 *Nat. Chem.* **2** 319–28
[10] Aldaye F A and Sleiman H F 2007 *J. Am. Chem. Soc.* **129** 13376–7
[11] Rothemund P W K 2006 *Nature* **440** 297–302
[12] Douglas S M, Dietz H, Liedl T, Högberg B, Graf F and Shih W M 2009 *Nature* **459** 414–8
[13] Kuzyk A, Yurke B, Toppari J J, Linko V and Törmä P 2008 *Small* **4** 447–50
[14] Gerdon A E, Oh S S, Hsieh K, Ke Y, Yan H and Soh H T 2009 *Small* **5** 1942–6
[15] Kershner R J *et al* 2009 *Nat. Nanotechnol.* **4** 557–61
[16] Kuzyk A, Laitinen K T and Törmä P 2009 *Nanotechnology* **20** 235305
[17] Voigt N V *et al* 2010 *Nat. Nanotechnol.* **5** 200–3
[18] Maune H T, Han S, Barish R D, Bockrath M, Goddard W A III, Rothemund P W K and Winfree E 2010 *Nat. Nanotechnol.* **5** 61–6
[19] Ding B, Deng Z, Yan H, Cabrini S, Zuckermann R N and Bokor J 2010 *J. Am. Chem. Soc.* **132** 3248–9
[20] Bui H, Onodera C, Kidwell C, Tan Y, Graugnard E, Kuang W, Lee J, Knowlton W B, Yurke B and Hughes W L 2010 *Nano Lett.* **10** 3367–72
[21] Bobadilla A D, Bellido E P, Rangel N L, Zhong H, Norton M L, Sinitskii A and Seminario J M 2009 *J. Chem. Phys.* **130** 171101
[22] Linko V, Paasonen S-T, Kuzyk A, Törmä P and Toppari J J 2009 *Small* **5** 2382–6
[23] Li H, Park S H, Reif J H, LaBean T H and Yan H 2004 *J. Am. Chem. Soc.* **126** 418–9
[24] Endres R G, Cox D L and Singh R R P 2004 *Rev. Mod. Phys.* **76** 195–214
[25] Breslauer K J, Frank R, Blockers H and Marky L A 1986 *Proc. Natl Acad. Sci. USA* **83** 3746–50
[26] Park S H, Barish R, Li H, Reif J H, Finkelstein G, Yan H and LaBean T H 2005 *Nano Lett.* **5** 693–6
[27] O'Neill P, Rothemund P W K, Kumar A and Fygenson D K 2006 *Nano Lett.* **6** 1379–83
[28] Tuukkanen S, Kuzyk A, Toppari J J, Häkkinen H, Hytönen V P, Niskanen E, Rinkiö M and Törmä P 2007 *Nanotechnology* **18** 295204
[29] Yan H, Park S H, Finkelstein G, Reif J H and LaBean T H 2003 *Science* **301** 1882–4
[30] Green N M 1975 *Adv. Protein Chem.* **29** 85–133
[31] Marek M, Kaiser K and Gruber H J 1997 *Bioconjug. Chem.* **8** 560–6
[32] Briman M, Armitage N P, Helgren E and Grüner G 2004 *Nano Lett.* **4** 733–6
[33] Warman J M, de Haas M P and Rupprecht A 1996 *Chem. Phys. Lett.* **249** 319–22
[34] Anderson J H and Parks G A 1968 *J. Phys. Chem.* **72** 3662–8
[35] Yamahata C, Collard D, Takekawa T, Kumemura M, Hashiguchi G and Fujita H 2008 *Biophys. J.* **94** 63–70
[36] Han Ha D, Nham H, Yoo K-H, So H, Lee H-Y and Kawai T 2002 *Chem. Phys. Lett.* **355** 405–9
[37] Kleine-Ostmann T, Jördens C, Baaske K, Weimann T, Hrabe de Angelis M and Koch M 2006 *Appl. Phys. Lett.* **88** 102102
[38] Pavanello M, Adamowicz L, Volobuyev M and Mennucci B 2010 *J. Phys. Chem.* B **114** 1416–23
[39] Barsoukov E and Macdonald J R 2005 *Impedance Spectroscopy: Theory, Experiment, and Applications* 2nd edn (Hoboken, NJ: Wiley)
[40] Xu B and Tao N J 2003 *Science* **301** 1221–3 and references therein
[41] Zuker M 2003 *Nucleic Acids Res.* **31** 3406–15
[42] http://mfold.rna.albany.edu/?q=mfold

Supplementary data

Defined-sized DNA triple crossover construct for molecular electronics: modification, positioning and conductance properties

Veikko Linko, Jenni Leppiniemi, Seppo-Tapio Paasonen, Vesa P Hytönen and J Jussi Toppari

1. Fabrication of TX tile constructs

Strand 7 with 5' thiol-modification (5' Thiol Modifier C6 S-S (Disulfide)) was purchased as HPLC-purified from Integrated DNA Technologies, IDT (Coralville, Iowa, USA). All other oligonucleotides were purchased from Biomers GmbH (Ulm, Germany) purified either by PAGE or by HPLC. Strands were diluted to a concentration of 10 µM in 40 mM Tris (pH 8) buffer containing 1 mM EDTA and 19 mM acetic acid. Magnesium acetate was included in the final reaction mixture with concentration of 12.5 mM. Therefore a buffer containing 40 mM Tris (pH 8), 1 mM EDTA, 19 mM acetic acid and 500 mM magnesium acetate was prepared and added to a master mix containing the following components:

- 5.8 µl 40 mM Tris (pH 8), 1 mM EDTA, 19 mM CH_3COOH, 500 mM $Mg(CH_3COO)_2$
- 0.8 µl 40 mM Tris (pH 8), 1 mM EDTA, 19 mM CH_3COOH
- 23.0 µl 10× T4 DNA Ligase buffer
- 0.5 µl T4 Polynucleotide Kinase (10,000 U/ml)

T4 Polynucleotide Kinase (New England Biolabs, Ipswich, MA, USA) was used to add phosphate groups to the 5' end of each strand except 5'thiol-modified stand 7. Each strand was modified separately by adding 1.5 µl of master mix to tubes containing 10 µl of strands of *tile A* (10 µM) or by adding 3.0 µl of master mix to tubes containing 20 µl of strands of *tile B* (10 µM). This was followed by incubation for one hour at 37 ºC.

The strand 7 was diluted to the same concentration (8.7 µM) as the other strands had after incubation with T4 kinase. Then the kinase modified strands and strand 7 were mixed. To achieve appropriate concentration of each tile a two-fold amount (20 µl) of strands 8 – 14 of *tile B* were used compared to strands 1 – 6 of *tile A* (10 µl). In addition, three-fold amount (60 µl) of 5'thiol-modified strands 7 compared to strands of *tile B* were used in order to hybridize them with each sticky end *d* of *tile B*. Complexes were formed by heating the mixture up to 90 ºC and cooling it down to 20 ºC at a rate 0.01 ºC/s in a PCR-machine (Biometra GmbH, Goettingen, Germany). After annealing the complexes were ligated using T4 DNA ligase (New England Biolabs) to make the complexes more stable for DEP. 800 units of T4 DNA ligase with T4 ligase buffer were added to the annealed complex:

- 260 µl of *tile B* - *tile A* - *tile B* -complex
- 7 µl 40 mM Tris (pH 8), 1 mM EDTA, 19 mM CH_3COOH
- 1.0 µl 40 mM Tris (pH 8), 1 mM EDTA, 19 mM CH_3COOH, 500 mM $Mg(CH_3COO)_2$

– 30 µl 10× T4 DNA Ligase buffer
– 2.0 µl T4 DNA Ligase (400,000 U/ml)

The mixture described above was incubated for two hours in dark at room temperature (RT, 22 ± 1 ºC) and stored at 4 ºC afterwards. The theoretical concentration of obtained complexes was 0.29 µM of strands 1 - 6 (*tile A*) and 0.58 µM of strands 8 – 14 (*tile B*).

Table S1. Sequences of strands used in *tile A* and *tile B*.

Strand	Sequence
1	5′-ATCGAGAGAC ATAACTGCTT GACCACGCTG TATCGGAACC TGACTCCTAA TCAGCA-3′
2	5′-AGGAGTCACT CTCGATGCCA GACG-3′
3	5′-GGTATAGTAT GCAACGTGAA TGAACAAGGT GAGGTGTCAA TGGAGATGAA TGTTC-3′
4	5′-ATCTCCATTG ACAGGTCAAG CAGTTATGTG GTTCTGCATA CTATACCGAA TGTTC-3′
5	5′-ATAGCACCAC TGCAAGGCCA GACG-3′
6	5′-CTTGCAGTCC TTGTTCATTC ACGTCGATAC AGCGTCCTCA GGTGCTATAA TCAGCA-3′
7	5′-5ThioMC6-D-TGGAGCGACA TG-3′
8	5′-AGATAACATA AGGACACTTA GGAATCCAGT ACTGACACAC AGTTGGAACA TTC-3′
9	5′-CAACTGTGTG AATGGGACTT TGCTGATT-3′
10	5′-AGCTGAACCT ACAGTCATAC GACTCGAACA CGTAGTATCA TCTAGCGTCT GGC-3′
11	5′-CTAGATGATA CTACGGCTAC TCAGTACTGG ATTCCTAAGT GAATTGGAC-3′
12	5′-GATCATGATG TTCGAGTCGT ATGACTGTAC TATCTCCTTA TGTTATCTCA TGTCGCTCCA-3′
13	5′-AAGTCCCATT GTAGCTCATG ATCGTCCAAT TGATAGCCCT GTTGACATGT CGCTCCA-3′
14	5′-TCAACAGGGG GTTCAGCTCA TGTCGCTCCA-3′

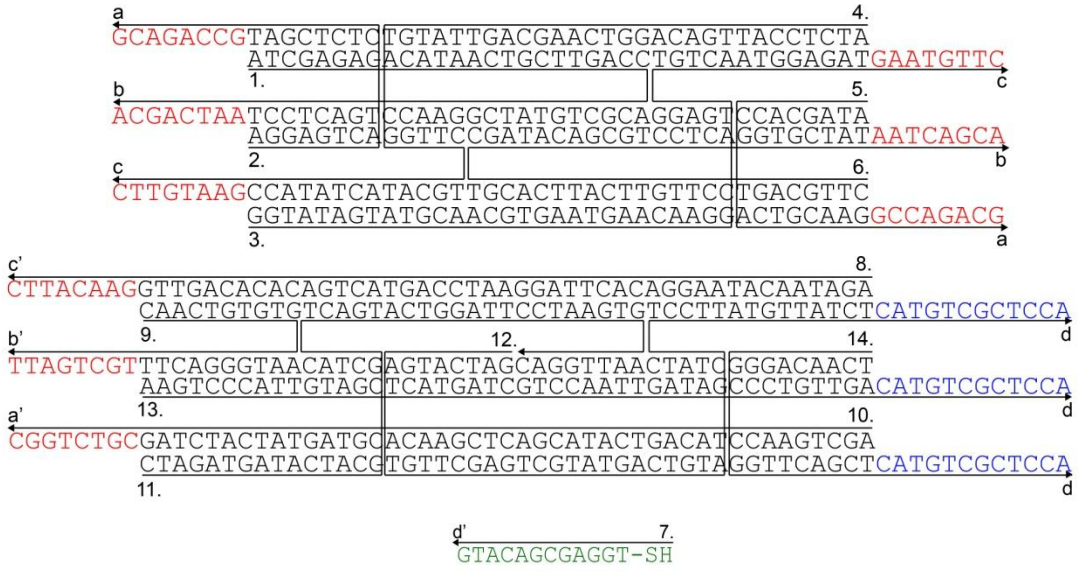

Figure S1. DNA strand structure and sequences of *tile A* and *tile B*. Sticky ends *a*, *b* and *c* are complementary to sticky ends *a'*, *b'* and *c'*. Strand 7 is complementary to sticky ends *d* of *tile B*. To be accurate, the SH-group indicated in a figure contains also a protection group (5' Thiol Modifier C6 S-S (Disulfide)) to avoid undesired S-S bonding between tiles.

2. Biotin-avidin modification of TX tiles

2.1. Biotin functionalization and streptavidin decoration

To study the biotin functionalization with one biotin per TX molecule we ordered the same strands previously used in DNA triple crossover molecules (TX tiles) [S1] except the strand 3 (Supplementary figure S2) with an internal biotin-TEG modification. The strand 3 was purchased from (TAG Copenhagen, Copenhagen, Denmark) and all other strands were purchased from Biomers GmbH. Strands were diluted to 20 mM Tris (pH 7.6), 2 mM EDTA. 12.5 mM $MgCl_2$ was included in the final reaction mixture and therefore a buffer containing 20 mM Tris (pH 7.6), 2 mM EDTA and 500 mM $MgCl_2$ was prepared. The reaction mixture is thus of the form:

- 20 µl Strand 1 (10 µM)
- 20 µl Strand 2 (10 µM)
- 20 µl Strand 3 (10 µM)
- 20 µl Strand 4 (10 µM)
- 20 µl Strand 5 (10 µM)
- 20 µl Strand 6 (10 µM)
- 20 µl Strand 7 (10 µM)
- 55 µl 20 mM Tris (pH 7.6), 2 mM EDTA
- 5 µl 20 mM Tris (pH 7.6), 2 mM EDTA, 500 mM $MgCl_2$

TX tile complexes were formed by heating and cooling by the same procedure as described above for the B-A-B complexes. The final concentration of each strand, as well as TX molecules, were 1 µM. TX tile : streptavidin ratio 1 µM : 1µM was used and after adding streptavidin to the annealed TX tiles, the solution was incubated overnight at 4 ºC before AFM imaging.

2.2. AFM imaging

A sample of 5 µL of streptavidin decorated TX tiles was incubated on a freshly cleaved mica surface for 3 min at room temperature and the sample was gently dried under nitrogen stream. Then the sample was washed with 10 µl of deionized water and dried under nitrogen stream. AFM imaging was performed by tapping mode in ambient conditions by Dimension 3100 AFM using NanoScope IVa controller (Veeco Instruments, NY, USA).

Table S2. Sequences of strands used in biotinylated TX tiles. The location of nucleotide analog Biotin-TEG is indicated by an asterisk (*).

Strand	Sequence
1	5′-GCAGACCGTA GAATCGCCTG CTCTGTATCA TAGATGTTTT CATCTATGTT TGCCGAACTG GACACTTACC TCTA -3′
2	5′-ACGACTAATC CGTCTTGTGG CGATTCTACG G-3′
3	5′-AAGCCATCTC CGAATGCCTG CGTTGCGGTA TCAGCGTT*TT CGCTGATTTT ACTTGTTCCT GCCGTTCATT GT-3′
4	5′-ATGTCGCACC AGTTCGGCAA TACAGAGCAC CAGTGGCATT CGGAGAT-3′
5	5′-TCTGCTAGAG GTAAGTGTGG AGTGGAACAA GTAACCGCAA CGCACCAAGG CT-3′
6	5′-GTCGTTATCG TGGACTCCTG CGACATAGCC TTGGACTGGA CAAGACGGAT TA-3′
7	5′-GGCTTACAAT GAACGGCACC ACGATA-3′

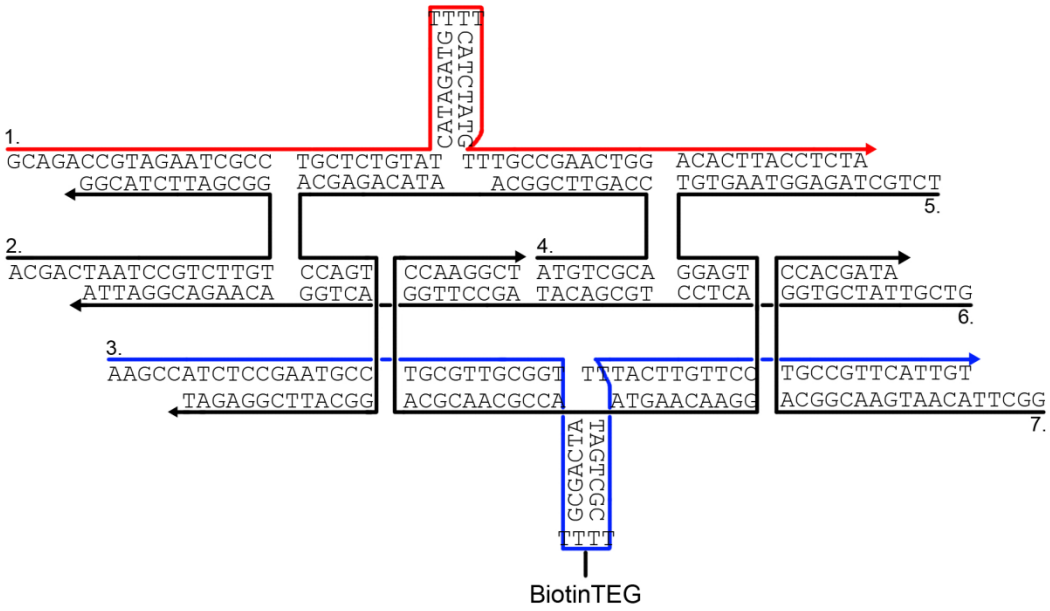

Figure S2. DNA strand structure of a TX tile functionalized with one biotin-TEG.

3. Spin-filtering of annealed TX tile construct solution

For filtering and buffer exchange we used Millipore Microcon YM-100 spin filters (MW cutoff of 100 kDa) (http://www.millipore.com/catalogue.nsf/docs/42424). The procedure was performed in the following way:

100 µl of annealed TX tile construct solution was mixed with 300 µl of Hepes/NaOH –based buffer (6.5 mM Hepes, 1 mM magnesium acetate and ~2 mM NaOH, pH ~7). Sample was spun for 12 min at 1000 relative centrifugal force (rcf) at 4 °C. After centrifugation, the eluate was removed and 400 µl buffer was added to the sample. Sample was spun once more for 7 min with 1000 rcf at 4 °C. This procedure left us with ~100 µl of sample retained in the spin filter. Finally, the spin filter was removed, placed upside down in a fresh tube and spun in a microcentrifuge for 2-3 min to collect the solution. We assume that nearly all structures are recovered from the filter membrane, thus filtering does not significantly change the concentration of B-A-B -complexes in solution.

4. Controlling the humidity inside the measurement chamber

Humidity in the humidity-tight measurement chamber was controlled by constantly feeding in either dry nitrogen (to dry the sample and environment) or alternatively water vapor-saturated air (to increase the relative humidity). The water vapor was generated by boiling autoclaved DI-water in a clean glass container and the air was pumped to the measurement chamber through the steam. Thus, in both cases there was a constant flow through the chamber and the relative humidity (RH) could be precisely tuned by pumping speed. RH and temperature were continuously measured by Honeywell HIH-3602-A humidity sensor. These values were also recorded to every measurement point.

5. Charging induced hysteresis in DC measurements

The hysteretic behavior observed in the measurements of the *IV* -characteristics at high humidity conditions is explained by currents due to charging of the total capacitance of the sample formed by the capacitance of the electrodes, parasitic stray capacitances and the capacitance of ions gathering on the electrodes. Most of these contributions yield negligible short time constants, i.e., not visible as hysteresis in our DC measurements. However, the polarization effect happens by the ions (i.e. ionized water molecules and counterions Na+, Mg++) gathered on the electrode, and this process has a quite slow timescale. This effectively causes a large parallel capacitance to the sample resistance, and is probably the main origin of the hysteresis seen in most of the DNA and reference samples (capacitances measured for completely clean samples, i.e. no salts, lead to time constants that would not be visible as hysteresis in the results). The amount of hysteresis varies from sample to sample and this is likely to be due to the slightly different salt concentrations and washing procedures applied from sample to sample. In addition, since our measurements are performed with very low DC voltages (0.3 V maximum), the reduction-oxidation processes of the ions at the electrodes are strongly suppressed.

In measurements, the DC bias voltage was changed in equal steps and after each step the sample was let to stabilize for $\tau_m \sim 0.5$ s before recording the current. In this case, one obtains for the measured current

$$I = \frac{V_n}{R} + I_0 \alpha \frac{1-\alpha^n}{1-\alpha} \quad (1)$$

where n means the nth *IV*-point measured and V_n is the corresponding bias voltage. Other parameters are: R the resistance of the sample, I_0 the maximum charging current at bias voltage transients (depends on the resistances of the measurement instruments) and $\alpha = \exp(-\tau_m/\tau)$ the exponential of the ratio between the stabilization time, τ_m, and the time constant of charging, τ. Figure 3(a) of the main paper shows this formula fitted to the measured data. The obtained resistance of the sample was 20 GΩ in that case, and time constants, τ, were typically of the order of 70 s.

6. AC impedance spectroscopy (AC-IS) of B-A-B -complexes

To take the environment of the trapped TX tile construct fully account, the following procedure was carried out in the AC-IS measurements:

1) The self-capacitance and the leakage current of the measurement setup were determined by measuring the impedance of an empty sample (only electrodes) in a dry environment. The obtained data was fitted with an equivalent circuit containing the resistor and one constant-phase element (CPE, $Z_{CPE} = 1/[Q(i\omega)^n]$, where ω is the angular frequency of the signal) in parallel. The leakage resistance is simply described by the resistor ($R_e \approx 0.3$ TΩ) and all stray capacitances of the setup can be incorporated into one constant-phase element [S2], which in fact turned out to be an ideal capacitor ($n = 1$, $Q =: C_e \approx 7$ pF). These values were kept constant during other data analysis and thus they were not free parameters in the fittings.

2) The control samples were measured (3 in total) and fitted with the equivalent circuit model (figure 4(b) in the article, black components). The equivalent circuit model was the same as in ref. [S3], i.e. a modified Randles circuit, where an additional diffusive element W_{diff} (Warburg impedance $Z_W = 1/[W(i\omega)^{1/2}]$) was added in parallel to the resistance R_s) [S2, S3]. This parallel

combination describes the area between electrodes, i.e., the resistance of "electrolyte" and the diffusive element due to ions migrating and diffusing along the SiO_2 surface. The other components describe so-called double-layer part, which is comprised of a double-layer capacitance C_{dl} (formed by ions on the electrode-"electrolyte" interface) and the charge-transfer resistance R_{ct} (charge moving through the double-layer via e.g. redox reactions) [S2, S3]. During the fitting W_{diff} and C_{dl} were replaced with general CPEs but it was found out that the exponents of CPEs converged to n = 0.5 for W_{diff} (pure Warburg impedance) and n ≈ 1 for C_{dl} (almost ideal capacitor). According to the fittings, the resistance of "electrolyte" was typically 1-4 GΩ and the charge-transfer resistance 20-30 GΩ. The sum of these two resistors roughly corresponds to the observed DC-resistance, and the high resistance of the charge-transfer process through the double-layer explains the poor DC-conductivity. These obtained parameters were also kept constant during the fitting of the TX tile samples.

3) The samples containing a single B-A-B -complex (3 in total) were measured and compared to the control samples. The charge-transfer resistance R_{ct} was kept constant during the fitting of the equivalent circuit shown in figure 4(b) in the article. In reality, the R_{ct} can slightly change when a TX tile construct is present, but it has a negligible contribution to the ac-conductivity since the impedance is large compared to other impedances parallel to it. Thus, all the other components were fitted including R_{DNA}, the resistance of the TX tile construct, which is located in parallel to the R_s and W_{diff}. The resistors R_s and R_{DNA} in parallel were considered as a single resistor $R_{s||DNA}$ during the fitting. Other fitted components were W_{diff} and C_{dl} (explained above) and additional components R_c (resistor) and Q_c (CPE). The latter two components together describe the modification of the double-layer and thus appear in parallel to the double layer part (for more details see ref. [S3]).

References

[S1] Li H, Park S H, Reif J H, LaBean T H and Yan H 2004 *J. Am. Chem. Soc.* **126** 418-9

[S2] Barsoukov E and Macdonald J R 2005 *Impedance spectroscopy: Theory, Experiment, and Applications* 2nd Ed (Hoboken, New Jersey: Wiley)

[S3] Linko V, Paasonen S-T, Kuzyk A, Törmä P and Toppari J J 2009 *Small* **5** 2382-86

Carbohydrate Polymers 89 (2012) 948–954

Contents lists available at SciVerse ScienceDirect

Carbohydrate Polymers

journal homepage: www.elsevier.com/locate/carbpol

Peptide-functionalized chitosan–DNA nanoparticles for cellular targeting

Elina Talvitie[a,c,*], Jenni Leppiniemi[b,c], Andrey Mikhailov[d], Vesa P. Hytönen[b,c,e], Minna Kellomäki[a,c]

[a] Department of Biomedical Engineering, Tampere University of Technology, FI-33101 Tampere, Finland
[b] Institute of Biomedical Technology, University of Tampere and Tampere University Hospital, FI-33014 University of Tampere, Finland
[c] BioMediTech, FI-33520 Tampere, Finland
[d] Department of Otolaryngology, University of Tampere and Tampere University Hospital, FI-33014 University of Tampere, Finland
[e] Center for Laboratory Medicine, Tampere University Hospital, FI-33520 Tampere, Finland

ARTICLE INFO

Article history:
Received 29 February 2012
Received in revised form 10 April 2012
Accepted 12 April 2012
Available online 21 April 2012

Keywords:
Chitosan
Nanoparticle
Gene delivery
Targeting

ABSTRACT

Chitosan–pDNA nanoparticles with various weight ratios (chitosan:pDNA 1:4–8:1) were characterized for particle size, zeta potential, morphology, and pDNA binding efficiency. For targeted gene delivery applications, nanoparticles were functionalized by coupling fluorescent dye and tyrosine kinase receptor B (TrkB) binding peptides on the particle surface. The targetability of the peptide-functionalized nanoparticles was demonstrated in TrkB positive murine transformed monocyte/macrophage cells (RAW 264). It was observed that weight ratio influenced DNA condensation and nanoparticle properties. An increase in the weight ratio decreased the average particle size, but increased the zeta potential. Cell culture studies showed that TrkB-peptide-functionalized nanoparticles bound to cells more effectively than nanoparticles functionalized with a control peptide. The length of the PEG spacer arm of the amine-to-sulfhydryl crosslinker used in the functionalization was found to positively correlate with the cellular attachment efficiency. This study suggests that the peptide-functionalization could be used to target chitosan–pDNA nanoparticles to specific cells.

1. Introduction

Cationic polymers and liposomes have been extensively studied as potential DNA carriers for non-viral gene delivery. Cationic polymers are positively charged and interact electrostatically with anionic DNA. These electrostatic interactions between polymer and DNA result in the formation of polymer–DNA complexes or nanoparticles (Opanasopit, Rojanarata, Apirakaramwong, Ngawhirunpat, & Ruktanonchai, 2009). Various cationic polymers such as polyethylenimine (PEI) (Ahn et al., 2008; Kunath et al., 2003; Wightman et al., 2001), poly-L-lysine (PLL) (Carlisle, Read, Wolfert, & Seymour, 1999; Mann, Richa, & Ganguli, 2008), polyamidoamine dendrimers (Navarro & Tros de ILarduya, 2009; Peng et al., 2010), and chitosan (Leong et al., 1998; Richardson, Kolbe, & Duncan, 1999) have all been reported to be able to condense DNA and have been used as gene carriers.

Non-viral carriers have several advantages when compared with unsafe viral vectors (retrovirus, adenovirus, adeno-associated viruses, herpes simplex virus, and lentivirus) (Corsi, Chellat, Yahia, & Fernandes, 2003). The non-viral systems can be tailored to target specific cells or tissues and they elicit only low host immune response. The non-viral systems provide an advantage in long-term storage, and they can also be produced in large volumes and at reasonable cost (Corsi et al., 2003; Mao et al., 2001). In gene delivery applications, the balance between stability and instability, the capability to protect DNA from nuclease degradation, targetability, and biocompatibility are important characteristics of efficient polymer–DNA complexes and nanoparticles (Mao et al., 2001).

Chitosan is a linear polymer composed of randomly repeating *N*-acetyl-D-glucosamines and D-glucosamines. Chitosan is obtained by alkaline deacetylation from chitin that is a natural polysaccharide found in the exoskeleton of crustaceans and insects and also in the cell walls of certain fungi (Muzzarelli et al., 2012). Chitosan has amino groups with a pK_a value of approximately 6.5. Thus, chitosan is positively charged and interacts with anionic DNA at acidic pH to form chitosan–DNA nanoparticles (Jayakumar et al., 2010). The molecular weight, degree of deacetylation, and the weight or charge ratio of chitosan to DNA has been shown to influence the properties of the chitosan–DNA delivery systems and their transfection efficiency (Huang, Fong, Khor, & Lim, 2005; Kiang, Wen, Lim, & Leong, 2004; Lavertu, Méthot, Tran-Khanh, & Buschmann, 2006; Strand et al., 2010). Conditions of nanoparticle synthesis such

Abbreviations: NHS, *N*-hydroxysuccinimide; PEG, polyethylene glycol; MAL, maleimide; TrkB, tyrosine kinase receptor B; RAW 264, murine transformed monocyte/macrophage cell line; PDI, polydispersity index; PEP, peptide; cPEP, control peptide.

* Corresponding author at: Department of Biomedical Engineering, Tampere University of Technology, FI-33101 Tampere, Finland. Tel.: +358 40 849 0976; fax: +358 3 3115 2250.
E-mail address: elina.talvitie@tut.fi (E. Talvitie).

0144-8617/$ – see front matter © 2012 Elsevier Ltd. All rights reserved.
http://dx.doi.org/10.1016/j.carbpol.2012.04.042

as the concentration of chitosan and DNA, ionic strength, and pH also influence chitosan–DNA particle properties like size and shape (Köping-Höggård, Mel'nikova, Vårum, Lindman, & Artursson, 2003; Mao et al., 2001; Romøren, Pedersen, Smistad, Evensen, & Thu, 2003). In addition to its cationic nature, chitosan is a biodegradable, biocompatible, and non-toxic material (Muzzarelli, 2010). Because of its favorable characteristics, chitosan is also studied in oral, nasal, and ocular drug delivery applications (Amidi et al., 2006; De Campos, Sánchez, & Alonso, 2001; Trapani et al., 2010; van der Lubben, Verhoef, van Aelst, Borchard, & Junginger, 2001; Yuan, Li, & Yuan, 2006).

Targeted delivery systems are essential for efficient and safe gene or drug delivery. Targetable nanoparticles can be achieved by conjugating targeting ligands such as small molecules, peptides, and proteins on the nanoparticle surface (Davis, 2002). Ligands enable the binding of the nanoparticles to specific target receptors on cells and internalization through various mechanisms. Functionalization of the nanoparticle surface does not only improve targetability but may also enhance cellular uptake, thereby making the gene transfer more efficient (Mao et al., 2001).

Some studies on chitosan–DNA delivery systems targeted to specific receptors have been reported. In these studies, nanoparticles were functionalized by conjugating transferrin (Mao et al., 2001), KNOB protein (Mao et al., 2001), and endosomolytic peptides GM225.1 and GM227.3 (MacLaughlin et al., 1998) to the nanoparticle surface. To improve nuclear uptake, delivery systems containing nuclear localization signal (NLS) peptides that attach to cytoplasmic transport receptors, have been investigated (Opanasopit et al., 2009). In addition, non-proteinaceous ligands such as folate (Chan, Kurisawa, Chung, & Yang, 2007; Mansouri et al., 2006) and hyaluronic acid (de la Fuente, Seijo, & Alonso, 2008) have been studied for targeting. Lactose (Hashimoto, Morimoto, Saimoto, Shigemasa, & Sato, 2006a), galactose (Gao et al., 2003; Kim, Park, Nah, Choi, & Cho, 2004), and mannose (Hashimoto et al., 2006b; Kim, Jin, Kim, Cho, & Cho, 2006) have been used as non-proteinaceous ligands in the production of chitosan derivatives for targeted gene delivery.

Brain-derived neurotrophic factor (BDNF) is a protein belonging to neurotrophins, i.e. a group of nerve growth factors that support the growth, differentiation, and survival of neuronal cells. Two neurotrophin receptors to which BDNF is able to bind exist on the cell surface: the low-affinity neurotrophin receptor p75 and the high-affinity receptor TrkB (García-Suárez et al., 1998; Ma et al., 2003). Therapeutic use of BDNF, e.g. in the treatment of neurodegenerative diseases is, however, restricted because of its molecular size, short half-life, and side effects. As a result, low molecular weight TrkB binding peptides have been developed (Ma et al., 2003) in order to mimic the actions of BDNF.

The aim of this study was to examine the functionalization of chitosan–pDNA nanoparticles by attaching TrkB binding targeting peptides and fluorescent dye on a nanoparticle surface. The conjugation of peptides was studied using crosslinkers with variable PEG spacer arm lengths. In addition, the effects of chitosan:pDNA weight ratio and surface modification on nanoparticle properties such as particle size and zeta potential were determined. To evaluate the binding of the nanoparticles to the cells, the peptide-functionalized chitosan–pDNA nanoparticles were studied in TrkB positive RAW 264 (murine transformed monocyte/macrophage) cells.

2. Materials and methods

2.1. Materials

Ultrapure chitosan PROTASAN UP B 80/20 with a molecular weight of 250 kDa and degree of deacetylation of 86% was purchased from FMC BioPolymer/NovaMatrix (Sandvika, Norway). Fluorescent dye DyLight 405 NHS ester as well as succinimidyl-([*N*-maleimidopropionamido]-#ethyleneglycol) ester (NHS-PEG$_n$-MAL) were purchased from Thermo Scientific (Rockford, IL, USA). Plasmid Id2.3 encoding green fluorescent protein (GFP) was obtained from Promega Corp. (Madison, WI, USA). GeneRuler^{TM} 1 kb DNA ladder, 6× DNA loading dye solution, and restriction enzyme PstI were from Fermentas (St. Leon-Rot, Germany). SYBR® Safe DNA gel stain was purchased from Invitrogen (Carlsbad, CA, USA). Other reagents were commercially available, higher-grade chemicals.

2.2. Peptide design and synthesis

Peptides were designed in a rational way on the basis of published TrkB binding sequences (Ma et al., 2003) and by inserting the sequence of the cleavage site for TeV protease between the N-terminal cysteine and the TrkB binding sequence. Peptide PEP (CENLYFQSG**SMAHPYFAR**) was used as a targeting peptide. Peptide cPEP (CENLYFQSGAYHMSAPFR) is a scrambled version of PEP with a randomized receptor-binding sequence. The recognition sequence for TeV protease is presented underlined and the TrkB binding sequence is presented in bold text. Both peptides have 18 amino acids and positive charge. All peptides were synthesized with FMOC technology at Storkbio (Tallinn, Estonia) and their purity (>90%) was verified by high performance liquid chromatography (HPLC) and their identity confirmed by mass spectrometry.

2.3. Cell culture

RAW 264 cell line was obtained from a local cryodepository and is descent from the original cells purchased from ATCC (Manassas, USA; clones TIB-71^{TM}) with less than 5 passages. The cells were maintained in Iscove's media supplemented with 5% fetal calf serum (Sigma, St. Louis, MO, USA) without any other nutritional supplements or antibiotics. The RAW 264 cells were maintained at a confluency lower than 50% in a humidified atmosphere at 5% CO_2.

2.4. Preparation of chitosan–pDNA nanoparticles

Chitosan nanoparticles loaded with plasmid DNA (pDNA) were prepared using complex coacervation. First, chitosan was dissolved in 100 mM acetic acid, 100 mM sodium acetate buffer overnight. Then, the pH of the chitosan solutions was adjusted to 5.5 with 10 M NaOH and the solutions were passed through a 0.2 μm syringe filter before use. Plasmid DNA was diluted in a 5 mM sodium sulfate solution. The chitosan and pDNA solutions were heated separately to 55 °C, followed by the immediate addition of the plasmid solution into the chitosan solution. The temperature of the solutions affects the size of the forming nanoparticles. At 55 °C using chitosan concentration of 50–400 μg/ml and DNA concentration of 40–80 μg/ml, uniform nanoparticles have been obtained (Mao et al., 2001). Finally, the mixture was vortexed for 30 s and then incubated at room temperature (RT, 22 ± 1 °C) for 30 min to complete the nanoparticle formation. The following chitosan to pDNA weight ratios were used: 1:4, 1:2, 1:1, 2:1, 4:1, and 8:1.

2.5. Functionalization of chitosan–pDNA nanoparticles

Targeting peptides and a fluorescent dye were coupled to amines at the surface of a nanoparticle after particle formation. The conjugation of the peptides was a two-step reaction, in which an amine-to-sulfhydryl crosslinker with polyethylene glycol (PEG) spacer arms, NHS-PEG$_n$-MAL, was used (Fig. 1). Three different crosslinkers with varying PEG spacer arm lengths and molecular

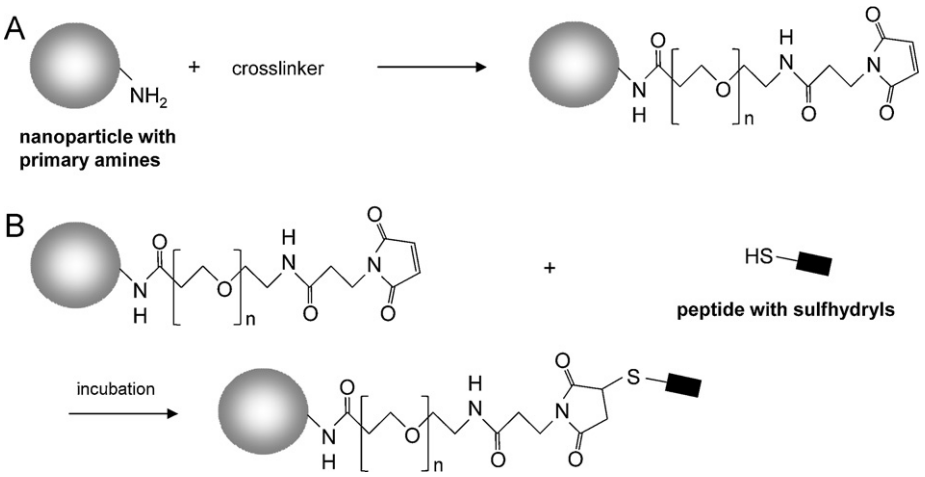

Fig. 1. Scheme for coupling a peptide to the surface of chitosan–pDNA nanoparticles using a heterobifunctional crosslinker with PEG spacer arms. (A) Coupling of NHS-PEG$_n$-MAL to the amines at the nanoparticle surface. (B) Reaction between NHS-PEG$_n$-MAL and peptide with N-terminal cysteine.

weights were studied: PEG_2 (17.6 Å, 425.39 g/mol), PEG_6 (32.5 Å, 601.60 g/mol), and PEG_{12} (53.4 Å, 865.92 g/mol).

To provide applicable conditions for the conjugation processes, the pH of the nanoparticle solution was increased to 7.0–7.2 by adding PBS buffer (100 mM sodium phosphate, 100 mM sodium chloride, pH 8). A 50-fold molar excess of crosslinker and a 16-fold molar excess of fluorescent dye to chitosan were mixed with the nanoparticle solution and incubated at RT for 1 h. Then, a 50-fold molar excess of peptide to chitosan was added into the nanoparticle solution and the incubation was continued at RT for 30 min. Non-reactive reagents and by-products were removed by dialysis in PBS buffer (50 mM sodium phosphate, 100 mM sodium chloride, pH 5.3) using a dialysis membrane with a molecular weight cut-off of 12,000–14,000 Da. The dialyzed nanoparticle solutions were stored at 4 °C.

2.6. Characterization of chitosan–pDNA nanoparticles

2.6.1. Particle size, polydispersity index, and zeta potential

A dynamic light scattering (DLS) instrument Zetasizer Nano ZS (Malvern Instruments Ltd., Worcestershire, UK) was used to determine the hydrodynamic diameter of the nanoparticles. The measurements were carried out at 25 °C using a scattering angle of 173°. Each sample was measured twice with three parallel measurements using a disposable sizing cuvette. The polydispersity index (PDI) was recorded for each nanoparticle as a measure of particle size distribution.

The zeta potential was defined by laser Doppler velocimetry (LDV) using the Zetasizer Nano ZS with Smoluchowski as a measurement model. The measurements were performed at 25 °C in disposable folded capillary cells. Each sample was measured three times.

2.6.2. Morphology

Morphology was studied using field emission scanning electron microscopy (FE-SEM, Zeiss ULTRA plus, Carl Zeiss NTS GmbH, Oberkochen, Germany). The samples were prepared for FE-SEM by pipetting a small amount of the nanoparticle solution onto a copper grid and incubating the solution for a few minutes. A filter paper was used to remove the excess nanoparticle solution. Before sample preparation, the nanoparticle solutions were dialyzed in PBS buffer (pH 5.3) or sterile water. Both carbon-coated and non-coated FE-SEM samples were examined.

2.6.3. Agarose gel electrophoresis

The capacity of chitosan to bind with pDNA was evaluated using agarose gel electrophoresis. Naked pDNA and nanoparticles with different chitosan to pDNA weight ratios (1:4, 1:2, 1:1, 2:1, 4:1, and 8:1) were studied. Samples mixed with a loading dye were loaded to a 0.8% agarose gel in Tris–borate EDTA (TBE) buffer, and run at 80 V (400 mA) for 1 h. The gel was prestained with SYBR® Safe DNA gel stain and visualized under UV light using a Bio-Rad ChemiDoc™ XRS molecular imager (Bio-Rad Laboratories, Inc., Hercules, CA, USA).

To study the protection effect of the nanoparticles to plasmid, PstI restriction enzyme was selected to cut the plasmid in two fragments. The following three samples were digested with PstI: the naked pDNA and the nanoparticles with the chitosan to pDNA weight ratios of 1:4 and 4:1. PstI was pipetted into a solution consisting of a digested sample, sterile water, and 10× buffer O. The mixture was incubated at 37 °C for 1 h and the reaction was stopped by adding 0.5 M EDTA (pH 8) to achieve a final concentration of 20 mM. After digestion, the samples were analyzed by gel electrophoresis as described above.

2.7. Cell culture studies

Estimation of binding efficiency was performed on a suspension of EDTA-detached RAW 264 cells naturally expressing the TrkB receptor. The peptide-bearing nanoparticles were added to the suspension of the cells at 1:5000 dilution with 10^6 cells per sample, incubated for 1, 6, or 22 h at room temperature in 5 mM Hepes containing 135 mM NaCl (pH 7.4), washed four times with PBS and then fixed in 4% paraformaldehyde in PBS. The fixed cells were measured using a Becton Dickenson FACSAria flow cytometer (BD Biosciences, Franklin Lakes, NJ, USA).

To distinguish whether the particles were bound to the receptors or internalized inside the cells, 100 E/ml of TeV protease was added to the cells before the addition of the nanoparticles. The cells were treated and analyzed as described above. Because the nanoparticles are supposed to bind to the cell surface via affinity interaction between the peptide and TrkB receptors, they should be released by the TeV protease that cleaves the peptide sequence between the nanoparticle and the recognition sequence of TrkB. Once the particles are internalized, however, the TeV treatment should not affect the fluorescence signal from the nanoparticles.

3. Results and discussion

3.1. Particle size, polydispersity index, and zeta potential

The chitosan–pDNA nanoparticles were formed by electrostatic interactions between chitosan and DNA. The electrostatic

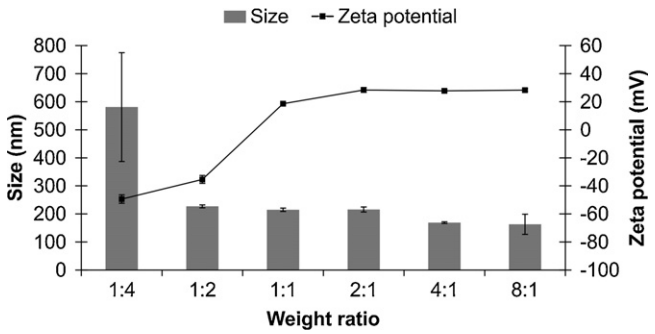

Fig. 2. Size (average hydrodynamic diameter) and zeta potential of nanoparticles prepared using different chitosan to pDNA weight ratios (w:w). The error bars represent the standard deviation.

interactions between the positively charged chitosan and negatively charged DNA resulted in phase separation (polymer-rich phase and polymer-poor phase) when these oppositely charged polyelectrolytes were mixed in an aqueous solution. The phase separation and coacervate formation was enhanced by using sodium sulfate as a coacervation agent (Leong et al., 1998).

The average hydrodynamic diameters for the chitosan–pDNA nanoparticles having different chitosan to pDNA weight ratios varied from 163 ± 36 nm to 581 ± 194 nm. The highest average diameter was obtained for the nanoparticles having the lowest chitosan to pDNA weight ratio. As shown in Table 1 and Fig. 2, the hydrodynamic diameter clearly showed a negative correlation with weight ratio.

Polydispersity indexes were elevated at low and high weight ratios (Table 1). The size distribution became bimodal at high weight ratio (w:w, 8:1), as smaller and larger particle populations were detected (peaks at 33 ± 3 nm, 190 ± 61 nm). This may indicate that the nanoparticles are aggregating or there are free molecules present in the sample. Monomodal particle size distributions were obtained at lower weight ratios. However, the weight ratio of 1:4 resulted in a remarkable particle size increase showing also high PDI and multimodal size distribution (two major peaks at 18 ± 2 nm and 662 ± 272 nm). The particle size distributions by volume are listed in Table 1 that shows the monomodal or multimodal size distributions.

The zeta potential of the nanoparticles varied from −49 mV to +28 mV (Table 1 and Fig. 2, measured at pH ~ 5.5). Zeta potentials of −49 mV and −35 mV were measured for the nanoparticles with weight ratios of 1:4 and 1:2, respectively. These results may indicate that there was an excess of pDNA in the mixture and that the binding of pDNA to chitosan was incomplete resulting in highly negative zeta potential. At weight ratios from 2:1 to 8:1, zeta potential remained at the level of approximately +28 mV showing condensation of pDNA and the formation of nanoparticles with free amines at the surfaces. Other studies have also shown similar changes in particle size and zeta potential when the charge ratio of the chitosan–DNA complexes was changed (Erbacher, Zou, Bettinger, Steffan, & Remy, 1998; Kim et al., 2004). Thus, weight or charge ratio has an evident connection to particle size and zeta potential.

3.2. Morphology

According to the FE-SEM studies, the morphology of the chitosan–pDNA nanoparticles seemed to be spherical. Aggregating nanoparticles were also observed, corresponding to the obtained DLS results. At the weight ratio of 4:1, the nanoparticles aggregated only slightly (Fig. 3A). However, aggregation was more obvious at the weight ratio of 8:1 (Fig. 3B). The size of the nanoparticles

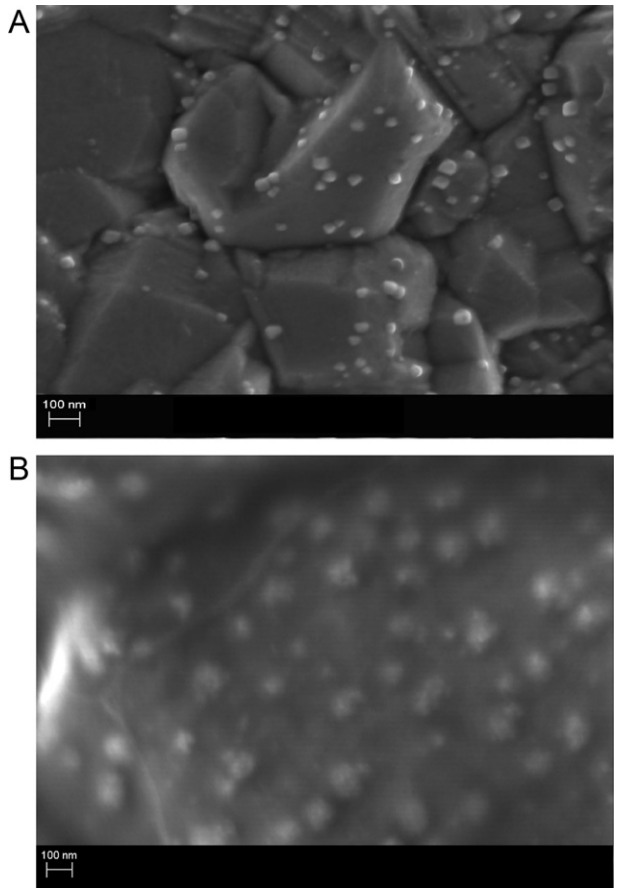

Fig. 3. Morphology of chitosan–pDNA nanoparticles studied by FE-SEM. Chitosan to pDNA weight ratio (A) 4:1 and (B) 8:1. Scale bar 100 nm.

(w:w, 4:1) estimated by FE-SEM analysis was approximately 40 nm, while according to the DLS measurement the size was 169 nm. In DLS analysis, the particle size was measured from the aqueous nanoparticle suspensions and chitosan has a tendency to swell when in contact with water. In contrast, the samples were dried for the FE-SEM studies, and this may explain the differences between the FE-SEM and DLS results (Aktas et al., 2005). Analogously, DNA requires water to form a natural helical conformation that collapses when dried (Dickerson et al., 1982).

Charge ratio has been reported to affect the shape of the chitosan–pDNA complexes. Liu et al. observed aggregates and irregular complexes at low charge ratio, but spherical complexes at higher charge ratios. They concluded that at high charge ratio chitosan is able to condense DNA completely to form spherical complexes (Liu et al., 2005). In addition, toroidal and rod-like structures have been observed (Danielsen, Vårum, & Stokke, 2004; Erbacher et al., 1998).

3.3. DNA binding capability

The capacity of the chitosan and pDNA to form nanoparticles together was evaluated by agarose gel electrophoresis. The naked plasmid migrated on the gel (Fig. 4, lane 2), whereas DNA loaded into the chitosan nanoparticles with weight ratio 1:1–8:1 (lanes from 5 to 8) was unable to migrate and remained in the gel loading wells, suggesting strong interaction between chitosan and DNA. At the weight ratios of 1:4 and 1:2, some plasmid was migrating freely on the gel (lanes 3 and 4). This was evidence that not all pDNA was tightly engaged by chitosan. In conclusion, it can be assumed that at the weight ratio of higher than 1:2, DNA was completely

Table 1
DLS analysis of particles. Average hydrodynamic diameter by volume, the distribution of hydrodynamic diameter by volume, the polydispersity index (PDI), and the zeta potential of non-functionalized and functionalized chitosan–pDNA nanoparticles at different chitosan to pDNA weight ratios (w:w).

Sample	Average diameter (nm)	Distribution of diameter by volume (nm). Percentual amount is indicated in parenthesis[a]		PDI	Zeta potential (mV)
w:w, 1:4	581 ± 194	18 ± 2 (6%)	662 ± 272 (91%)	0.362 ± 0.097	−49.4 ± 3.0[b]
w:w, 1:2	227 ± 5	227 ± 5 (100%)		0.139 ± 0.008	−35.4 ± 2.8[b]
w:w, 1:1	215 ± 6	215 ± 6 (100%)		0.107 ± 0.017	+18.6 ± 0.7[b]
w:w, 2:1	216 ± 9	216 ± 9 (100%)		0.187 ± 0.011	+28.4 ± 1.7[b]
w:w, 4:1	169 ± 3	169 ± 3 (100%)		0.188 ± 0.012	+27.8 ± 1.1[b]
w:w, 8:1	163 ± 36	33 ± 3 (11%)	190 ± 61 (89%)	0.248 ± 0.017	+28.3 ± 0.9[b]
Functionalized					
w:w, 4:1; blank	166 ± 3	166 ± 3 (100%)		0.215 ± 0.004	+19.6 ± 1.3[c]
w:w, 4:1; PEG_2		173 ± 6 (40%)	5000 ± 390 (60%)	0.259 ± 0.040	+18.9 ± 1.4[c]
w:w, 4:1; PEG_6		159 ± 13 (49%)	4740 ± 1050 (51%)	0.285 ± 0.053	+19.8 ± 1.6[c]
w:w, 4:1; PEG_{12}		193 ± 13 (44%)	4860 ± 540 (53%)	0.275 ± 0.058	+17.5 ± 0.8[c]

[a] Size distributions containing <5% of total are not shown.
[b] Particle solution, pH ~ 5.5.
[c] Nanoparticles in dialysis buffer, pH 5.3.

coupled with chitosan and remained in the loading well. Similar findings have been made earlier and suggest that the interaction between chitosan and pDNA become more effective when weight or charge ratio increases (Xu, Capito, & Spector, 2008; Zheng et al., 2007). Kiang et al. reported the influence of molecular weight and degree of deacetylation on the capability of chitosan to bind DNA. According to their study, chitosans with lower molecular weight or degree of deacetylation require a higher charge ratio to condense DNA completely (Kiang et al., 2004).

When pDNA and two samples of the chitosan nanoparticles were digested with restriction enzyme PstI, plasmid was cut into two fragments, 4120 bp and 1197 bp. The nanoparticles containing an excess amount of plasmid (w:w, 1:4) released most of the DNA (Fig. 4, lane 10). This demonstrated that at weight ratio of 1:4 plasmid was partly located on the nanoparticle surface or remained unbound and free in the solution and, therefore, exposed to enzymatic digestion with PstI. Nevertheless, part of the plasmid remained in the well with chitosan. In the case of the nanoparticles containing an excess amount of chitosan (w:w, 4:1), no released DNA was seen after PstI digestion. Therefore, at weight ratio of 4:1 plasmid was most probably located mainly inside the particle and chitosan protected it from digestion. These findings are in line with the zeta potential results.

3.4. Functionalization of chitosan–pDNA nanoparticles

The nanoparticles with chitosan to pDNA weight ratio 4:1, having the initial particle size of 169 nm, were selected for the functionalization studies because they were able to bind pDNA completely according to agarose gel electrophoresis and that they had the monomodal particle size distribution. The functionalization potential of these nanoparticles was studied by conjugating fluorescent dye DyLight 405 NHS ester and NHS-PEG_n-MAL crosslinkers of different sizes to amine groups of chitosan. This was followed by the conjugation of sulfhydryl-containing peptide (PEP, cPEP) to the maleimide group of crosslinker.

The used heterobifunctional crosslinker had two different reactive groups, NHS (*N*-hydroxysuccinimide) ester and maleimide group. NHS esters react with amines forming covalent amide bonds and releasing *N*-hydroxysuccinimide. In the two-step conjugation procedure NHS ester reaction is followed by maleimide reaction. Maleimides are sulfhydryl-reactive, and the double bond of maleimide may undergo a specific alkylation reaction with sulfhydryl group to form a stable thioether bond (Hermanson, 1996; Mattson et al., 1993).

As expected, surface modification increased the particle size. After coupling with DyLight 405, PEG crosslinker, and peptide, the size of the particles varied from 159 ± 13 to 193 ± 13 nm (Table 1). In addition, the functionalization seemed to partly induce the aggregation process since large aggregates with diameter ~5 μm appeared in all functionalized particles (Fig. 5). If these aggregates are excluded from the data analysis, the hydrodynamic diameter of the particles was 173 ± 6 nm with the shortest PEG_2 spacer arm and 159 ± 13 nm with the PEG_6 spacer arm. By contrast, the nanoparticles functionalized with the longest PEG spacer arm (PEG_{12}) were slightly larger with the average diameter of 193 ± 13 nm. MacLaughlin et al. have studied the effect of non-covalently attached pH-sensitive endosomolytic peptides on the complex size and zeta potential. The size of the complexes

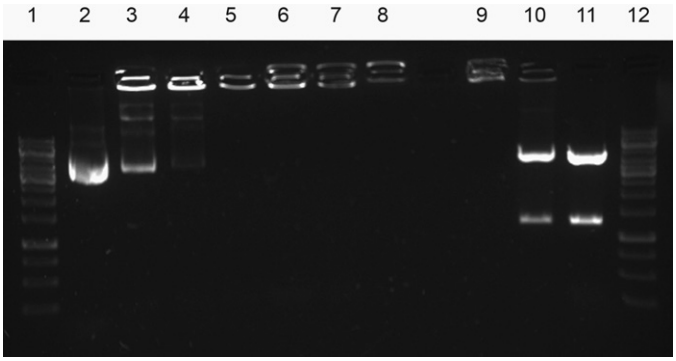

Fig. 4. Agarose gel electrophoresis of chitosan–pDNA nanoparticles having different chitosan to pDNA weight ratios (w:w). Lane 1: DNA ladder; lane 2: naked plasmid; lane 3: w:w, 1:4; lane 4: w:w, 1:2; lane 5: w:w, 1:1; lane 6: w:w, 2:1; lane 7: w:w, 4:1; lane 8: w:w, 8:1; lane 9: digested w:w, 4:1; lane 10: digested w:w, 1:4; lane 11: digested plasmid; and lane 12: DNA ladder.

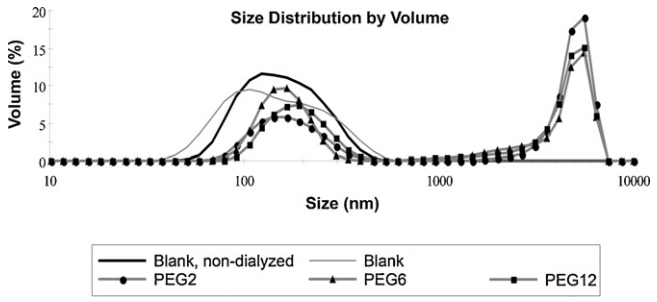

Fig. 5. Particle size distribution by volume of chitosan–pDNA nanoparticles functionalized with fluorescent dye DyLight 405 and different crosslinkers conjugated with peptide PEP. Nanoparticles without any functionalization (blank) were used as a control.

Table 2
Fluorescence of cells incubated for 1, 6, and 22 h with chitosan–pDNA nanoparticles. As a control measurement, the fluorescence of cells incubated for 22 h in the presence of TeV protease is shown. The results are indicated as mean*10^3 ± CV*10^3.

Incubation time	PEG_2		PEG_6		PEG_{12}	
	PEP	cPEP	PEP	cPEP	PEP	cPEP
1 h	7.5 ± 0.1	3.7 ± 0.2	8.0 ± 0.1	1.7 ± 0.1	9.2 ± 0.1	2.9 ± 0.3
6 h	10.4 ± 0.1	5.0 ± 0.3	12.7 ± 0.1	3.3 ± 0.3	10.8 ± 0.1	4.2 ± 0.3
22 h	19.3 ± 0.1	9.5 ± 0.2	21.6 ± 0.1	17.0 ± 0.3	22.9 ± 0.1	6.9 ± 0.3
22 h TeV protease	15.2 ± 0.1	6.6 ± 0.2	17.1 ± 0.1	12.4 ± 0.3	20.6 ± 0.1	5.7 ± 0.3

increased with increasing peptide amount. However, at higher peptide proportions (charge ratio of plasmid to peptide 1:1.5) the complex size decreased (MacLaughlin et al., 1998). Studies of the chitosan–DNA complexes functionalized with NLS peptides showed that at high chitosan to DNA weight ratios (8:1 and higher) the particle size was smaller compared with the complexes without NLS peptide. At lower weight ratios the particle size increased when NLS was added (Opanasopit et al., 2009).

The zeta potential of the peptide-functionalized nanoparticles varied between +18 and +20 mV (Table 1, measured at pH 5.3). These values are almost equal to the zeta potential of the dialyzed blank nanoparticles, +20 mV, indicating that this functionalization does not change the zeta potential of the particles. However, as the particles are more stable when the zeta potential is highly negative (<−30 mV) or highly positive (>+30 mV), we can conclude that the functionalized and even our dialyzed blank nanoparticles have a tendency to aggregate. Interestingly, the zeta potential of the non-dialyzed, blank nanoparticle was higher, +28 mV, at pH 5.5 indicating that they were more stable before dialysis. An increase in the number of surface peptides has been reported to diminish the zeta potential of the complexes containing endosomolytic peptides (MacLaughlin et al., 1998).

3.5. Cell culture studies

Targeting ligands enable ligand conjugated nanoparticles to be transported to the target cells by binding to the receptors on the cell surface. Our results demonstrate that the decoration of the chitosan–pDNA nanoparticles with affinity peptide (PEP) against TrkB significantly increased the binding of these nanoparticles to their target cells in the time-dependent manner. Table 2 illustrates the fluorescence of the cells after 1, 6, and 22 h incubation with the peptide-functionalized nanoparticles. FACS studies also showed that the longer PEG spacer arm was beneficial for TrkB binding. Clearly less efficient binding was seen with scrambled control peptide (cPEP). It is noticeable that the longer spacer gives higher specificity between targeting and scrambled peptides, as well as higher absolute binding of the nanoparticles. This behavior could be explained by the lower sterical hindrance of the peptides attached to the longer spacer, as well as the higher hydrophilicity of the longer PEG spacer reducing unspecific binding by van der Waals interaction.

Pretreatment with TeV protease specifically removes affinity peptides from the termini of the PEG spacer. As expected, the TeV treated samples demonstrated a lower fluorescence signal in all experimental groups (Table 2). However, the TeV treated functionalized particles still showed more binding compared with the particles decorated with the scrambled peptide, possibly suggesting either fast nanoparticle internalization or incomplete cleavage of the peptides by TeV. Our data show that the treatment of the affinity peptide-bearing nanoparticles with TeV protease partially reverses the effects of peptides on the binding and internalization of the particles. However, in our earlier studies (results not shown), we noticed that when TeV protease was added after 1 or 12 h incubation, fluorescence was higher compared with the samples pretreated with TeV. This proposes the fast dynamics of the steps critical for internalization. Finally, we propose that the measured fluorescence in the presence of TeV protease was obtained from the internalized nanoparticles, and that cell uptake was enhanced when the length of PEG spacer arm was increased.

4. Conclusions

Nanoparticles can be used in gene delivery as efficient and protective carriers for DNA. Targeting enables the delivery of therapeutic agents to the specific, predetermined cells. In targeted delivery, the availability of the delivered therapeutic agent can be improved and, hence nonspecific delivery can be avoided. This reduces unwanted effects and also decreases the amount of materials needed for efficient treatment.

Chitosan–pDNA nanoparticles with various chitosan to pDNA weight ratios were prepared, and the properties of the nanoparticles were affected by the weight ratio. Targeting peptides were successfully coupled on the nanoparticle surface, and surface modification only slightly reflected to the particle properties. The functionalization of the nanoparticles with TrkB binding affinity peptide was shown to enhance the binding to the cells having TrkB receptors in a specific and time-dependent manner. The PEG spacer arm length of the NHS-PEG_n-MAL crosslinker was found to positively correlate with the binding efficiency.

Acknowledgments

This study was financially supported by the European Community 6th Framework Programme (NanoEar, contract number: NMP4-CT-2006-026556), Academy of Finland (project number 115796), and Tampere Graduate Program in Biomedicine and Biotechnology (TGPBB). The authors thank Tommi Manninen and Weikai Zhang (University of Tampere) for plasmid propagation and extraction, Katri Paavilainen (Tampere University of Technology) for her assistance in nanoparticle preparation and characterization, and Ulla Kiiskinen (University of Tampere) for her excellent technical assistance.

References

Ahn, H. H., Lee, M. S., Cho, M. H., Shin, Y. N., Lee, J. H., Kim, K. S., et al. (2008). DNA/PEI nano-particles for gene delivery of rat bone marrow stem cells. *Colloids and Surfaces A: Physicochemical and Engineering Aspects*, *313-314*, 116–120.

Aktas, Y., Andrieux, K., Alonso, M. J., Calvo, P., Gürsoy, R. N., Couvreur, P., et al. (2005). Preparation and in vitro evaluation of chitosan nanoparticles containing a caspase inhibitor. *International Journal of Pharmaceutics*, *298*, 378–383.

Amidi, M., Romeijn, S. G., Borchard, G., Junginger, H. E., Hennink, W. E., & Jiskoot, W. (2006). Preparation and characterization of protein-loaded *N*-trimethyl chitosan nanoparticles as nasal delivery system. *Journal of Controlled Release*, *111*, 107–116.

Carlisle, R. C., Read, M. L., Wolfert, M. A., & Seymour, L. W. (1999). Self-assembling poly(L-lysine)/DNA complexes capable of integrin-mediated cellular uptake and gene expression. *Colloids and Surfaces B: Biointerfaces*, *16*, 261–272.

Chan, P., Kurisawa, M., Chung, J. E., & Yang, Y. Y. (2007). Synthesis and characterization of chitosan-g-poly(ethylene glycol)–folate as a non-viral carrier for tumor-targeted gene delivery. *Biomaterials*, *28*, 540–549.

Corsi, K., Chellat, F., Yahia, L., & Fernandes, J. C. (2003). Mesenchymal stem cells, MG63 and HEK293 transfection using chitosan–DNA nanoparticles. *Biomaterials*, *24*, 1255–1264.

Danielsen, S., Vårum, K. M., & Stokke, B. T. (2004). Structural analysis of chitosan mediated DNA condensation by AFM: Influence of chitosan molecular parameters. *Biomacromolecules*, *5*, 928–936.

Davis, M. E. (2002). Non-viral gene delivery systems. *Current Opinion in Biotechnology*, *13*, 128–131.

De Campos, A. M., Sánchez, A., & Alonso, M. J. (2001). Chitosan nanoparticles: A new vehicle for the improvement of the delivery of drugs to the ocular surface. Application to cyclosporin A. *International Journal of Pharmaceutics*, *224*, 159–168.

de la Fuente, M., Seijo, B., & Alonso, M. J. (2008). Novel hyaluronic acid–chitosan nanoparticles for ocular gene therapy. *Investigative Ophthalmology & Visual Science*, *49*, 2016–2024.

Dickerson, R. E., Drew, H. R., Conner, B. N., Wing, R. M., Fratini, A. V., & Kopka, M. L. (1982). The anatomy of A-, B-, and Z-DNA. *Science*, *216*, 475–485.

Erbacher, P., Zou, S., Bettinger, T., Steffan, A. M., & Remy, J. S. (1998). Chitosan-based vector/DNA complexes for gene delivery: Biophysical characteristics and transfection ability. *Pharmaceutical Research*, *15*, 1332–1339.

Gao, S., Chen, J., Xu, X., Ding, Z., Yang, Y. H., Hua, Z., et al. (2003). Galactosylated low molecular weight chitosan as DNA carrier for hepatocyte-targeting. *International Journal of Pharmaceutics*, *255*, 57–68.

García-Suárez, O., Hannestad, J., Esteban, I., Sainz, R., Naves, F. J., & Vega, J. A. (1998). Expression of the TrkB neurotrophin receptor by thymic macrophages. *Immunology*, *94*, 235–241.

Hashimoto, M., Morimoto, M., Saimoto, H., Shigemasa, Y., & Sato, T. (2006). Lactosylated chitosan for DNA delivery into hepatocytes: The effect of lactosylation on the physicochemical properties and intracellular trafficking of pDNA/chitosan complexes. *Bioconjugate Chemistry*, *17*, 309–316.

Hashimoto, M., Morimoto, M., Saimoto, H., Shigemasa, Y., Yanagie, H., Eriguchi, M., et al. (2006). Gene transfer by DNA/mannosylated chitosan complexes into mouse peritoneal macrophages. *Biotechnology Letters*, *28*, 815–821.

Hermanson, G. T. (1996). *Bioconjugate techniques* (1st ed.). San Diego, CA: Academic Press.

Huang, M., Fong, C. W., Khor, E., & Lim, L. Y. (2005). Transfection efficiency of chitosan vectors: Effect of polymer molecular weight and degree of deacetylation. *Journal of Controlled Release*, *106*, 391–406.

Jayakumar, R., Chennazhi, K. P., Muzzarelli, R. A. A., Tamura, H., Nair, S. V., & Selvamurugan, N. (2010). Chitosan conjugated DNA nanoparticles in gene therapy. *Carbohydrate Polymers*, *79*, 1–8.

Kiang, T., Wen, J., Lim, H. W., & Leong, K. W. (2004). The effect of the degree of chitosan deacetylation on the efficiency of gene transfection. *Biomaterials*, *25*, 5293–5301.

Kim, T. H., Park, I. K., Nah, J. W., Choi, Y. J., & Cho, C. S. (2004). Galactosylated chitosan/DNA nanoparticles prepared using water-soluble chitosan as a gene carrier. *Biomaterials*, *25*, 3783–3792.

Kim, T. H., Jin, H., Kim, H. W., Cho, M. H., & Cho, C. S. (2006). Mannosylated chitosan nanoparticle-based cytokine gene therapy suppressed cancer growth in BALB/c mice bearing CT-26 carcinoma cells. *Molecular Cancer Therapeutics*, *5*, 1723–1732.

Kunath, K., von Harpe, A., Fischer, D., Petersen, H., Bickel, U., Voigt, K., et al. (2003). Low-molecular-weight polyethylenimine as a non-viral vector for DNA delivery: Comparison of physicochemical properties, transfection efficiency and in vivo distribution with high-molecular-weight polyethylenimine. *Journal of Controlled Release*, *89*, 113–125.

Köping-Höggård, M., Mel'nikova, Y. S., Vårum, K. M., Lindman, B., & Artursson, P. (2003). Relationship between the physical shape and the efficiency of oligomeric chitosan as a gene delivery system *in vitro* and *in vivo*. *The Journal of Gene Medicine*, *5*, 130–141.

Lavertu, M., Méthot, S., Tran-Khanh, N., & Buschmann, M. D. (2006). High efficiency gene transfer using chitosan/DNA nanoparticles with specific combinations of molecular weight and degree of deacetylation. *Biomaterials*, *27*, 4815–4824.

Leong, K. W., Mao, H. Q., Truong-Le, V. L., Roy, K., Walsh, S. M., & August, J. T. (1998). DNA–polycation nanospheres as non-viral gene delivery vehicles. *Journal of Controlled Release*, *53*, 183–193.

Liu, W., Sun, S., Cao, Z., Zhang, X., Yao, K., Lu, W. W., et al. (2005). An investigation on the physicochemical properties of chitosan/DNA polyelectrolyte complexes. *Biomaterials*, *26*, 2705–2711.

Ma, Z., Wu, X., Cao, M., Pan, W., Zhu, F., Chen, J., et al. (2003). Selection of trkB-binding peptides from a phage-displayed random peptide library. *Science in China Series C Life Sciences*, *46*, 77–86.

MacLaughlin, F. C., Mumper, R. J., Wang, J., Tagliaferri, J. M., Gill, I., Hinchcliffe, M., et al. (1998). Chitosan and depolymerized chitosan oligomers as condensing carriers for in vivo plasmid delivery. *Journal of Controlled Release*, *56*, 259–272.

Mann, A., Richa, R., & Ganguli, M. (2008). DNA condensation by poly-L-lysine at the single molecule level: Role of DNA concentration and polymer length. *Journal of Controlled Release*, *125*, 252–262.

Mansouri, S., Cuie, Y., Winnik, F., Shi, Q., Lavigne, P., Benderdour, M., et al. (2006). Characterization of folate–chitosan–DNA nanoparticles for gene therapy. *Biomaterials*, *27*, 2060–2065.

Mao, H. Q., Roy, K., Troung-Le, V. L., Janes, K. A., Lin, K. Y., Wang, Y., et al. (2001). Chitosan–DNA nanoparticles as gene carriers: Synthesis, characterization and transfection efficiency. *Journal of Controlled Release*, *70*, 399–421.

Mattson, G., Conklin, E., Desai, S., Nielander, G., Savage, M. D., & Morgensen, S. (1993). A practical approach to crosslinking. *Molecular Biology Reports*, *17*, 167–183.

Muzzarelli, R. A. A. (2010). Chitins and chitosans as immunoadjuvants and non-allergenic drug carriers. *Marine Drugs*, *8*, 292–312.

Muzzarelli, R. A. A., Boudrant, J., Meyer, D., Manno, N., DeMarchis, M., & Paoletti, M. G. (2012). Current views of fungal chitin/chitosan, human chitinases, food preservation, glucans, pectins and inulin: A tribute to Henri Braconnot, precursor of the carbohydrate polymers science, on the chitin bicentennial. *Carbohydrate Polymers*, *87*, 995–1012.

Navarro, G., & Tros de ILarduya, C. (2009). Activated and non-activated PAMAM dendrimers for gene delivery in vitro and in vivo. *Nanomedicine: Nanotechnology, Biology, and Medicine*, *5*, 287–297.

Opanasopit, P., Rojanarata, T., Apirakaramwong, A., Ngawhirunpat, T., & Ruktanonchai, U. (2009). Nuclear localization signal peptides enhance transfection efficiency of chitosan/DNA complexes. *International Journal of Pharmaceutics*, *382*, 291–295.

Peng, S. F., Su, C. J., Wei, M. C., Chen, C. Y., Liao, Z. X., Lee, P. W., et al. (2010). Effects of the nanostructure of dendrimer/DNA complexes on their endocytosis and gene expression. *Biomaterials*, *31*, 5660–5670.

Richardson, S. C. W., Kolbe, H. V. J., & Duncan, R. (1999). Potential of low molecular mass chitosan as a DNA delivery system: Biocompatibility, body distribution and ability to complex and protect DNA. *International Journal of Pharmaceutics*, *178*, 231–243.

Romøren, K., Pedersen, S., Smistad, G., Evensen, Ø., & Thu, B. J. (2003). The influence of formulation variables on in vitro transfection efficiency and physicochemical properties of chitosan-based polyplexes. *International Journal of Pharmaceutics*, *261*, 115–127.

Strand, S. P., Lelu, S., Reitan, N. K., de Lange Davies, C., Artursson, P., & Vårum, K. M. (2010). Molecular design of chitosan gene delivery systems with an optimized balance between polyplex stability and polyplex unpacking. *Biomaterials*, *31*, 975–987.

Trapani, A., Lopedota, A., Franco, M., Cioffi, N., Ieva, E., Garcia-Fuentes, M., et al. (2010). A comparative study of chitosan and chitosan/cyclodextrin nanoparticles as potential carriers for the oral delivery of small peptides. *European Journal of Pharmaceutics and Biopharmaceutics*, *75*, 26–32.

van der Lubben, I. M., Verhoef, J. C., van Aelst, A. C., Borchard, G., & Junginger, H. E. (2001). Chitosan microparticles for oral vaccination: Preparation, characterization and preliminary in vivo uptake studies in murine Peyer's patches. *Biomaterials*, *22*, 687–694.

Wightman, L., Kircheis, R., Rössler, V., Carotta, S., Ruzicka, R., Kursa, M., et al. (2001). Different behavior of branched and linear polyethylenimine for gene delivery *in vitro* and *in vivo*. *The Journal of Gene Medicine*, *3*, 362–372.

Xu, X., Capito, R. M., & Spector, M. (2008). Plasmid size influences chitosan nanoparticle mediated gene transfer to chondrocytes. *Journal of Biomedical Materials Research*, *84A*, 1038–1048.

Yuan, X. B., Li, H., & Yuan, Y. B. (2006). Preparation of cholesterol-modified chitosan self-aggregated nanoparticles for delivery of drugs to ocular surface. *Carbohydrate Polymers*, *65*, 337–345.

Zheng, F., Shi, X. W., Yang, G. F., Gong, L. L., Yuan, H. Y., Cui, Y. J., et al. (2007). Chitosan nanoparticle as gene therapy vector via gastrointestinal mucosa administration: Results of an in vitro and in vivo study. *Life Sciences*, *80*, 388–396.